Scholars' Mine

Doctoral Dissertations   Student Theses and Dissertations

Summer 2018

Mitigation of environmental hazards of sulfide mineral flotation with an insight into froth stability and flotation performance

Muhammad Badar Hayat

Department: Mining and Nuclear Engineering

Recommended Citation

MITIGATION OF ENVIRONMENTAL HAZARDS OF SULFIDE MINERAL

FLOTATION WITH AN INSIGHT INTO FROTH STABILITY AND

FLOTATION PERFORMANCE

by

MUHAMMAD BADAR HAYAT

A DISSERTATION

Presented to the Faculty of the Graduate School of the

MISSOURI UNIVERSITY OF SCIENCE AND TECHNOLOGY

In Partial Fulfillment of the Requirements for the Degree

DOCTOR OF PHILOSOPHY

in

MINING ENGINEERING

2018

Approved by:

Dr. Lana Alagha, Advisor
Dr. Nassib Aouad
Dr.Neil L.Anderson
Dr.Mary R. Reidmeyer
Dr Muthanna Al-Dahhan

ABSTRACT

Today's major challenges facing the flotation of sulfide minerals involve constant variability in the ore composition; environmental concerns; water scarcity and inefficient plant performance. The present work addresses these challenges faced by the flotation process of complex sulfide ore of Mississippi Valley type with an insight into the froth stability and the flotation performance. The first project in this study was aimed at finding the optimum conditions for the bulk flotation of galena (PbS) and chalcopyrite ($CuFeS_2$) through Response Surface Methodology (RSM). In the second project, an attempt was made to replace toxic sodium cyanide (NaCN) with the biodegradable chitosan polymer as pyrite depressant. To achieve an optimum flotation performance and froth stability, the third project utilized two types of nanoparticles; silica (SiO_2) and alumina (Al_2O_3) as process aids. The fourth project investigated the impact of water chemistry on the process outcomes in an attempt to replace fresh water with sea water. In the last project, five artificial intelligence (AI) and machine learning (ML) models were employed to model the flotation performance of the ore which will allow the building of intelligent systems that can be used to predict the process outcomes of polymetallic sulfides. It was concluded that chitosan can be successfully used as a biodegradable depressant. Alumina nanoparticles successfully enhanced both froth stability and flotation performance while silica nanoparticles did not. Seawater had a negative effect on both the froth stability and the grade of lead (Pb) and copper (Cu) but it improved the recoveries of both Pb and Cu minerals. Hybrid Neural Fuzzy Interference System (HyFIS) ML model showed the best accuracy to be adopted for automated sulfide ore flotation process in the future.

ACKNOWLEDGMENTS

First and foremost, I would like to acknowledge my advisor Dr. Lana Alagha.I sincerely appreciate her continuous support, patience, and devoted guidance throughout my Ph.D study. I see her as my mentor and anything which I may achieve in my future life is dedicated to her.I humbly thank her for changing my life for better.May Allah bless her and her family.

My deep appreciation goes to Dr. Mary Reidmeyer (a great human being) for her guidance in operating and providing access to the mineral processing equipment. I would like to thank Dr. Muthanna Al Dahhan for his support in providing the chemical engineering lab facilities. I would also like to mention my gratitude to Dr. Nassib Samir Aouad for his continuous support throughout my stay. Regarding Dr Neil Anderson, I have not seen a better teacher in my life. I feel proud to have him on my commitetee.

I will always be indebted to Dr. Muhammad Usman Khan, Dr. Muhammad Akram and Dr. Syed Muhammad Tariq for putting me on track of academics and PhD studies.

Contributions of beautiful mind and heart of Danish Ali and Keitumetse Monyake to my research is immeasurable.I am thankful to Syed Muhammad Sannan, Frank Schott and Zhongqing Xiao for helping me in carrying out experiments. Ontlametse Molatlhegi, Ashraf Alsafasfeh, Simin Khatibi and Mostafa Khodakarami were great.

I would like to express my gratitude to my parents, my wife and role model Yasmeen Aziz, brothers Aslam and Faisal Hayat, sisters , inlaws, talented cousins, loving uncles, aunts, friends and my beautiful daughters for their everlasting support and love.

TABLE OF CONTENTS

LIST OF ILLUSTRATIONS

LIST OF TABLES

1. INTRODUCTION

1.1. POLYMETALLIC SULFIDE MINERALS

When sulfur anion combines with a metal or semi-metal cation, the resulting compound is termed as a sulfide mineral. This serves as the standard definition for sulfide minerals, but compounds having anions such as As or Sb are also included in the wider definition of these minerals. In addition, sulfo salts are also included in the sulfide mineral family. These sulfo salts are generally composed of Ag, Cu, Pb, As, Sb, Bi and S. Hundreds of minerals are included in the sulfide mineral group, but only four minerals namely pyrite, galena, sphalerite, pentlandite and chalcopyrite are well known [1]. Sulfides can be regarded as the most important ore minerals as these are main sources of base metals like copper, lead, zinc, nickel and cobalt [2].

Sulfide minerals generally occur together rather than individually. As an example, in a deposit of galena, it is not unusual to find sphalerite, pyrite, and chalcopyrite. At times sulfide minerals occur along with precious metals like gold and silver [2], [3]. Table 1.1 shows how sulfide minerals occur in association with each other throughout the world.

Sulfide mineral deposits are formed via two processes (i) crystallization of basic magmas, and (ii) sedimentation of brine solutions. Sulfide deposits which are formed as a result of igneous activity are mostly enriched with sulfide minerals like chalcopyrite, pyrite, pyrrhotite and Pentlandite [4]. Sulfide deposits associated with sedimentary rocks, on the other hand have galena, sphalerite and pyrite as the major form of sulfide minerals. Limestone is mainly the major host sedimentary rock especially in the Mississippi Valley region (USA) [3].

Table 1.1. Major Type of sulfide ore deposits [5].

Type	Major Ore Minerals*	Examples
Sulfide nickel deposits	po, pn, py, cpy, viol	Sudbury, Ontario, Canada
Merensky reef platinum	po, pn, cpy	Merensky Reef, RSA
Tin and tungsten skarns	py, cass, sph, cpy, wf	Pine Creek, CA, USA
Zinc–lead skarns	py, sph, gn	Ban Ban, Australia
Copper skarns	py, cpy	Carr Fork, Utah, USA
Porphyry copper/molybdenum	py, cpy, bn, mbd	Bingham Canyon, Utah;USA Climax, CO, USA
Polymetallic veins	py, cpy, gn, sph, ttd	Camsell River, NWT, Canada
High sulfidation ores	py, enar, cov, ten, Au	Summitville, CO, USA
Cyprus-type massive sulfides	py, cpy	Cyprus
Besshi-type massive sulfides	py, cpy, sph, gn	Japan
Creede-type epithermal veins	py, sph, gn, cpy, ttd, asp	Creede, CO, USA
Kuroko-type	py, cpy, gn, sph, ttd, asp	Japan
Quartz pebble U–gold	py, uran, gold	Witwatersrand, RSA
Sandstone-hosted lead–zinc	py, sph, gn	Laisvall, Sweden
Sedimentary exhalative lead–zinc	py, sph, gn, cpy, asp, ttd, po	Sullivan, BC, Canada Tynagh, Ireland
Mississippi Valley type	py, gn, sph	Missouri, USA

Where asp–arsenopyrite, Au–gold, bn–bornite, cass–cassiterite, cov–covellite, cpy–chalcopyrite, enar–Enargite, gn–galena, mbd–molybdenite, PGM–platinum group minerals, pn–pentlandite, po–pyrrhotite, py Pyrite, sph–sphalerite, ten– tennantite, ttd– tetrahedrite, uran–uraninite, viol–violarite, wf–wolframite.

Among sulfide deposits lead–zinc ores are the most extensively found throughout the world. Main areas where lead–zinc ores occur are the United States, Europe, South America, Africa, Balkan Peninsula, Australia, and Russia. Copper–lead–zinc ores share a common origin with lead-zinc ores. The only difference is the addition of copper as an extra valuable mineral in copper–lead–zinc ores. The most important geological formations in which lead–zinc and Copper–lead–zinc ores occur are (i) hydrothermal vein fillings and bodies, (ii) massive sulfide deposits and (iii) sedimentary deposits. The first type of deposits is found mainly in North America, Mexico, Russia and Peru. The second type (massive) of deposits is mostly found in Canada, Spain, and Turkey. The Viburnum Trend in Missouri is famous over the world for having the most sedimentary deposits (third type) [6], [7]. The complex Cu–Pb–Zn ores account for a 15% share of total world production. These ores contain 7.5% of the total world copper. [8].

1.2. EXTRACTION OF BASE METALS FROM SULFIFDE ORES

Extraction of metals from complex sulfide ores requires multi-stage mineral processing. Flotation is the only technique in mineral processing that has been used successfully to process these ores [9]. Froth flotation uses the surface chemistry of minerals in a three–phase system that consists of solids, gas and water. Hydrophobic mineral particles are captured selectively and carried by air bubbles, to the froth product,

whereas hydrophilic minerals are discharged as tailings or rejected [10]. The two

flotation methodologies used to process these ores are sequential flotation and bulk

flotation. In sequential flotation each mineral in the ore is separated in different steps.

Bulk flotation requires flotation of copper and lead minerals together in one step, while

zinc and iron minerals are depressed. This is followed by activation of the flotation of

zinc minerals. The bulk concentrate of copper and lead is then separated in different

steps. A typical bulk flotation circuit for complex lead–zinc sulfide ore is shown in

Figure 1.1.
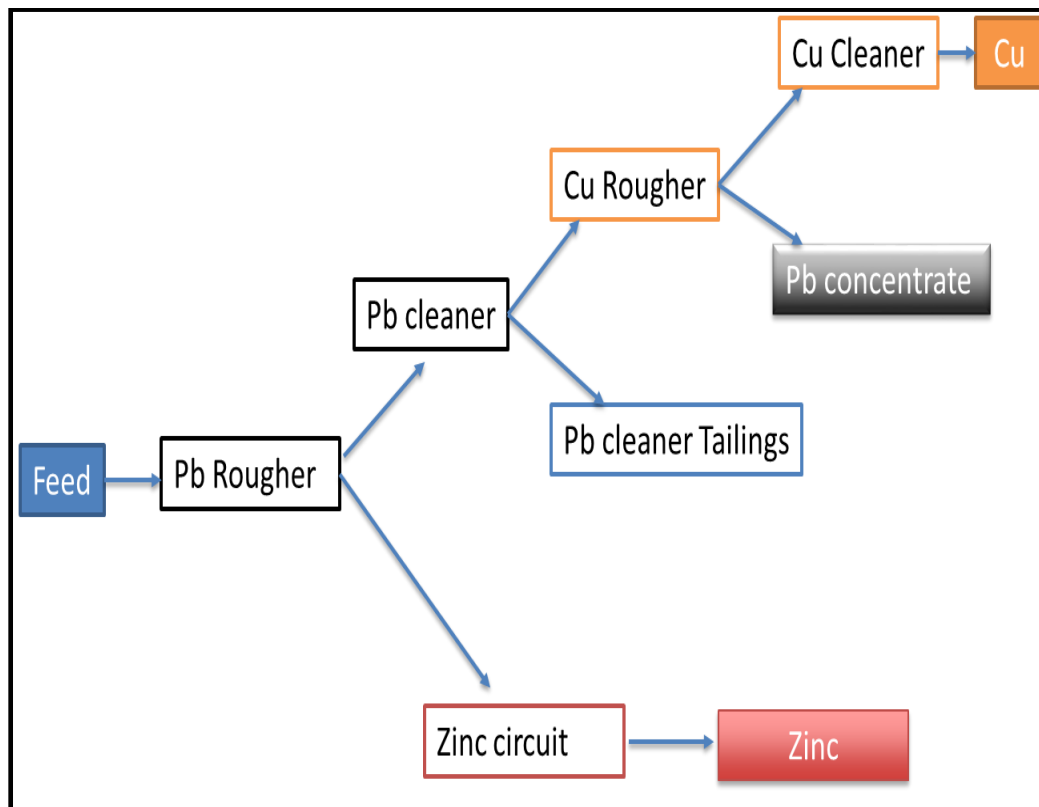
Figure 1.1. Typical Bulk flotation of complex sulfide ores.

Each flotation methodology has its own pros and cons and adopting anyone method heavily depends upon the geology of the ore. However the most widely used method for treating complex sulfide ores is bulk flotation. Bulk flotation is normally carried out at an alkaline PH with sodium cyanide and $ZnSO_4$ as pyrite and sphalerite depressants [9].

1.3. STATEMENT OF THE PROBLEM

Froth flotation is known to be one of the key enabling technologies that allow the selective separation of values from uneconomic mineral resources. Froth flotation utilizes the differences in the wettability of minerals in a three–phase system that consists of solids, gas and water. Despite the extensive and successful use of this process in ore enrichment, there are many challenges facing flotation operations of polymetallic sulfides. Froth zones in the case of sulfide mineral flotation have not been studied thoroughly. This makes it difficult to achieve the desired grade and recovery of metallic sulfide minerals [11]. Another challenge facing mineral processing plant is the continuous changes in the geology of the mine, which makes it difficult to achieve peak performance with constant variability of ore composition. Human experts on the behavior of flotation plants are few and far between and even if one is found, unfortunately may not be able to formulate his knowledge in a precise, convenient and certain manner. It is therefore of utmost importance to develop automatic monitoring and control system to run the processing plants [12].There are also environmental concerns over toxic sodium cyanide (used as iron depressant) as discharge products of sulfide flotation processes. Recent leakages of sodium cyanide at mines throughout the world have raised the need

for eliminating sodium cyanide from the mineral processing industry as it uses 20 % of the total world production of cyanide [13]–[15]. Another major challenge facing mineral processing operations in general and sulfide mineral froth flotation processes in particular, is water supply. The severity of this challenge can be assessed through this quote; "The water required to operate a flotation plant may outweigh all of the other uses of water at a mine site, and the need to maintain a water balance is critical for the plant to operate efficiently" [16].

To address these challenges, future research efforts must focus on three major areas:

1. A comprehensive understanding of the froth layer. Understanding the factors effecting the stability and mobility of froth is very important to control the recovery and flow of froth. Froth stability is of crucial importance as it affects both the grade and recovery of the concentrate. By increasing the stability of the froth, the recovery also increases but the selectivity and thus the grade of the froth decrease due to the recovery of gangue material. Conversely, if the froth is unstable the overall concentrate recoveries will decrease, but this may enhance the grade. Therefore acquiring the correct stability of the froth is of paramount importance [17].

2. Integrating green chemicals to replace "toxic reagents." Toxic reagents, like NaCN used in sulfide mineral flotation need to be replaced with biodegradable reagents. This will not only reduce the environmental hazards, but will also help to improve the sustainability of the process.

3. Reducing freshwater intake. Currently, freshwater resources are becoming scarcer day by day. There is a need to conserve these resources. It is therefore required to cut down the freshwater usage in the sulfide mineral flotation process.

4. Currently, in order to achieve peak flotation performance on daily basis, plant operators change the input variables of flotation plant based on the sampling results from the lab and froth color. There are a lot of inefficiencies in the plant operations due to human errors. The integration of artificial intelligence and machine learning to current plant practices will cut down human errors and can enhance the performance of flotation plant.

This research work will contribute to the existing efforts to integrate and implement sustainability into the flotation process of complex sulfide ores and will address the challenges facing it. To accomplish this purpose, bulk flotation of complex sulfide ores containing galena, sphalerite, pyrite, chalcopyrite and dolomite was carried out using biodegradable reagents, nanoparticles and seawater. The effect of these materials on the froth stability was also quantified. Moreover, artificial intelligence and machine learning models were employed to contribute to the development of automatic plants of the future.

1.4. OBJECTIVES OF THE CURRENT WORK

The proposed research aims to contribute to the existing efforts to integrate and implement sustainability into the flotation process of complex sulfide ores. To accomplish this purpose, bulk flotation of complex sulfide ores containing galena,

sphalerite, pyrite, chalcopyrite and dolomite was carried out. The specific objectives of the current work were as follows:

1. To optimize operation parameters used in froth flotation of complex sulfide minerals using statistical techniques. The seven control parameters investigated include collector (sodium isopropyl xanthate) dosage, frother (MIBC) dosage, impeller speed, air rate, pyrite depressant (NaCN) dosage, sphalerite depressant ($ZnSO_4$) dosage and flotation time.

2. To investigate the possibility of replacing toxic NaCN with biodegradable polymer chitosan as pyrite depressant. Sodium cyanide interferes with the body's ability to adsorb oxygen which may result in death. A dosage of 200 to 300 mg of sodium cyanide is considered fatal [18].Chitosan was chosen because of its biodegradability and abundance, and its recent success as a depressant of pyrite in single mineral flotation tests.

3. To study the effect of nanomaterials on froth stability and flotation performance. Recently, nanomaterials were found to increase the recovery of barite via flotation processes. Nanomaterials provided an opportunity to control the froth stability without altering the operational parameters of the flotation process[19]. Motivated by these results nano–sized Fe_2O_3 and Al_2O_3 were used to study the effect of these nano materials in sulfide mineral flotation.

4. To explore the possibility of using seawater as process water in order to save freshwater resources. The salinity of water affects froth stability and flotation performance. This study will test the effect of seawater salinity on sulfide ore flotation and will pave the way for its usage at plant scale.

5. To carry out artificial intelligence (AI) and machine learning (ML) modelling to predict the flotation performance of complex sulfide ores under different operational variables. To date, at plant scale, this has been done mainly through empirical methods. The empirical approach is not effective with regards to cost and control. Therefore, application of AI and ML is significant to optimize plant performance and rule out the human errors.

Based upon the literature review above, key areas regarding froth stability to be explored through current research are identified in Table 1.2.

1.5. BROADER IMPACTS AND INTELECTUAL MERIT OF THE PRESENT WORK

This research is a pioneering effort toward introducing nanomaterials and biodegradable reagents as process aids in the flotation of complex sulfide ores to further improve the sustainability of the process by increasing the economic gain and reducing the environmental impact. The economic gain was evaluated based on froth stability and its consequent effect on the recovery and the grade of the concentrate products. Further improvement in economics and plant operation was obtained through optimization of plant through statistical, AL and ML modelling. The environmental profile of the flotation process was examined by quantifying the effect of seawater on the process outcomes to explore the potential of using seawater to reduce the freshwater intake. To the best of the candidate's knowledge and based on extensive literature search, this study has undertaken these tasks to investigate these effects in the flotation of run-of-mine complex sulfide ores for the first time.

1.5.1. Broader Impact. This research will contribute immensely to the

existing body of knowledge on froth flotation efficiency and froth stability in mineral

processing. Results generated from this study will be beneficial at different frontiers.

1.5.1.1. Economic benefits. Froth stability has a major effect on the

mineral grade and recovery in flotation process. A 1% increase in mineral recovery

Table 1.2. Technology gap assessment.

Key components	Current technology	Proposed technology
The use of biodegradable reagents to replace toxic depressants in sulfide mineral flotation	Biodegradable polymers have been used in simulated ores and single mineral flotation. These polymers have shown promising results during the fundamental studies.	Naturally occurring complex sulfide ores from Missouri were used for the first time to explore the impact of these polymers on froth stability. Results provided useful information to industry professionals.
Nano materials as process aids to enhance froth stability	Nano materials have been reported to increase froth stability in single mineral flotation tests.	Effectiveness of nano materials in the flotation of real complex sulfide ores was tested.
Artificial intelligence and Machine learning models for process	Till date Hybrid artificial intelligence and machine learning models have not been employed in mineral flotation process	A total of five AI or ML models namely ANN, RF, Mamdani, ANFIS and HyFIS were developed in this study.
Froth flotation using seawater	The effect of seawater and flotation chemicals in stabilizing the froth in coal flotation and copper-molybedenite ore has been studied. These studies helped to reduce the reagent consumption at processing plants. Freshwater resources have also been saved by this study.	Seawater containing different ions will be used in a lab scale Denver flotation cell. The effect of inorganic electrolytes on froth stability and flotation performance in Sulfide ores will be studied.

during flotation is a great economic benefit. Understanding the factors affecting froth stability will benefit many industries besides the mineral processing industry, including food, emulsions, firefighting, shampoo, dish washing, petroleum, and many others. The use of nanomaterials to optimize froth stability has the potential of making froth stability a controllable factor. This development will enhance separation efficiency and selectivity of the flotation process. Moreover AI and ML modelling of the process will ensure peak performance of the plant.

      1.5.1.2. Environmental benefits. The replacement of the toxic depressant, NaCN, by the bio-degradable chitosan polymer will contribute towards more sustainable mineral processing operations by reducing the environmental footprint. Furthermore, the utilization of seawater will help to save freshwater resources and decrease the toxic waste produced at the plant sites.

      1.5.2. Intellectual Merit. This work has contributed to a better understanding about the factors that influence the froth phase stability. Considerable information has been generated through the different phases of this work that and will broaden the knowledge in the field of sulfide mineral flotation. The findings of this study should also advance the fundamental knowledge in different areas in science and engineering as follows:

1. Understanding the interaction mechanism between mineral particles in the flotation pulp and the polymer through electro kinetic measurements has contributed to the fields of polymer and colloid science.

2. Understanding the effect of nanoparticles in controlling froth stability has contributed to the field of nanotechnology.

3. The effect of seawater on froth flotation performance will contribute towards understanding the effect of ions in water towards effectiveness of foaming agents.

4. AI and ML modelling will contribute towards integration of new technologies to the mineral processing industry and will pave the way for automatic plants of the future.

1.6. ORGANIZATION OF THESIS

This thesis includes eight sections discussing the challenges and possible remedial strategies concerning complex sulfide ore flotation.

Section 1: This Section presents the purpose of this project. It includes the formation and geology of sulfide minerals. General extraction strategies for complex sulfide ores are briefly introduced. The problems in sulfide mineral processing are outlined. The impact of this study on different disciplines of science and its intellectual merit is depicted. The specific objectives and outline of the thesis are included herein.

Section 2: This Section reviews the background of this project. It contains fundamentals of froth flotation and the reagents and equipment used in the flotation process. Specific details on the sulfide mineral flotation processes are included. Statistical methods regarding the optimization of flotation process are discussed with a special emphasis on response surface methodology (RSM). Literature regarding the application of biodegradable polymers as reagents, nano material usage for froth stability, and the possibility of seawater usage in sulfide ore flotation is reviewed. Factors affecting froth stability and methods used for measuring froth stability are illustrated.

Section 3: This Section describes the application of response surface methodology (RSM) for modeling and the optimization of seven process variables of sulfide ore flotation. A three-level Box–Behnken design combined with RSM was employed for modeling and optimizing seven operation parameters of the bulk flotation of galena and chalcopyrite. Quadratic mathematical models were derived for the prediction of Pb, Cu, Zn, and Fe recovery. These models were then used to find the optimum operational parameters to achieve the desired flotation results.

Section 4: This Section investigates the possibility of using chitosan polymer as a potential selective green depressant of pyrite in the bulk flotation of galena (PbS) and chalcopyrite ($CuFeS_2$) from sphalerite (ZnS) and pyrite (FeS_2) using sodium isopropyl xanthate as a collector and 4-methyl-2-pentanol (MIBC) as a frother. Results of the investigation are presented.

Section 5: This Section focuses on the possibility of using nano materials as froth stabilizing agents. The flotation tests of sulfide ore in the presence of Al_2O_3 and SiO_2 nanoparticles were conducted. Froth stability tests using the nano materials were also carried out.

Section 6: This Section aims at understanding the challenges of using seawater in sulfide mineral flotation and its effect on froth stability. Flotation reagents' dosages were varied to find the optimum dosages in case of seawater flotation. Correlation among froth stability, grade and recovery of the concentrates was explored to better understand and tackle the challenges of using seawater as process water.

Section 7: This Section describes the application of AI and ML for modeling of seven process variables to predict the grade and recovery of Pb, Cu, Zn, and, Fe in the

bulk flotation of galena and chalcopyrite. This will lay the ground work toward adoptation of enhanced automated flotation performance in future.

Section 8: This Section encompasses the main conclusions and contributions of this project, and includes recommendations for future research in the sulfide mineral flotation process.

2. LITERATURE REVIEW

2.1. FROTH FLOTATION PROCESS

Froth flotation was patented in 1906 and is considered the most versatile and important mineral processing technique [9]. It has found widespread use in the mineral processing industry especially in processing of low–grade ores. For efficient separation , froth flotation needs to be employed for particle sizes ranging from10 to 100 μm [20]. The froth flotation process exploits the difference in surface hydrophobicity of mineral particles. Hydrophobic mineral particles are selectively captured and carried by air bubbles to the froth product, whereas hydrophilic minerals are discharged as tailings or rejected. The effectiveness of particle bubble attachment depends on three things: collision, attachment and detachment [21].

2.1.1. Probability of Collision. When a bubble of radius R_b rises through slurry, it creates a disturbance in the form of streamlines around itself. Due to this disturbance created around the bubble, any particle outside the limiting radius Rc does not collide with the bubble (Figure 2.1).

The probability of collision P_c is defined as the fraction of particles in line with the rising bubble that actually collide with the bubble. In order to calculate this probability, different models are used to measure probability of collision [21].One of the most widely used models is given in Equation 1.

Where D_b is the bubble size, D_p is the particle size, and, Re is the Reynolds number of the bubble [22], [23]. The equation indicates that within effective size range for flotation, the decrease in bubble size and the increase in particle size enhance the probability of collision.

$$P_c = \left[\frac{3}{2} + \frac{4Re^{0.72}}{15}\right]\left(\frac{D_p}{D_b}\right)^2 \qquad (1)$$
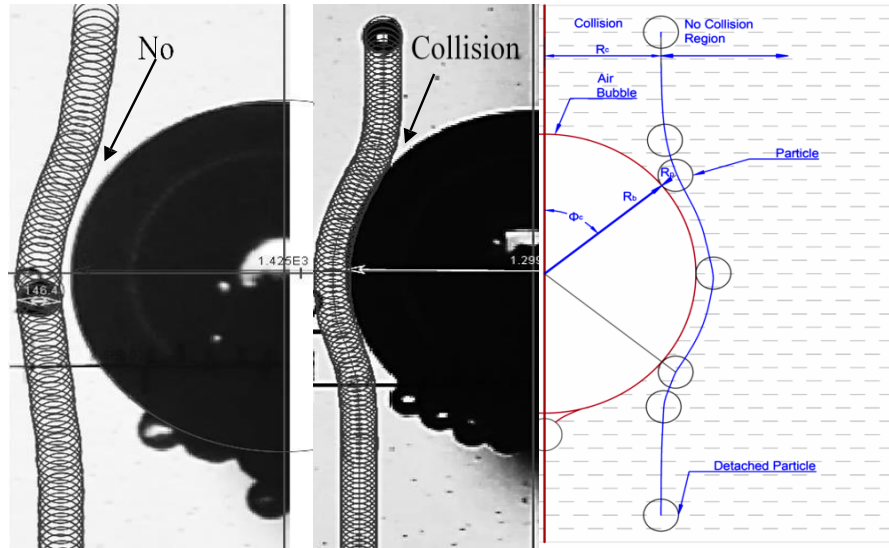
Figure 2.1. Collision pattern amongst bubble and particle [21].

2.1.2. Probability of Adhesion. Once particle –bubble collision happens,

a three step process takes place for the particle to get attached to the bubble as shown in

Figure 2.2. During first step, liquid film between particle and bubble becomes thin to a

critical level (hcr), secondly this film ruptures to form a three phase contact (TPC) nuclei

of critical wetting radius (rcr), thirdly TPC line expands to form a stable wetting

parameter with penetration depth (h) depending upon the hydrophobicity of the

particle[24], [25]. The time it takes to complete all these steps is called attachment

time(tat), while the time taken for thining and rupturing of film1.1.1. (First two steps) is

termed as induction time (ti).
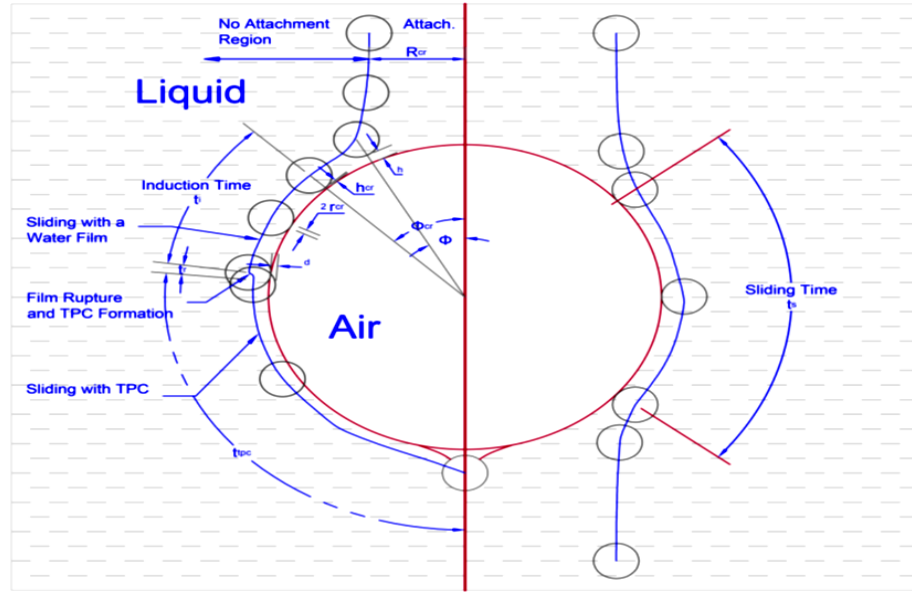
Figure 2.2. Particle –bubble attachment process ([21], [24], [26]).

For particle bubble attachment another important time to consider is the sliding time (t_s). It is the time taken by the particle to slide along the bubble surface. A smaller induction time as compared to sliding time results in particle getting attached to the bubble and vice versa. The model for calculating probability of attachment(P_a) is given by Equation 2 [27]:

$$P_a = sin^2 \left[2 \arctan exp \left(- \frac{(45 + 8Re^{0.72}) u_b t_i}{15 D_b \left(\frac{D_b}{D_p} + 1 \right)} \right) \right] \qquad (2)$$

Here U_b is bubble rising velocity. Equation 2 indicates that probability of attachment increases with the increase in particle hydrophobicity (induction time) t_i, particle size and bubble rising velocity. On the other hand probability of attachment

seems to decrease with increasing bubble size. From these observations it can be concluded that for increasing probability of particle bubble attachment, smaller bubbles and larger particle size with higher degree of hydrophobicity are preferred.

2.1.3. Probability of Detachment. After attachment as the bubble laden with particles moves up, some of the particles get detached and fall back into the pulp phase. The cause for the detachment is the increase of detaching forces as compared to the adhesive forces. The probability of detachment is calculated by Equation 3 [28].

$$P_d = \left[1 + \left(\frac{3(1 - \cos\theta_d)\gamma}{g\left(\rho_b - \rho_w\left(\frac{1}{2} + \frac{3}{4}\cos\frac{\theta_d}{2}\right)\right)}\right)\left(\frac{1 + \frac{D_p}{D_b}}{D_p^2}\right)\right] \tag{3}$$

Where ρ_b is bubble density, ρ_w is water density θ_d is polar position for detachment. Equation 3 suggests increase of Probability of detachment with increase in particle size and bubble diameter. It can therefore be concluded for increase in recovery, smaller particle size, small bubble size and more hydrophobic particles are recommended.

These probabilities of collision, attachment and detachment define the flotation performance. As reported in literature, there are around 100 variables that affect these probabilities and flotation performance [29]. These process variables include physiochemical factors such as water chemistry, reagents chemistry, temperature, interfacial forces and hydrodynamic factors such as circuit design, cell type and aeration rate. Moreover, feed characteristics such as mass flowrate, mineralogy, liberation size, and particle size distribution are detrimental factors of the process outcome [30]. A froth flotation cell consists mainly of two major zones (i) two-phase

pulp zone (ii) three-phase froth zone. Efficient flotation depends on the characteristics of both the pulp and the froth zone [31].

      2.1.4. Reagents Used in Froth Flotation. Froth flotation separates minerals on the basis of surface properties. For a mineral to get attached to the bubbles, it should have a certain degree of hydrophobicity owing to its surface properties. The selective attachment of hydrophobic minerals to air bubbles determine the efficiency and performance of the process. In order to change the surface properties in favor of flotation various reagents are used in the flotation process. These reagents include Collectors, frothers and regulators [32].

      2.1.4.1. Collector. Collectors are the organic compounds which render the mineral surface hydrophobic by adsorbing onto its surface [33]. Collector molecules can be ionizing or non-ionizing. Non ionizing collectors do not dissociate in water and work by covering the mineral surface in form of a thin film, hence making the mineral surface hydrophobic. Ionizing collectors however dissociate into ions when dissolved in water. Non ionizing collectors normally consist of complex hetero type molecules. These molecules consist of a polar and non-polar group. Non polar group is a hydrocarbon while polar group can be of any type. Ionizing collectors are classified on the basis of type of ion, responsible for inducing hydrophobic effect to the mineral. Detailed classification of collectors is illustrated in Figure 2.3 [9], [34].

      In an ionizing collector, polar group attaches to the mineral surface through electrical, physical or chemical attraction while non polar hydrophobic group extends into the solution imparting hydrophobicity to the mineral as shown in Figure 2.4.
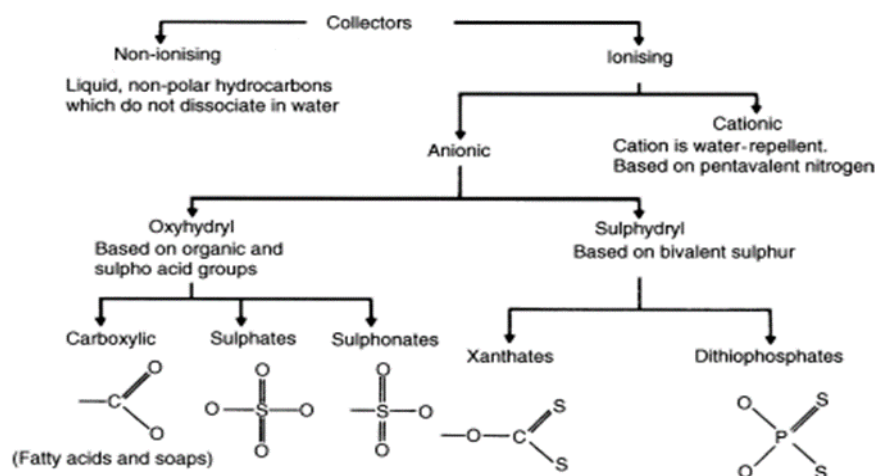
Figure 2.3. Classification of collectors [9].
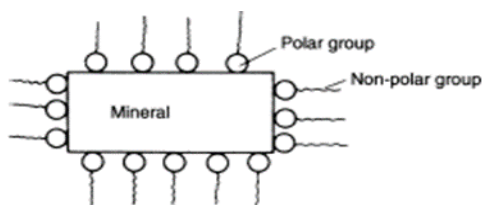
Figure 2.4. Working mechanism of ionizing collectors [9].

2.1.4.2. Frothers. Frothers are nonionic heteropolar compounds. These are responsible for the stabilization of bubble formed in pulp phase, thus help in formation of a stable froth. These reagents also assist in achieving the desired flotation kinetics. The hydroxyl, ester or carbonyl groups determine the frothing ability of a frother. Alcohols, polyglycols, aloxyparaffins are regarded as the three main classes of the frothers. Frother has a non-polar hydrophobic tail and a polar end which forms hydrogen bonding with water as shown in Figure 2.5.

Frothers do not form any bond with the mineral. This is the reason, frothers are not specific for different group of minerals [35][36].
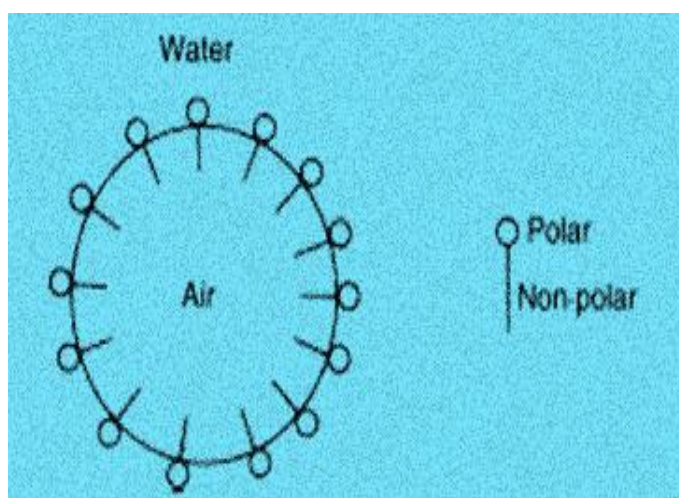
Figure 2.5. Functioning of frother[9].

Most widely used frothers are alcohols as these carry no collector properties. This lack of collector property makes these frothers ideal for flotation process. Pine oil and Cresol (cresylic acid),$CH_3C_6H_4OH$ are the most widely used natural frothers. Synthetic frothers based on high molecular weight alcohols and polyglycol ethers have also become popular among froth flotation plants. Methyl iso butyl carbinol (MIBC) is the most widely used synthetic frother[9].

2.1.4.3. Modifying reagents. Modifying reagents is the most important class of reagents used in sulfide mineral flotation. Collector selectivity and efficiency heavily depends upon the careful use of these reagents. These reagents sometimes enhance the adsorption of collector on specific minerals while other times depress the adsorption of

collector. These modifying reagents are therefore can be classified generally into two groups, activators and depressants [37]. The classification of modifying reagents on the basis of type is shown in Figure 2.6.
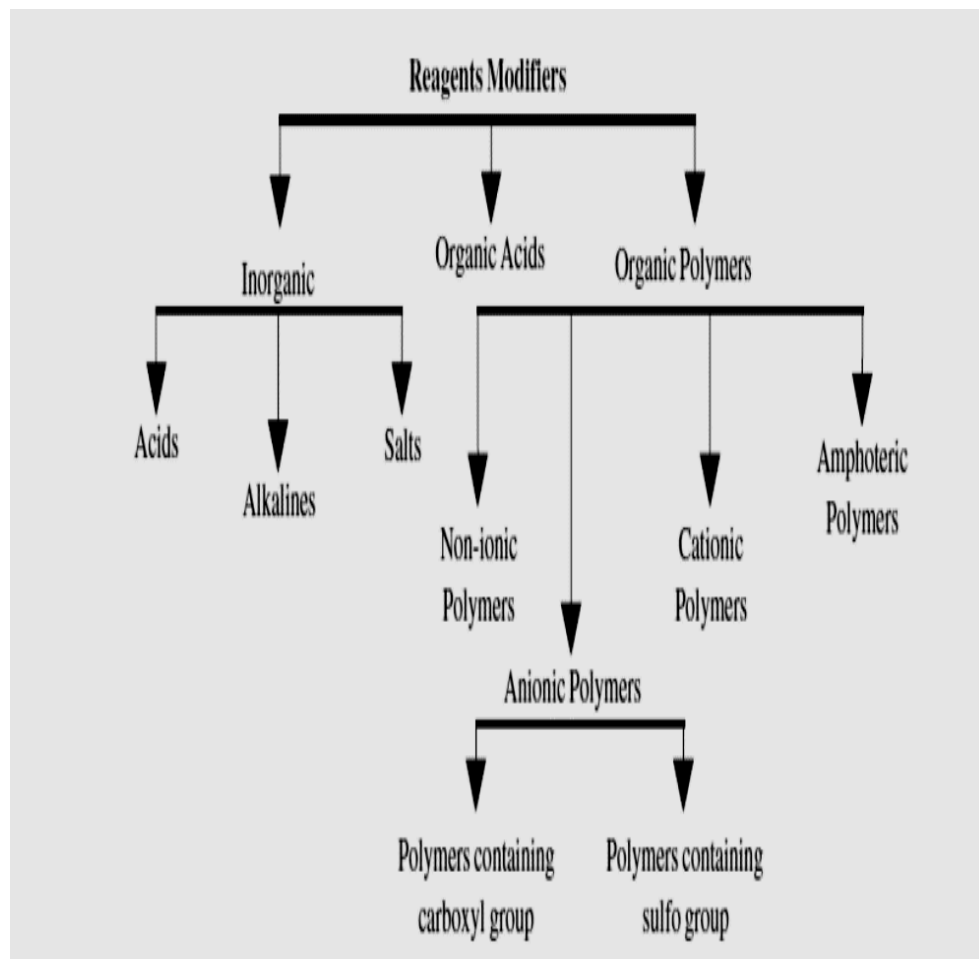
Figure 2.6. Classification of modifying reagents on basis of type[37].

2.1.4.4. Activators. Activators are chemicals that facilitate the adsorption of collectors on mineral surfaces . These are generally salts which dissociate in water to form ions. Sodium sulfate, lead nitrate, copper sulfate and hydrogen sulfate are amongst widely used activators[34].PH modifiers like lime and sulfuric acid can also be regarded

as activators ,as change in pH caused by these ensure selective adsorption of collector[38].

  2.1.4.5. Depressants. Depressants render minerals hydrophilic, thus retarding their flotation. There are many types of depressants and phenomenon associated with these is varied and complicated. Depressants can however be generally classified into inorganic and organic depressants. Inorganic depressants are extremely useful when two are more minerals in the pulp have same floatability. Amongst the most widely used inorganic depressants are lime and cyanide ions. Sodium silicate, permanganates, ferro cyanide and sulfur dioxide are some examples of the inorganic depressants. Organic depressants are the ones with molecular weights higher than 10,000.The depressing mechanism of organic depressants is not clear. Polysaccharides, polyethers and polyphenols are some examples of organic depressants[9], [38]. Slime coatings are considered as natural depressants. Slime coating occurs when colloidal mineral matter form a coat on the surface of the mineral and hence inhibit the adsorption of collectors that results in decreasing the flotation recovery and deteriorating the quality of the concentrate products.

  2.1.5. Equipment in Flotation. Mechanical and column flotation cells are the two most widely used machines to carry out froth flotation in mineral industry. In column flotation cells, the flotation feed has a counter current contact with air bubbles. Hydrophobic feed particles move down under the action of gravity colloid with the air bubbles that move in upward direction. Hydrophilic particles on the other hand follow the downward motion under gravity. This way separation takes place on basis of surface properties of minerals. The froth zone consists of an approximately 1 m froth bed. Wash

water is distributed over the top of the froth to ensures the production of high grade concentrates by washing away any entrained gangue particles (Figure 2.7) [38][31], [39], [40].
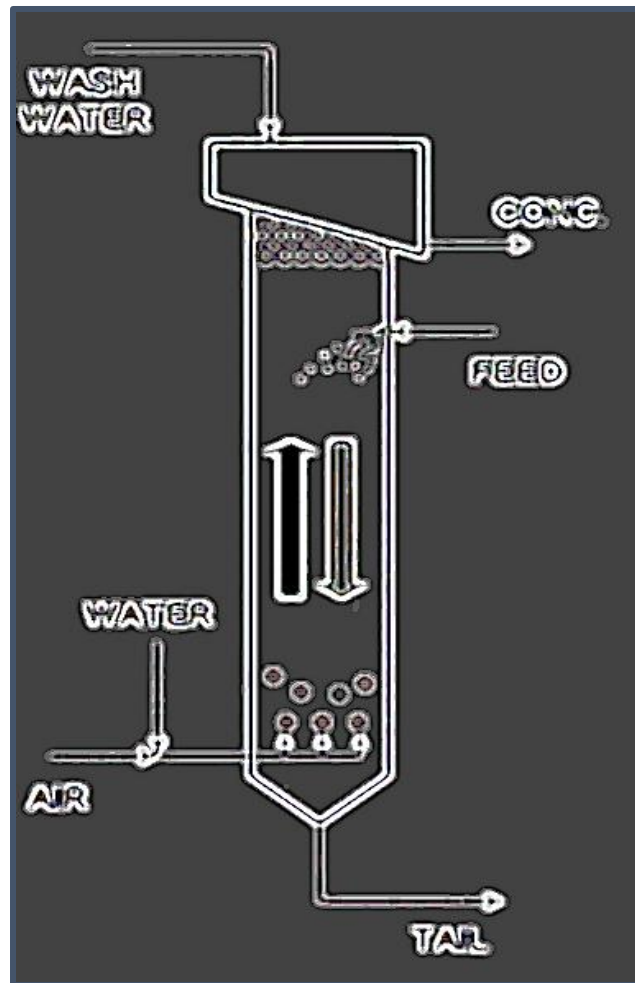
Figure 2.7. Column flotation cell [40].

Opposed to column flotation cells, mechanical flotation cells have a mechanically driven impeller which disperses the slurry and breaks the incoming air into bubbles. Due to the intense agitation of slurry in mechanical cells, the probability of entrainment and transportation of gangue particles to the concentrate is high. Thus mechanical flotation

cells may achieve higher recovery than column flotation cells but usually have lower

quality concentrates[41][9].A typical Denver flotation cell is shown in Figure 2.8.
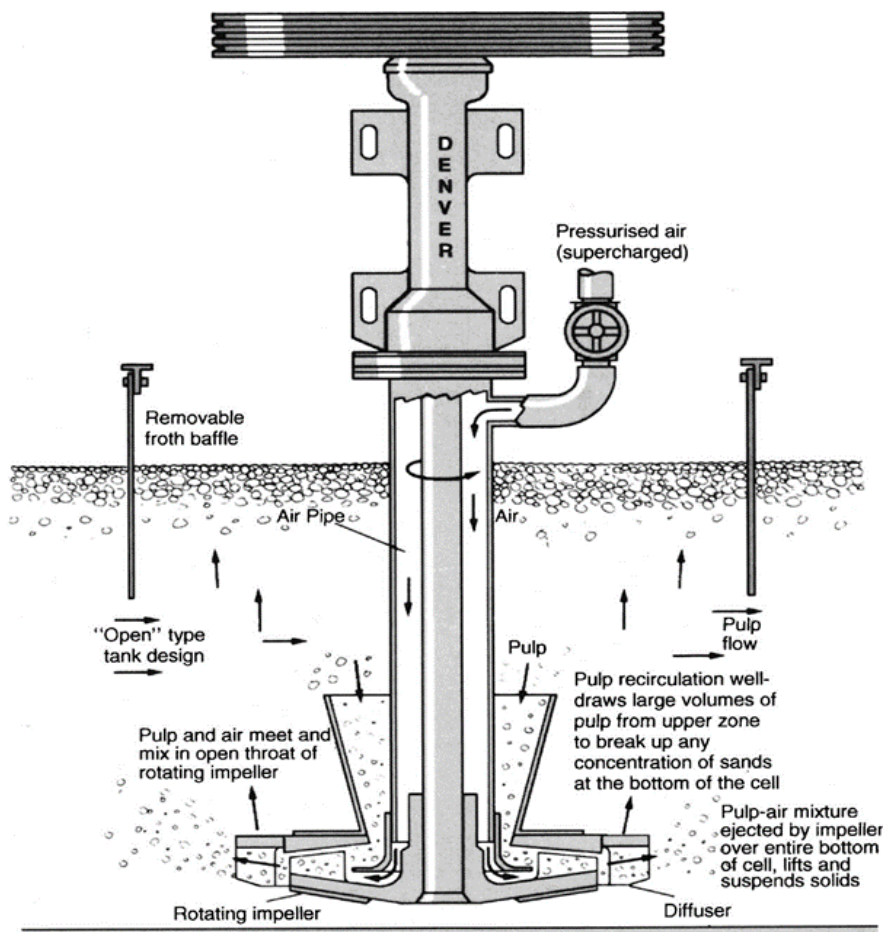
Figure 2.8. Schematic diagram of a typical Denver D-R flotation cell [9].

2.2. SULFIDE MINERAL FLOTATION

Flotation has exclusive success in treating complex sulfide ores. It is therefore

regarded as the source of 95 percent base metals in the world. Sulfides are the largest

group of minerals which are treated by flotation[42]. Complex sulfide ores from run-of-

mine contain chalcopyrite, galena, sphalerite and pyrite as the main valuable minerals which are the most important sources of copper, iron, lead and zinc metals. Processing of such complex ores is of vital importance[7].Sequential and bulk flotation of sulfide ores is carried out to process sulfide ores. Different minerals are processed at different stages when carrying out sequential flotation. Bulk flotation on the other hand requires flotation of copper and lead minerals together in one step, while depressing the zinc and iron minerals. This is followed by the activation and consequent flotation of zinc minerals. Bulk concentrate of copper and lead is then processed at later stages to separate copper from zinc [9].

For sulfide minerals, xanthates are the most extensively used collectors. The xanthates are however not selective and can get adsorbed on different types of sulfides which is one of the drawback in application of these chemicals. This problem is solved by adding modifiers to enhance the selectivity of these collectors[43]. Two major groups of sulfide mineral collectors are shown in Figure 2.9. Thionocarbamates, thiourea, derivatives of phosphoric acid, glyoxalidine, mercapto-benzo-thiazoles and aminothiophenols are amongst the most important collectors for sulfide minerals[43]. Sodium and potassium Iso propyl xanthate, Potassium amyl xanthate, ditiophosphate are commonly used frothers in sulfide mineral flotation[44][45].

In sulfide mineral processing, MIBC, DOW 250, pine oil and glycol are the most commonly used frother [35][36].

Modifying reagents affect the adsorption of collector on sulfide mineral surfaces in different ways under different conditions. For example, $CuSO_4$ acts as an activator for the flotation of sphalerite. It coats the sphalerite surface with copper which enhances the
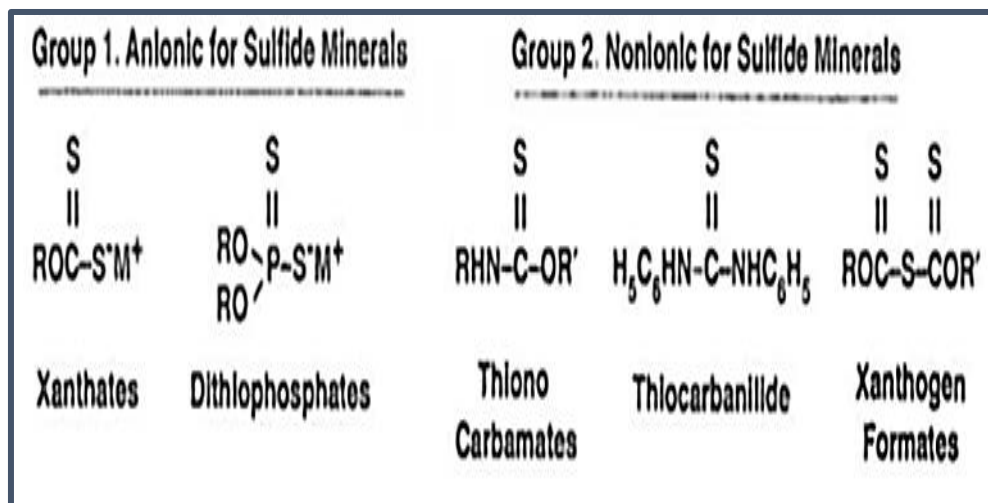
Figure 2.9. Collectors in sulfide minerals [33].

adsorption of collector on the sphalerite surface, thus enhancing its floatability. On the other hand, sodium cyanide which is a depressant for sphalerite, dissolves copper from the sphalerite surface. This inhibits the adsorption of collector on sphalerite surface to make it less floatable.. In certain cases modifying reagents act as collector scrubbers. In such instances, modifying reagents remove the coatings of collector from certain minerals making these minerals unable to float. In sulfide mineral processing, Sodium sulfide depresses the flotation of galena and sphalerite by this phenomenon. Some modifying reagents have the ability to make the surface of minerals hydrophilic by adsorbing onto the surfaces of these minerals. Modification of the pulp's pH is another popular way to control the floatability of various minerals. This can be understood by the non-floatability of pyrite under alkaline conditions, however at neutral or acidic PH, pyrite becomes floatable[37]. Starch, soda ash, NaCN, Lime, $ZnSO_4$, Na_2SiO_3 and dextrin are some of the most common modifying reagents used in sulfide mineral flotation[37].

2.3. OPTIMIZATION OF SULFIDE MINERAL FLOTATION

Sulfide mineral flotation is a complex and an expensive process involving various reagents with a number of different variables involved. Optimization of all those important variables is of utmost importance for designing an efficient and economical floatation set up. With flotation of such complex sulfide, it's important to obtain the optimum conditions and characteristics which will yield the desired output. Response surface methodology (RSM) is an excellent alternative to the factorial design especially when a quadratic effect is expected for a factor, as a higher number of experiments would be required with higher level factorial design required in the aforementioned situation. Response surface methodology (RSM) can be used for analyzing a problem in which the relationship between the response variable (dependent variable) and all the influencing variables for that outcome is unknown with the objective being the optimization of the response variable [46], [47]. RSM starts with finding a proper approximation function, a low or a high order polynomial, to define the relationship between the response and the independent variables. Due to the ease in parameter estimation and flexibility in application, second-order polynomial models are widely used in RSM [48]. In general, central composite design (CCD), Box − Behnken design (BBD) and Doehlert designs are the most common methods in RSM.

RSM has been employed by different researchers for experimental design and optimization of the independent variables. Martinez et al. [49] used factorial experimental design methodology for designing the floatation tests for evaluating the effect of the three important variables on the grade and recovery of celestite and obtained the optimum value for each variable. Obeng et al. [50] used the central composite design for designing

the experimental set up for evaluating the effect of four different independent variables on the three-product cyclone performance. Kalyani et al. [51] used the response surface methodology to obtain the optimum values for the three involved independent variables in the process of coal flotation. Aslan and Fidan [52] used Box – Behnken combined with response surface methodology for evaluating and optimizing the three most important variables involved in lead floatation. The variables studied were potassium amyl xanthate (KAX) as a collector, sodium sulfide (Na$_2$S) and pH .Aslan et al. [53] used response surface methodology for optimizing the four process variables (kerosene dosage, sodium silicate dosage, agitation speed and scrubbing time) in graphite concentrate production with central composite design used for designing the experimental layout. Mehrabani et al. [54] used response surface methodology for optimizing the three control variables (activator (CuSO$_4$) dosage, collector (potassium amyl xanthate (PAX)) dosage and pH) to maximize the separation efficiency in zinc – lead flotation. Central composite design (CCD) is the most popular RSM method and is widely used for experimental design and optimization work [46], [55]. Box – Behnken design (BBD) is however slightly more efficient than central composite design [56].

2.4. APPLICATION OF BIODEGRADABLE POLYMERS IN SULFIDE MINERAL FLOTATION

Sulfide mineral flotation utilizes a variety of chemical reagents to achieve efficient separation of different minerals. Some of these reagents bring harmful impacts to the environment because of the toxic nature of these reagents [57]. Among these toxic reagents, cyanide is regarded as the most toxic one. Cyanide in form of sodium cyanide is used in sulfide mineral flotation to depress ferro and zinc containing sulfide minerals.

This ability of cyanide was discovered in the nineteenth century and since that time it has been used as one of the main reagents in sulfide mineral flotation [58][59][60][61]. Due to recent advances in polymer field, a number of polymers have been discovered which are very adoptable and can be cheaply prepared [59].Owing to this advancement, polymers have been tried to replace harmful reagents in sulfide mineral flotation. Among other polymers, polyacrylamide-based polymers are the most extensively employed in sulfide mineral flotation as multifunctional reagents. Different functional groups can be attached to Polyacrylamide polymers. This gives these polymers a unique capability to be used as collectors, depressants, activators, or modifiers. Polyacrylamide polymers (PAMs) with different functional groups have been successfully used to depress ferrous sulfide minerals in sulfide mineral flotation and ash minerals in coal flotation [62][58]. Another promising polymer Chitosan has recently been successfully tested as a depressant for ferro minerals in simulated sulfide mineral flotation. Chitosan has a lot of positive aspects which indicate it's broader application in future mineral processing systems. It is abundant, biodegradable, and bio compatible, while conventional depressants for ferro minerals (NaCN) is highly toxic [63][64][65][66]. The structure of Chitosan polymer is shown in Figure 2.10.

2.5. FROTH STABILITY AND ITS MEASUREMENT

Extensive research work has been done to study the flotation pulp while froth layer has not been investigated as thoroughly. During last two decades, froth structure and stability has attracted more attention due to its critical role in achieving the desired mineral grade and recovery[11]. Both the mobility and stability of froth zone contribute
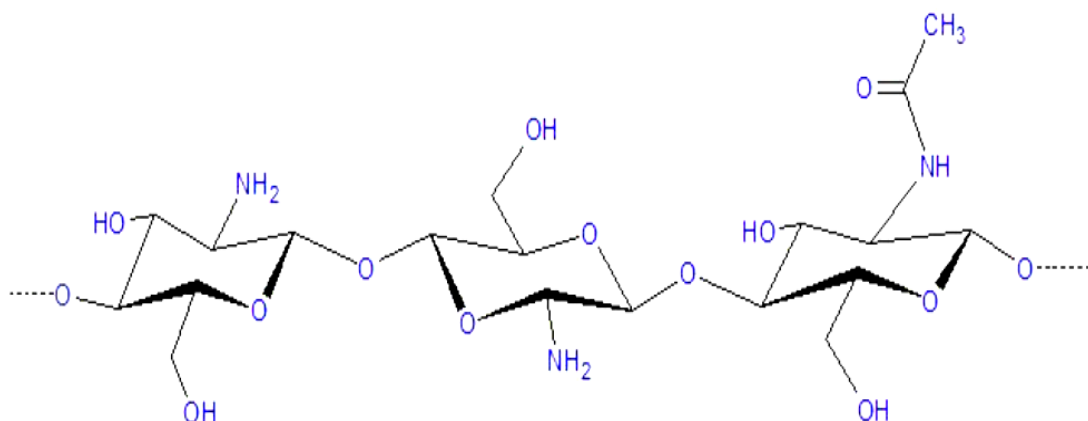
Figure 2.10. Structure of Chitosan Polymer[67].

to the overall outcome of any flotation process. The mobility of the froth can be described

as the froth's ability to move from the flotation cell into the launder, whilst stability of

the froth phase is the time of the froth's persistence or the froth's ability to resist bubble

rupture and coalescence[32] .Froth stability is of crucial importance as it affects both the

grade and recovery of the concentrate. By increasing the stability of the froth, the

recovery also increases but the selectivity and thus the grade of the froth decreases due to

the recovery of gangue material. Conversely, if the froth is unstable the overall

concentrate recoveries will decrease, but this may enhance the grade[68], [69][70].

Acquiring the correct stability of the froth is therefore of paramount importance[17].

The bubbles in the froth phase are separated by thin films. Three of these films

combine together at 120 degree to form a plateau border. Four of these plateau borders

form a vertex. Plateau borders in the froth phase make a branched network of channels as

shown in Figure 2.11 [11][71]. Bubbles transform shape from sphere to angular as it

moves up the froth. The liquid content also drops with the height of the froth[72].

2.5.1. Factors Affecting Froth Stability. Froth stability is effected by a number of factors. A deep understanding of influence of these factors upon froth stability can lead to controlling froth stability and hence flotation performance. Some of the
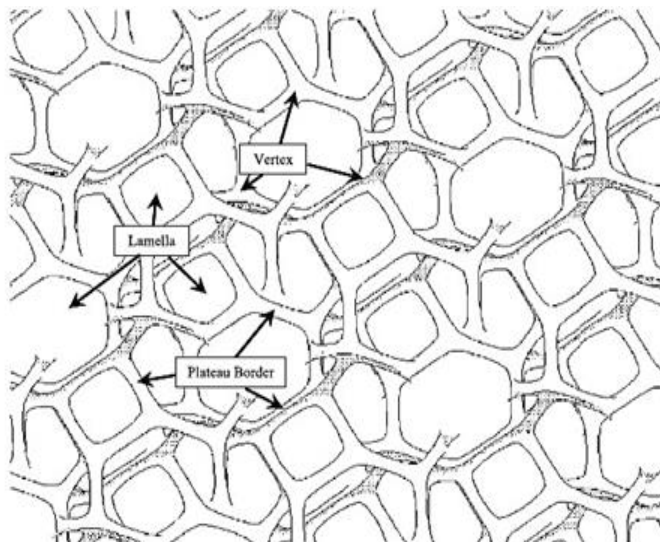
Figure 2.11. Branched network of channels in the froth [11].

major factors influencing froth stability include the type and the concentration of the frother, the nature and the concentration of the particles, the size of the particles, the shape of the particles, the conditioning time of the flotation feed, the temperature, the air rate and the salt concentration [73].

2.5.1.1. Frother type. It has been observed that frother of higher molecular weights tend to produce more viscous and stable froths. It can be seen from Figure 2.12 that the retention time of the froth and hence its stability depends upon the type of frother used. It is clear from Figure 2.12 that frothers of intermediate molecular weight (Poly

Propylene Glycol (PPG) 400 and PPG 725) produced more stable froth as compared to

lower(PPG 192 and MIBC) and higher (PPG 1000) molecular weight frothers [74].

Frother's structure also plays an important role in respect of froth stability., Frothers with

polyglycol structures tend to produce stable froths as compared to alcohol based frothers

[75], [76].It is therefore important to consider the appropriate type of the frother to be

used while designing a froth flotation operation.
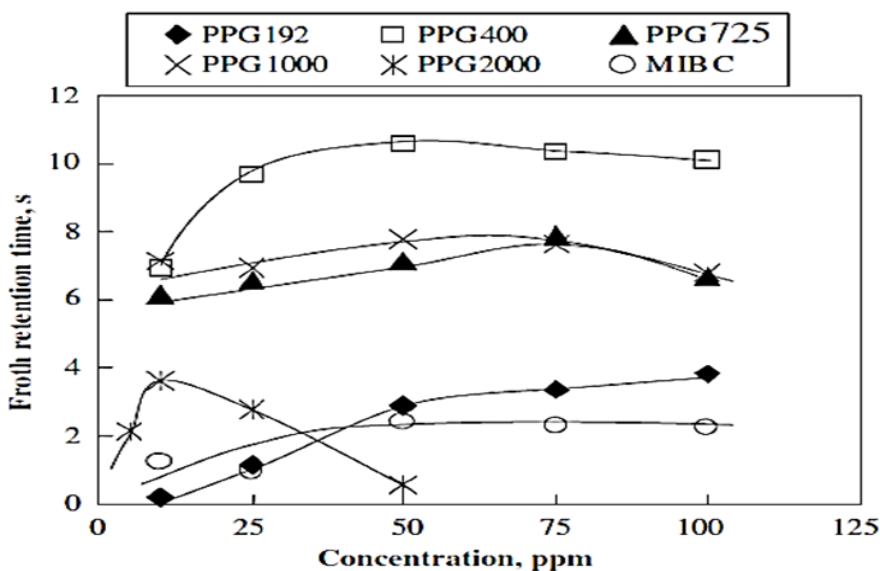
Figure 2.12. Effect of frother type on froth retention time[77].

2.5.1.2. Frother concentration. Frother concentration controls size of the

bubbles by controlling the coalescence of the bubbles. As frother concentration is

increased, bubble coalescence decreases. This decrease in bubble coalescence increases

the froth stability. The bubble coalescence is totally prevented at a particular

concentration. This concentration is known as Critical Coalescence Concentration

34

(CCC).Increase in frother concentration above this critical concentration loses its effect

on bubble size and hence froth stability (Figure 2.13). It is therefore recommended to use

other parameters like sparger design and shape to control any further froth stability once

frother reaches this concentration. Frother is believed to decrease the bubble size as it

reduces the surface tension induced by the addition of surfactants. An icrease in frother

concentration thus decreases bubble size [78].
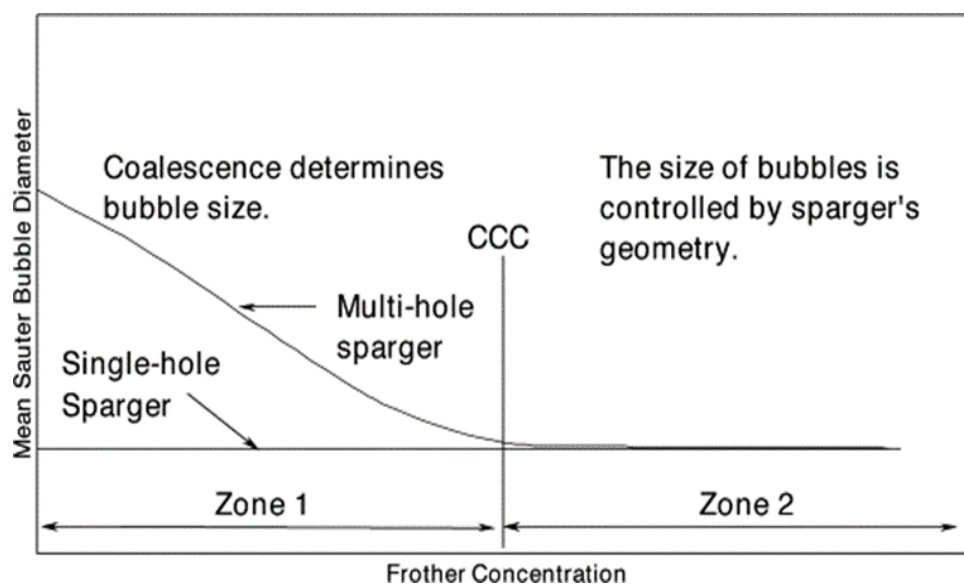
Figure 2.13. Effect of frother concentration on bubble coalescence[78].

2.5.1.3. Size and shape of the particle. Froth stability has been reported to be

influenced by the particle size. During investigation on Platinum Group Metal (PGM)

ore, froth stability was found to increase as particle size decreased (Figure 2.14) [79].

Another study using silica particles also reported more stable froths in case of finer silica

particles. Ability of finer particles to yield stable froths is attributed to the capillary

mechanism of these particles owing to the smaller size of these as compared to the film thickness. In case of coarse particles, a decrease in froth stability is caused by rupturing of the foam films due to the large size of these particles [80].

In addition to particle size, particle shape is also important in determining the stability of froth. Investigations reveal that rounded particles take 0.08 more seconds to rupture the foam film as compared to the sharp edged particles. This property lets round particles to produce more stable froths as compared to flat or sharp edged particles [79], [80].
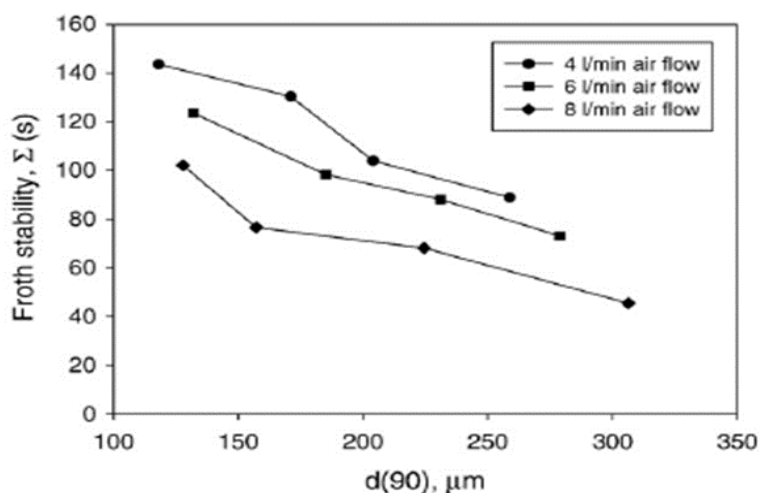
Figure 2.14. Effect of particle size on froth stability[79].

2.5.1.4. Concentration of the particles. Concentration of the particles in conjunction with hydrophobicity and particle size effects froth stability in a positive manner. In a fundamental study carried out with silica particles, when silica particle concentration increased from 0 to 10 % , the froth stability increased by increasing the

bubble life time and hydrated thickness[81]. Another investigation on silica particles have also reported an increase in froth stability with the increase in particle concentration [81]. This increase in foam stability can be explained by the decrease in the film drainage at higher particle concentration [82], [83].

  2.5.1.5. Conditioning time of feed particles. Dynamic froth stability is affected by the conditioning time of the particles. An inverse relationship has been observed between froth stability and conditioning time. During a study carried on platinum ore, considerable decrease in dynamic froth stability was observed as the conditioning time was increased (Figure 2.15).
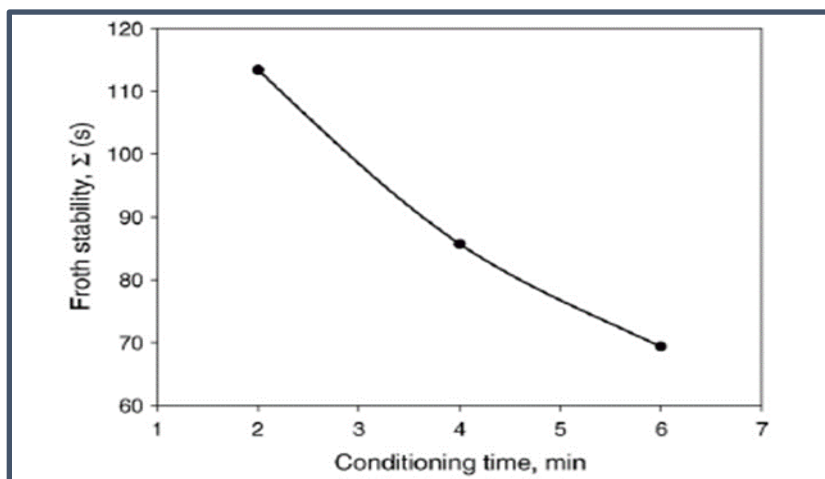
Figure 2.15. Relationship between conditioning time and froth dynamic froth stability[79].

  As conditioning time is increased, collector adsorption on mineral surface also increases. This results in an increase in the hydrophobicity of the particles above the critical values which destabilizes the froth [79], [80].

2.5.1.6. Salt concentration and temperature. Salt concentration and temperature are also prominently found to affect froth stability. As temperature of solution increases, froth stability decreases. On the other hand an increase in salt concentration increases froth stability[73].

2.5.2. Froth Stability Assessment. Different methods can be used to assess the stability of the froth layer. Water recovery and the change in the froth appearance are used as indicators of froth stability. The methods of water recovery and bubble burst rate in combination are proven to give the best estimate of froth stability[17]. Some of the popular methods for froth stability assessment are given below

2.5.2.1. Froth maximum height at equilibrium. It is one of the most widely used technique for measuring froth stability [84][85]. As air is introduced in the cell, the froth starts growing. Pictures are taken during the froth growth until it reaches a maximum equilibrium height depending upon its stability. The froth maximum height at equilibrium is measured directly. The higher the value of maximum height at equilibrium, the more stable is the froth and vice versa [80], [86] .

2.5.2.2. Froth growth velocity. Froth growth velocity is an important parameter to quantify froth stability [87]. It is measured by recording the time the froth takes in reaching maximum equilibrium height. Higher velocity indicates more stable froth [80], [86].

2.5.2.3. Dynamic froth stability factor. Dynamic froth stability factor will be calculated using the following Equation 4:

$$\sum = \frac{V_f}{Q} = \frac{H_{max}A}{Q_1} \tag{4}$$

Where Σ = dynamic froth stability, V_f = foam volume, H_{max} =total foam height, Q = gas volumetric flow rate, A is cross sectional area of the cell[73], [80], [86]. A stable froth tends to have a higher dynamic froth stability factor. In general, the recovery of the minerals increases with the increase in the stability of the froth.

2.5.2.4. Air recovery. Air recovery is the fraction of air which flows over the top of flotation cell lip in form of unburst bubbles[88][89]. It can be calculated by Equation 5 [80], [90].

$$\alpha = \frac{Q_{air\ concentrate}}{Q_{airpulp}} \tag{5}$$

Where α is air recovery, Q_{air} concentrate is air flow rate in the concentrate and Q_{air} pulp is air flow rate entering cell. Larger value of air recovery indicates stable froth and vice versa.

2.5.2.5. Bubble burst rate. Video footage of the top of the froth is recorded to measure the top-of-froth bubble burst rate. More bursting events indicate unstable froth [91][92][80][93].

In the course of this study dynamic froth stability was used as the measure of froth stability in different flotation tests carried out. Froth growth velocity, air recovery, froth maximum height were also measured but are not included in this dissertation.

2.6. NANO MATERIALS FOR FROTH STABILITY

Froth stability can be achieved by selecting the optimum flotation process variables. Frothing agents are also widely used to stabilize the froth. In addition to these techniques small solid particles can also provide stability to froth due to their attachment with planar or curved liquid interfaces. The main factors effecting froth stability with respect to feed particles are concentration, shape, hydrophobicity and size [94]. Different researchers have found that as percentage of solids in froth increase, rate of detachment in the froth phase is decreased and vice versa [95].Results from the study conducted by R. M. Rahman,et.al [96] show that particle size strongly effects froth recovery. Fine particles tend to enhance froth recoveries while the coarse particles have more probability of detachment from the froth zone. The role of flotation reagents has also been studied since it has a major effect on the surface chemistry of different components of the froth layer. Colloidal particles, for example, are found to stabilize air bubbles. These colloidal particles can thus be used as froth stabilizer in the flotation process [97]. Starch particles are also found to improve froth stability by reducing film drainage and increasing viscosity of foaming solution as reported by [98]. In a recent study an increase in the recovery of barite was achieved by utilizing nanosized Fe_2O_3 and Al_2O_3 at deep froths [19]. It has also been reported that nano particle are expected to considerably improve the performance of the column flotation cells [19]. Flotation experiments on ultramafic nickel ores and glass beads have demonstrated that conventional water-soluble molecular collectors could be partially or completely replaced by colloidal hydrophobic nanoparticle flotation collectors. For a good recoveryof beads polystyrene nanoparticles can be more effective than

conventional molecular collector requires [99][100]. Frother blends with combinations of alcohol and propylene glycols have been reported to increase froth stability and grade and recovery of the flotation process[101]. All of the previous studies were performed on model systems that consist of either a single pure mineral or artificially mixed pure minerals. Therefore, this study investigated the effect of nanoparticle addition on the processing of real complex sulfide ore.

2.7. SULFIDE MINERAL FLOTATION IN SEA WATER

One of the major challenges facing mineral processing operations in general and froth flotation process in particular is water supply. The availability of water is a long-term concern for most mining operations. "The water required to operate a flotation plant may outweigh all of the other uses of water at a mine site, and the need to maintain a water balance is critical for the plant to operate efficiently"[16] . At US mines, plant water can be re used to save fresh water resources. However, water reuse results in increased salinity in site water ponds, which is largely driven by evaporation and ongoing salt inputs from soil, minerals and groundwater [102]. The use of waste or sea water containing inorganic electrolytes can save the fresh water resources from being used [103] [104].Improved bubble stability has been reported by several researchers in flotation in saline conditions. Inorganic salts help in stabilizing bubbles by decreasing coalescence. These salts also increase the ability of frother to reduce the surface tension of solutions hence stabilizing the froth [105]. Frothers can also be replaced by inorganic electrolytes such as NaCl [103], [104]. Keeping this in mind, there is a possibility to effectively use waste water treated by inorganic electrolytes for the flotation of minerals.

Ejtemal, et.al concluded that copper uptake by sphalerite decreases in the presence of calcium and magnesium ions [106]. This finding suggests to remove these ions to enhance copper activation of sphalerite. Moimane et.al conducted study on PGM-bearing ore from the Merensky reef [107]. Results indicated that as the ionic strength of the plant water increased, the recoveries of PGM increased and the effect on decreasing the concentrate grade was minimal. Therefore, it was concluded that the practice of water recycle and reuse should not impose any adverse impact during beneficiation of the tested ore. A similar study needs to be conducted on complex ores such as sulfide ores to test the flotation efficiency when sea water. Optimum reagent concentrations especially the frothers and collectors can be determined, thus saving cost of reagents and helping in maintaining a clean environment.

2.8. CFD SIMULATION OF FROTH

As bubble coalescence and bursting rate determines the stability of the froth and hence the flotation performance, prediction of coalescence and bursting is highly desirable but is very complex, and limited success has been had in this regard [72]. Recently an electro-resistivity technique have been developed for measuring a proxy for froth bubble sizes as a function of height above the pulp–froth interface which can be used in combination with the photographic techniques. Empirical observations have been made in the past to optimize the flotation process and enhance the stability of the froth. Reagents including frothers, collectors and depressants are varied to find the optimum dosages. Various flotation tank designs have been tried to find the best option. This approach however is costly and time consuming; hence a CFD-model approach will

be very cost effective in designing froth flotation process. Combining the pulp and froth models into a single simulation is long desirable. However achieving this is very challenging due to complex mass transfer across the pulp froth interface [108][72]. Eulerian–Eulerian approach has been used recently in a CFD model to study the solid concentration on froth stability.Good agreement was found between experimental and simulation results regarding the effect of solid concentration on gas hold-up and axial pressure profile [109]. The model however lacks simulating the froth zone. Froth phase transportation model was developed, comprising different types of cumulative air recovery functions with best fit to the measured surface velocity distribution in coal flotation. It was found that coal laden froth can be described in a convincing manner through the cumulative air recovery function expressed in power-law form. Detachment of particle from bubble is a key parameter which can be understood better with increase in knowledge pertaining to contact line motion. Computer simulations can significantly help in understanding this dynamic parameter [95], [110].

2.9. APPLICATION OF ARTIFICIAL INTELLIGENCE AND MACHINE LEARNING IN FROTH FLOTATION

Mineral deposits are gradually depleting, mines are becoming deeper and ore grades are becoming lower every day. On the other hand demand for minerals is increasing day by day due to increase in population and the advancement of technology. This increasing gap between supply and demand can only be met by cost effective and high productivity plants. It is therefore a dire need to increase the efficiency and production rate of the mineral processing plants which can be sustainable for a long time in future. The only answer to this challenge is to develop automatic control systems

which are free from human inefficiencies and should give peak performance round the clock in a systematic way [12]. Artificial intelligence and machine learning models are therefore of utmost importance for the sustainability of mineral processing industry. There are few people who have worked in implementing AI and ML models to identify the micro-processes that affect the coal flotation process. Multi-layered artificial neural network have been tried for predicting ash reduction in coal [111]. In phosphate flotation process, a multilayer feed forward neural network has been successfully used to predict the effect of different operational variables on the recovery and grade of siliceous phosphate [112]. Interface level in column flotation cell has been controlled through AI modelling [113]. Artificial Neural Network (ANN) has also found application in performance prediction of sulfide ores containing copper and molybdenum [114]. Controllers based on fuzzy logic model have been implemented to control a copper flotation plant [115]. ANN has also been utilized for predicting the metallurgical performance of iron ore flotation plant. Mamdani Fuzzy logic (MFL) model has been reported to satisfactorily predict iron and copper recoveries. Operational method, bacteria type and time were used as input for the model [116]. Another study used multi layered ANN for developing predict models for grade and recovery of copper and molybdenum. Collector dosage, frother dosage, F-oil dosage, pH of pulp, particle size, moisture content, solid percentage, and copper, molybdenum and iron grade in feed were used as the input parameters to predict the metallurgical performance [117]. Owing to the previous success of AI and ML models implementation in flotation process, this study is tasked to implement five different AI and ML models for modelling of complex sulfide ore flotation.

3. PROCESS OPTIMIZATION AND MODELING OF COMPLEX SULFIDE ORE FLOTATION USING RESPONSE SURFACE METHODOLOGY

3.1. BACKGROUND

Froth flotation is a widely used ore beneficiation method for the processing of mineral ores. It is a complex and an expensive process involving the application of various task-specific reagents. In addition to these reagents, operational parameters such as airflow rate, agitation, feed flow rate, pulp density, etc. are also involved and can largely influence the process efficiency. Optimization of all those important chemical and operational variables is of utmost importance for designing an efficient and economical floatation set up.

Response surface methodology (RSM) can be used to analyze problems where the relationship between the response variables (dependent variables) and all the influencing variables for that outcome is unknown with the objective being the optimization of the response variable [46], [47]. RSM starts with finding a proper approximation function, a low or a high order polynomial, to define the relationship between the response and the independent variables. Due to the ease in parameter estimation and flexibility in application, second-order polynomial models are widely used in RSM [48]. In general, central composite design (CCD), Box – Behnken design (BBD) and Doehlert designs are the most common methods in RSM. RSM has been employed by different researchers for experimental design and optimization of the independent variables in froth flotation. Kalyani et al. [51] used the response surface methodology to obtain the optimum values for the collector dosage, frother dosage and pulp density in the process of coal flotation. Aslan and Fidan [52] used Box – Behnken combining with response surface methodology

for evaluating and optimizing the dosage of potassium amyl xanthate, sodium sulfide dosage and pH in lead flotation. Central Composite Design (CCD) is the most popular RSM method and is widely used for experimental design and optimization work [46], [55] despite that the Box – Behnken design (BBD) is slightly more efficient than central composite design [56] This is explained by the equations that calculate the number of experiments for both designs. The BBD generates less number of experiments given by $N=k^2+k+c_p$ while in CCD the number of experiments is given by $N= k^k + 2k +c_p$ where k is the number of variables and c_p is the number of central points [52], [56].

In this work, three-level Box-Behnken design in combination with the response surface methodology (RSM) has been employed to develop a functional relationship between the seven independent process variables and the metallurgical performance of complex sulfide ore of Missisipi Valley type ore containing chalcopyrite, galena and sphalerite as the main valuable minerals with pyrite and dolomite being the main gangue mineral. No laboratory data is available on the optimization and modeling of process variables of froth flotation related to sulfide ore used in this study .The seven operational control parameters investigated in this study includes the collector (sodium isopropyl xanthate) dosage, frother (MIBC) dosage, impeller speed, air rate, pyrite depressant (NaCN) dosage, sphalerite depressant ($ZnSO_4$) dosage & flotation time. Quadratic mathematical models were derived for the prediction of the recoveries of Pb, Cu, Zn & Fe as well as the grade of the concentrate products with respect to these metals. These models were used thereafter to find the optimum operational parameters to achieve the desired flotation results.

3.2. METHODOLOGY AND MATERIALS

Details of materials and methods used in this study are given below. All lab scale equipment were provided by Missouri University of Science and technology, USA.

3.2.1. Materials. Complex sulfide ore samples of Mississippi Valley-type were obtained from a mine located in North America. This ore was characterized using various techniques as shown in the following sections. In order to adjust pH of the flotation pulp, hydrochloric acid and sodium hydroxide were used. Sodium isopropyl xanthate, sodium cyanide and zinc sulfate were used as a collector, a pyrite depressant and a sphalerite depressant, respectively. Fisher Scientific, USA was the provider of all these reagents. The 4-Methyl-2-pentanol (MIBC) which was used as frother was obtained from ACROS, USA Inc. All flotation reagents were used without further purification. All flotation tests were conducted using tap water.

3.2.2. Preparation of the Flotation Feed. Run of mine ore was crushed in two stages. During primary stage, laboratory scale jaw crusher was used to crush the large samples of ore. Cone crusher was used as a secondary crusher to further reduce the ore size. Homogenized samples from crushed ore were taken using coning and quartering sampling method. These samples were stored in airtight bags at a temperature of -10 ^{0}C to avoid oxidation. Prior to the flotation experiment, feed samples were taken out of the refrigerator and dry ground for ~20 minutes in a batch rod mill of 20.16 cm diameter and 24.5 cm length. A total of 21 steel rods were used as the grinding media.

3.2.3. Characterization of Flotation Feed. Feed was characterized in detail. Particle size distribution and composition of feed is discussed in detail.

3.2.3.1. Particle size distribution. In order to determine the particle size distribution of the feed, screens of 200, 230, 270, 325, and 400 US mesh were used. Sieving process was performed as per the protocols defined by the American Society for Testing and Materials (ASTM) protocols.The composite particle size distribution as determined by sieve analysis is shown in Figure 3.1. The 80 % passing size (P_{80}) of the flotation feed was approximately 58 microns.
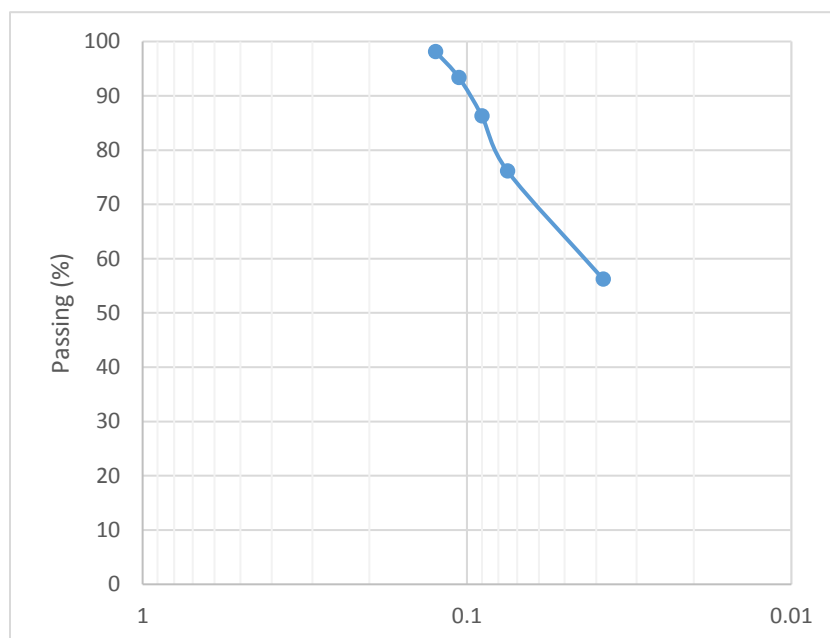
Figure 3.1. Particle size distribution of the flotation feed.

3.2.3.2. Mineralogical composition of feed. The Mineralogical composition of the feed was determined by Mineral Liberation Analysis (MLA). MLA analysis was carried out at the Center for Advanced Mineral & Metallurgical Processing (CAMP) in Montana Tech of the University of Montana, USA. Figure 3.2 shows the mineralogical composition as determined through the MLA analysis.
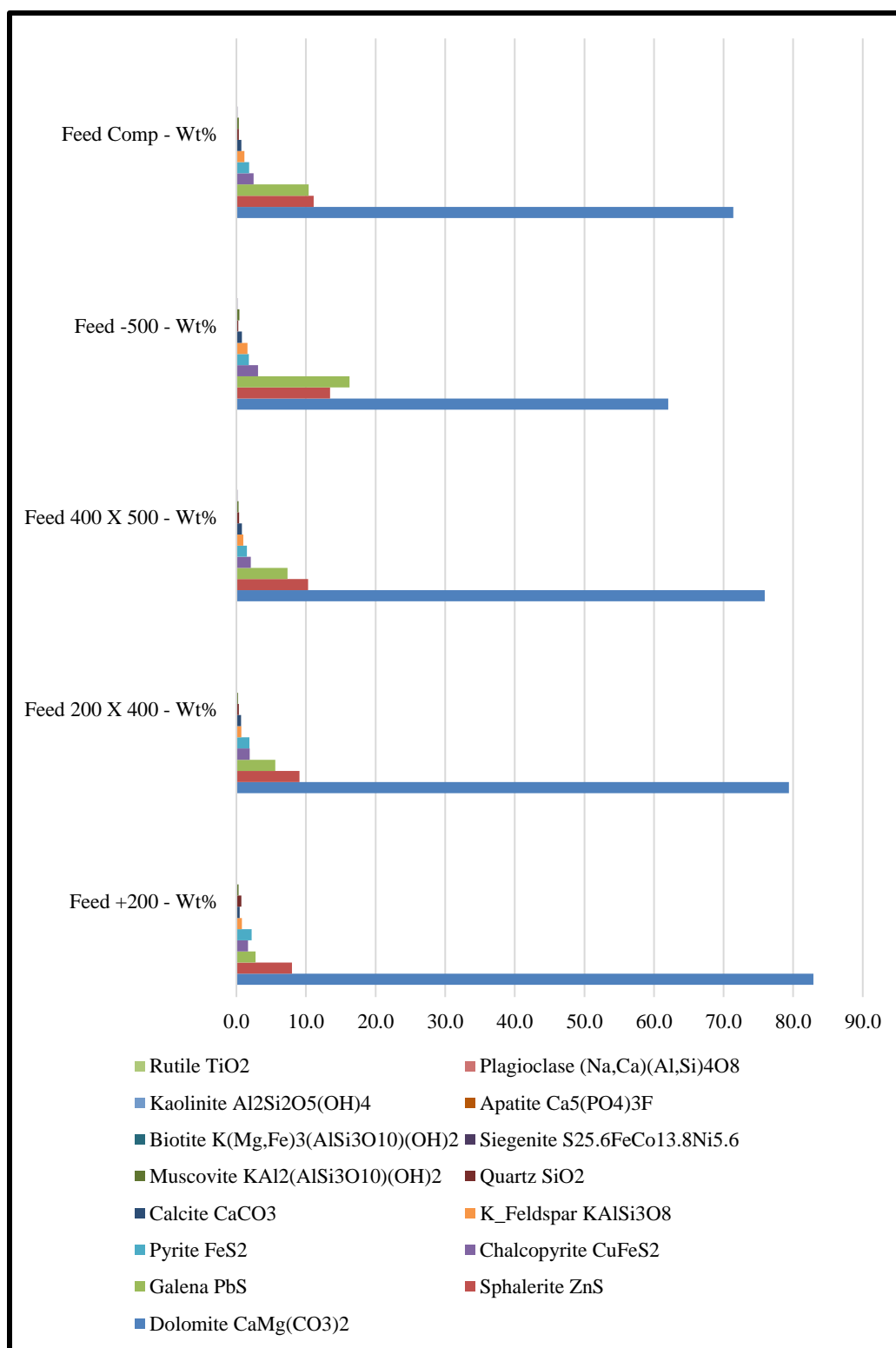
Figure 3.2. Mineralogical Composition of feed.

Valuable sulfide minerals constitute around 15-20 % of the feed, while up to 70 to 80 % of the feed consists of gangue minerals mainly dolomite, in addition to pyrite, quartz, muscovite and K-Feldspar .

3.2.3.3. Elemental analysis of feed. The total concentration of each element (Cu, Pb, Zn and Fe) was analyzed using Inductively Coupled Plasma Optical Emission Spectrometer ICP-AES (Thermo Fisher ICP/OES iCAP6000 series) after a complete sample dissolution by mixed acid digestion (HCl and HNO_3). Samples which assayed greater than 30% of Pb were titrated by EDTA titration as atomic adsorption spectroscopy was not possible at such high percentage of Pb. During EDTA titration lead in the feed sample was converted to lead sulfate, which was then dissolved in ammonium acetate and titrated with EDTA, using Xylenol Orange as an internal indicator. Samples were titrated until a bright yellow, permanent color appeared. Results of elemental analysis yielded feed to contain 5.0 % Pb, 4.3 % Zn, 0.88 % Cu and 2.3% Fe.

3.2.4. Batch Fotation Experiments. Bulk flotation of galena and chalcopyrite was carried out in a Denver flotation cell with an impeller diameter of 3.88 inches and a 1-liter flotation tank. In all the experiments, natural pH and solids concentration (as per industrial application) was kept constant at 7.9 and 45%, respectively, while other factors were varied (dosages of the collector, depressant and frother; impeller speed; flotation time and air rate). Sodium isopropyl xanthate was used as the collector while methyl isobutyl carbinol (MIBC) was used as the frother The depressants used include sodium cyanide (NaCN) and zinc sulfate ($ZnSO_4$) that were used to depress the flotation of pyrite and sphalerite, respectively. The depressants were added first followed by the collector and the frother. All reagents were given a 3 minutes conditioning time except

for MIBC which was conditioned for 2 minutes. After flotation, the froth (concentrate) was collected, dried, weighed and assayed for Pb, Cu, Zn, and Fe. The assays were determined using ICEP-OES and EDTA titration methods as applicable. Recovery was then calculated based on the dry concentrate weight (C), feed weight (F), feed assay of each element (f), concentrate assay of each element (c) using Equation 6.

$$R = \frac{Cc}{FF} * 100$$

(6)

3.2.5. Box-Behnken Design. The Box-Behnken method (BBD) is one of the major response surface methods used in experimental design [56]. This method is a class of second order rotatable design based on three level incomplete factorial designs. It was explained by [56] that, for three factors as shown in the graphical representations for three factors in BBD can be in the form of a cube with one center point and edge mid-points as shown in Figure 3.3.

Three interlocking 2^2 factorial designs with one center point is also a graphical representation of the method as shown in Figure 3.4. One advantage of the BBD method is that it eliminates combinations where all factors are simultaneously at their highest or lowest levels hence avoids occurrence of unsatisfactory results [56]. Using this design, optimum flotation conditions can be achieved with minimum number of experiments.

In this study, therefore BBD was used to design the sets of experiments required to maximize the recovery and the grade of lead and copper in the concentrate produced from bulk flotation of galena and chalcopyrite. As stated earlier, pyrite and sphalerite were depressed using sodium cyanide and zinc sulfate, respectively. The seven control
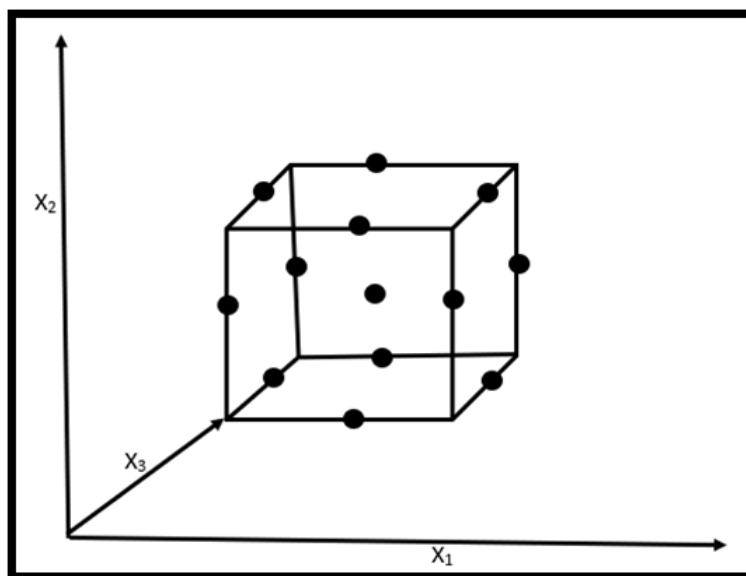
Figure 3.3. Box–Behnken design cube.
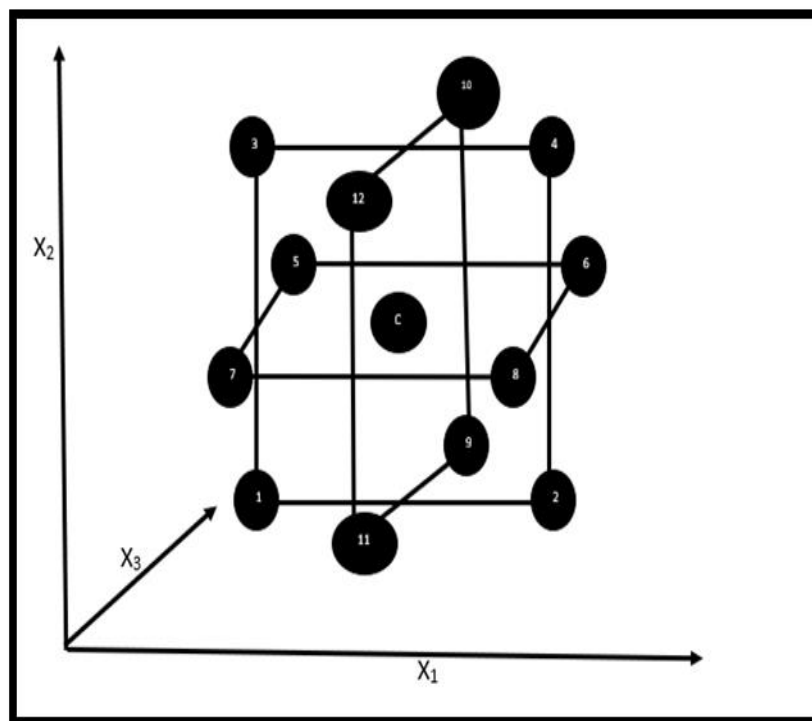
Figure 3.4. Interlocking three 2^2 factorial design.

parameters investigated in this study include collector (sodium isopropyl xanthate) dosage, frother (MIBC) dosage, impeller speed, air rate, pyrite depressant (NaCN) dosage, sphalerite depressant (ZnSO$_4$) dosage & flotation time. All other parameters were kept constant. A total of 62 sets of experiments were designed using BBD method. In each set of experiments, the combinations of seven variables used were different. Impeller speed was tested at three levels: 800 rpm, 1300 rpm and 1800 rpm. Three dosage of NaCN were used during flotation tests: 5g/ton, 52.5g/ton and 100 g/ton. As for ZnSO$_4$, three dosage were also used: 200g/ton, 450g/ton and 700 g/ton. Sodium Isopropyl Xanthate was tested at three dosage: 100 g/ton, 275g/ton and 450 g/ton. MIBC was added at the rate of 50g/ton, 200g/ton and 350 g/ton. Air flow rate was kept at 3 liter/min, 6 liter/min and 9 liter/min. Froth was collected for 2 mins, 5 mins and 8 mins during different experiments. Table 3.1 sumarises the levels of variables employed in this study.

3.3. RESULTS

A total number of 62 sets of experiments were designed using the BBD method. In these tests, different combinations of collector (sodium isopropyl xanthate) dosage, frother (MIBC) dosage, impeller speed, air rate, pyrite depressant (NaCN) dosage, sphalerite depressant (ZnSO4) dosage and flotation time were tested. Each set consisted of two number of experiments. The results of the experiments in form of grade and recovery of the metals like Pb, Cu, Fe, and Zn were analyzed using "Minitab 17.0" statistical software. Quadratic models were fitted to the results to predict and optimize the outputs. A total of eight quadratic models were fitted. These models describe equations for response variables including Pb grade, Pb recovery, Cu grade, Cu recovery,

Table 3.1. Three level experimental design with seven variable factors.

	Variable levels		
Variables	Low	Center	High
Impeller speed (rpm)	800	1300	1800
Air flow rate (l/min)	3	6	9
Collection time (mins)	2	5	8
NaCN dosage (g/ton)	5	52.5	100
MIBC dosage (g/ton)	50	200	350
ZnSO4 dosage (g/ton)	200	450	700
Xanthate dosage (g/ton)	100	275	450

Zn grade, Zn recovery, Fe grade and Fe recovery. Models for the response variables were

chosen through a stepwise procedure with an alpha (α) value of 0.05. Resulting models

are given by the Equations 7 through 14.

$$
\begin{aligned}
\text{Pb grade} = {}& 42.68 - 0.02240\ A + 0.00614\ B + 0.2147\ C + 0.01171\ D \\
& - 5.285\ E + 0.01382\ F - 1.964\ G - 0.002050\ C*C + 0.2540\ E*E \\
& - 0.000006\ F*F - 0.000082\ A*B + 0.00410\ A*G - 0.00934\ C*E \\
& + 0.01404\ C*G
\end{aligned}
\tag{7}
$$

$$
\begin{aligned}
\text{Pb recovery} = {}& -30.00 - 0.1247\ A + 0.3430\ B - 0.1602\ C - 0.0764\ D - 2.291\ E \\
& + 0.04151\ F + 26.77\ G - 0.000454\ B*B - 1.740\ G*G + 0.000274\ A*D \\
& - 0.03840\ B*G
\end{aligned}
\tag{8}
$$

$$Zn\ grade = 3.97 + 0.01068\ A + 0.00528\ B - 0.0163\ C + 0.00138\ D \quad (9)$$
$$+ 0.3026\ E - 0.000806\ F - 0.040\ G - 0.000011\ B*B + 0.000157\ C*C$$
$$- 0.000131\ A*C + 0.000010\ A*D - 0.001245\ A*G - 0.000071\ B*C$$
$$- 0.000014\ B*D + 0.000006\ B*F + 0.000021\ C*F - 0.000533\ D*E$$
$$- 0.000005\ D*F + 0.000592\ D*G$$

$$Zn\ recovery = 9.95 - 0.02382\ A + 0.0379\ B - 0.2095\ C - 0.02808\ D \quad (10)$$
$$+ 0.498\ E + 0.00070\ F + 3.743\ G - 0.000072\ B*B + 0.001027\ C*C$$
$$- 0.1530\ G*G + 0.000056\ A*D + 0.000039\ B*F - 0.01059\ B*G$$

$$Cu\ grade = 4.029 + 0.02070\ A + 0.00789\ B - 0.008668\ D - 0.000497\ F \quad (11)$$
$$- 0.7230\ G - 0.000008\ A*A - 0.000001\ F*F - 0.000080\ A*B + 0.000012\ B*F$$
$$+ 0.001485\ D*G$$

$$Cu\ recovery = 14.5 + 0.0332\ A + 0.1264\ B - 0.1713\ C - 0.0529\ D \quad (12)$$
$$- 0.00283\ F + 4.61\ G - 0.000163\ A*B + 0.000128\ B*F - 0.04830\ B*G$$
$$+ 0.01120\ D*G$$

$$Fe\ grade = 5.826 + 0.00142\ A - 0.00395\ B - 0.02490\ C + 0.003290\ D \quad (13)$$
$$- 0.2140\ E + 0.001594\ F - 0.4057\ G + 0.000005\ B*B - 0.000001\ F*F$$
$$- 0.000014\ A*D + 0.000446\ A*E + 0.000527\ A*G + 0.000003\ B*D$$
$$- 0.000007\ C*F + 0.004741\ C*G$$

$$Fe\ recovery = -19.92 - 0.0500\ A + 0.0537\ B - 0.4153\ C - 0.0069\ D \quad (14)$$
$$+ 3.884\ E + 0.01755\ F$$
$$+ 7.93\ G + 0.002636\ C*C - 0.628\ G*G + 0.000117\ A*D - 0.00836\ B*E$$
$$- 0.00432\ D*E$$

Where, A = Sodium isopropyl xanthate dosage, B = MIBC dosage, C = NaCN dosage, D = $ZnSO_4$ dosage, E = Air flow rate, F = Impeller speed and, G = Time.

For estimation of the significance of these model, the analysis of variance (ANOVA) was applied. Using a 5% significance level, a model is considered highly significant if the P-value (significance probability value) is less than 0.05. Table 3.2

describes the results of the ANOVA analysis performed on these models. It can be

seen that all the fitted models are significant (p-value < 0.05).

Table 3.2. ANOVA analysis results of the developed models.

		Sum of square	DOF	Mean square	F-value	P-value
Pb grade	Model	2785.64	14	198.97	60.28	<0.05
	Residual	155.13	47	3.30		
Pb Recovery	Model	22253.7	11	2023.1	76.08	<0.05
	Residual	1329.6	50	26.6		
Zn grade	Model	103.225	19	5.4329	37.65	<0.05
	Residual	6.060	42	0.1443		
Zn recovery	Model	1764.49	13	135.730	38.57	<0.05
	Residual	168.91	48	3.519		
Cu grade	Model	60.7158	10	6.0716	105.49	<0.05
	Residual	2.9354	51	0.0576		
Cu recovery	Model	9949	10	994.9	37.24	<0.05
	Residual	1362.5	51	26.72		
Fe grade	Model	18.0208	15	1.20139	41.72	<0.05
	Residual	1.3246	46	0.02880		
Fe recovery	Model	4988.69	12	415.72	32.4	<0.05
	Residual	628.63	49	12.83		

Figures 3.5, 3.6, 3.7 and 3.8 represents the predicted against the actual values for % recovery and the % grade of the flotation concentrates (froth) of Pb, Cu, Zn and Fe, respectively. Predicted values were derived from the mathematical models as presented by Equation 7 to 14. 1:1 correlation line for each of the plot is also shown in Figures 3.5, 3.6, 3.7 and 3.8.
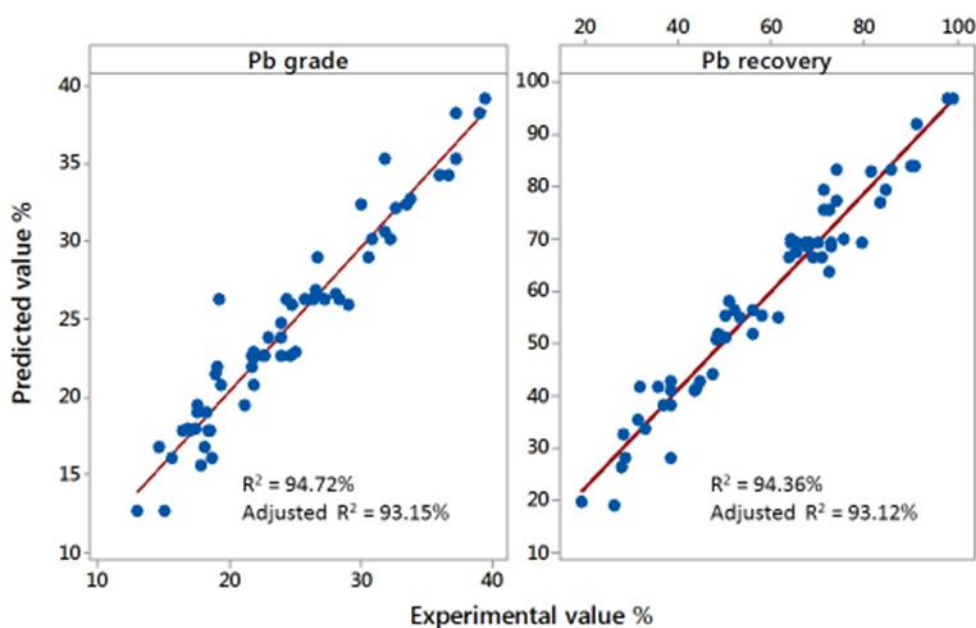
Figure 3.5. Actual vs predicted values of Pb grade (%) and Pb recovery (%).

The closer the points to the line, the better the agreement between the predicted values and the actual values. Values of R-square and adjusted r square for the developed models are also provided. The coefficient of multiple determinations, R^2 was found to be higher
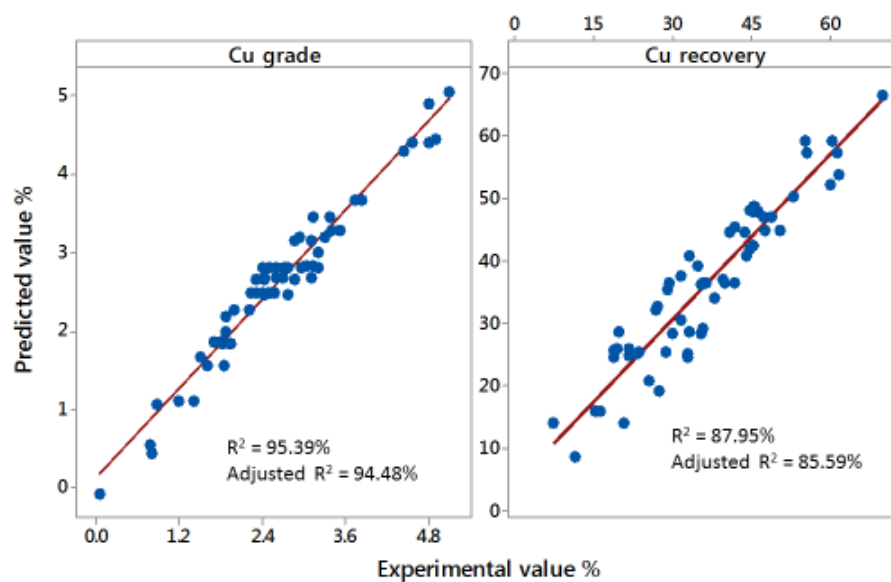
Figure 3.6. Actual vs predicted values of Cu grade (%) and Cu recovery (%).
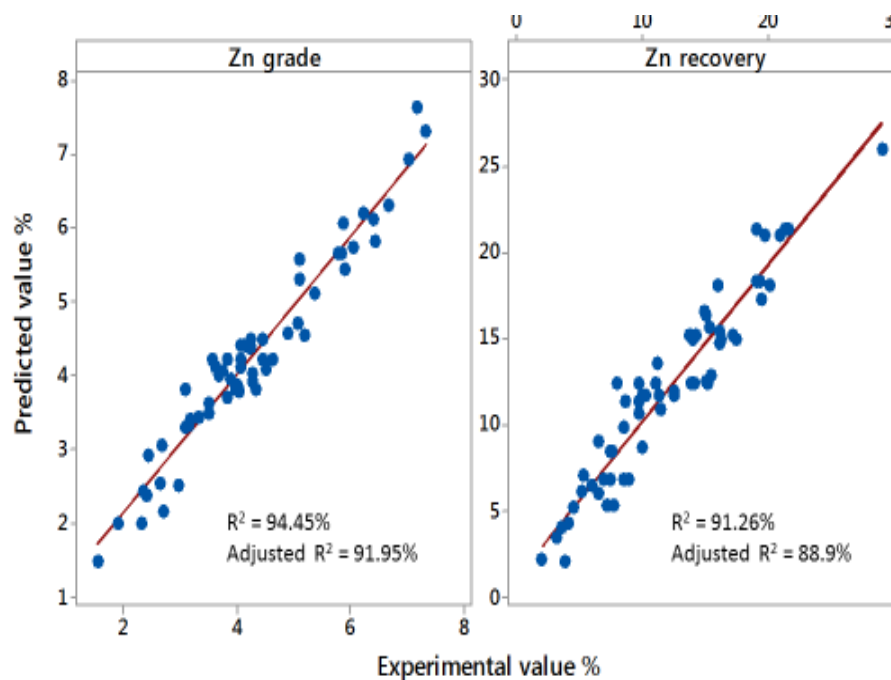
Figure 3.7. Actual vs predicted values of Zn grade (%) and Zn recovery (%).
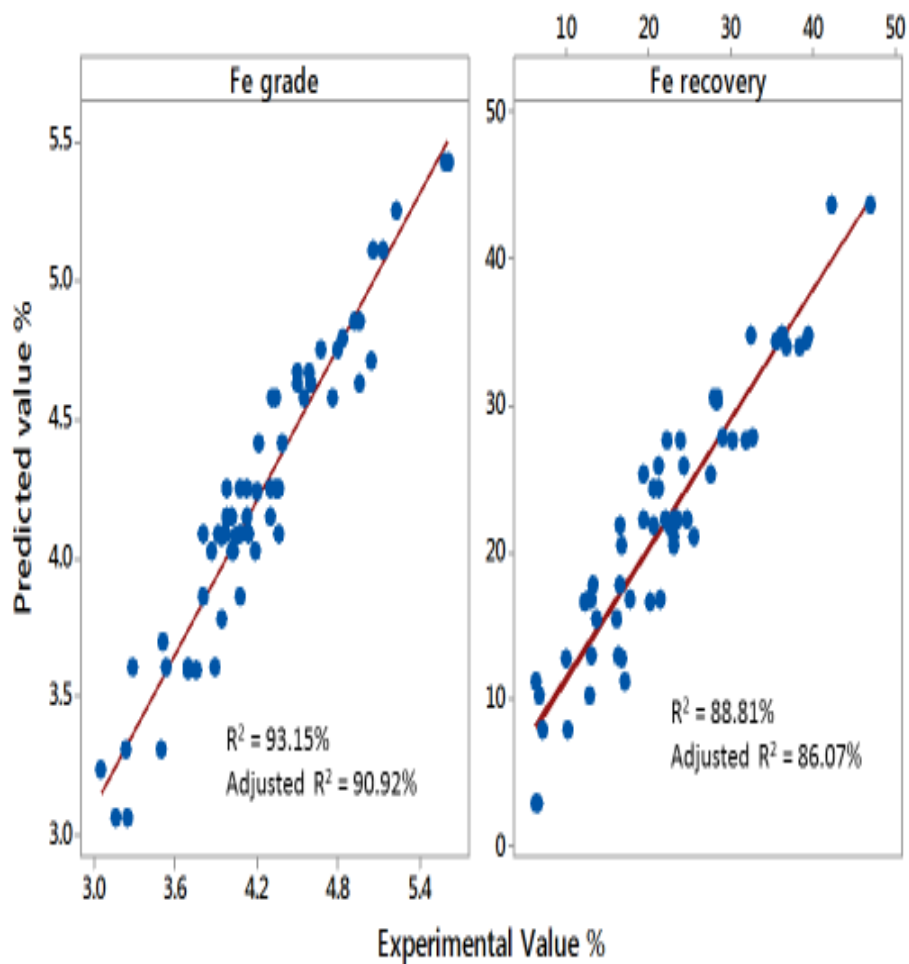
Figure 3.8. Actual vs predicted values of Fe grade (%) and Fe recovery (%).

than 85% in all cases. Thus model can explain more than 85% of the total variations in the system. The high value of R^2 specifies the reliability of the quadratic equations in the given experimental domain.

Three-dimensional surface plots provide valuable information regarding the interaction effects of different operational variables on flotation. In this study interaction effects of seven operational variables of flotation on grade and recovery of Pb, Zn and Cu

were studied. These three-dimensional (3D) plots for the measured responses were

based on the model equations. Only those interaction effects which were important and

had a significance level of at least 95 %, have been discussed in this paper. One factor

considered as constant in each plot was held constant at center level. Figure 3.9 shows the

3D response surface relationship between the dosage of sodium isopropyl xanthate and

the flotation time and its influence on Pb grade in the concentrates at the center values of

other variables. It can be seen that increasing the sodium isopropyl xanthate

concentration above 100 g/ton of ore decreases the grade. This can be due to the fact that
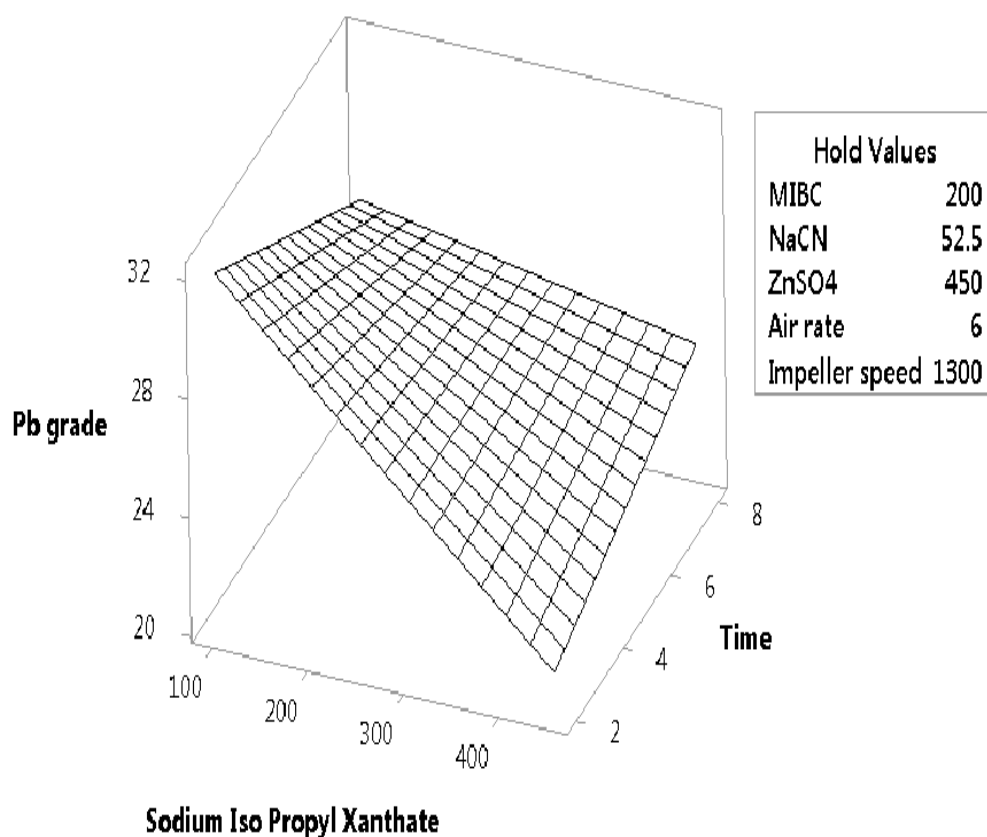
Figure 3.9. Effect of collector (sodium isopropyl xanthate) dosage and flotation time on Pb Grade.

excess amount of collector adsorbs on all mineral surfaces, therefore, reducing the selectivity. With regards to time, the maximum grade was achieved at the lowest flotation time of 2 minutes at 100 g/ton of the xanthate collector. Allowing more flotation time provides more chances for the gangue minerals to report to the concentrate thus reducing the grade.

Figure 3.10 represents the effect of NaCN and impeller speed on Pb grade. As indicated, at a dosage below 50g of NaCN per ton of ore, increasing the dosage of sodium cyanide resulted in increasing the Pb grade. Increasing the value of NaCN decreases the inclusion of pyrite in the product hence increasing the grade of Pb in the concentrate. An increase in the value of NaCN above 50 g/ton however adversely effects the Pb grade as an excess amount of NaCN can get coated on galena particles, this inhibits the adsorption of sodium isopropyl xanthate collector on galena particles thus, making galena less hydrophobic. As a result, the selectivity of the flotation process is reduced resulting in lower Pb grade. Impeller speed also affected the Pb grade in a similar fashion. The lower impeller speed (900 rpm) was ineffective to provide the appropriate mixing which reduced the bubble-particle collision for high density mineral galena (containing Pb) and , hence a reduction in Pb grade. On the other hand, a higher impeller speed (1800 rpm) stirs up the system to extreme thus increasing the chances of entrained gangue minerals reporting to the product. This reduces the selectivity of flotation process thus reducing the Pb grade in the product. Impeller speed of 1500 rpm was found to be the optimum value for achieving the best Pb grade in the product as it avoids both extreme conditions.

Figure 3.11 bears interesting observation in terms of the interaction effects of flotation time and NaCN dosage. It is observed that at a dosage of 50 g/ton of NaCN, the

highest Pb grade can be achieved. It is interesting to note that an increase in the

flotation time does not affect the Pb grade when we consider the interaction effect of

NaCN and time. This suggests that an optimum amount of NaCN is not effected by the

flotation time in case of Pb grade in concentrate. It is interesting to observe in Figure 3.12

that at a lower dosage (200 g/ton) of $ZnSO_4$, Pb recovery of the product decreases as the

dosage of sodium isopropyl xanthate increases. This suggests that in the absence of

enough $ZnSO_4$,
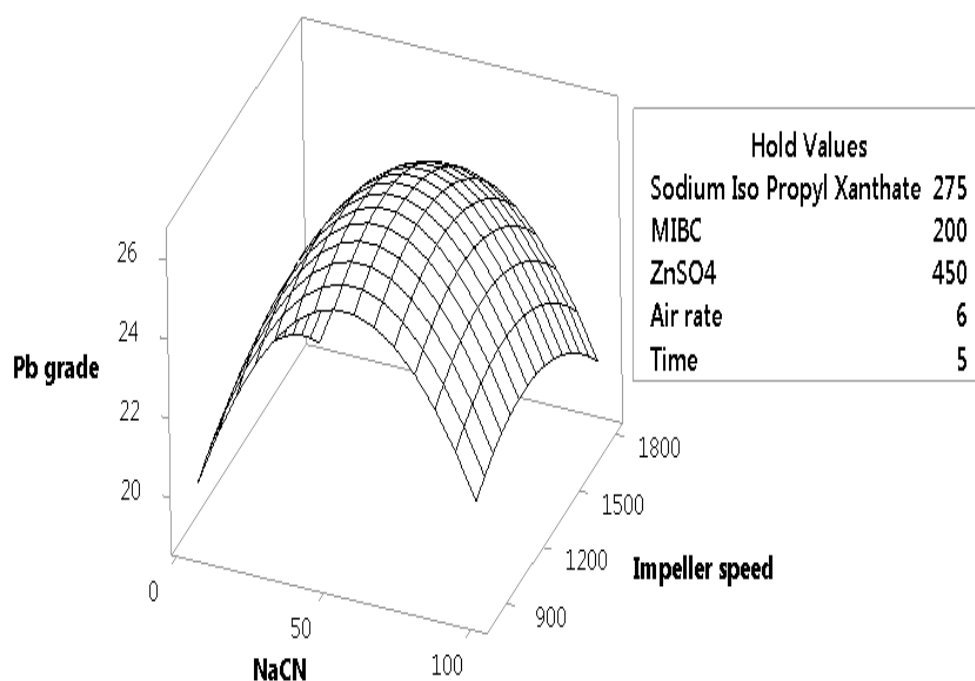
Figure 3.10. Effect of NaCN dosage and impeller speed on Pb Grade.
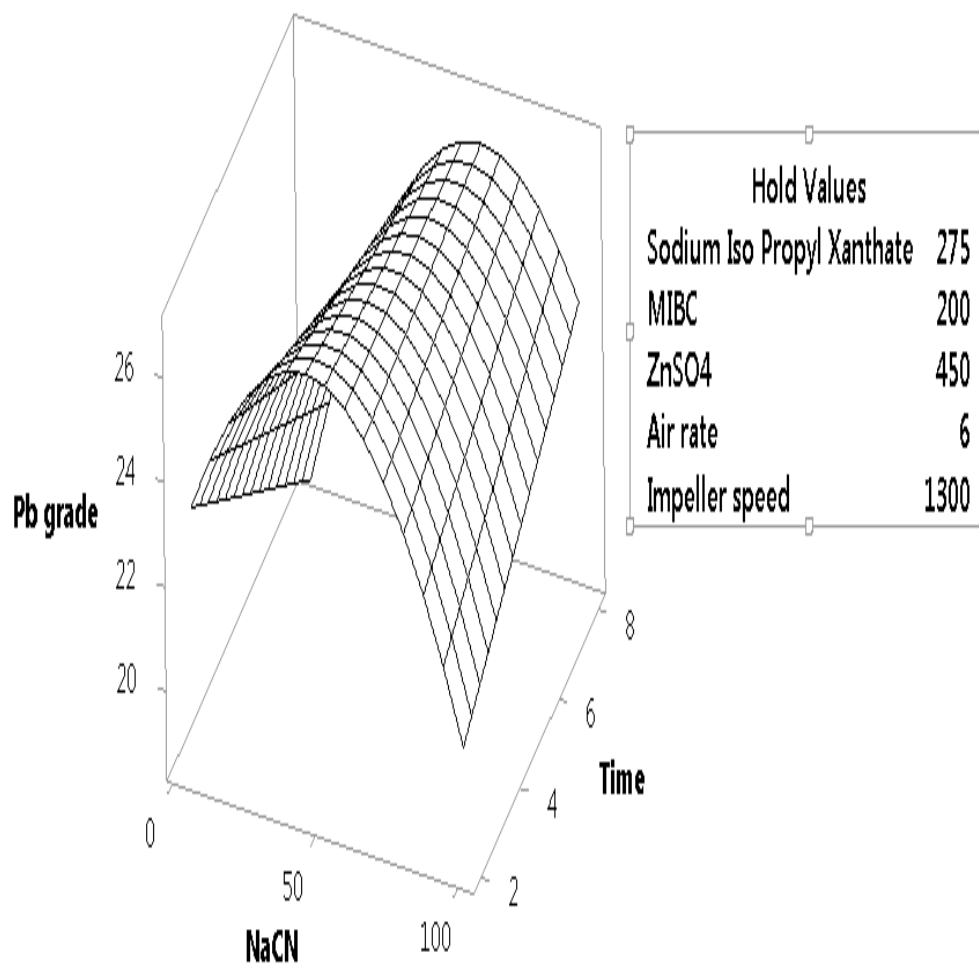
Figure 3.11. Effect of NaCN dosage and flotation time on Pb Grade.

the excess amount of collector (sodium isopropyl xanthate) does not preferably adsorb on galena surface thus reducing the Pb recovery. However, when highest dosages of collector and $ZnSO_4$ are used, $ZnSO_4$ prevents the adsorption of collector onto sphalerite thus increasing the efficiency of the collector to make galena hydrophobic. This results in higher recovery of galena in the final concentrate.
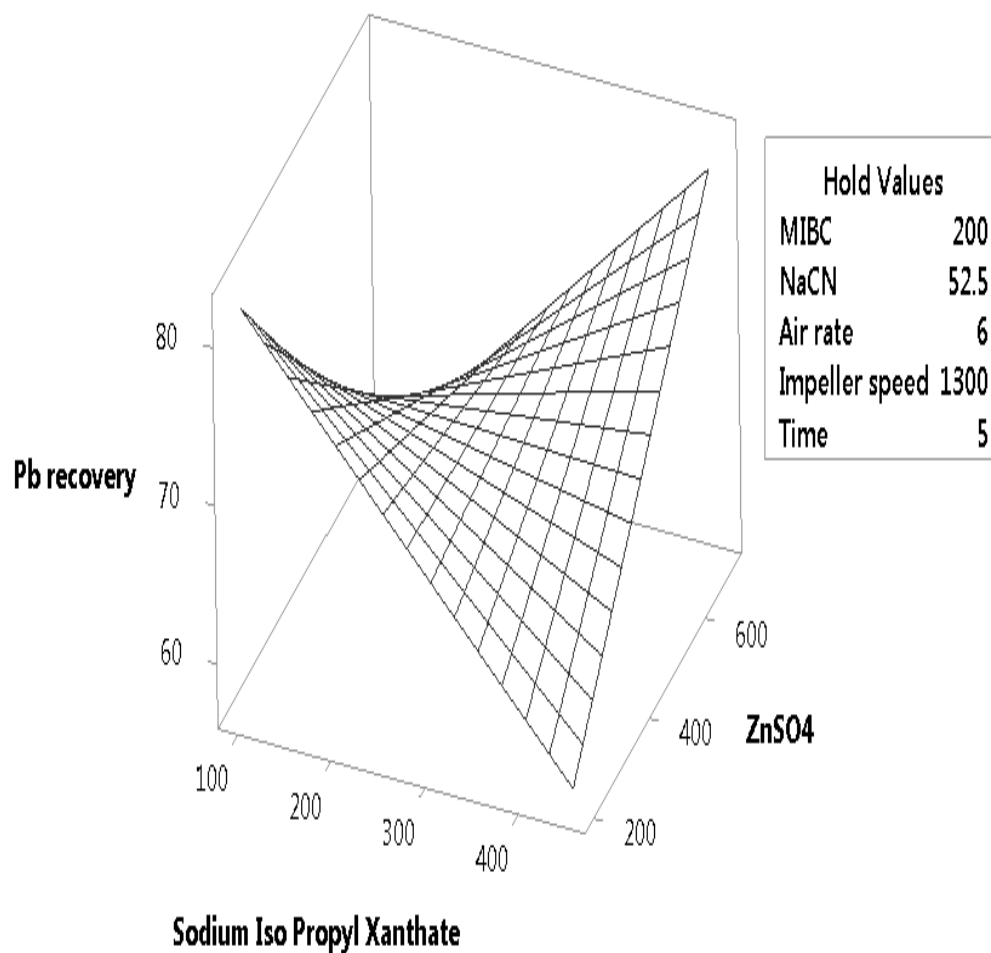
Figure 3.12. Effect of the collector (sodium isopropyl xanthate) and Zinc Sulfate (ZnSO₄) dosages on Pb recovery.

Highest Pb recovery was achieved at frother (MIBC) concentration of 100 g/ton and flotation time of 8 minutes as shown in Figure 3.13. At a higher frother concentration, Pb recovery is decreased. This can be explained by the fact that higher frother concentration strongly decreases the surface tension of the solution; thus decreasing the froth stability and recovery.
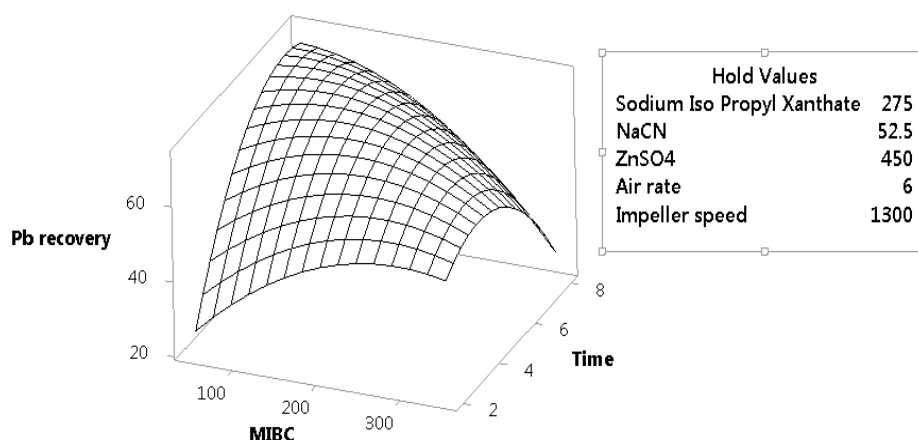
Figure 3.13. Effect of the frother (MIBC) concentration and flotation time on Pb recovery.

$ZnSO_4$ acts as a depressant for Zn containing sphalerite. The 3D plot of the interaction effect of $ZnSO_4$ and sodium isopropyl xanthate, in Figure 3.14, shows that at a 100 g/ton dosage of the collector (sodium isopropyl xanthate), an increase in the dosage of $ZnSO_4$ decreases the Zn grade. Zn grade can be seen to increase (Figure 3.15) in the product as flotation time increases at a collector dosage of 100 g/ton. This undesirable effect can be attributed to the increasing probability of sphalerite mineral entrainment as its probability of collision with bubble increases with more time at hand.

According to the 3D plot of MIBC and $ZnSO_4$ interaction effect on Zn grade as shown in Figure 3.16, an increase in the dosage of $ZnSO_4$ decreases the Zn grade which is expected as $ZnSO_4$ acts as a depressant for sphalerite.
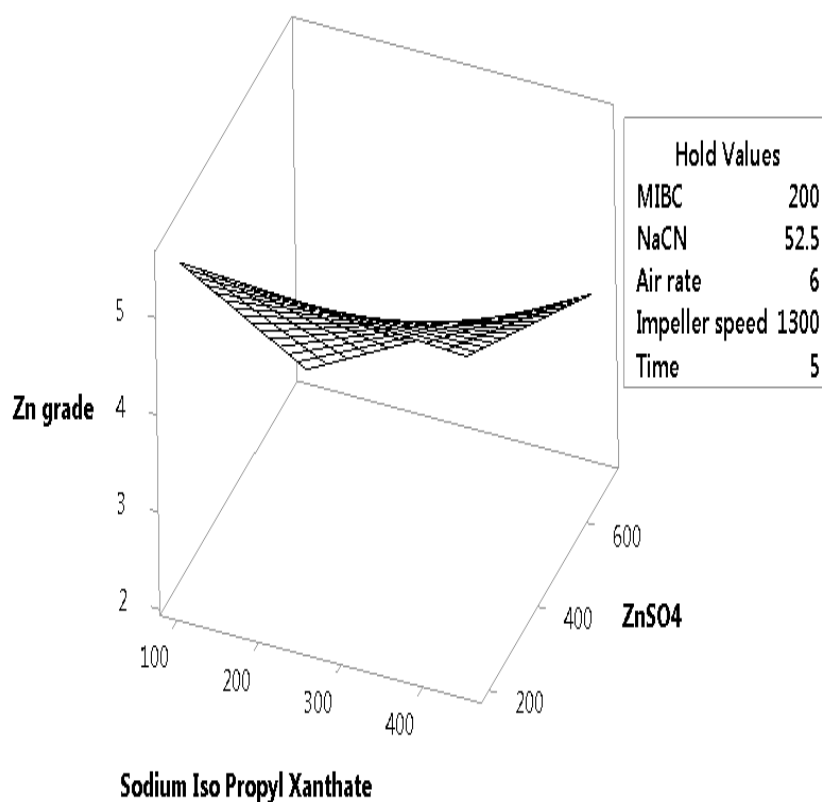
Figure 3.14. Effect of the collector (sodium isopropyl xanthate) dosage and Zinc Sulphate (ZnSO$_4$) concentration on Zn grade.

Figure 3.17 suggests using the highest MIBC dosage and the lowest Impeller speed to achieve the lowest Zn grade in the product. Figures 3.19, 3.20 and 3.21 show the response surface relationship between ZnSO$_4$ and air rate, impeller speed, flotation time with Zn grade, respectively. The highest level of ZnSo$_4$, air rate and impeller speed with the lowest flotation time is found to depress Zn grade most efficiently. At a lower dosage (100 g/ton) of sodium isopropyl xanthate, Zn recovery decreases as the dosage of ZnSO$_4$ decreases (Figure 2.22), which is expected. However, at a higher dosage
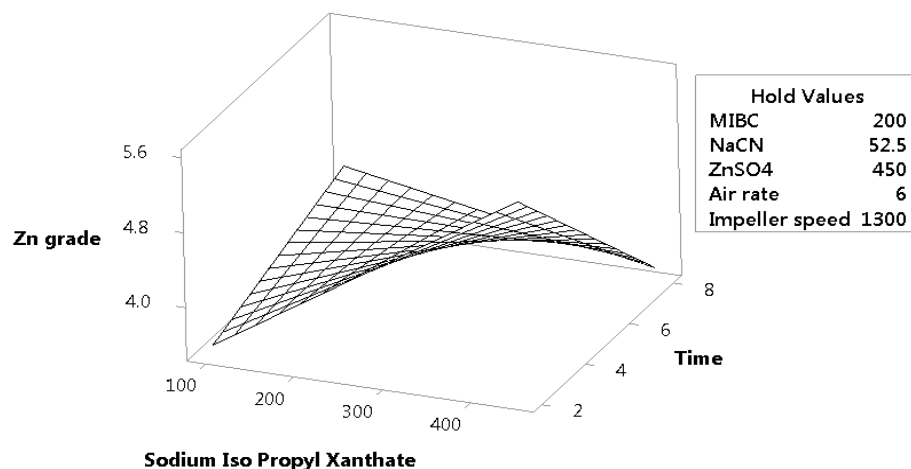
Figure 3.15. Effect of the collector (sodium isopropyl xanthate) dosage and flotation time on Zn.
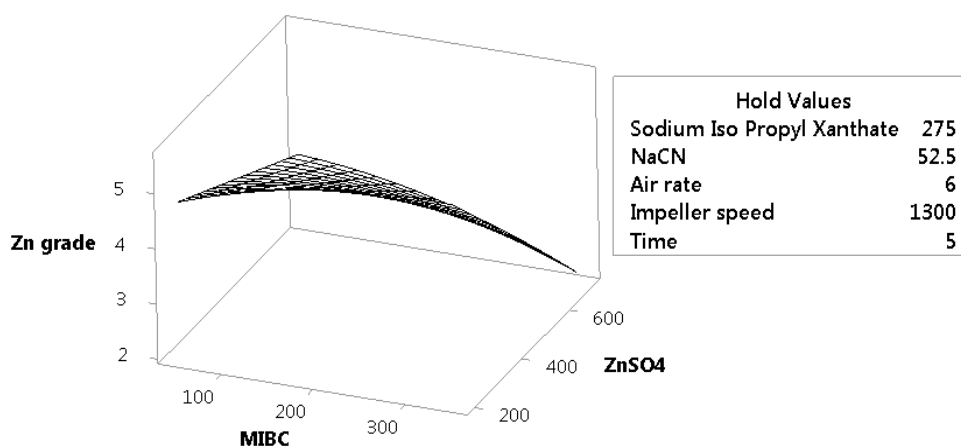
Figure 3.16. Effect of the frother (MIBC) and Zinc Sulphate ($ZnSO_4$) concentrations on Zn grade.

(400 g/ton) of sodium isopropyl xanthate, Zn recovery increases even with increasing amount of $ZnSO_4$. This phenomenon suggests that higher dosage of collector (sodium isopropyl xanthate) diminishes the effect of $ZnSO_4$ as sphalerite depressant.

Figures 3.23 and 3.24 suggest that in order to achieve the lowest Zn recovery in the concentrate without destabilizing the forth, lower level of MIBC (100 g/ton), impeller speed (900 rpm) and time (2 minutes) should be used to carry out the flotation.

Figure 3.25 illustrates that the highest Cu grade in the product can be achieved with a lower dosage of sodium isopropyl xanthate (100 g/ton) and the highest concentration of MIBC (300 g/ton). Lower dosage of collector increases the selectivity of the collector and the higher concentration of MIBC stabilizes the froth and increases the particle-bubble collision between the chalcopyrite mineral and air bubbles. Figure 3.26 suggests that the highest Cu grade can be achieved at the lowest levels of MIBC (100 g/ton) and Impeller speed (900 rpm). These mild flotation conditions allow only the highly hydrophobic minerals to make it to the concentrate.
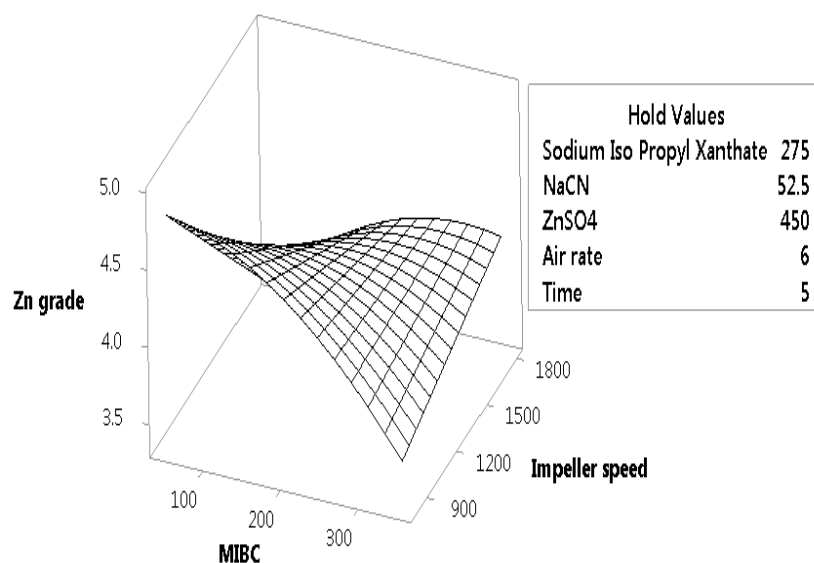
Figure 3.17. Effect of the frother (MIBC) concentration and impeller speed on Zn grade.
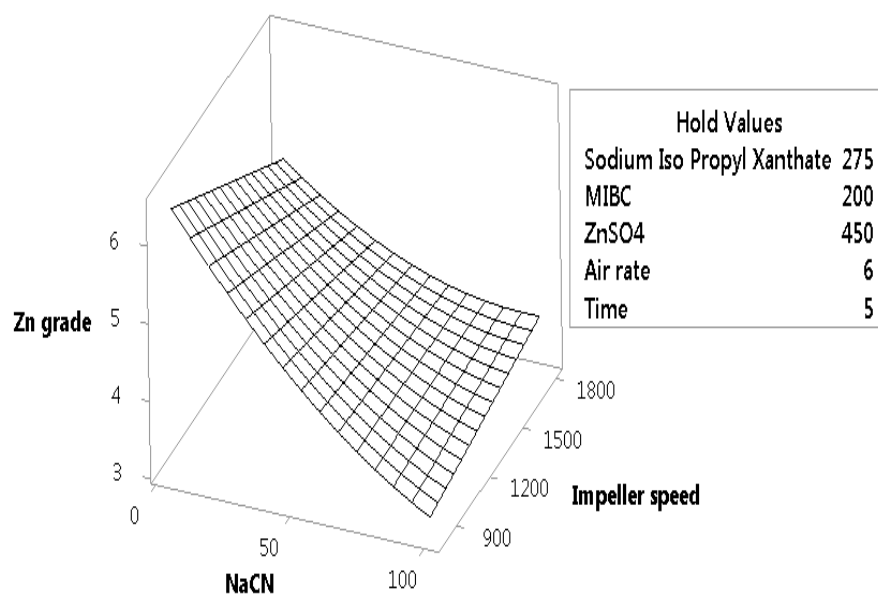
Figure 3.18. Effect of the NaCN dosage and impeller speed on Zn grade.
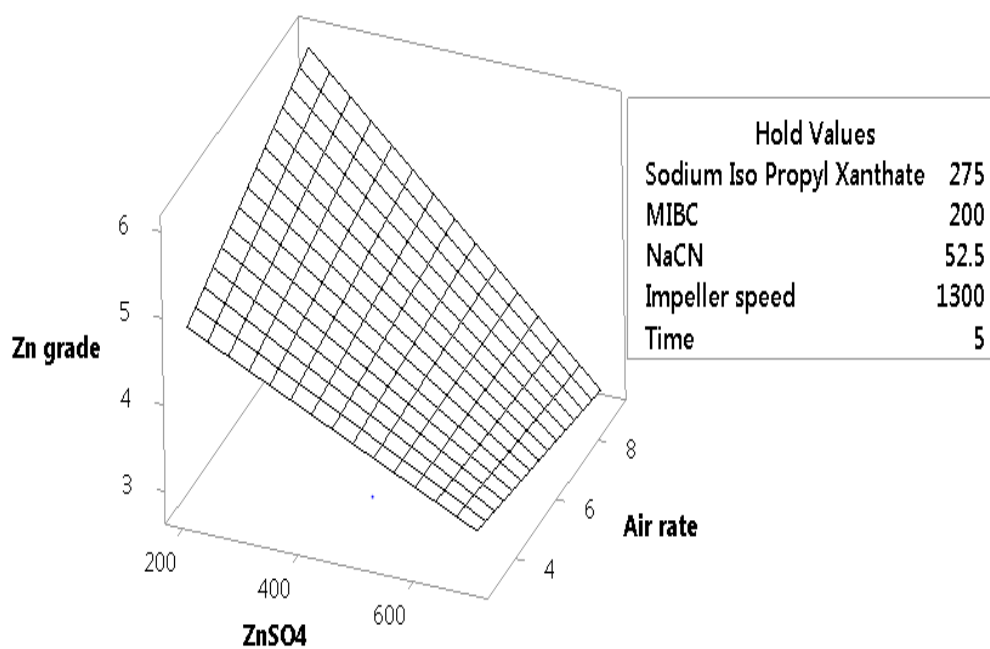
Figure 3.19. Effect of Zinc Sulphate (ZnSO$_4$) concentration and air flow rate on Zn grade.
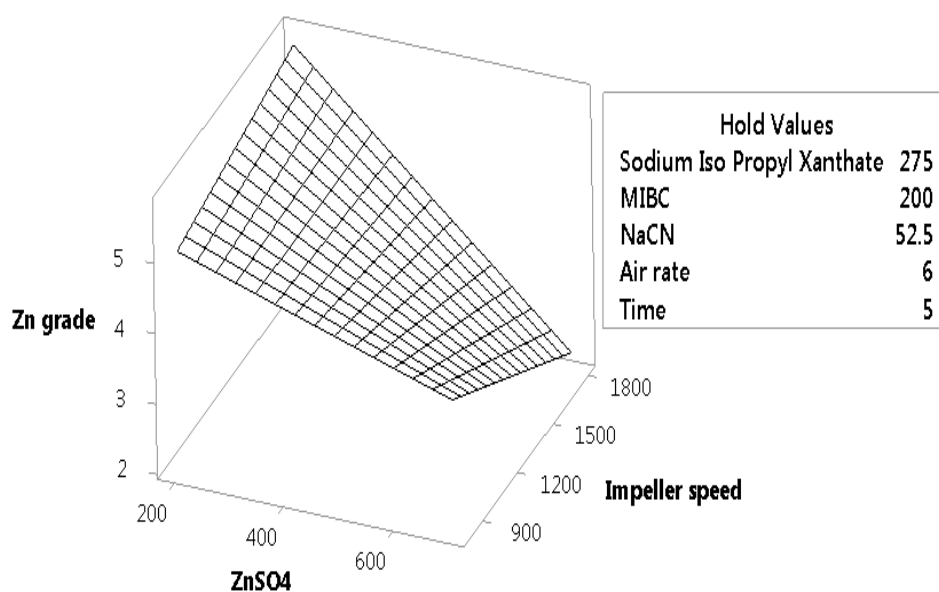
Figure 3.20. Effect of Zinc Sulphate (ZnSO$_4$) concentration and impeller speed on Zn grade.
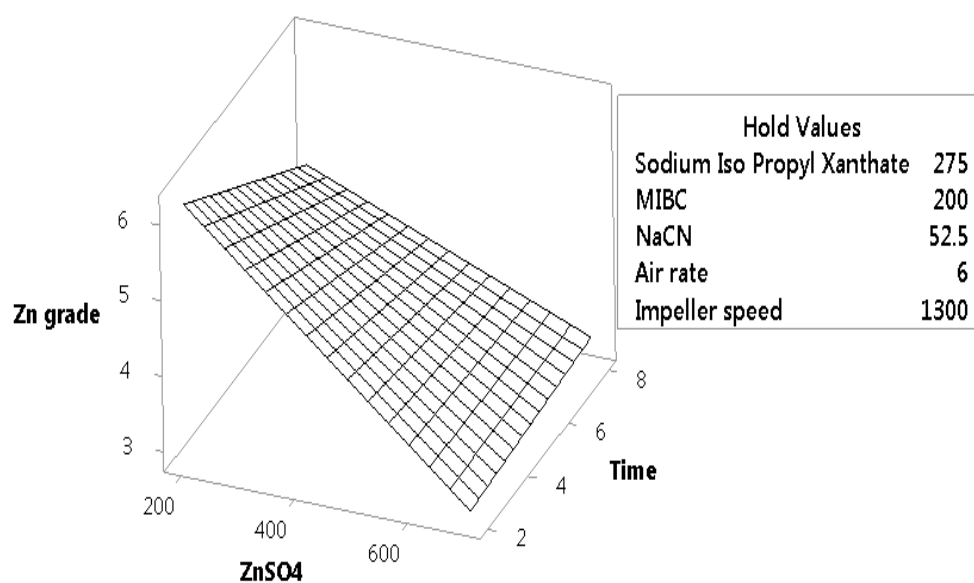
Figure 3.21. Effect of Zinc Sulphate (ZnSO$_4$) concentration and flotation time on Zn grade.
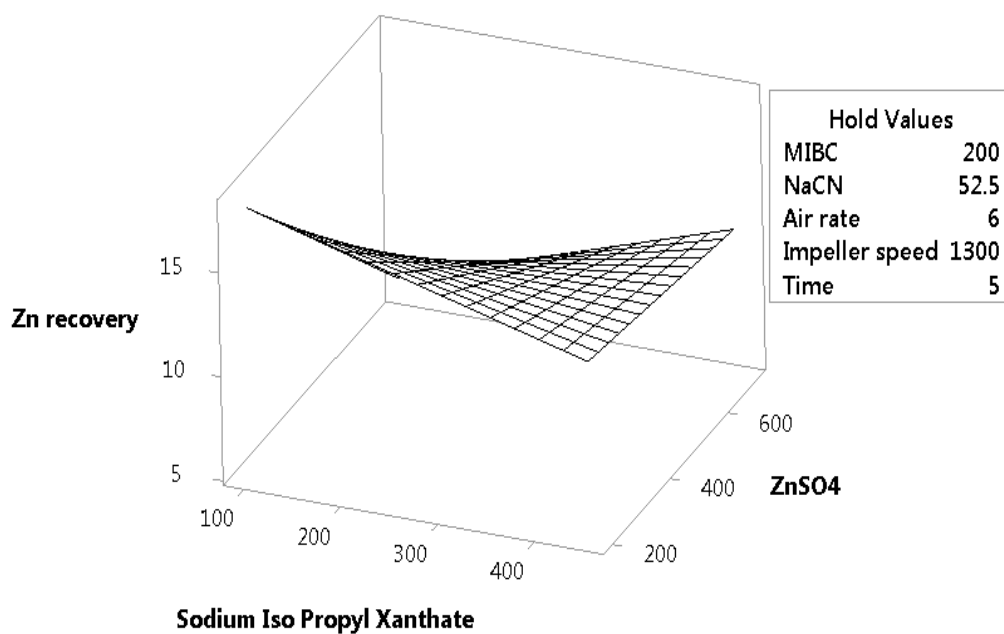
Figure 3.22. Effect of the collector (sodium isopropyl xanthate) dosage and Zinc Sulphate (ZnSO$_4$) concentration on Zn recovery.
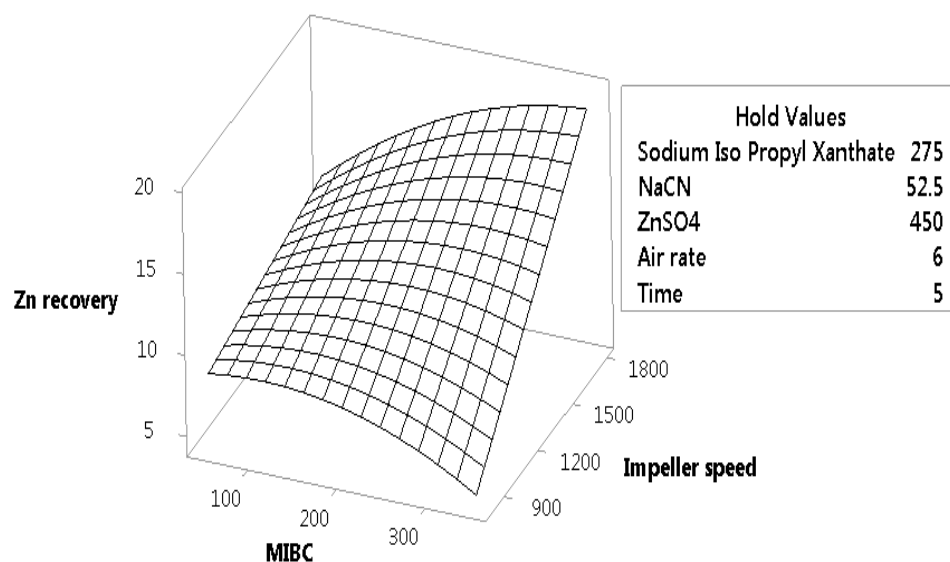
Figure 3.23. Effect of the frother (MIBC) concentration and impeller speed on Zn recovery.
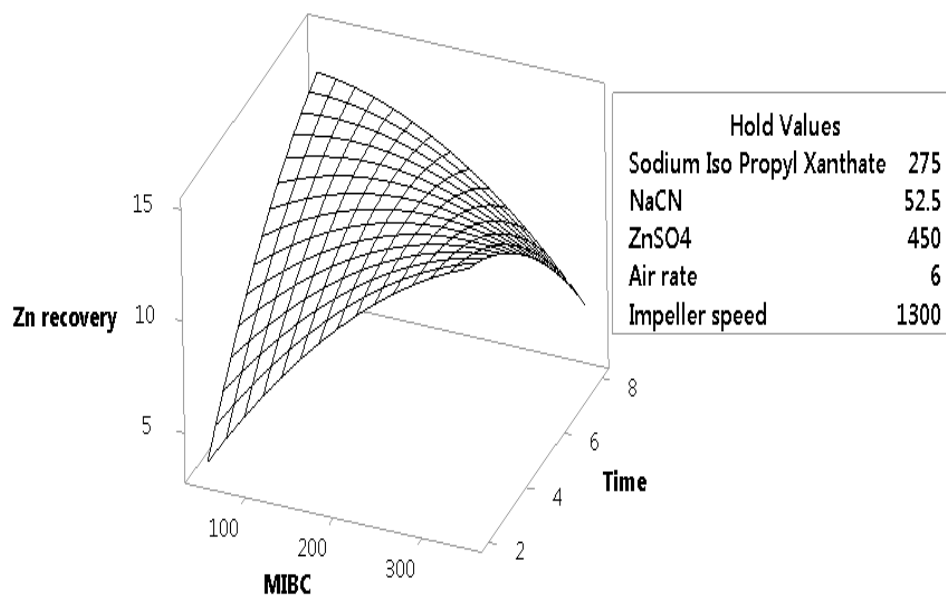
Figure 3.24. Effect of the frother (MIBC) concentration and flotation time on Zn recovery.
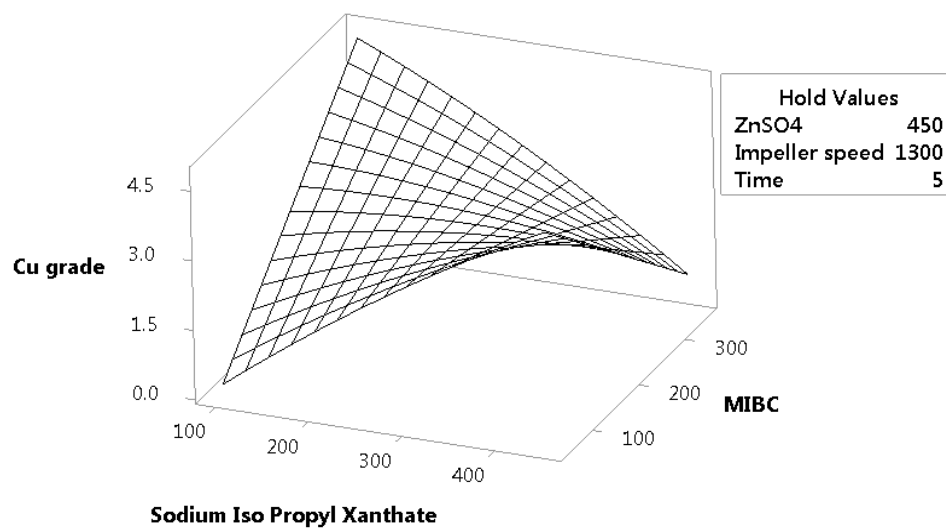
Figure 3.25. Effect of the collector (sodium isopropyl xanthate) dosage and frother (MIBC) concentration on Cu grade.
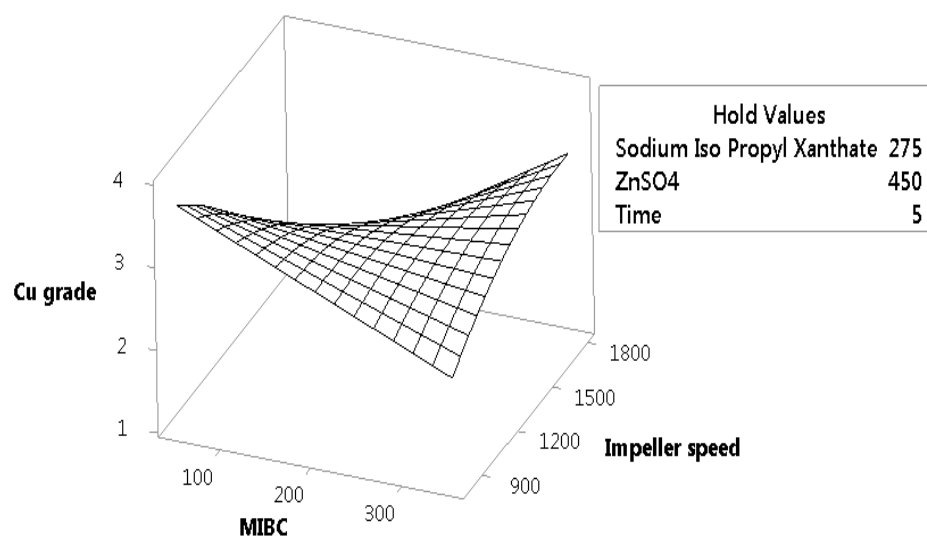
Figure 3.26. Effect of the frother (MIBC) concentration and impeller speed on Cu grade.
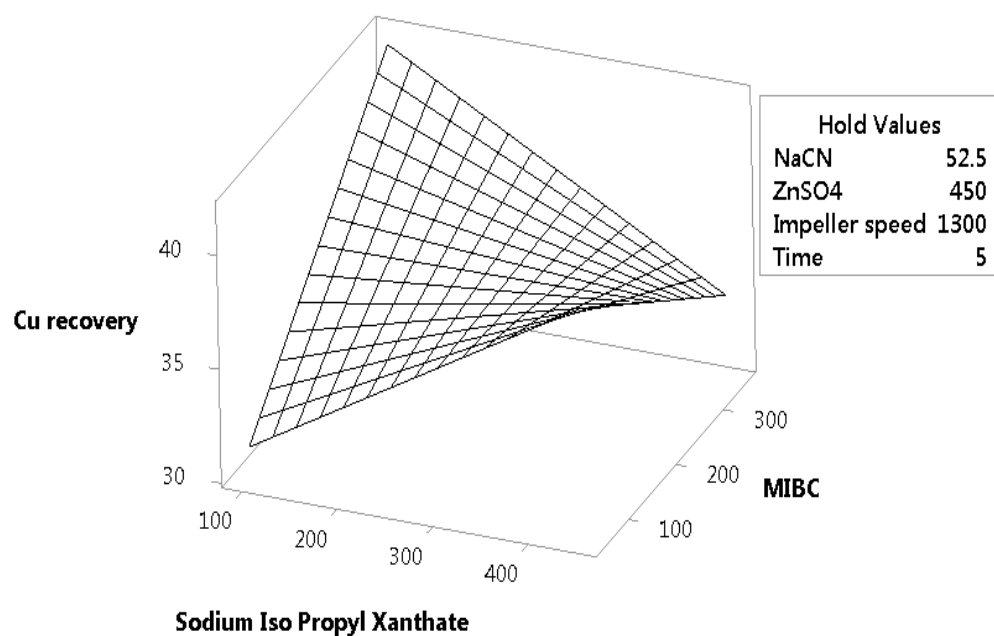
Figure 3.27. Effect of the collector (sodium isopropyl xanthate) dosage and frother (MIBC) concentration on Cu recovery.

In the presence of highest dosage of MIBC (300 g/ton), Cu recovery appears to increase as the impeller speed increases (Figure 3.28). This can be attributed to an improved mixing and suspension of ore particles at higher levels of impeller speed. With regards to flotation time, Cu recovery appears to increase with an increase in the flotation time as demonstrated by Figure 3.29. Maximum recovery is observed at a flotation time of 8 minutes and MIBC concentration of 100 g/ton. Figures 3.30, 3.31 and 3.32 suggest that an increase in the dosage of NaCN proportionally depresses the Fe
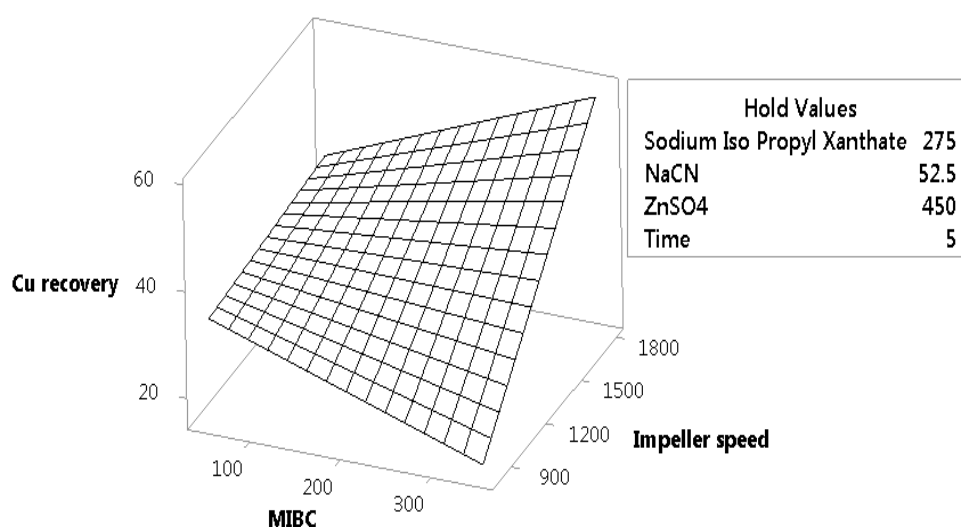
Figure 3.28. Effect of the frother (MIBC) concentration and impeller speed on Cu recovery.

grade. Lowest Fe grade is achieved at the highest dosage of NaCN which is 100 g/ton. Variation in the dosages of Sodium isopropyl xanthate, MIBC and $ZnSO_4$ do not affect

the Fe grade in the concentrate. These results demonstrate the pronounced effect of

NaCN in depressing Fe containing Pyrite.
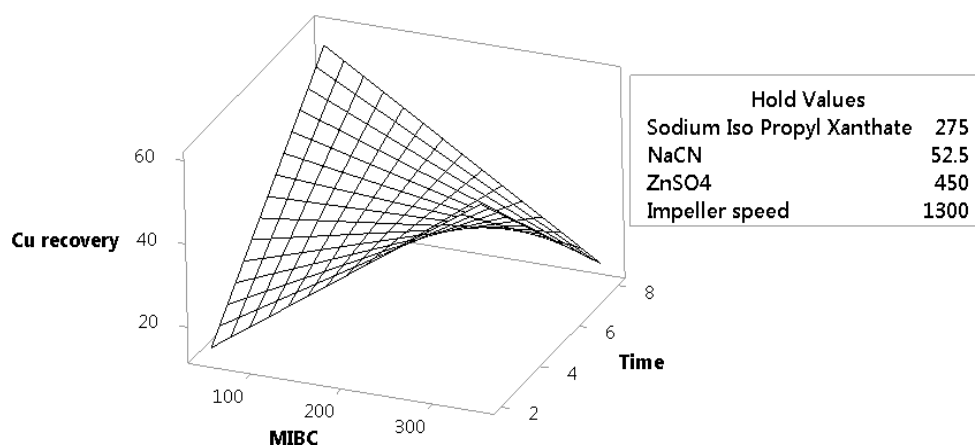
Figure 3.29. Effect of the frother (MIBC) concentration and flotation time on Cu recovery.
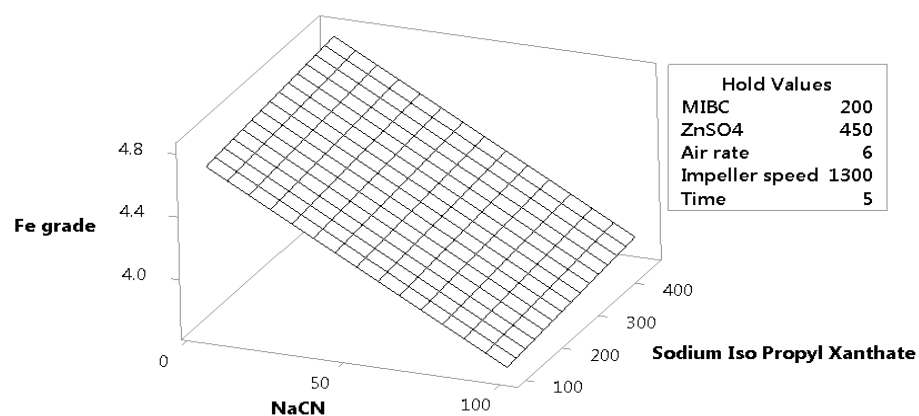
Figure 3.30. Effect of the NaCN and collector (sodium isopropyl xanthate) dosages on Fe grade.

Figures 3.33 and 3.34 also demonstrates the effect of NaCN as a Fe depressant. The highest level of Fe depression is accomplished at the highest dosage of NaCN (100 g/ton). A higher level of air rate and impeller speed also depresses the Fe grade more efficiently. This may be due to the lesser chances of entrainment of gangue particles at these extreme conditions.
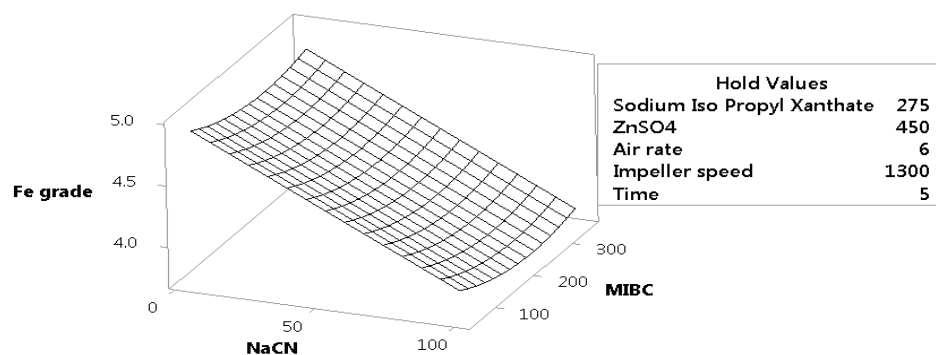
Figure 3.31. Effect of the NaCN dosage and frother (MIBC) concentration on Fe grade.
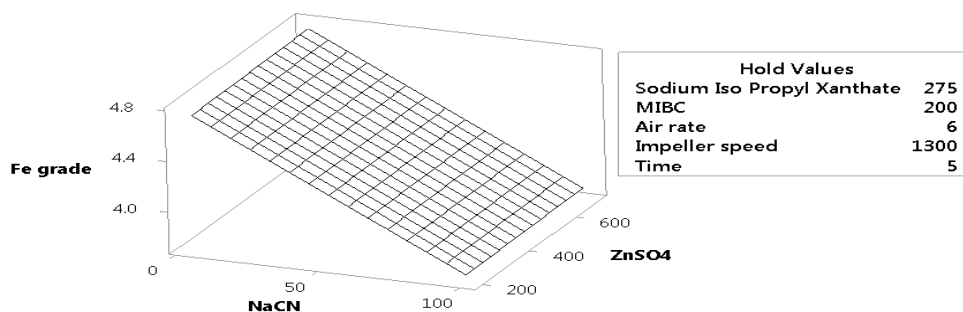
Figure 3.32. Effect of the NaCN dosage and Zinc Sulphate (ZnSO₄) concentration on Fe grade.
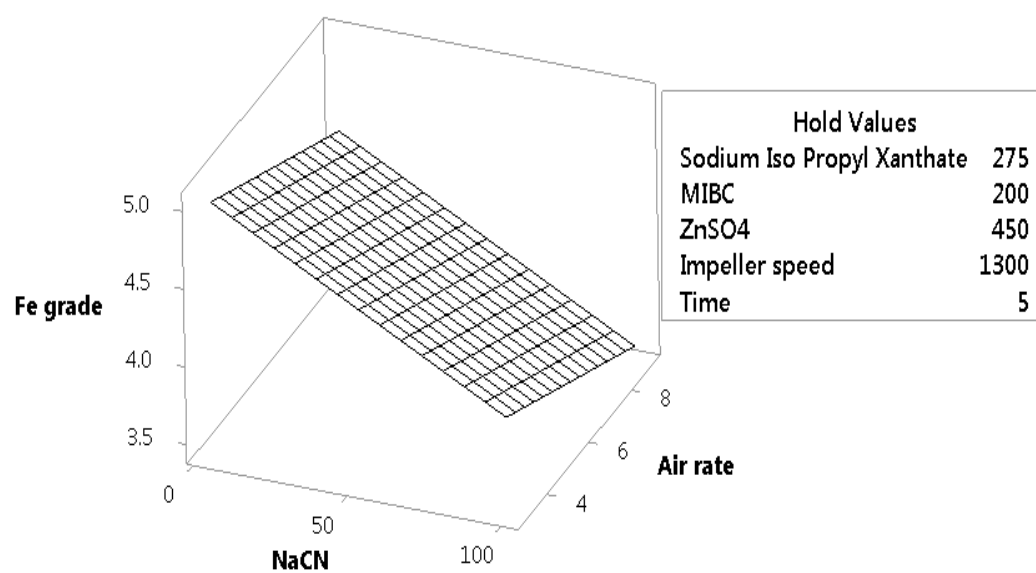
Figure 3.33. Effect of the NaCN dosage and air flow rate on Fe grade.
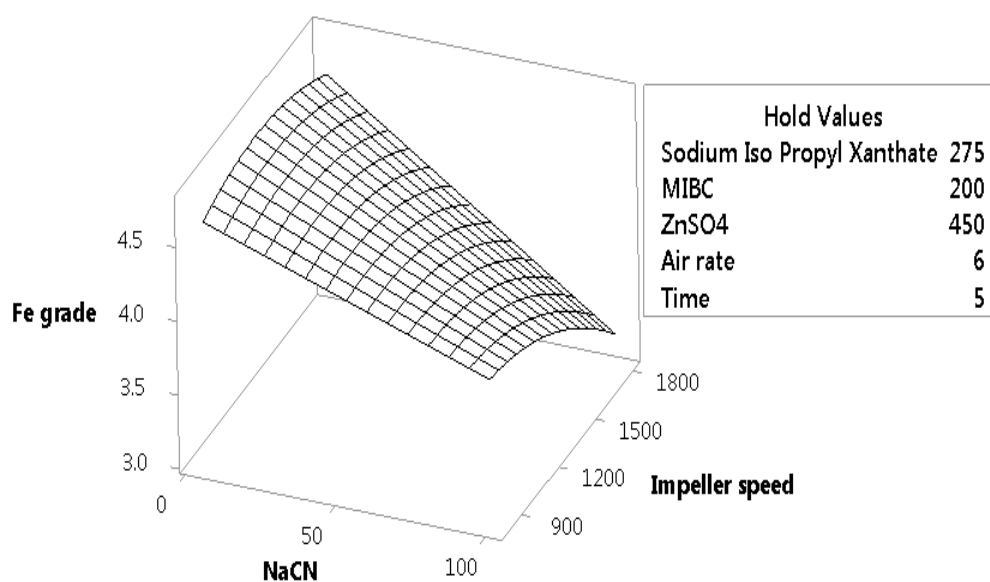
Figure 3.34. Effect of the NaCN dosage and impeller speed on Fe grade.

A lesser flotation time only allows the most likely particles to report to the concentrate. As flotation time is increased more gangue particles get the allowance to get to the concentrate through entrainment. Figure 3.35 shows the same as the lowest Fe grade in the concentrate can be observed at the lowest flotation time (2 minutes) used during this study.
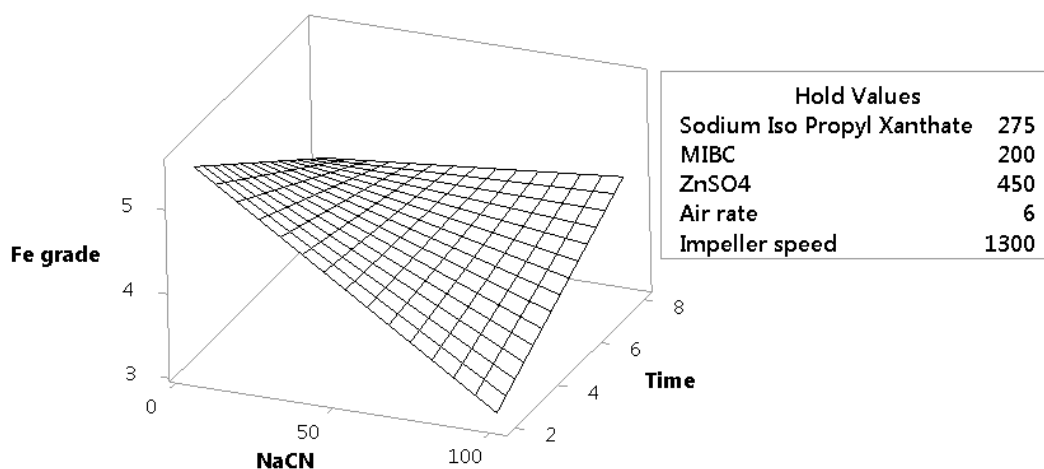
Figure 3.35. Effect of the NaCN dosage and flotation time on Fe grade.

Similar to Fe grade, Fe recovery does not appear to be effected by the dosages of sodium isopropyl xanthate, MIBC, $ZnSO_4$ and air rate as can be seen in Figures 3.36, 3.37, 3.38 and 3.39, respectively. Figures 3.36, 3.37, 3.38 and 3.39 also shows that an increase in NaCN dosage can be very effective in reducing the Fe recovery.

At the highest dosage of NaCN and the lowest level of impeller speed, Fe recovery is minimum as shown in Figure 3.40. High dosage of NaCN(100 g/ton) is therefore

recommended for depressing Fe. Lower impeller speed decreases the probability of entrainment of hydrophilic particles thus reducing the hydrophilic pyrite minerals.
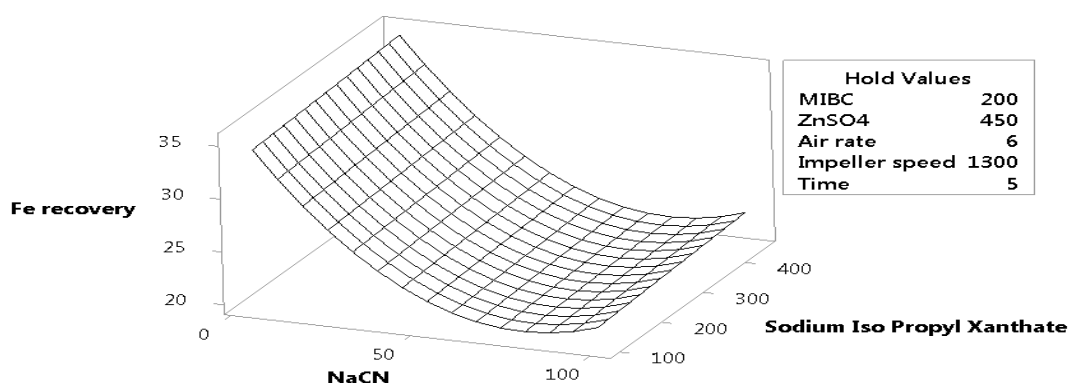
Figure 3.36. Effect of the NaCN and collector (sodium isopropyl xanthate) dosages on Fe recovery.
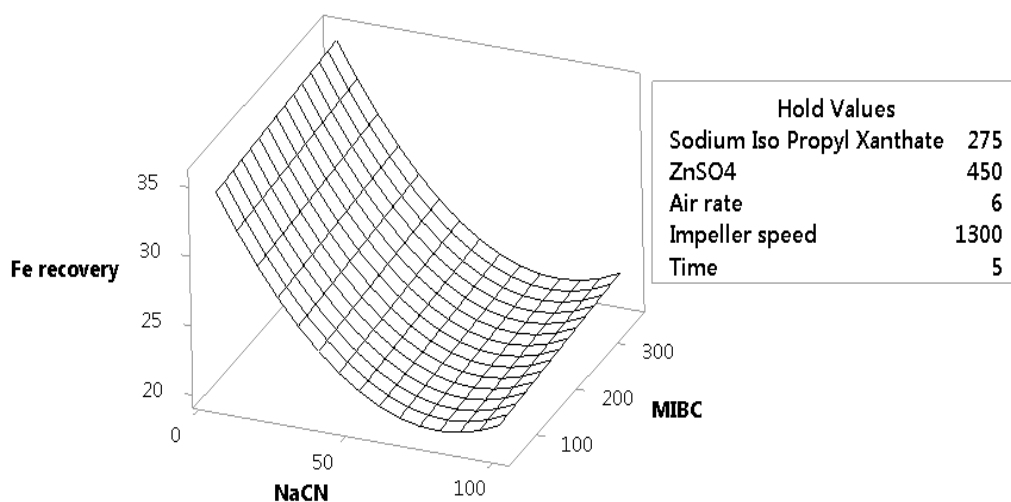
Figure 3.37. Effect of the NaCN dosage and frother (MIBC) concentration on Fe recovery.
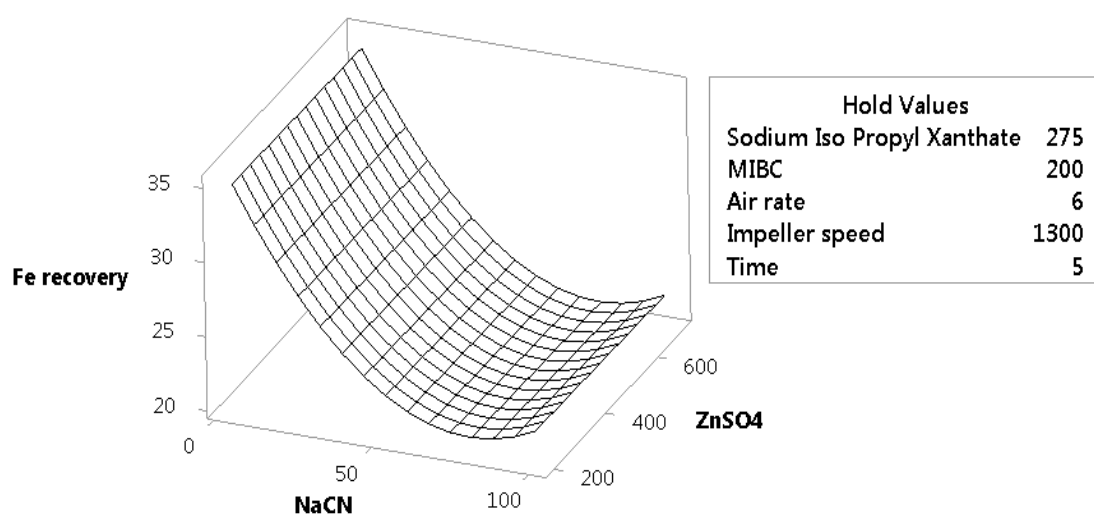
Figure 3.38. Effect of the NaCN dosage and Zinc Sulphate ($ZnSO_4$) concentration on Fe recovery.
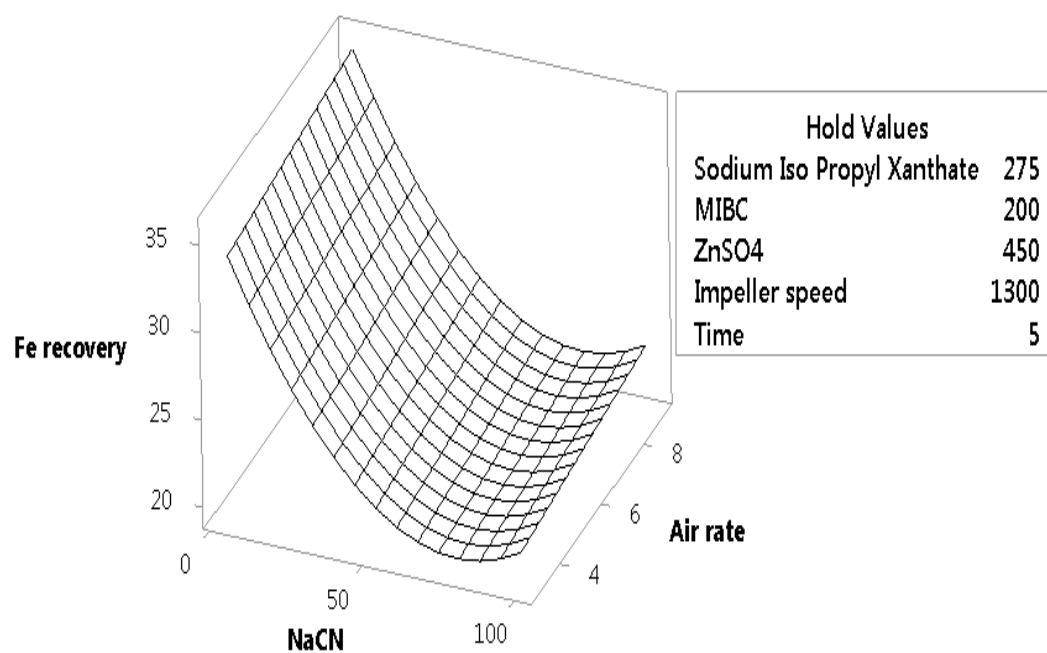
Figure 3.39. Effect of the NaCN dosage and air flow rate on Fe recovery.
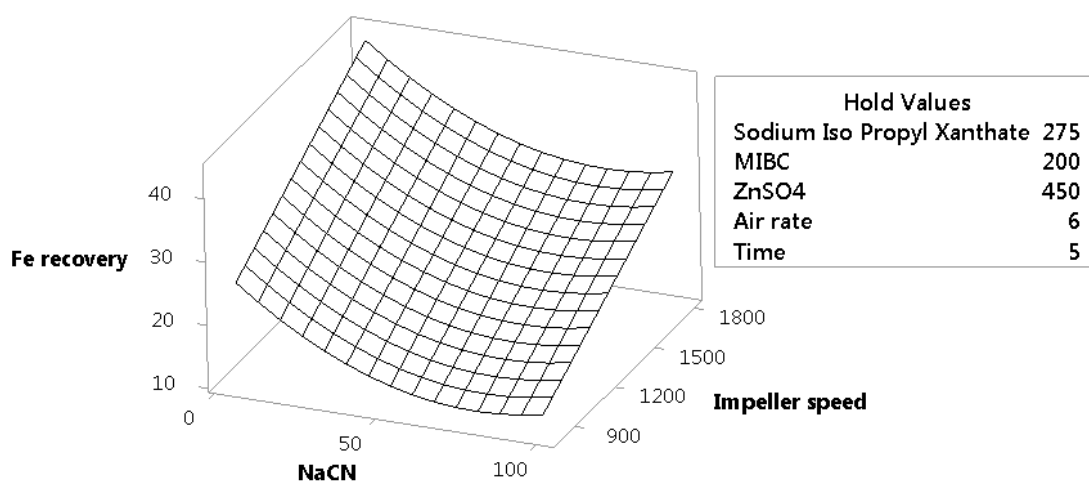
Figure 3.40. Effect of the NaCN dosage and impeller speed on Fe recovery.

3.4. DISCUSSION

Response optimizer in Minitab [17] was employed to find the optimum conditions to maximize the Pb grade, Pb recovery, Cu grade and Cu recovery using the model Equations 7, 8, 11 and 12, respectively within the experimental range of the study. The optimum flotation conditions found for maximum Pb grade of 43.8 % were 450 g/ton of sodium isopropyl xanthate, 50 g/ton of MIBC, 73g/ton of NaCN, 700 g/ton of ZnSO4, 3 l/min of air, 1200 rpm of impeller speed and 8 min of flotation time. Optimum flotation variables for maximum Pb recovery were found to be 113 g/ton of sodium isopropyl xanthate, 342 g/ton of MIBC, 5g/ton of NaCN, 206 g/ton of $ZnSO_4$, 3 l/min of air, 1800 rpm of impeller speed and 2 min of flotation time. Here maximum Pb recovery target was kept at 98 %.

For maximizing Cu grade, 450 g/ton of sodium isopropyl xanthate, 50 g/ton of MIBC, 200 g/ton of $ZnSO_4$, 800 rpm of impeller speed, and 2 min of flotation time were found to be the best fit values of significant operation parameters. A Cu grade of 7.2 % is predicted to be achieved at these optimal flotation conditions. For a target maximum Cu recovery of 98 % optimum flotation conditions were predicted to be 193 g/ton of sodium isopropyl xanthate, 350 g/ton of MIBC, 5 g/ton of NaCN, 200 g/ton of ZnSO4, 1800 rpm of impeller speed, and 2 min of flotation time. It was found in the study that NaCN and air rate do not effect the Cu grade significantly. In Cu recovery, air rate was not optimized as it did not contribute significantly to the Cu recovery.

Results of the response optimizer showed that in order to achieve the desired results, which were minimizing the grade and recovery of Zn and Fe and maximizing the grade and recovery of Pb and Cu, the following values of flotation variables should be used, 450 g/ton of sodium isopropyl xanthate, 50 g/ton of MIBC, 80g/ton of NaCN, 700 g/ton of ZnSO4, 3 l/min of air, 1254 rpm of impeller speed, and 8 min of flotation time. These optimum conditions yielded a maximum recovery for Pb and Cu to be 82.4 % and 66.14 %, respectively, and maximum grade for Pb and Cu to be 41.67 % and 5.35 %, respectively.

=

4. FLOTATION BEHAVIOR OF COMPLEX SULFIDE ORES IN THE PRESENCE OF BIODEGRADABLE POLYMERIC DEPRESSANTS

4.1. BACKGROUND

Chitosan is a well-known polymer and has found extensive use across different industries amongst which wastewater treatment [118], agriculture, food [119][120] and textile industry are some examples [121][122].To date effectiveness of chitosan has been demonstrated during flotation of single mineral or artificial mixtures of minerals [63].It has been efficaciously employed to selectively depress the recovery of chalcopyrite ($CuFeS_2$) to 30% in a mixture of chalcopyrite and galena (PbS) [64]. In single mineral flotation, it has been able to depress both galena and pyrite. However, during flotation tests at a pH of 4, it depressed 45 % more pyrite as compared to galena. This indicates its preferential adsorption on pyrite and thus it can selectively depress it [65]. It should be noted that all these observations were made in artificially mixed mineral samples. Motivated by these observations, this study was aimed to test the possibility of replacing sodium cyanide by chitosan polymer as a selective pyrite depressant in the bulk flotation of complex sulfide ore sample containing galena (PbS), chalcopyrite ($CuFeS_2$), sphalerite (ZnS), pyrite (FeS_2), dolomite (Ca $Mg(CO_3)_2$), and marcasite (a polymorph of pyrite).

4.2. METHODOLOGY AND MATERIALS

Details of materials and methods used in this study are given below. All lab scale equipment was provided by Missouri University of Science and Technology, USA.

4.2.1. Materials. A complex sulfide ore sample was obtained from a mine located in North America. Detailed characterization of the feed can be found in Section 3. Natural pure galena, pyrite, sphalerite and chalcopyrite mineral samples were purchased from Ward's Scientific USA. Each mineral was crushed using a manual mortar/pestle grinder. The fine powder of each mineral was utilized in zeta potential measurements. The chitosan polymer used in this work was of analytical grade. The polymer was purchased from ACROS USA Inc. The molecular weight of chitosan used in this study is 800,000 Da and its structure is given in Figure 4.1 [67].
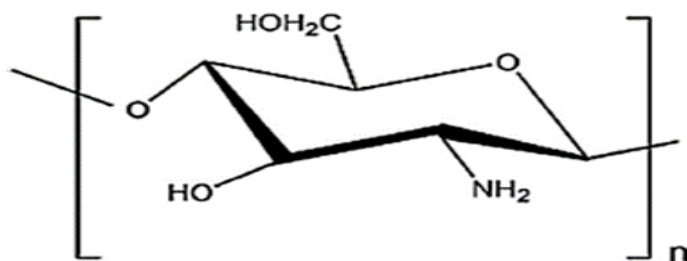
Figure 4.1. Structure of biodegradable polymer Chitosan Polymer.

Hydrochloric acid and sodium hydroxide (Fisher scientific USA) were used as PH modifiers. Sodium isopropyl xanthate (industrial grade) was used as a collector. Sodium cyanide and zinc sulphate were used as depressants. Both of these reagents were of industrial grade. The 4-Methyl-2-pentanol (MIBC) was purchased form ACROS USA Inc and was used as frother without further purification. Tap water was used throughout the tests unless otherwise stated.

4.2.2. Methods. Details of flotation experiments. Zeta potential measurements for electrokinetic studies and froth stability tests performed to examine the stability of the froth in case of chitosan polymer are illustrated below.

4.2.2.1. Batch flotation tests. Bulk flotation of galena and chalcopyrite was carried out in Denver flotation cell with an impeller diameter of 3.88 inches and a 2-liter flotation tank. A feed slurry of 30 % solids was used in all experiments. Unadjusted pH of 7.9 was maintained in all the flotation experiments. Depressants (polymers, sodium cyanide and zinc sulphate) were added first followed by the addition of xanthate collector. Frother was the last reagent to be added. Dosages of sodium cyanide, zinc sulphate, sodium isopropyl xanthate & MIBC were kept the same for all flotation experiments at a dosage of 2.26 g/ton, 680 g/ton, 317 g/ton and 470 g/ton of ore, respectively. These dosages were found to be optimum as per plant studies. Agitator was set at a rotation rate of 1000 rpm. Air flow rate was kept at 6 liter /min. Agitator speed and airflow rate were also kept constant during all flotation experiments. Four sets of flotation tests were carried out. In the first set, no depressants were used and the ore was floated in the presence of the collector and the frother as the only reagents. Second set of flotation experiments was performed using conventional depressants sodium cyanide and zinc sulphate. Third set of flotation experiments was carried out using chitosan as the only depressant. Four different dosages 50 g/ton, 100 g/ton and 300 g/ton and 500g/ton of chitosan were tested. In the fourth and last set, NaCN was tested at dosages of 50 g/ton, 100 g/ton, 300 g/ton and 500g/ton to be compared to the chitosan over the same dosage amounts. The dosages of all the reagents used are given in Table 4.1. After flotation, both the froth products (concentrates) and tailings were collected, dried, weighed, and assayed

for Cu, Pb, Zn, and Fe contents. The elemental analysis of the concentrate and tailings products was calculated using Scanning Electron Microscopy equipped with Energy Dispersive X-ray Spectroscopy (SEM-EDS). Various products obtained from flotation process were pressed into 0.5 inch diameter pellets using 3851-0 Carver Hydraulic press (Carver Inc. Wabash, USA). These pellets were coated with gold palladium powder using a sputter-coater (Hitachi E-1030). After coating, Energy-Dispersive X-ray Spectroscopy (EDS) analysis of the samples was carried out using Hitachi Model S-4700 field-emission microscope. Accelerating voltage was kept at 25 kV, emission current at 10.00 μAmp, working distance of 12mm, and magnification at 400x. Results of the EDS analysis were gathered and analyzed by EDAX Inc. Genesis software [67].

Table 4.1. Reagent (g/ton of ore) used in the different sets of flotation experiments [67].

Experiment sets	NaCN (g/ton)	ZnSO$_4$ (g/ton)	Sodium Iso propyl xanthate (g/ton)	MIBC (g/ton)	Chitosan (g/ton)
First	0	0	317	470	0
Second	2.26	680	317	470	0
Third	0	0	317	470	50,100,3 00,500
Fourth	50,100,300, 500	680	317	470	0

4.2.2.2. Zeta potential measurement. The mineral samples purchased from Wards Science were ground in an agate mortar. The mineral suspensions containing 0.05 wt % solids in 1 mmol/L KNO_3 were sonicated for 15 min then allowed to settle for 5-10 min. The pH of all the suspensions was maintained at a value of 7.9. Zeta potential measurements were carried out using Zetasizer nano ZS, ZEN3600, by Malvern Instruments Limited, Worcestershire, UK. Laser Doppler Micro-electrophoresis was used to measure the velocity of mineral particles in the solution under an electric field. Smoluchowski model was then used to calculate zeta potential.

4.2.2.3. Froth stability tests. For each flotation experiment an identical froth stability experiments was run. All conditions were kept same as in the flotation experiment, except the size of the cell used. In Froth stability experiments an especially designed high wall cell was used to prevent the overflow of froth. This gave an opportunity to record the rise of froth in the cell and to measure its velocity and maximum equilibrium height. The set up for froth stability experiment is shown in Figure 4.2.

After introducing air in the cell, a five minute video depicting the rise of froth was recorded. Video was then analyzed through video analysis software "Tracker" to calculate the maximum equilibrium height and rising velocity of the froth. A paper scale was attached at one end of the cell to calibrate the software measuring tool. A mass point was used to track the height of the froth after every 200 frames. Two graphs were plotted by the software elaborating the relationship between Time (second) vs height (cm) and Time (sec) vs velocity (cm/sec) (Figure 4.3).
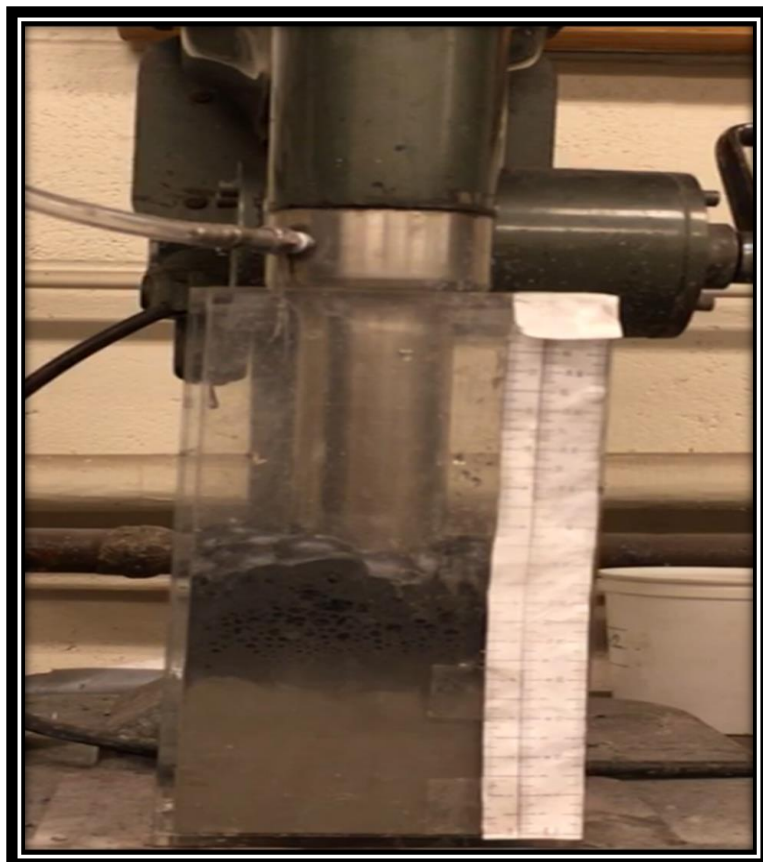
Figure 4.2. Froth stability experimental set up with high wall cell to prevent overflow of froth.

4.3. RESULTS

In this study performance of the polymer chitosan as a selective pyrite depressant was investigated. In this regard, recovery of lead, copper, zinc and iron elements was calculated in the froth products in the presence of chitosan at different dosages and compared with the recoveries of these elements when NaCN was used as a depressant.

Recovery values were in turn compared with the results obtained when flotation was conducted without any depressants.
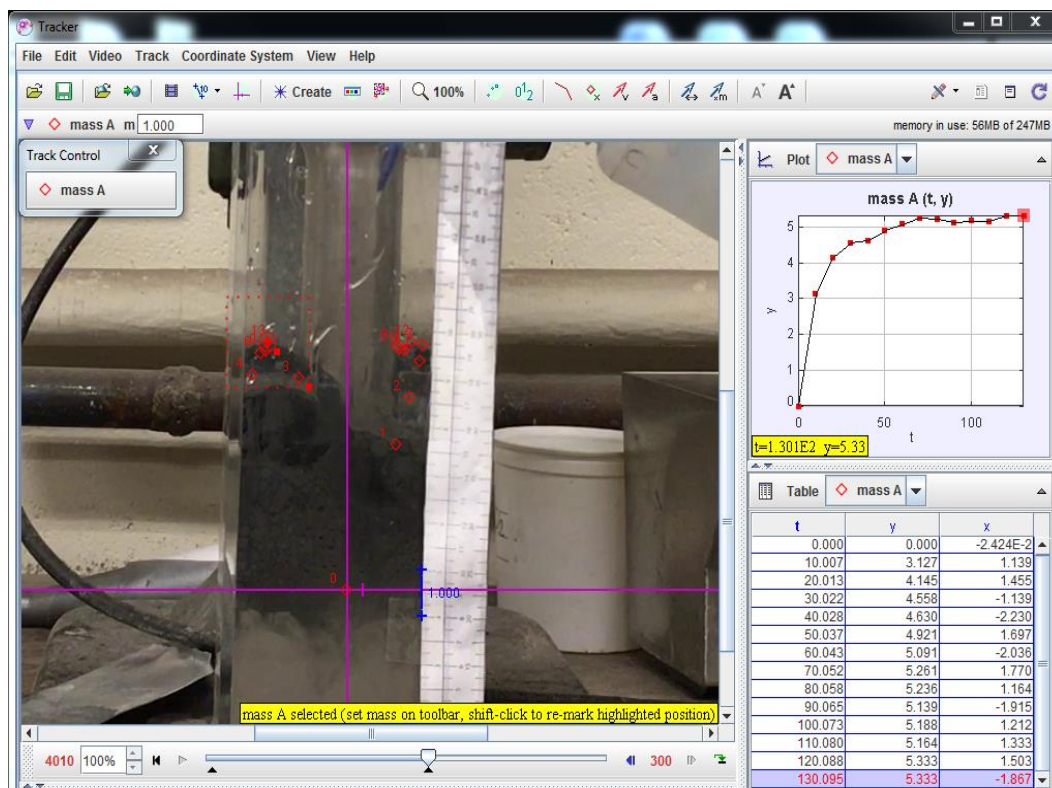
Figure 4.3. Tracker software plotting graph between y (height of froth in cm) vs
t (time in seconds).

4.3.1. Zeta Potential. Zeta potential measurements were conducted on mineral

suspensions with and without the addition of chitosan polymer to fundamentally explore

and compare the surface properties and interaction mode of the polymer with galena,

pyrite, chalcopyrite &sphalerite. As shown in Figure 4.4, the particles of all the minerals

were negatively charged at pH 7.9 with pyrite has the largest negative charge value of ~ -

36mV compared with – 7.5 mV ~ , -20 mV, and -18.5 mV for galena, chalcopyrite, and

sphalerite, respectively. These values are consistent with the values reported in literature

at similar pH range [123], [124]. Addition of chitosan polymer to mineral suspensions

resulted in increasing the values of surface charge to more positive values for all minerals

which means that chitosan was adsorbed on the surface of these minerals. For example, at 500g/ton of polymer, the zeta potential value of galena, chalcopyrite, pyrite & sphalerite increased from -7.5, -20 ,– 36 & -18.5 mV to +12, -10 , +5, and 4.5 mV, respectively. Figure 4.4 also exhibited that as the dosage of the polymer increased, the measured value of surface charge become more positive for all minerals. For example, increasing the chitosan dosage from 50 g/t to 100 g/t, resulted in increasing the value of zeta potential of pyrite suspensions from -12.3 to 13.4 mV, respectively. As expected and shown in Figure 4.4, chitosan polymer has stronger interaction with pyrite minerals compared to galena and chalcopyrite. At 100 g/t of chitosan, the value of zeta potential of pyrite suspension dramatically shifted from -36 to +10 mV while in the case of galena, the value of zeta potential slightly shifted from -7.5 to -1.9 mV. Moreover, the interaction of chitosan with chalcopyrite surfaces is stronger in comparison with galena. The zeta potential value of chalcopyrite suspensions was shifted from -20 to -8mV at 100 g/t of chitosan. Zeta potential of sphalerite increased from -18.5 to 5.4. Sphalerite will not be discussed further as it is out of scope of this study and another research project. The results were very consistent with what was previously published in literature when chitosan was used in the flotation of model sulfide mineral suspensions [125]–[127][128][124][123][129].

The adsorption mechanism of chitosan on sulfide minerals has not been comprehensively explained yet. There are only few studies that attempted to examine the adsorption behavior and elucidate the selectivity of chitosan towards pyrite and chalcopyrite compared to galena. In general, the interaction mechanism between chitosan and certain ion on mineral surfaces is due to chelation [130][131][132] . Both amino

groups (-NH$_2$ and O=C-NH$_2$) and the hydroxyl groups (C-OH) are anticipated to be the major binding site for chitosan adsorption on mineral surfaces [133][134]. It has been also reported that the adsorption capacity of chitosan and the consequent formation of polymer-ion complex can be influenced by many factors such as solution pH [135] , physical type of chitosan and the degree of deacetylation [136][137]. X-ray photoelectron spectroscopy were used to understand the selective adsorption of chitosan on chalcopyrite-galena mixtures as well as pyrite-galena mixtures [64]. In their work, they compared the binding energy values of mineral surfaces before and after treatment with chitosan polymer. In the case of comparative adsorption of the chitosan on chalcopyrite versus galena, results indicated that chitosan adsorbed on both minerals with larger binding energy shift of amino groups in the case of chitosan-chalcopyrite system compared with chitosan-galena system. More binding energy shifts reflects a stronger adsorption of the polymer on mineral surface. Result suggested that that in the case of chalcopyrite, both amine group and amide group in the chitosan molecules are involved with the formation of ammonium (protonated amine) complex which was absent in the case of galena-chitosan system. The larger binding energy shift of amino groups and the appearance of ammonium complex on the surface of chalcopyrite suggest chemical adsorption rather than a physiosorption which was the proposed mode of adsorption of chitosan on galena. Similar surface studies using XPS were performed on chitosan/pyrite system. The results suggested the formation of protonated amine on the surface of pyrite after chitosan adsorption with large binding energy shift of amine groups in chitosan molecules from 399.5 eV before adsorption to 399.8eV after adsorption suggested that chemical adsorption rather than physiosorption may be occurred between chitosan and

pyrite surface. Other studies [138] suggested that the preferential adsorption of chitosan on different mineral surfaces is related to the electron affinity of constituent metals. The higher the electron affinity of the constituent metal, the stronger is the interaction between the amine groups in chitosan molecules and the mineral surface. Thus, chitosan adsorb more preferentially on chalcopyrite surface compared to galena since the electron affinities of copper ions and iron ions are larger than galena.
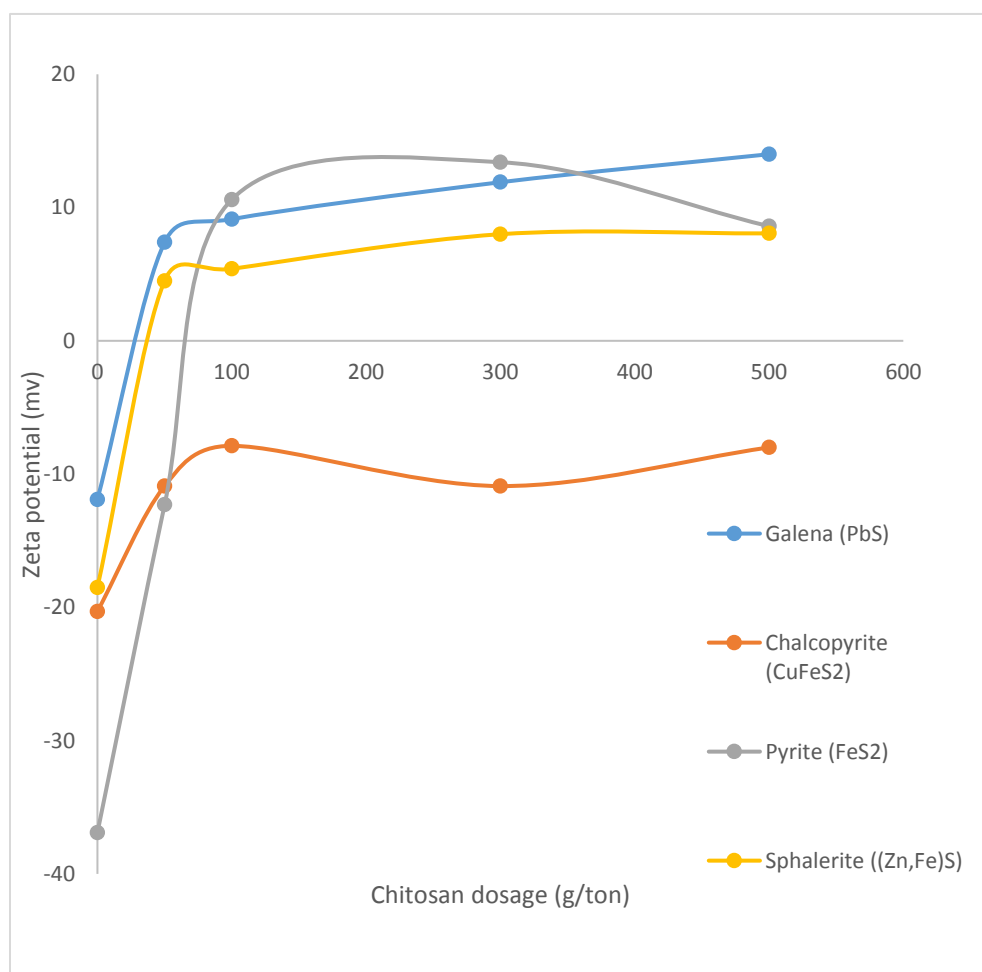
Figure 4.4. Zeta potential measurements of mineral suspensions as a function of chitosan dosage at pH ~ 8 [67].

4.3.2. Flotation Experiments. Details of flotation experiments regarding **b**aseline experiments using Sodium Cyanide (NaCN)**, i**nfluence of Chitosan dosage on the flotation performance sulfide minerals**, i**nfluence of flotation time on the recovery of galena, chalcopyrite and pyrite in the presence of chitosan polymer**,** and froth stability and performance are given below.

4.3.2.1. Baseline experiments using Sodium Cyanide (NaCN). From literature the dosages to be tested for chitosan were selected to be 50,100,300 & 500 g/ton. These dosages were chosen as the polymers like Polyacrylamide (PAM) and its derivatives have been applied in sulphide mineral flotation with the same dosages [139]. Although initial experiments suggested 2.2 g/ton of NaCN as optimum dosage, still NaCN was tested at dosages of 50, 100, 300 & 500 g/ton to be compared to chitosan at same dosages. Figure 4.5 shows the results of flotation experiments with optimum chitosan dosage of 50 g/ton with equivalent NaCN dosage.
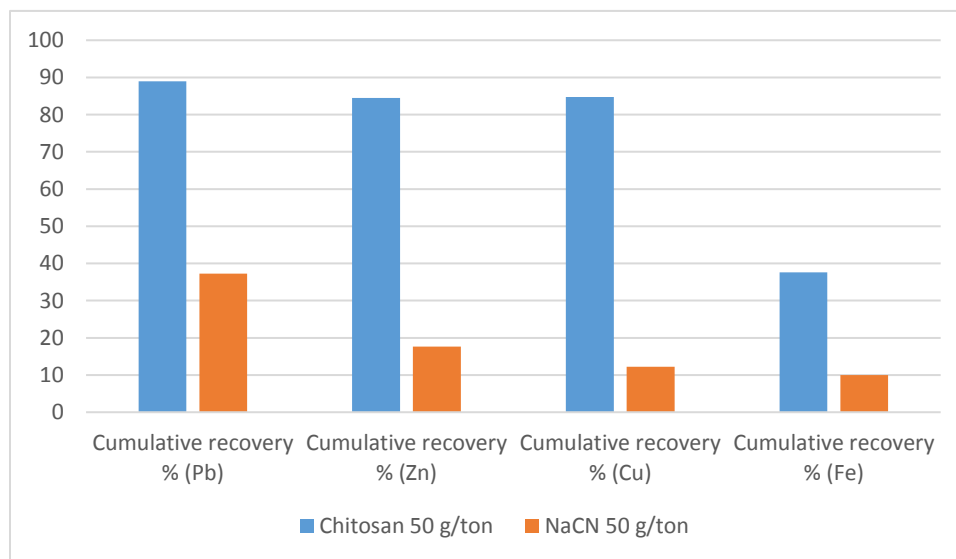
Figure 4.5. Flotation results of chitosan & NaCN at a dosage of 50 g/ton [67].

It can be seen from Figure 4.5 that NaCN at a dosages of 50 g/ton greatly reduced the recovery of valuable metals like copper and lead along with zinc & iron. Similar trend was observed for NaCN at higher dosages of 100,300 & 500 g/ton. As a result, keeping in mind the economics and efficiency of flotation process, an optimum dosage of 2.26 g/ton of NaCN was found to be most feasible to be compared to chitosan dosages of 50 to 500 g/ton.

4.3.2.2. Influence of Chitosan dosage on the flotation performance sulfide minerals. Four different dosages of chitosan polymer were used in the flotation experiments. Results were compared with the flotation results in presence and absence of optimum dosage of conventional depressants which is the NaCN. Figures 4.6, 4.7, 4.8 and 4.9 show the flotation recoveries and concentrate grades of lead, copper, iron and zinc respectively.
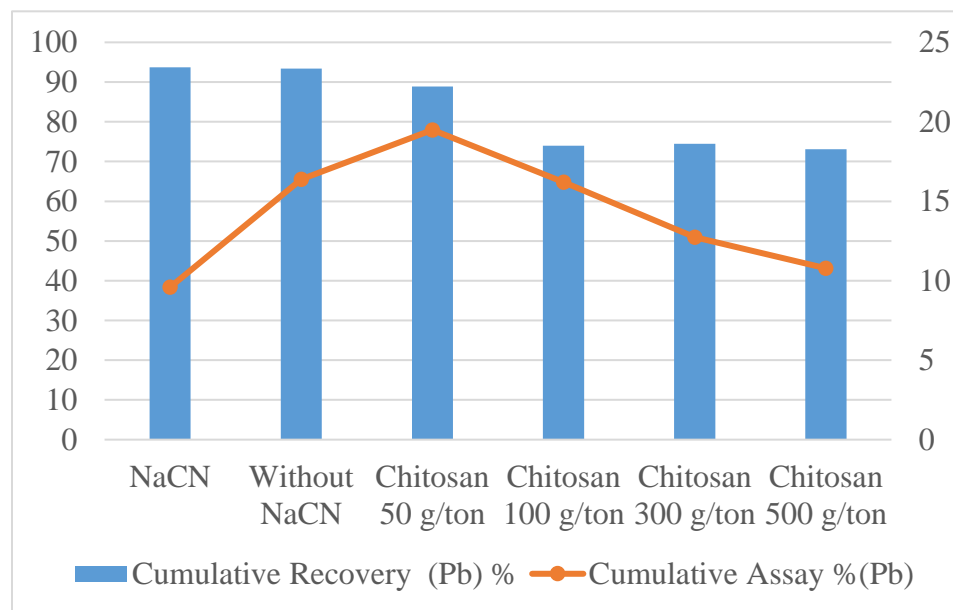
Figure 4.6. Lead recovery and concentrate grade as a function of chitosan dosage in comparison with NaCN depressant [67].
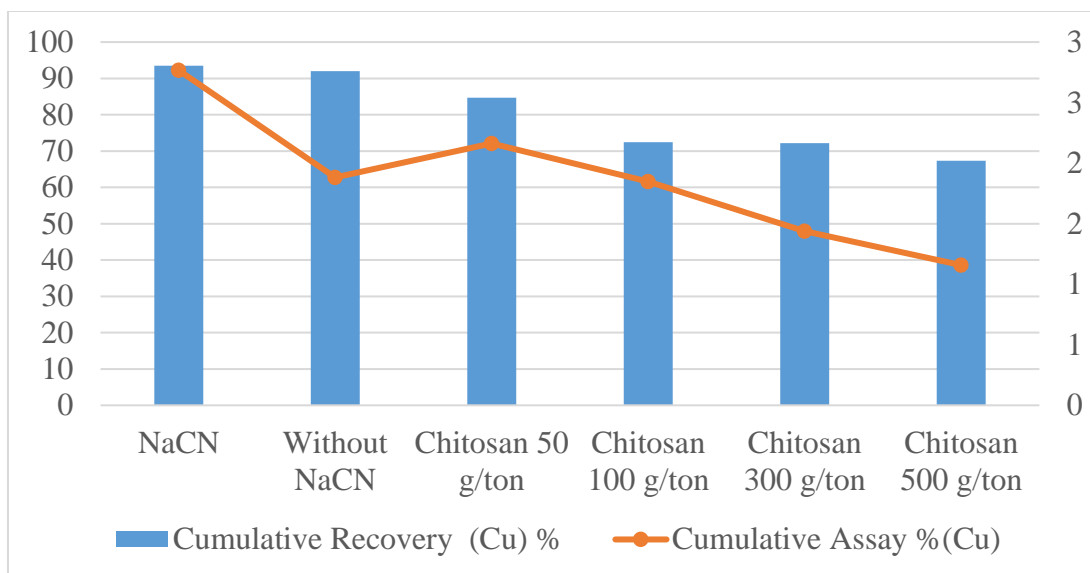
Figure 4.7. Copper recovery and concentrate grade as a function of chitosan dosage in comparison with NaCN depressant [67].
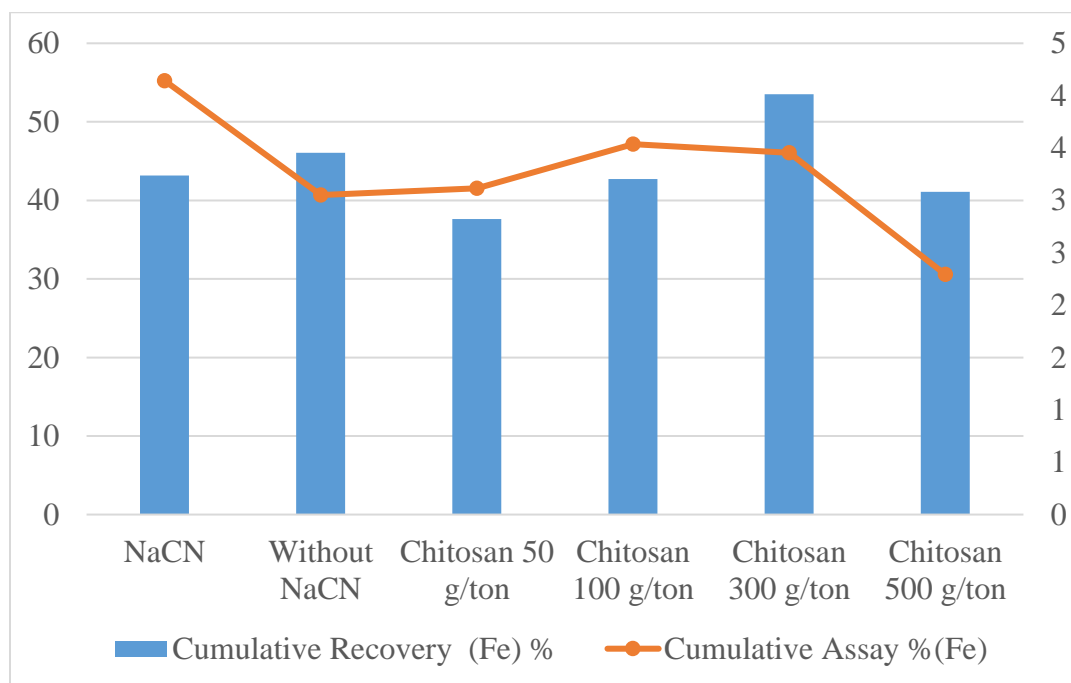
Figure 4.8. Iron recovery and concentrate grade as a function of chitosan dosage in comparison with NaCN depressant [67].
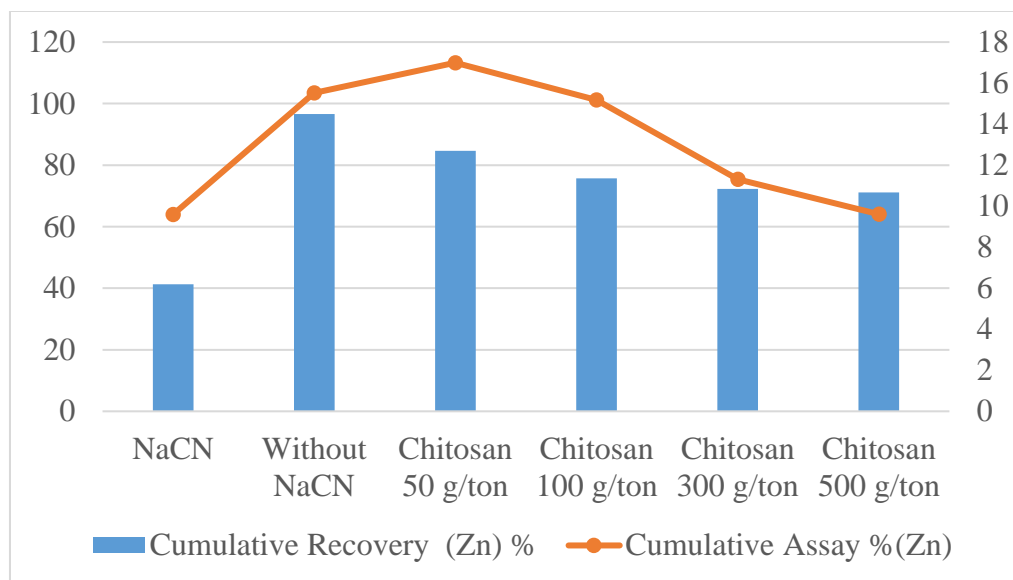
Figure 4.9. Iron recovery and concentrate grade as a function of chitosan dosage in comparison with NaCN depressant [67].

NaCN reduced zinc recovery by 42 % as compared to chitosan at 50 g/ton (Figure 4.9). This was understandable as $ZnSO_4$ which is a depressant of sphalerite was added with NaCN and not with chitosan. Testing zinc recovery with a combination of chitosan and $ZnSO_4$ was not in the scope of this study and will be carried out as separate research project. At a dosage of 50g/ton, chitosan was able to depress iron recovery more than 5.6 % than the conventional depressants (Figure 4.8). Chitosan did also reduce the recovery of lead by 4.8 % (Figure 4.6) and that of copper by 8.8 % (Figure 4.7) as compared to conventional depressant NaCN, which was not desirable as bulk flotation of chalcopyrite and galena was the major focus of this experiment. However chitosan at 50 g/ton proved to be a better and more selective depressant for pyrite in bulk flotation of galena and chalcopyrite. Results also revealed that increasing the dosage to 100 g/ton and up, caused a decrease in the recovery of both galena and chalcopyrite. As for the enrichment of

minerals in the concentrates, at 50g/ton of chitosan, the concentrate grade of galena increased to 20% compared to 10% when NaCN was used. However, the concentrate grade of chalcopyrite and pyrite slightly decreased from 2.7% and 4.2% with NaCN to 2.2% and 3% with 50g/t chitosan, respectively. As for pyrite, it is interesting to see that increasing the polymer dosage to 100 g/ton and higher resulted in an increase in the recovery of pyrite in the concentrate which might be due to competitive adsorption at higher dosages of polymer. In general, the preferential adsorption of chitosan on pyrite and chalcopyrite is due to the ability of the polymer to chemically bond to the mineral surface which results in stronger adsorption compared to galena. It was proposed that [129] the amine groups and the hydroxyl group in the chitosan structure (Figure 4.1) can react with the mineral surfaces and form a stable complex through chemisorption mechanism which resulted in its stronger flotation depression compared to galena. The adsorption of chitosan polymers on galena is anticipated to physiosprotion mechanism through hydrophobic interactions between the mineral surface and the amide group of chitosan molecules. In single mineral flotation tests it was found that chitosan was a selective depressant for galena-sphalerite and galena-pyrite but not as such for galena - chalcopyrite mixture at higher pH than 3 [140].This was confirmed by the zeta potential studies carried out in this study (Figure 4.4) which show preferential adsorption of chitosan on sphalerite and pyrite as compared to chalcopyrite and galena. This can therefore be concluded that chitosan can be introduced as a depressant for sphalerite and pyrite in bulk flotation of chalcopyrite and galena. As stated previously, sphalerite discussion will be topic of another research project.

4.3.2.3. Influence of flotation time on the recovery of galena, chalcopyrite and pyrite in the presence of chitosan polymer. At an optimum dosage of 50 g/ton of chitosan, froth products were collected after 0, 2, 4 & 8 mins of flotation. After 4 minutes of flotation 86.3 % of cumulative lead recovery, 79.6 % of cumulative copper recovery & 33% of cumulative iron recovery was observed as shown in Figure 4.10. Doubling the flotation time to 8 minutes increased recovery of lead and copper only by 2.6 & 5%, respectively. However, the undesirable recovery of Fe in the product increased by 4.5%. This shows that most of lead and copper are floated in the initial 4 minutes of flotation. After 4 minutes selective flotation ceases and all minerals are recovered at the same rate. It therefore seems that depending upon the plant economics, four minutes of flotation time may be regarded as optimum.
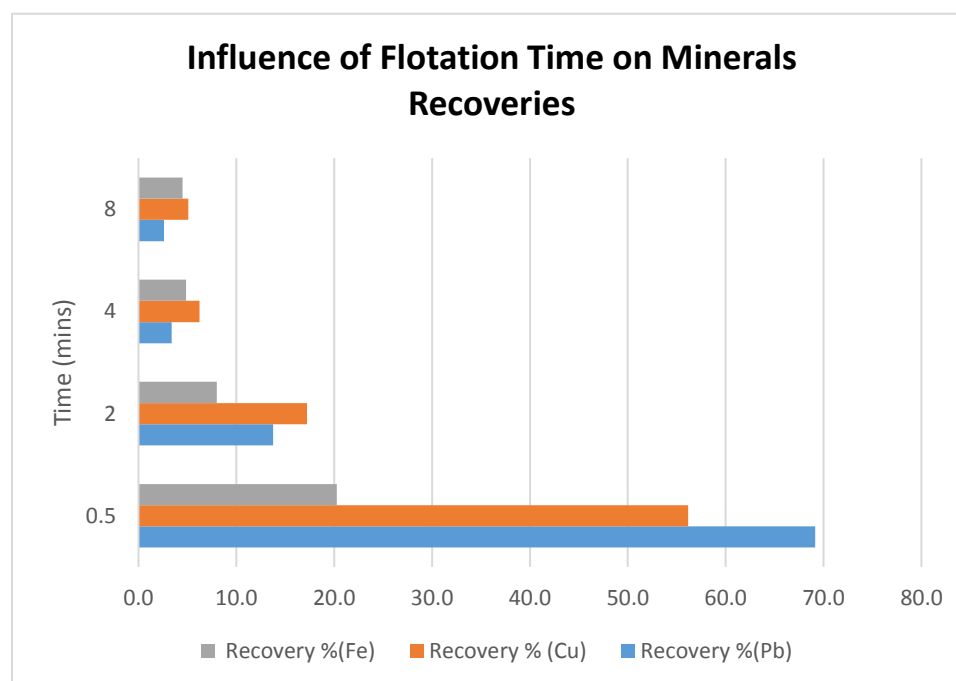
Figure 4.10. Influence of flotation time on flotation recoveries of galena, pyrite and chalcopyrite at a chitosan's dosage of 50 g/ton [67].

4.3.2.4. Froth stability and performance. Dynamic froth stability was calculated at different dosages of chitosan and NaCN to see the effect of these on froth performance and stability. Figures 4.11, 4.12, and 4.13 show these effects.
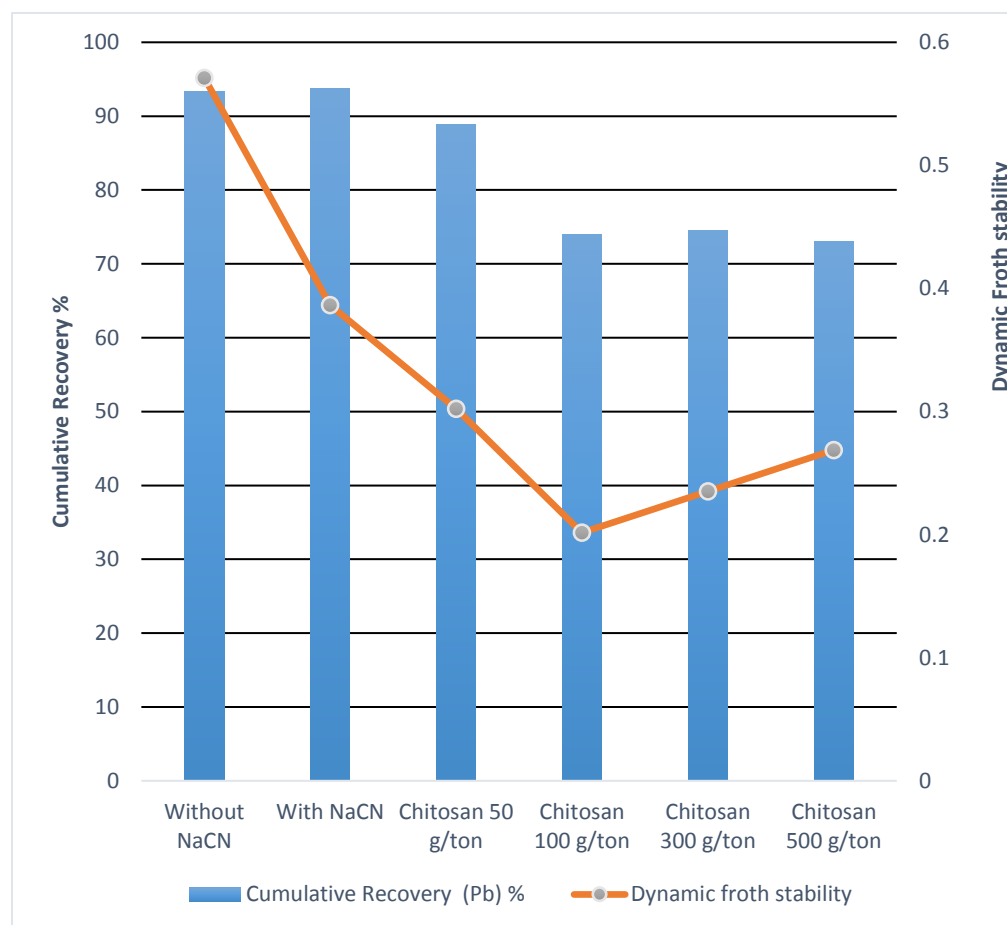
Figure 4.11. Effect of Chitosan dosage on dynamic froth stability and Pb recovery.

It can be seen from Figures 4.11, 4.12, and 4.13 that dynamic froth stability tends to decrease with increase in chitosan dosage. Decrease in stability can be attributed to less number of solid particles in froth due to depressing effect of chitosan.
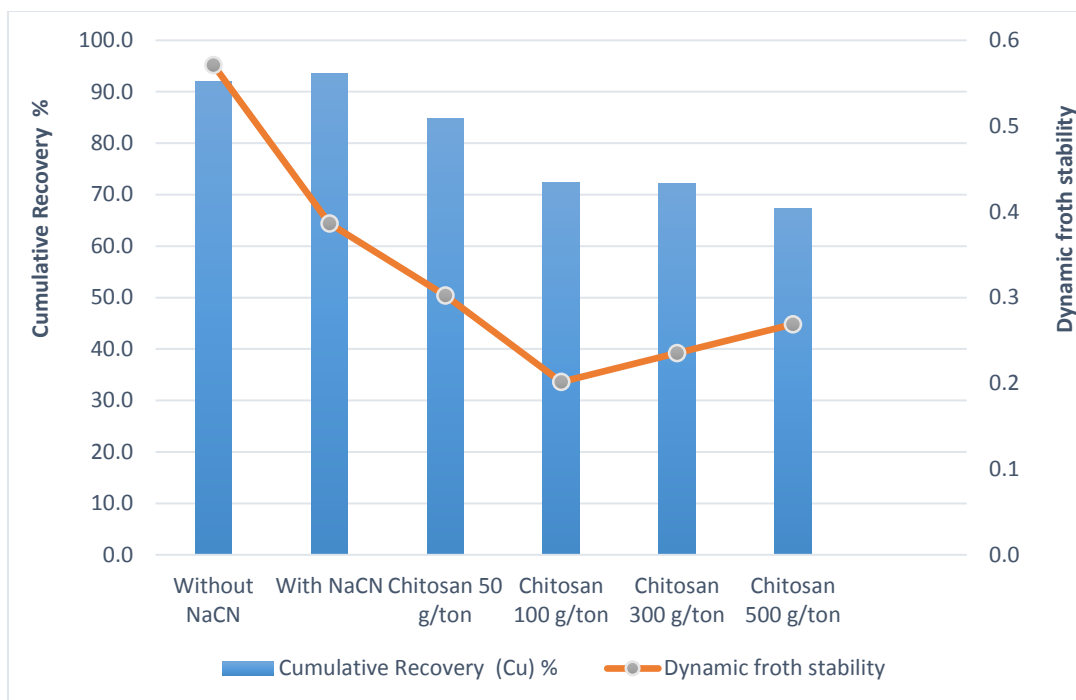
Figure 4.12. Effect of Chitosan dosage on dynamic froth stability and Cu recovery.
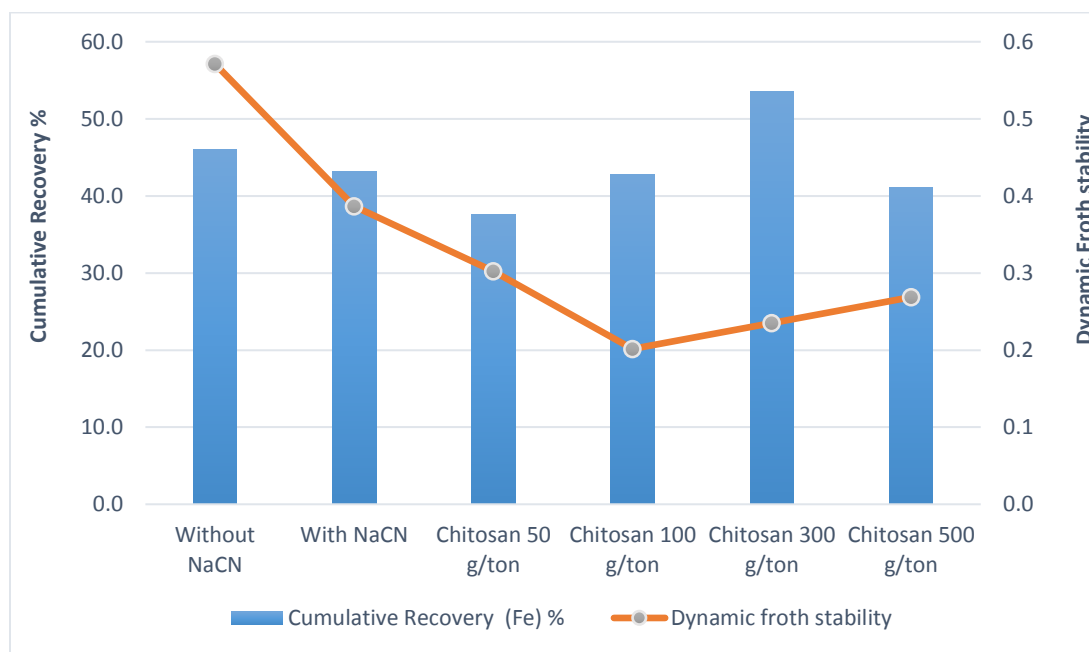
Figure 4.13. Effect of Chitosan dosage on dynamic froth stability and Fe recovery.

4.4. DISCUSSION

The objective of this study was to investigate the potential of replacing the toxic depressant NaCN used in the flotation of sulfide minerals to depress pyrite, by the biodegradable chitosan polymer. Bulk flotation tests of sulfide mineral samples contain galena; chalcopyrite; pyrite and sphalerite were carried out in laboratory scale Denver flotation cell to compare the depression capability of NaCN and chitosan polymer, separately. It was found that chitosan was effective in depressing pyrite minerals. Sphalerite depression is out of scope of this study. Chitosan depressed 5.6% more pyrite as compared to conventional depressants. It was however noted that at higher dosages, chitosan depressed chalcopyrite and galena which was not desired in this case. The optimum dosage of chitosan was 50 g/ton. At this dosage, galena had the highest recovery while pyrite had the lowest recovery. Findings obtained from zeta potential measurements were consistent with those obtained from flotation test. Zeta potential measurements of galena, chalcopyrite and pyrite suspensions before and after chitosan addition revealed that chitosan has stronger and preferential interaction with pyrite surface as indicated by the dramatic shift in the zeta values of the mineral before and after the addition of chitosan. This study shows that chitosan has a bright prospect to be used in sulfide mineral flotation as iron Sulfide depressant.

5. EFFECT OF NANOPARTICLES ON DYNAMIC FROTH STABILITY AND FLOTATION PERFORMANCE OF COMPLEX SULFIDE ORE

5.1. BACKGROUND

Foams are the end products in a lot of processing industries including mining, food, and cosmetics. This makes understanding foam formation and stability very important. Foams are defined as mixtures of immiscible fluids containing a dispersed gas phase and a continuous liquid phase [141]. In mineral processing industry foam/froth stability and structure is very important as froth stability is the key factor determining the efficiency of the process. If froth collapses, hydrophobic mineral particles drop back into the flotation cell, thus causing loss of the product [73], [87], [142], [143]. To prevent collapse of the foam/froth and increase its stability, different industries use proteins and surfactants to modify the liquid gas interface of the foam [144]. In mineral flotation, frothers, along with feed particle size, particle hydrophobicity, and particle concentration play a vital role in the stability and mobility of the froth phase. Achieving critical values of these factors can help immensely in the stabilization of froth [82][19].Recently, interest has been growing among the researchers to examine the ability of nanosized particles to stabilize the foams. Nanosized particles are believed to act as surfactants when adsorbed to a fluid-fluid interface [144][121], [145][146][94], [147]–[150]. It has been found that nanoparticles have great ability to be adsorbed onto a liquid-air interface due to the high adsorption energies of these particles. Once adsorbed, these nanoparticles act as steric barriers inhibiting bubble coalescence resulting in very stable froths [42]. The aforementioned observations from the literature make a strong case for nanoparticles to be utilized in the froth flotation process to enhance the stability of froth.Nanoparticles

have not been used in mineral processing industry for this purpose to date. The objective of this study is therefore to investigate the possibility of controlling dynamic froth stability and flotation performance through nanomaterials in flotation of complex sulfide ores. Two types of nanomaterials, aluminum oxide (Al_2O_3) and silicon dioxide (SiO_2), are used in this study. This study is aimed to contribute towards making froth stability an easily controllable factor to enhance the efficiency of flotation performance.

5.2. METHODOLOGY AND MATERIALS

Details of the materials and methods used during this study are given below. All the lab scale equipment was provided by Missouri University of Science and Technology, USA.

5.2.1. Materials. Complex sulfide ore samples of Mississippi Valley-type (MVT) were obtained from a mine located in North America. This ore was characterized using various techniques. Detailed characterization of feed can be found in Section 3. In order to adjust the pH of the flotation pulp, hydrochloric acid and sodium hydroxide were used. Sodium isopropyl xanthate, sodium cyanide and zinc sulfate were used as collector, pyrite depressant and sphalerite depressant, respectively. Fisher Scientific, USA, was the provider of all these reagents. The 4-Methyl-2–Pentanol Isobutyl Carbinol (MIBC), which was used as a frother, was obtained from ACROS, USA Inc. All flotation reagents were used without further purification. Nanomaterials were obtained from Sky Spring Nanomaterials Inc., USA. The properties of the two nanoparticles used in this study are given in Table 5.1. All flotation tests were conducted using deionized water.

Table 5.1. Properties of nanoparticles used.

Material	Purity %	Particle size(nm)	Point of zero charge (PZC) (pH)
Gamma-Al2O3	99.9	20	6.2
SiO2	99.9	15-20	< 2

5.2.2. Methods. Nanoparticle suspensions was prepared by mixing one milligram (0.001 g) of sodium silicate in 40 mL of deionized water. After preparing sodium silicate solution, 0.14 g of nanoparticles was added to the solution. Nanoparticle solution was then sonicated to attain a stable suspension using vibra-cell sonicator from Sonics & Materials Inc., USA, as shown in Figure 5.1.

Once the sonicator was turned on, an energy knob was placed at level 4. The tuning button was then pressed to see if the power needle was below or above 20. If the power needle showed any value other than 20, the tuning knob was rotated until it approached 20. This ensured the probe crystal achieved resonance frequency. During the tuning process, the probe was kept in the air. After tuning, the probe was inserted into the beaker containing nanoparticle solution. The probe was kept one inch from the bottom of the beaker. The energy knob was moved from level 4 to 10. The start button was pressed to start the sonication process. The sonication process ran for 3 minutes.

Figure 5.1. Vibra-cell sonicator for stabilizing nanoparticle suspensions.

5.2.3. Design of Experiments. The face-centered rotatable central composite

design was used to design both the flotation and froth stability experiments. A central

composite design consists of a factorial or fractional factorial design having center points.

This factorial design is supplemented with a group of "star points" that help in estimate

the curvature of test results, as shown in Figure 5.2.

Rotatable face-centered central composite design is a form of central composite

design in which the star points are at the center of each face of the factorial space, so $\alpha = \pm 1$[151]. Table 5.2 lists the details of the experiment sets carried out during this study.

Each set consisted of two experiments. A total of 56 sets of experiments were performed.

Twenty-eight flotation experiment sets were carried out, including 14 sets of experiments

for each nanoparticle. Similarly, 28 sets of froth stability experiments were

performed, including 14 sets of experiments for each nanoparticle.
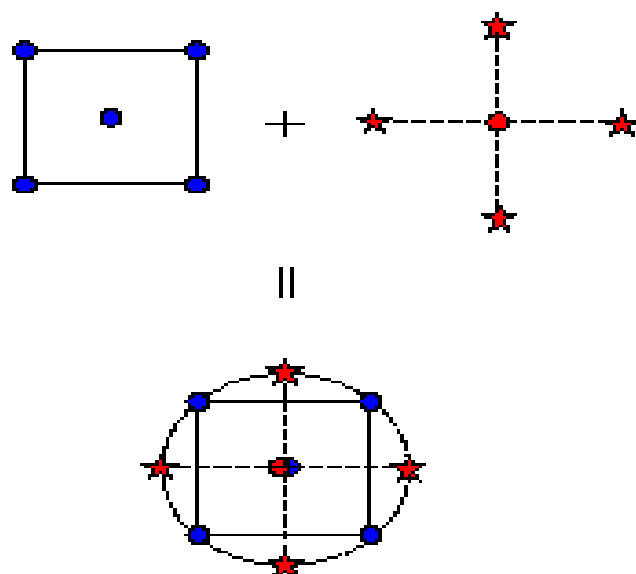
Figure 5.2. Central composite design.

5.2.3.1. Froth flotation experiments. Bulk flotation of galena and chalcopyrite

was carried out in Denver flotation cell with an impeller diameter of 3.88 in and a 1L

flotation tank. In all the experiments, unadjusted pH and solids concentration (as per

industrial application) were kept constant at 7.9 and 45% respectively. The optimum

operation parameters, which were found through statistical analysis in Section 3, were

also kept constant. The values of these operation parameters were 450 g/ton of sodium

isopropyl xanthate, 80g/ton of NaCN, 700 g/ton of $ZnSO_4$, 3 l/min of air, 1456 rpm of

impeller speed, and 8 min of flotation time. As frother (MIBC) has pronounced effect

on froth stability, so its value was also varied between 0 to 50 g/ton of ore. Two types of

Table 5.2. General experimental design for flotation and froth stability tests.

Std Order	Run Order	Pt Type	Blocks	Frother(g/ton)	Nanoparticle (g/ton) (Al_2O_3 & SiO_2)
1	1	1	1	0	0
6	2	0	1	25	5
2	3	1	1	50	0
5	4	0	1	25	5
7	5	0	1	25	5
3	6	1	1	0	10
4	7	1	1	50	10
8	8	-1	2	0	5
9	9	-1	2	50	5
10	10	-1	2	25	0
12	11	0	2	25	5
13	12	0	2	25	5
14	13	0	2	25	5
11	14	-1	2	25	10

nanoparticles, Al_2O_3 and SiO_2, were added before the frother in variable amounts to test

the effect of each on flotation performance. The sequence of reagent addition in froth

flotation experiments is given in Figure 5.3.
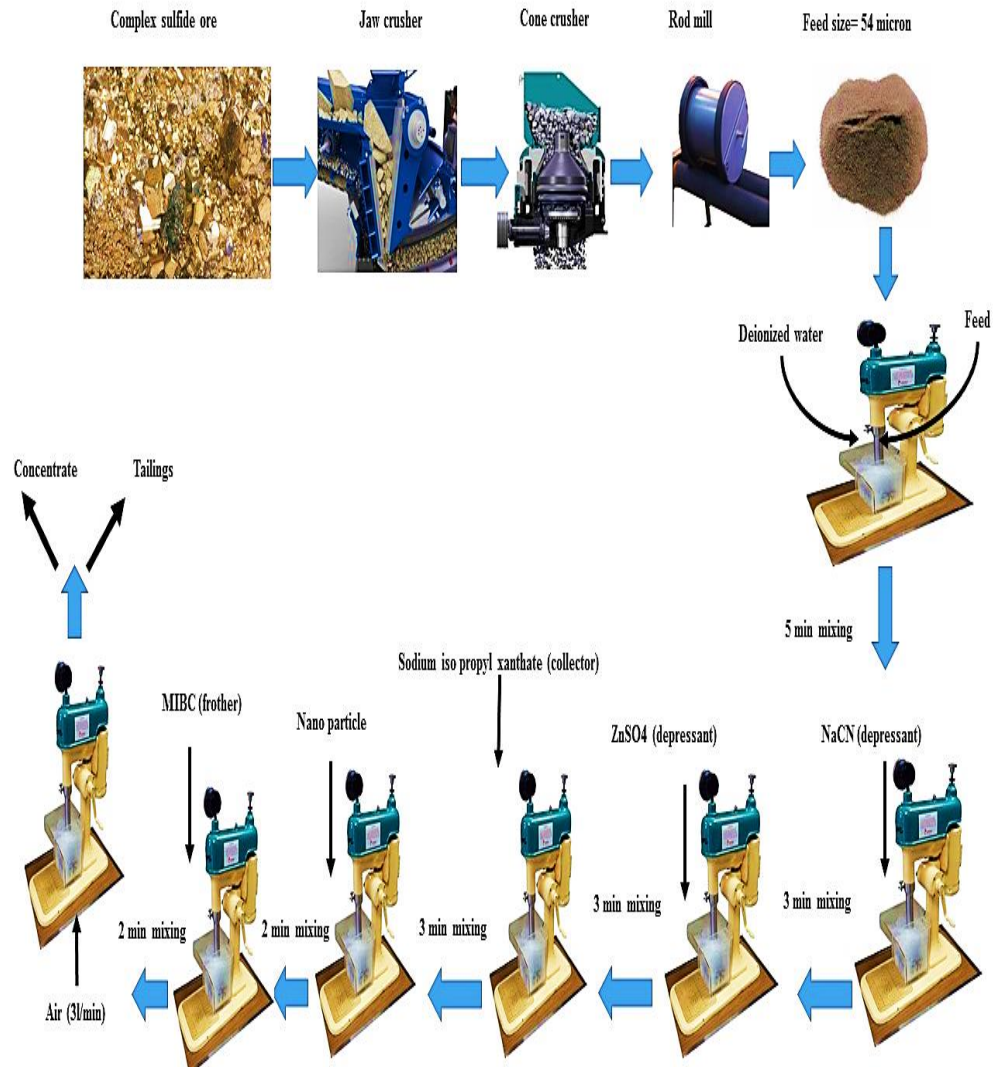
Figure 5.3. Sequence of reagent addition for froth flotation tests involving nano materials[152]–[156].

5.2.3.2. Froth stability experiments. For each flotation experiment, an identical froth stability experiments was run. All conditions were kept the same as in the flotation experiment, except the size of the cell used. In froth stability experiments, a specially designed high wall cell was used to prevent the overflow of froth. Further details of the experiments are discussed in Section 4.

5.3. RESULTS

Fifty-six sets of experiments using the face-centered central composite design method were designed and conducted. In these tests, collector (sodium isopropyl xanthate) dosage, impeller speed, air rate, pyrite depressant (NaCN) dosage, sphalerite depressant (ZnSO$_4$) dosage, and flotation time were kept constant. Only frother and nanoparticle dosage was varied to test the effect of these on flotation performance and froth stability. Each set consisted of two experiments. The results were analyzed using Minitab 17.0 software.

5.3.1. Froth Flotation Results. Fourteen sets of flotation experiments were performed for each type of nanomaterial to study its effect on flotation performance of bulk flotation of galena and chalcopyrite. After flotation, the froth (concentrate) was collected, dried, weighed and assayed for Pb, Cu, Zn, and Fe. The assays were determined using ICEP-OES and EDTA titration methods as applicable. Recovery was then calculated based on the dry concentrate weight (C), feed weight (F), feed assay of each element (f), and concentrate assay of each element (c). Table 5.3 shows the grade and recovery of different metals achieved in the ore when Al$_2$O$_3$ nanoparticles were used as flotation aid.

Grade and recovery of Pb, Cu, Zn and Fe achieved in case of application of SiO$_2$ nano material is depicted by Table 5.4.

5.3.2. Froth Stability Results. For each type of nanoparticle, 14 sets of froth stability tests were carried out to analyze the effect of nanoparticles on the dynamic froth stability of the flotation process. Data collected from froth stability tests using Al$_2$O$_3$ nanoparticles is shown in Figure 5.4.

Table 5.3. Grade and recovery of Pb, Zn, Cu and Fe plus dynamic froth stability obtained in case of flotation when Al_2O_3 was used as flotation aid.

Dynamic Froth Stability	47.3	44.68	55.26	37.3	40.9
Fe Recovery	6.54	3.069	8.349	4.83	6.24
Fe Grade (%)	2.280	2.470	2.652	1.872	2.189
Zn Recovery (%)	4.25	2.828	5.12	5.12	3.85
Zn Grade (%)	1.81	1.024	1.7961	1.95	2.1311
Cu Recovery (%)	45.87	12.27	50.96	47.88	48.99
Cu Grade (%)	2.85	1.5	3.49	3.2	3.38
Pb Recovery (%)	94.32	47.71	91.88	96.86	90.36
Pb Grade (%)	59.04	54.26	63.82	63.82	59.04
Al2O3 (g/ton)	5	0	10	0	5
Frother (g/ton)	25	0	50	50	25
Blocks	1	1	1	1	1
Pt Type	0	1	1	1	0
Run Order	1	2	3	4	5
Std Order	5	1	4	2	7

Table 5.3. Grade and recovery of Pb, Zn, Cu and Fe plus dynamic froth stability obtained in case of flotation when Al_2O_3 was used as flotation aid (cont.).

6	**3**	**9**	**10**	**8**	**11**	**13**	**14**	**12**
6	7	8	9	10	11	12	13	14
0	1	-1	-1	-1	-1	0	0	0
1	1	2	2	2	2	2	2	2
25	0	50	25	0	25	25	25	25
5	10	5	0	5	10	5	5	5
59.04	54.26	63.82	59.04	54.26	59.04	59.75	60.29	62.84
82.46	53.3	89.02	98.72	39.51	83.34	82.36	86.3	85.69
3.16	2.25	3.4	3.14	1.78	3.37	2.59	3.01	2.85
47.64	20.99	49.5	50.89	16.9	51.27	45.15	39.17	45.87
1.81	1.4848	1.41	2.2986	0.89	2.46	1.8	1.4704	1.82
3.974	2.91	4.56	3.974	2.828	3.974	3.85	3.974	4.41
2.350	2.652	2.262	1.872	2.262	2.652	2.262	2.3	2.1
6.79	9.05	6.512	4.22	4.76	9.152	6.29	5.988	6.38
49.36	26.32	46.28	41	35.5	40.78	45.74	40.9	47.96

Table 5.4. Grade and recovery of Pb, Zn, Cu and Fe plus dynamic froth stability obtained in case of flotation when SiO_2 was used as flotation aid.

Dynamic Froth Stability	30.78	33.74	52.98	30.72	36.20	37.66
Fe Recovery (%)	8.21	8.85	8.63	8.40	8.13	8.17
Fe Grade (%)	2.751	2.420	2.516	2.639	2.810	2.650
Zn recovery (%)	5.21	6.03	6.25	5.46	5.84	5.19
Zn Grade (%)	1.780	2.104	2.253	2.134	2.003	2.130
Cu Recovery (%)	53.62	27.75	62.2	61.8	61.21	56.67
Cu Grade (%)	3.14	2.33	3.36	3.98	3.23	3.49
Pb Recovery (%)	96.92	57.03	82.85	86.48	92.62	96.74
Pb Grade (%)	55.97	47.15	44.14	57.28	58.52	58.75
SiO2 (g/ton)	5	0	10	0	5	5
Frother (g/ton)	25	0	50	50	25	25
Blocks	1	1	1	1	1	1
Pt Type	0	1	1	1	0	0
Run Order	1	2	3	4	5	6
Std Order	5	1	4	2	7	6

Table 5.4. Grade and recovery of Pb, Zn, Cu and Fe plus dynamic froth stability obtained in case of flotation when SiO_2 was used as flotation aid (cont.).

3	9	10	8	11	13	14	12
7	8	9	10	11	12	13	14
1	-1	-1	-1	-1	0	0	0
1	2	2	2	2	2	2	2
0	50	25	0	25	25	25	25
10	5	0	5	10	5	5	5
57.37	52.09	59.27	53.36	57.67	61.05	56.13	57.26
55.49	98.75	99.24	53.42	89.07	92.58	95.8	94.54
3.18	3.32	3.26	2.66	3.35	3.18	3.35	3.17
30.3	56.64	53.86	26.24	50.97	40.64	56.4	51.83
1.447	2.130	2.250	1.712	1.932	2.050	2.003	2.070
2.97	5.87	5.68	4.62	4.44	5.19	6.35	5.26
3.250	2.517	2.801	3.620	3.260	2.751	2.630	2.820
5.94	8.48	9.25	7.36	7.58	7.98	8.21	9.35
20.68	41.08	36.72	26.86	40.48	37.40	37.62	36.60
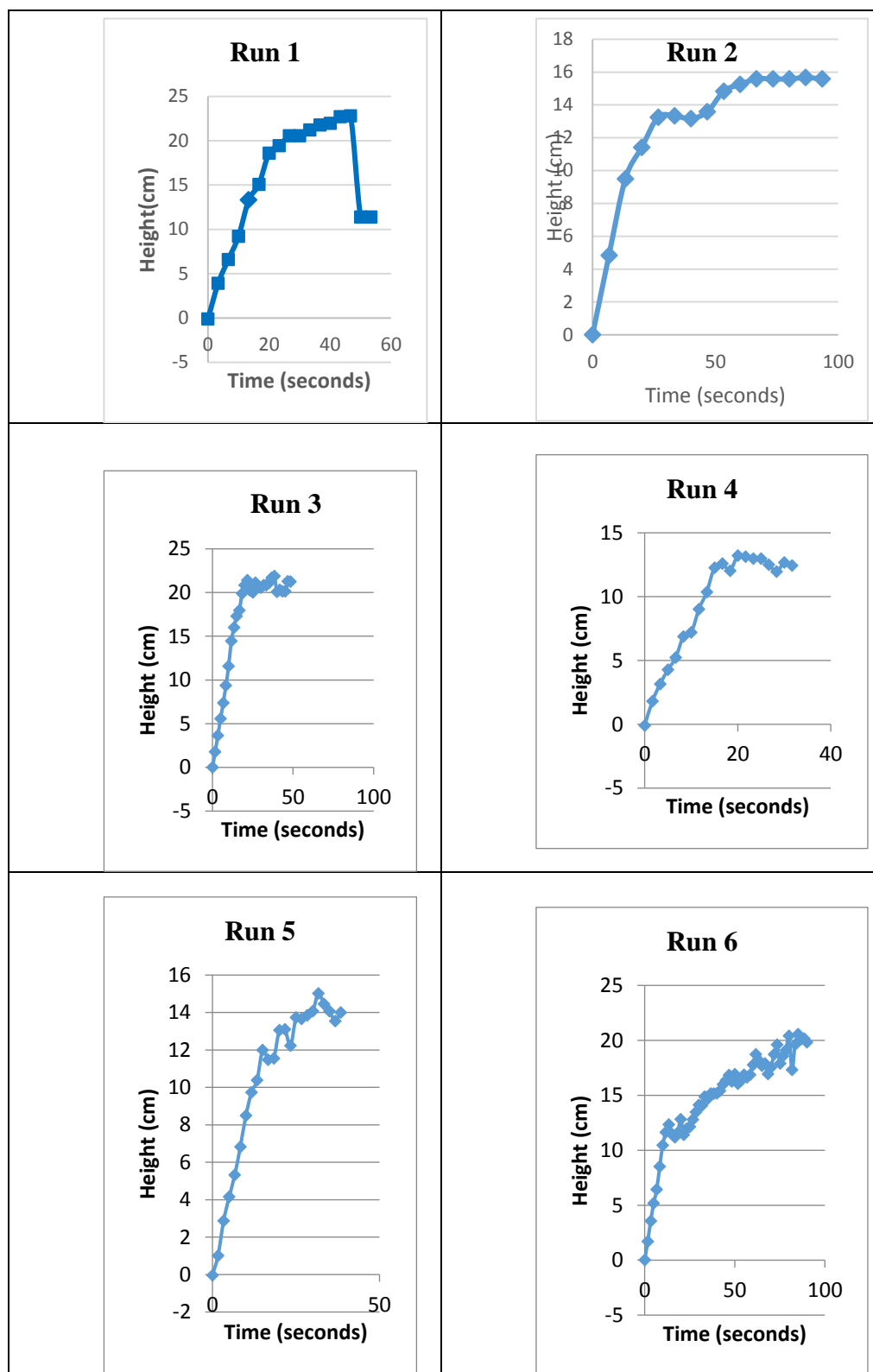
Figure 5.4. Time vs froth height data obtained via tracker software for 14 experimental runs conducted using Al_2O_3 nanoparticles as flotation aid.
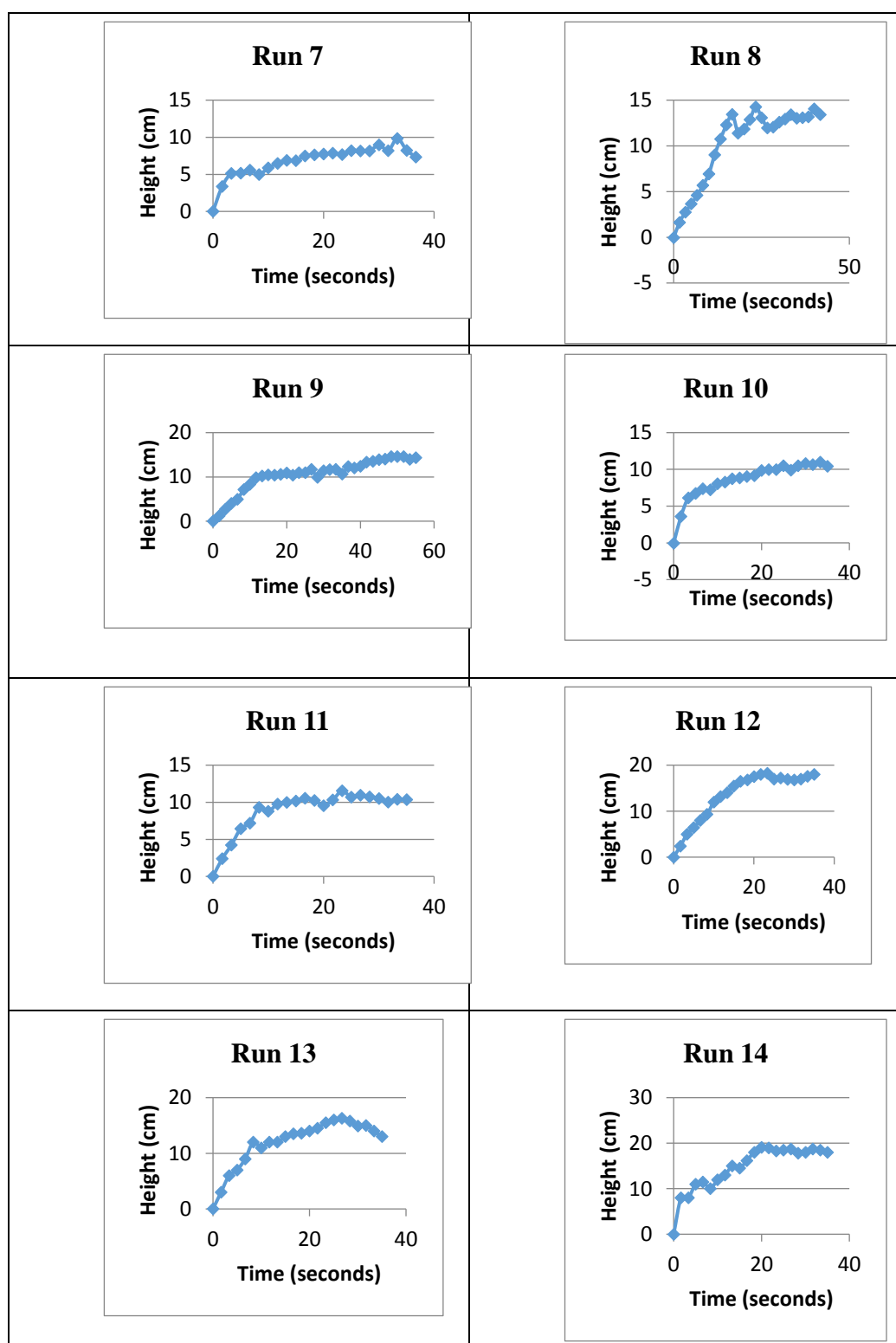
Figure 5.4. Time vs froth height data obtained via tracker software for 14 experimental runs conducted using Al_2O_3 nanoparticles as flotation aid.(cont.).

SiO$_2$ nanoparticles were also used in 14 sets of experiments to find out the effect of these particles on froth stability. Figure 5.5 gives the graphs of froth height vs time measured during these experiments. All data was obtained through Tracker software.
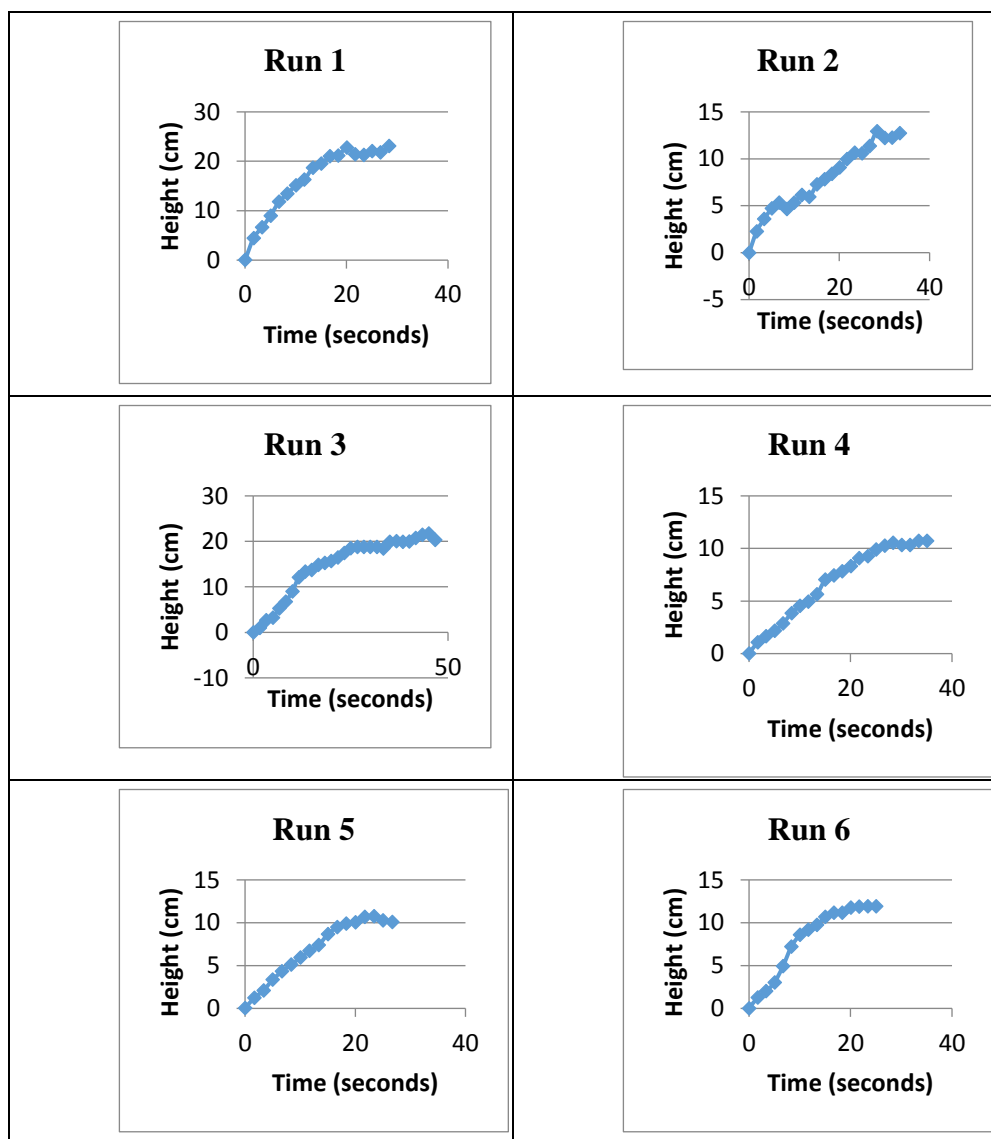
Figure 5.5. Time vs froth height data obtained via tracker software for 14 experiment runs conducted using SiO$_2$ nanoparticles as flotation aid.
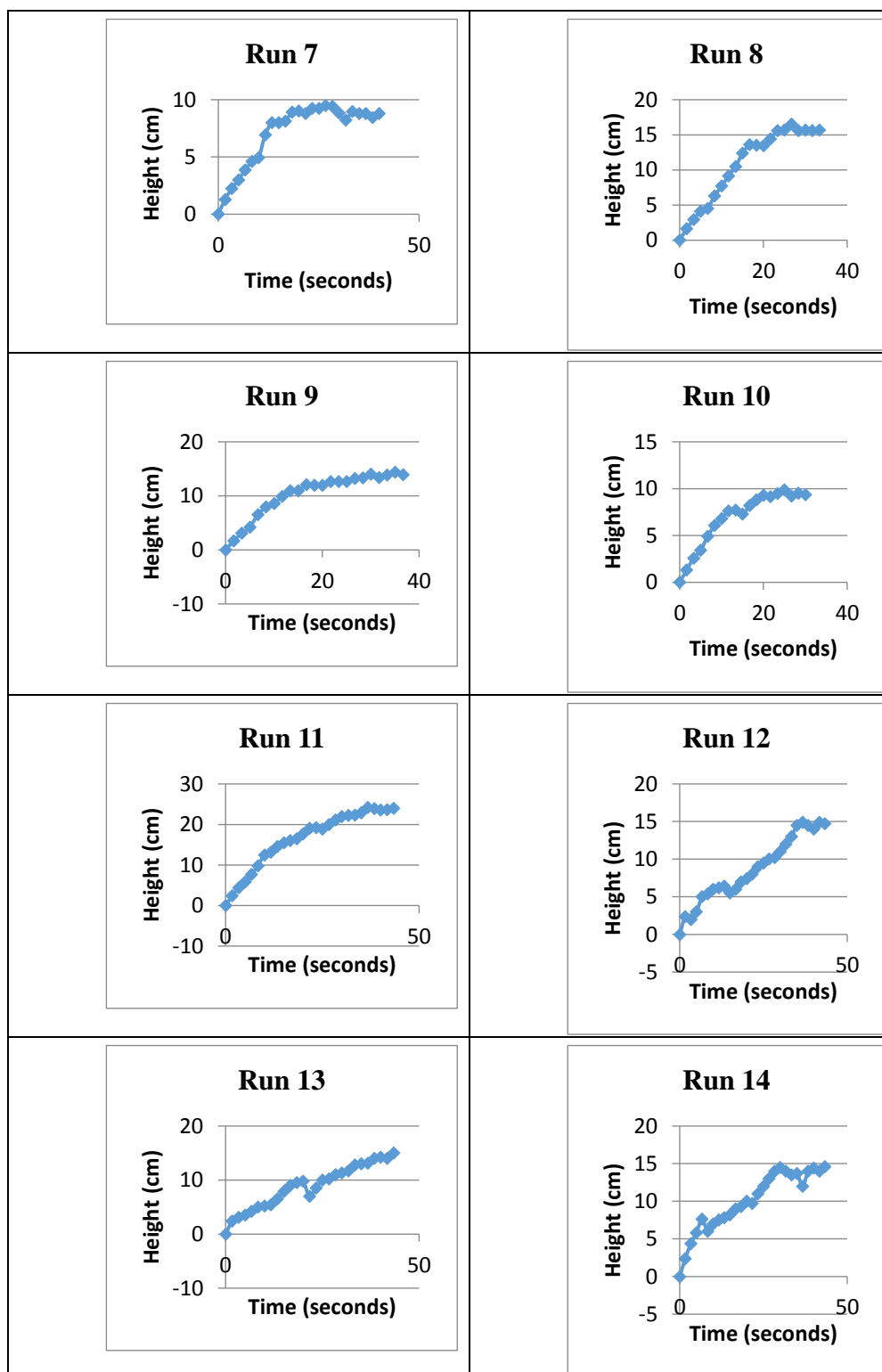
Figure 5.5. Time vs froth height data obtained via tracker software for 14 experiment runs conducted using SiO_2 nanoparticles as flotation aid (Cont.).

5.3.3. Mathematical Modelling. Quadratic models were fitted to the

flotation and froth stability experimental results. A total of nine models were fitted for

experiments involving each nanoparticle. These models describe equations for response

variables including Pb grade, Pb recovery, Cu grade, Cu recovery, Zn grade, Zn recovery,

Fe grade, Fe recovery and dynamic froth stability. Models for the response variables were

chosen through a stepwise procedure with an alpha (α) value of 0.05. Resulting models

from froth stability and flotation experiments involving Al_2O_3 nanoparticles are given by

Equations 7 through 15:

$$\text{Pb grade} = 54.671 + 0.1912 \text{ Frother} \tag{7}$$

$$\begin{aligned} \text{Pb Recovery} &= 46.84 + 2.373 \text{ Frother} \\ &- 0.02917 \text{ Frother*Frother} \end{aligned} \tag{8}$$

$$\text{Cu grade} = 1.843 + 0.0656 \text{ Frother} - 0.000705 \text{ Frother*Frother} \tag{9}$$

$$\begin{aligned} \text{Cu Recovery} &= 16.72 + 1.756 \text{ Frother} \\ &- 0.02204 \text{ Frother*Frother} \end{aligned} \tag{10}$$

$$\begin{aligned} \text{Zn Grade} &= 1.221 + 0.07024 \text{ Frother} - 0.1835 \ Al_2O_3 \\ &- 0.001171 \text{ Frother*Frother} + 0.01991 \ Al2O3*Al_2O_3 \end{aligned} \tag{11}$$

$$\text{Zn Recovery} = 2.934 + 0.04156 \text{ Frother} \tag{12}$$

$$\text{Fe} = 2.0136 + 0.0581 \ Al_2O_3 \tag{13}$$

$$\begin{aligned} \text{Fe recovery} &= 2.808 + 0.0434 \text{ Frother} + 0.6042 \ Al_2O_3 \\ &- 0.00492 \text{ Frother*}Al_2O_3 \end{aligned} \tag{14}$$

$$\text{Dynamic Froth Stability} = 46.60 - 0.1476 \text{ Frother} \tag{15}$$
$$- 1.837 \text{ Al}_2\text{O}_3$$
$$+ 0.0726 \text{ Frother*Al}_2\text{O}_3$$

Analysis of variance (ANOVA) was implied to estimate the significance of these models. Table 5.5 describes the results of the ANOVA analysis performed on these models. It can be seen that all fitted models are significant (p-value < 0.05).

Figure 5.6 represents the predicted against actual values for dynamic froth stability along with % grade and % recovery of Pb, Cu, Zn, and Fe in case for Al_2O_3 nanoparticles. A 1:1 correlation line for each of the plots is shown in Figure 5.6. The closer the points to the line, the better the agreement between the predicted values and the actual values.

The coefficient of multiple determinations, R^2 was found to be 90.65 %, 91.83%, 82.84% , 93.68% , 86.79 %, 92.19 %, 62.17 %, 94.71 %, 78.88 % for Pb grade, Pb recovery, Cu grade, Cu recovery, Zn grade, Zn recovery, Fe grade, Fe recovery and dynamic froth stability respectively. The R^2 value is higher than 80% in all cases except in case of Fe grade, meaning that these models could explain more than 80% of the total variations in the system and 60% for Fe grade. The high value of R^2 indicates the reliability of quadratic equations under the given experimental domain.

Models obtained through flotation and froth stability experiments involving SiO_2 nanoparticles with 95 % confidence interval are given through Equations 16 to 24: Analysis of variance (ANOVA) was applied to the models through Equations 16 to 24.All models gave a p-value < 0.05.This ensures that all models are significant within a confidence interval of 95%. Table 5.6 describes the results of the ANOVA analysis performed on these models. Figure 5.7 embodies the predicted against the actual values

for dynamic froth stability in addition to % grade and % recovery of Pb, Cu, Zn and Fe, respectively. A linear correlation line for each of the plots is also shown in Figure 5.7. The coefficient of multiple determinations, R^2, was found to be 92.95%, 94.09%, 86.78%, 86.73%, 83.78 %, 83.83%, 29.68%, 79.81 %, 91.07% for Pb grade, Pb recovery, Cu grade, Cu recovery, Zn grade, Zn recovery, Fe grade, Fe recovery, and dynamic froth stability, respectively. R^2 value is higher than or equal to approximately 80% in all cases except Fe grade. This means that the models could explain more than 80% of the total variations in the system except for Fe grade. An R^2 value of 29.68% is very low for Fe grade, and thus the results from this model may not be very accurate for Fe grade.

5.3.4. Optimization. Response optimizer in Minitab 17.0 was employed to find the optimum conditions to achieve maximum Pb grade, Pb recovery, Cu grade, Cu recovery and dynamic froth stability, while minimizing the grade and recovery of Zn and Fe for both Al_2O_3 and SiO_2 nanoparticle aided flotation. All the results were computed using Equations 7 to 24 within the experimental range of the study. The optimum flotation conditions found when Al_2O_3 nanoparticles were used as flotation aid were 35.3 g/ton of frother (MIBC) and 2.2 g/ton of Al_2O_3 nanoparticles, as shown in Figure 5.8.

The corresponding values of Pb grade, Pb recovery, Cu grade, Cu recovery, Zn grade, Zn recovery,Fe grade, Fe recovery, and dynamic froth stability achieved at these conditions Figure 5.9 gives the optimum flotation conditions of frother (MIBC) and SiO_2 nanoparticles to achieve the desired results.The optimum values of MIBC and SiO_2 were found to be 21.7 g/ton and 10 g/ton respectively. The values of Pb grade, Pb recovery, Cu

Table 5.5. ANOVA analysis results of the developed models for flotation and froth stability experiments using Al_2O_3 nanoparticles.

		Sum of square	DOF	Mean square	F-value	P-valu
Pb grade	Model	137.09	1	137.09	116.37	<0.0
	Residual	14.137	12	1.178		
Pb Recovery	Model	4278.6	2	2139.3	61.84	<0.0
	Residual	380.5	11	34.6		
Zn grade	Model	2.195	4	0.548	14.78	0.00
	Residual	0.334	9	0.037		
Zn recovery	Model	6.47	1	6.47	141.67	0.00
	Residual	0.548	12	0.045		
Cu grade	Model	4.130	2	2.065	26.55	<0.0
	Residual	0.855	11	0.077		
Cu recovery	Model	2256.93	2	1128.46	84.06	<0.0
	Residual	147.67	11	13.42		
Fe grade	Model	0.505	1	0.505	19.72	0.00
	Residual	0.307	12	0.0256		
Fe recovery	Model	37.54	3	12.515	59.71	<0.0
	Residual	2.096	10	0.2096		
Dynamic froth stability	Model	504.162	3	168.054	12.45	0.00
	Residual	134.957	10	13.496		
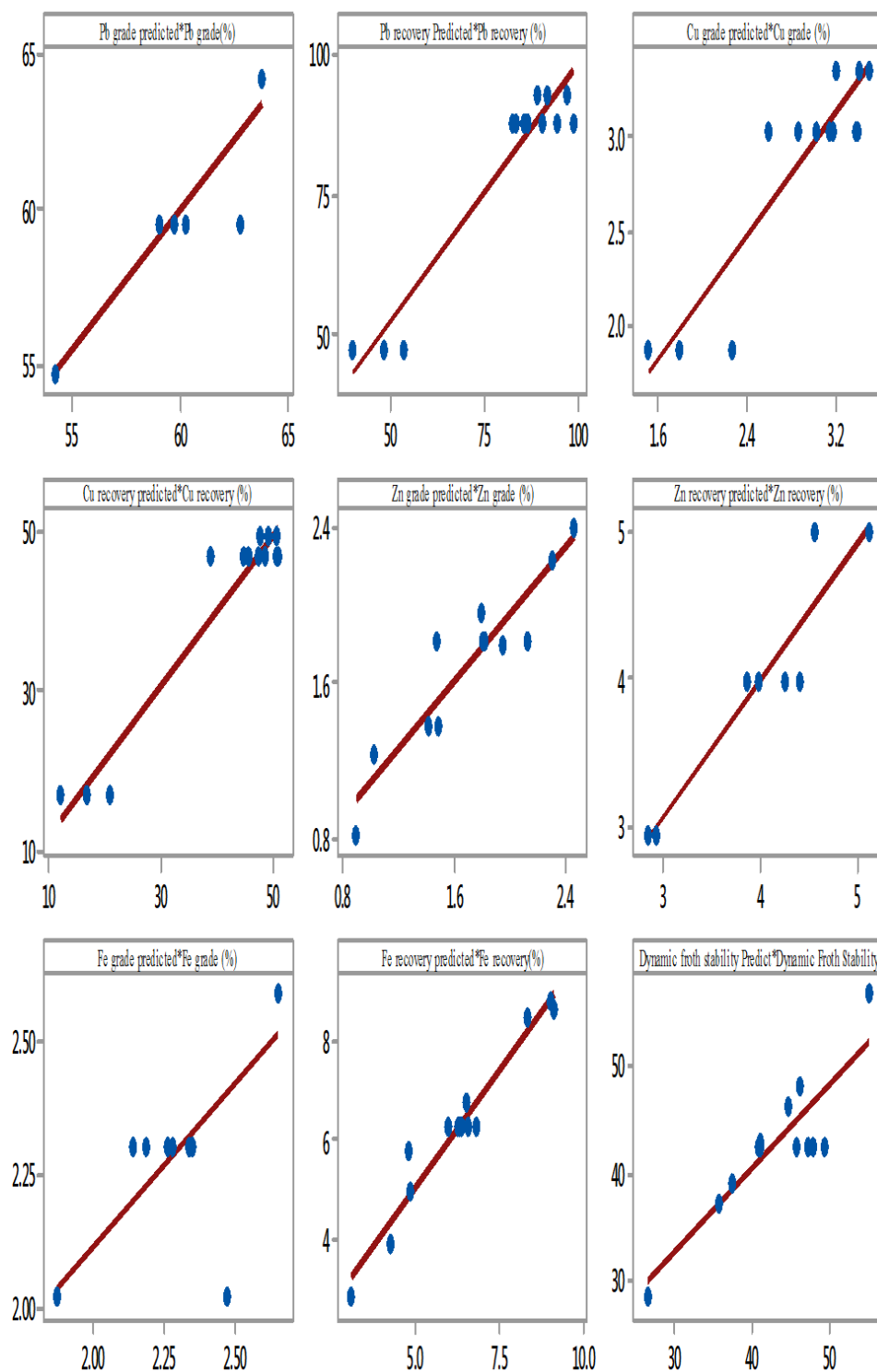
Figure 5.6. Plot showing the actual vs predicted values of Pb grade, Pb recovery, Cu grade, Cu recovery, Zn grade, Zn recovery, Fe grade, Fe recovery and dynamic froth stability in case of Al_2O_3 nanoparticles used in flotation.

$$\text{Pb grade} = 47.54 + 0.6988 \text{ Frother} + 1.017 \text{ SiO2}$$
$$- 0.00989 \text{ Frother*Frother}$$
$$- 0.04672 \text{ Frother*SiO2} \tag{16}$$

$$\text{Pb Recovery} = 55.31 + 2.469 \text{ Frother} - 0.03576 \text{ Frother*Frother} \tag{17}$$

$$\text{Cu grade} = 2.378 + 0.03130 \text{ Frother} + 0.0842 \text{ SiO2}$$
$$- 0.002940 \text{ Frother*SiO2} \tag{18}$$

$$\text{Cu Recovery} = 28.10 + 1.362 \text{ Frother} - 0.01439 \text{ Frother*Frother} \tag{19}$$

$$\text{Zn Grade} = 2.1275 + 0.00060 \text{ Frother} - 0.0673 \text{ SiO2}$$
$$+ 0.001552 \text{ Frother*SiO2} \tag{20}$$

$$\text{Zn recovery} = 6.199 - 0.0121 \text{ Frother} - 0.3095 \text{ SiO2}$$
$$+ 0.00770 \text{ Frother*SiO2} \tag{21}$$

$$\text{Fe Grade} = 3.086 - 0.01079 \text{ Frother} \tag{22}$$

$$\text{Fe recovery} = 9.131 - 0.0090 \text{ Frother} - 0.3020 \text{ SiO2}$$
$$+ 0.00628 \text{ Frother*SiO2} \tag{23}$$

$$\text{Dynamic Froth Stability} = 35.10 - 0.0632 \text{ Frother} - 1.334 \text{ SiO2}$$
$$+ 0.0706 \text{ Frother*SiO2} \tag{24}$$

grade, Cu recovery, Zn grade, Zn recovery, Fe grade, Fe recovery and dynamic froth stability obtained at these conditions were 58.08%, 92.06%, 3.26%, 50.88 %, 1.80%, 4.51%, 2.85%, 7.27% and 35.7% respectively.

5.4. DISCUSSION

Results from froth flotation tests carried with nano material Al_2O_3, with nano material SiO_2 and without the aid of nanomaterials are as shown in Figure 5.10.

Table 5.6. ANOVA analysis results of the developed models for flotation and froth stability experiments using SiO_2 nanoparticles.

		Sum of square	DOF	Mean square	F-value	P-value
Pb grade	Model	273.92	4	68.48	29.66	<0.05
	Residual	20.77	9	2.309		
Pb Recovery	Model	3451.73	2	1725.87	87.54	<0.05
	Residual	216.86	11	19.71		
Zn grade	Model	0.534	3	0.17825	17.22	<0.05
	Residual	0.1035	10	0.010352		
Zn recovery	Model	8.37	3	2.79	17.28	<0.05
	Residual	1.614	10	2.79		
Cu grade	Model	1.591	3	0.530	21.88	<0.05
	Residual	0.242	10	0.02423		
Cu recovery	Model	1824.63	2	912.31	35.39	<0.05
	Residual	279.29	11	25.39		
Fe grade	Model	0.436	1	0.436	5.06	0.044
	Residual	1.034	12	0.0861		
Fe recovery	Model	7.500	3	2.5001	13.17	0.001
	Residual	1.8977	10	0.1898		
Dynamic froth stability	Model	655.24	3	218.415	33.99	<0.05
	Residual	64.25	10	6.425		
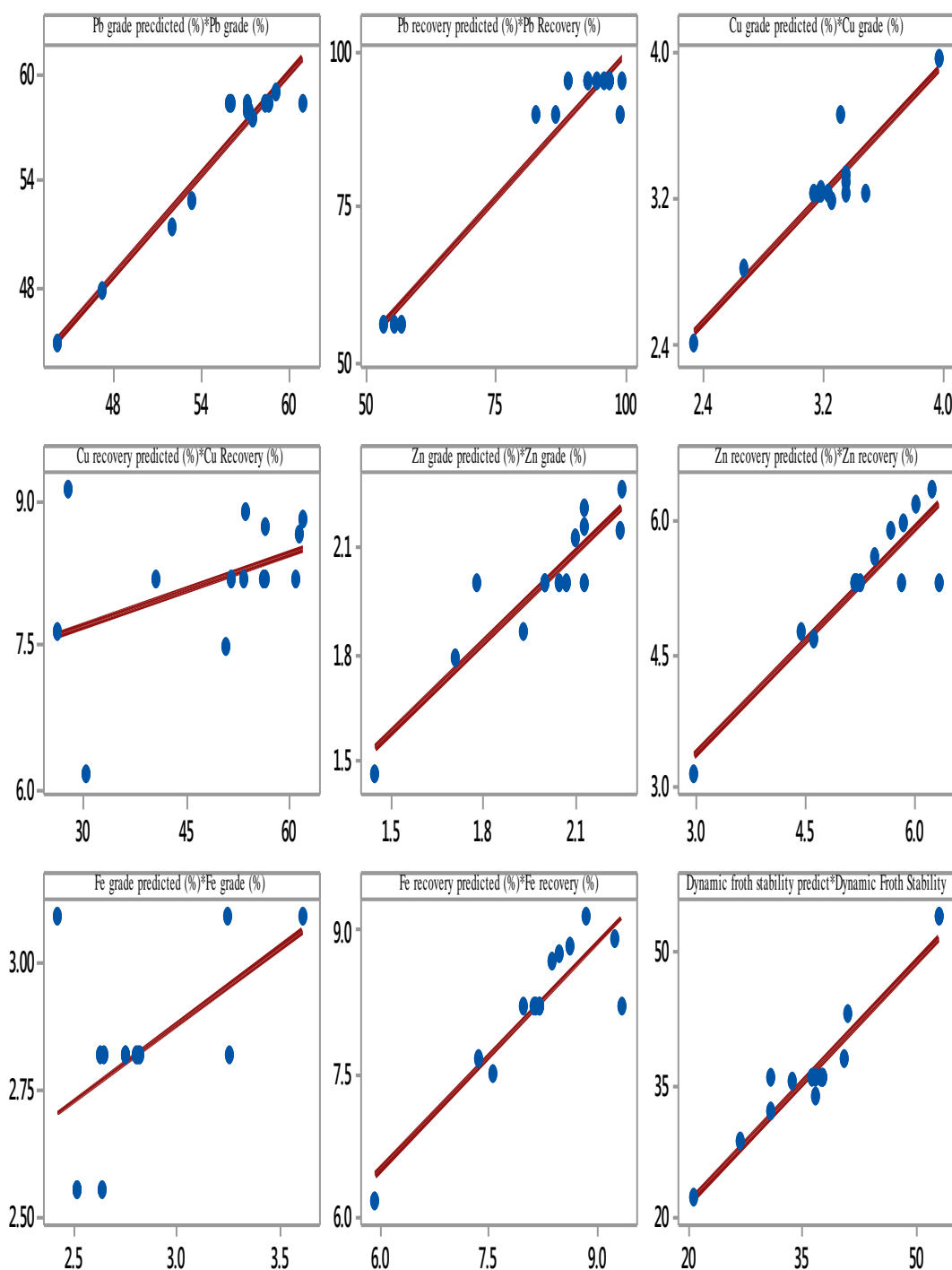
Figure 5.7. Plot showing the actual vs predicted values of Pb grade, Pb recovery, Cu grade, Cu recovery, Zn grade, Zn recovery, Fe grade, Fe recovery and dynamic froth stability in case of SiO_2 nanoparticles used in flotation.

From Figure 5.10, it can be seen that the addition of Al2O3 nanoparticles increase dynamic froth stability by 26.4%, while there was no significant increase in the dynamic froth stability when SiO2 nanoparticles were used. As nanoparticles increase the froth stability being adsorbed onto liquid air interface and preventing the bubble coalescence (Figure 5.11), it can be established from the above observation that SiO2 nanoparticles do not get adsorbed while Al2O3 nanoparticles do get ad Effect of nano particles Al2O3 concentration on dynamic froth stability is given by Figure 5.12.It is observed that at frother concentration below 10 g/ton, froth stability decreases with the increase of Al2O3 concentration from 0 to 10 g/ton. At frother concentration above 30 g/ton, situation is reversed as froth stability starts to increase with the increase in dosage of Al2O3 nanoparticles. This signifies the joint action of frother and nano particles as it seems that frother helps adsorb nano particles onto the liquid film between mineral laden air bubbles. Regarding the effect of nanoparticles on flotation performance, there was 0.85 % increase in Pb grade when Al2O3 nanoparticles were added in the system while Pb grade decreased by 2% when SiO2 nanoparticles were added. The addition of Al2O3 nanoparticles increased Pb recovery by 3%, while there was no significant increase observed for SiO2 nanoparticles. Cu grade was not significantly influenced by the addition of both type of nanoparticles. Cu recovery, however unexpectedly decreased when either types of nanoparticles were added. The decrease in Cu recovery was found to be 4% for SiO_2 nanoparticles and 3.5% for Al_2O_3 nanoparticles. Both types of nanoparticles had no effect on Zn grade. A decrease of 0.8 % was detected in Zn recovery by virtue of addition of both types of nanoparticles. Al_2O_3 nano particle addition decreased both Fe grade and recovery. SiO_2 nanoparticles, however, resulted in a rise of

0.6% in Fe grade and 0.7% in Fe recovery, which was not desired as Fe was targeted to be depressed.
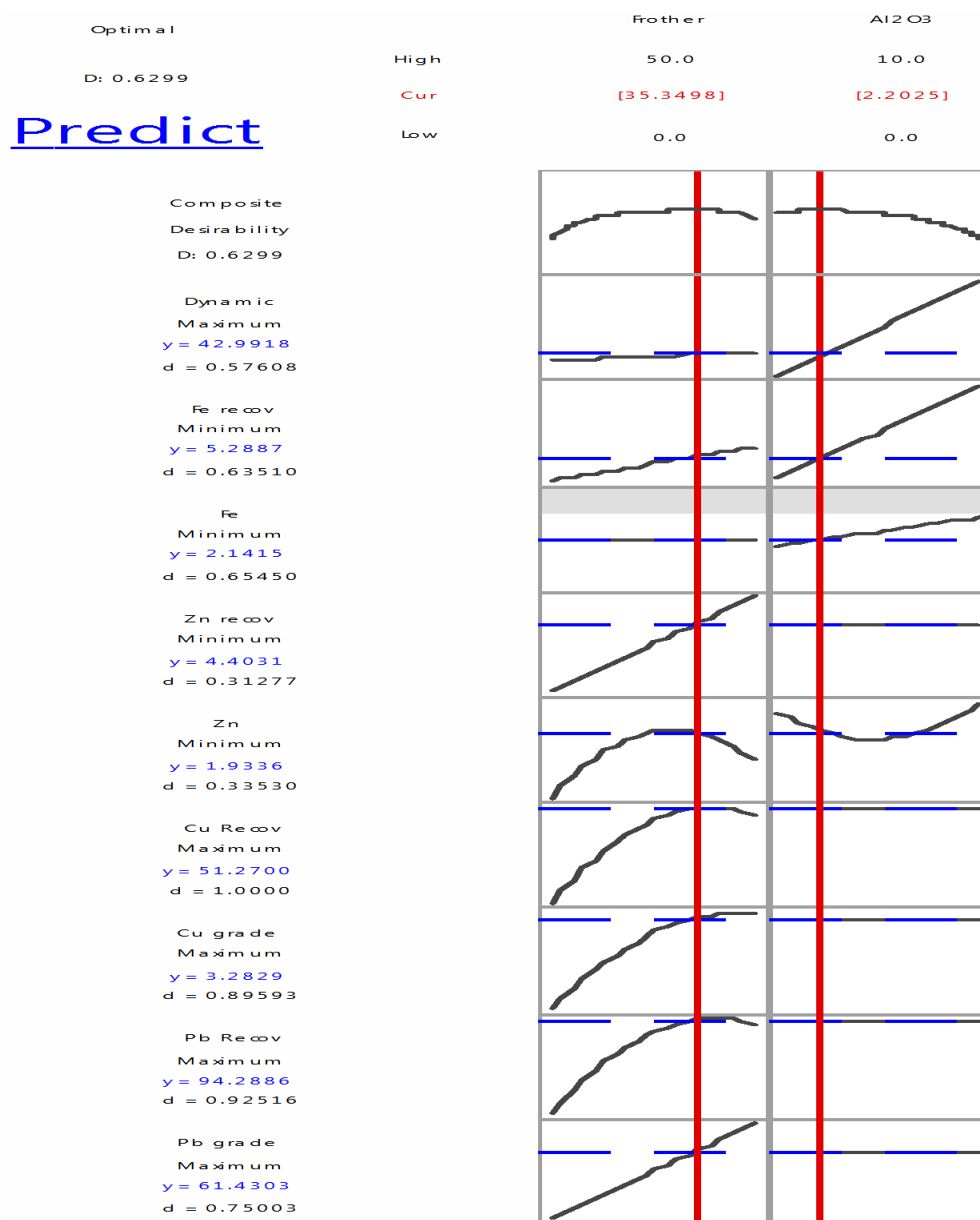
Figure 5.8. Optimum concentrations of frother (MIBC) and Al2O3 nanoparticles and corresponding values of Pb grade, Pb recovery, Cu grade, Cu recovery, Zn grade, Zn recovery, Fe grade, Fe recovery and dynamic froth stability.
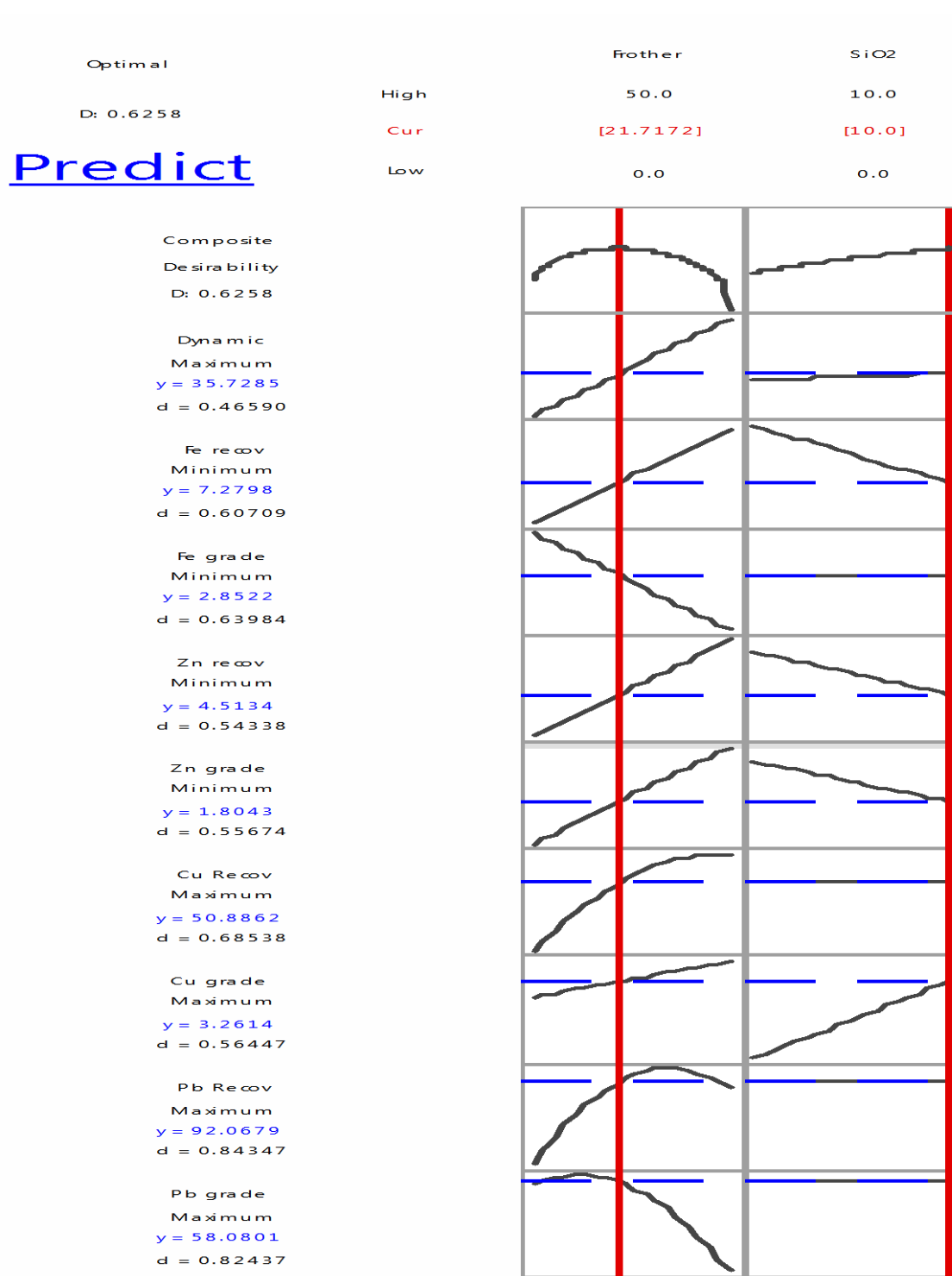
Figure 5.9. Optimum concentrations of frother (MIBC) and SiO_2 nanoparticles and corresponding values of Pb grade, Pb recovery, Cu grade, Cu recovery, Zn grade, Zn recovery, Fe grade, Fe recovery and dynamic froth stability.
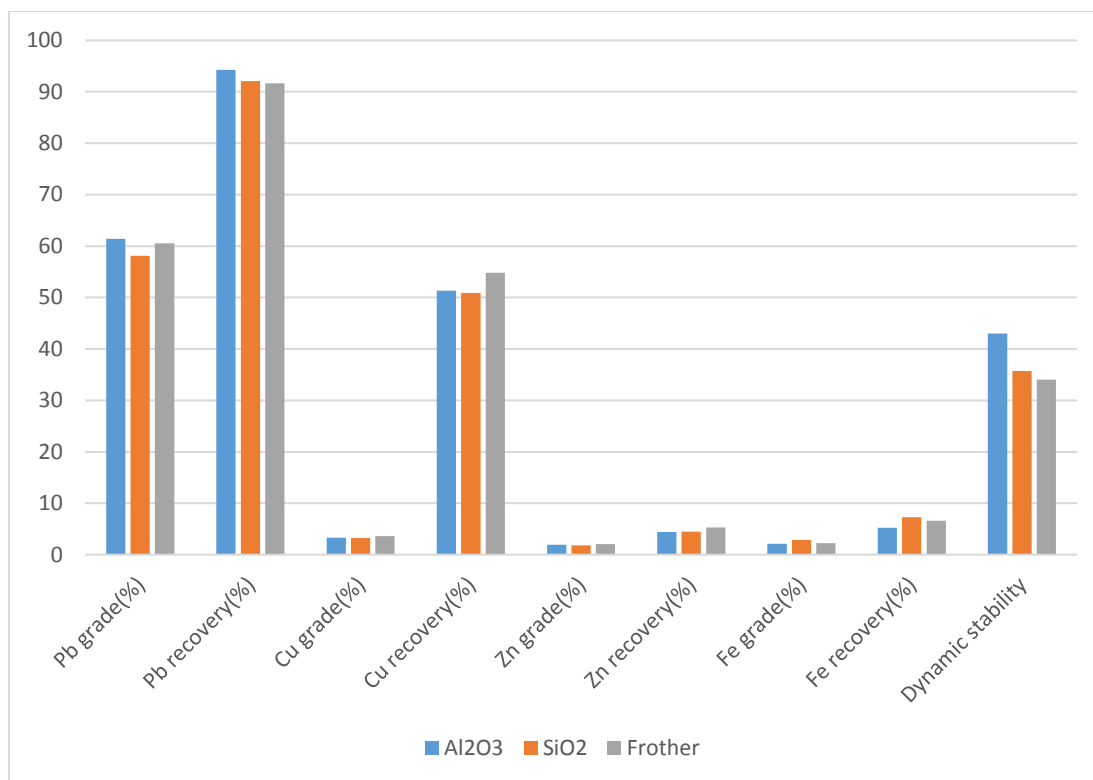
Figure 5.10. Comparison of Pb grade, Pb recovery, Cu grade, Cu recovery, Zn grade, Zn recovery, Fe grade, Fe recovery and dynamic froth stability achieved in case of froth flotation tests carried with and without the aid of nanomaterials. Two types of nano materials namely Al_2O_3 and SiO_2 were used. Results from the flotation tests without nano materials are represented by frother columns.

Based on the observations done during this study, it can be concluded that nanoparticles can have positive influence on froth stability and flotation performance of complex sulfide ore flotation. However, it is important to select the correct type of nanoparticles for each ore type. In the current study, Al_2O_3 was found to be a suitable type of nano particle for sulfide ore flotation because it not only enhanced the forth stability but also increased the Pb grade and recovery, thus enhancing flotation performance. On the other hand, SiO_2 nanoparticles were not able to augment froth stability or flotation performance.
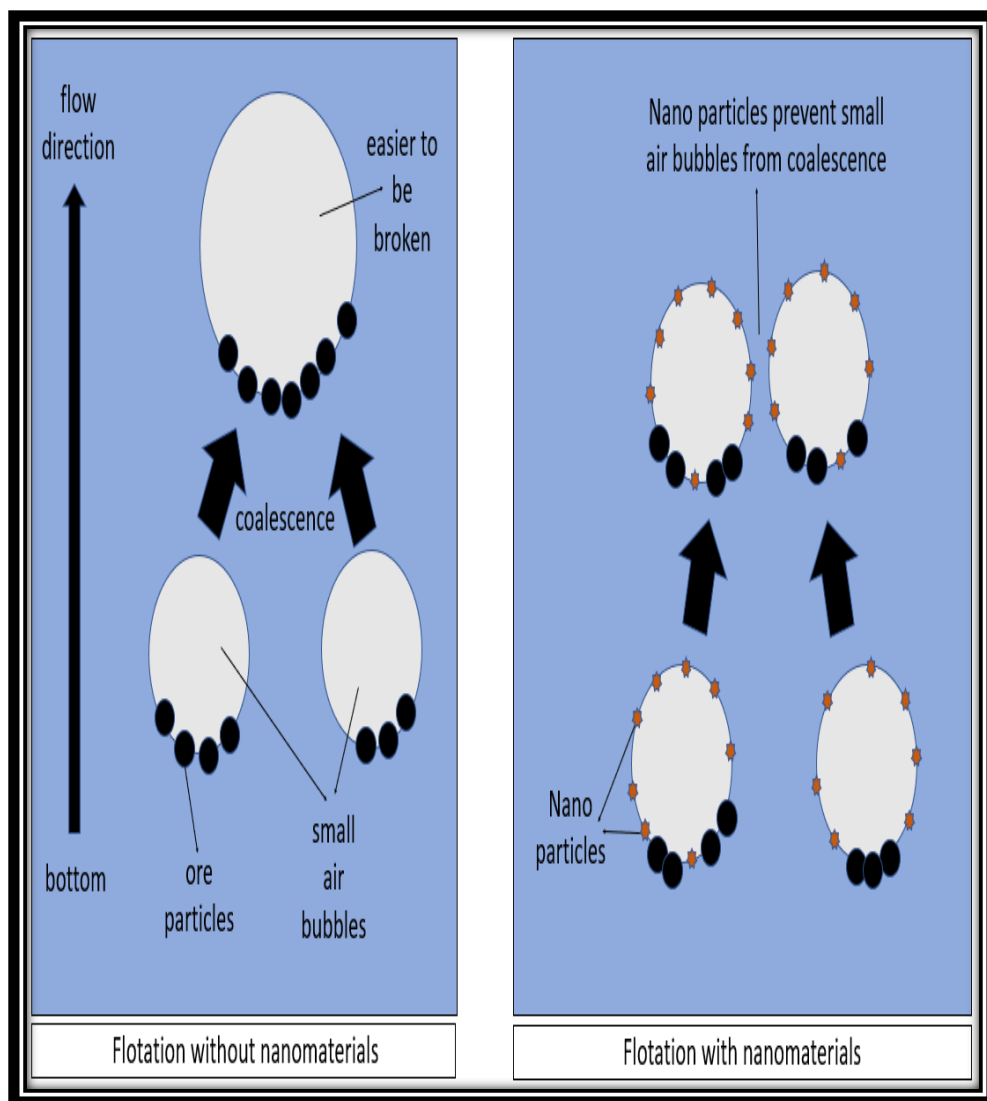
Figure 5.11. Nanoparticles adsorption on the liquid-air interface. Nanoparticles effectively prevent small air bubbles from coalescence to form large bubbles.

It is recommended to carry out fundamental research to uncover the reasons of preferential adsorption of Al_2O_3 nanoparticles on liquid air interface in the case of sulfide ore flotation. More types of nanoparticles should also be tried to determine the most suitable type of nanoparticles to control froth stability and flotation performance of complex sulfide ores.
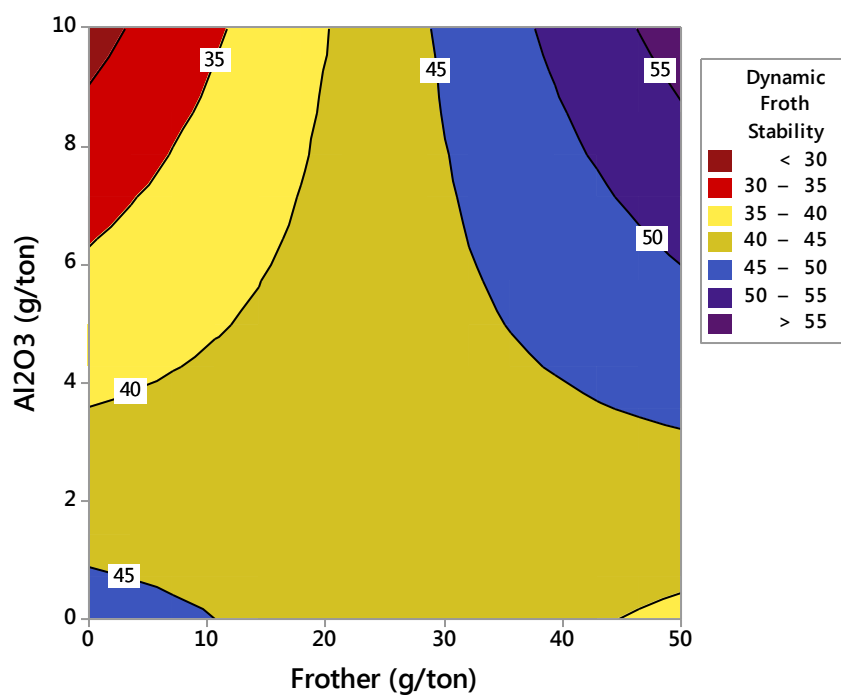
Figure 5.12. Effect of nano particles Al$_2$O$_3$ concentration on dynamic froth stability.

6. EFFECT OF THE USE OF SEA WATER ON DYNAMIC FROTH STABILITY AND GRADE AND RECOVERY OF PB AND CU IN COMPLEX SULFIDE ORE FLOTATION

6.1. BACKGROUND

Freshwater resources are becoming scarce as fresh water resources like rivers and groundwater are becoming depleted in dry regions. In arid regions, the importance of saving freshwater resources is increasing. Mineral deposits are normally found in remote areas with limited freshwater resources. The Atacama Desert, which is the heart of Chilean Copper Industry is a prime example of the problems pertaining to freshwater resources. As mineral processing plants use extensive amounts of water, especially in flotation, water scarcity is being considered as one of the major challenges being faced by the mining and processing industry. In this scenario, use of seawater as replacement of fresh water is becoming one of the most promising solutions to make mineral processing a sustainable option in future [122], [123]. The biggest challenge facing the use of seawater as processing water is achieving the same recoveries and grade of minerals as in fresh water [122]. Froth stability plays a very important role in determining concentrate grade and recovery in flotation operations, in order for the mineral processing industry to achieve sustainability, there is an urgent need to study the effect of seawater on froth stability and flotation performance [68].

This study is aimed at investigating the effect of seawater on dynamic froth stability and flotation performance in flotation of complex sulfide ores. The regression equations will be computed to obtain the reagent amounts necessary for the desired grade and recovery when seawater will be replaced with fresh water.

6.2. METHODOLOGY AND MATERIALS

Details of materials and methods used in this study are given below. All the lab equipment was provided by Missouri University of Science and Technology, USA.

6.2.1. Materials. Mississippi Valley-type (MVT) sulfide ore was obtained from a mine located in North America. This ore was characterized using various techniques. Complex sulfide ore has never been processed in seawater before this study to the knowledge of the author. MVT deposits are found throughout the world as shown in Figure 6.1.

Figure 6.1. MVT deposits found throughout the world.

Some of these MVT deposits are situated in countries like Saudi Arabia, Iraq and Australia, all near the coast. These countries also have challenges with respect to limited freshwater resources [124].

Detailed characterization of feed can be found in Section 3. Hydrochloric acid and sodium hydroxide were used as pH modifiers. Sodium isopropyl xanthate, sodium

cyanide and zinc sulfate were used as collector, pyrite depressant and sphalerite depressant, respectively. These chemicals were obtained from Fisher Scientific, USA. The 4-Methyl-2- pentanol isobutyl carbinol (MIBC) which was used as frother was obtained from ACROS, USA Inc. All flotation reagents were used without further purification. Sea salt was obtained from Lake Products Company LLC, Florissant, Mo, USA, as shown in Figure 6.2. Flotation tests were conducted using both tap and seawater.

Figure 6.2. Sea salt obtained from Lake Products Company LLC.
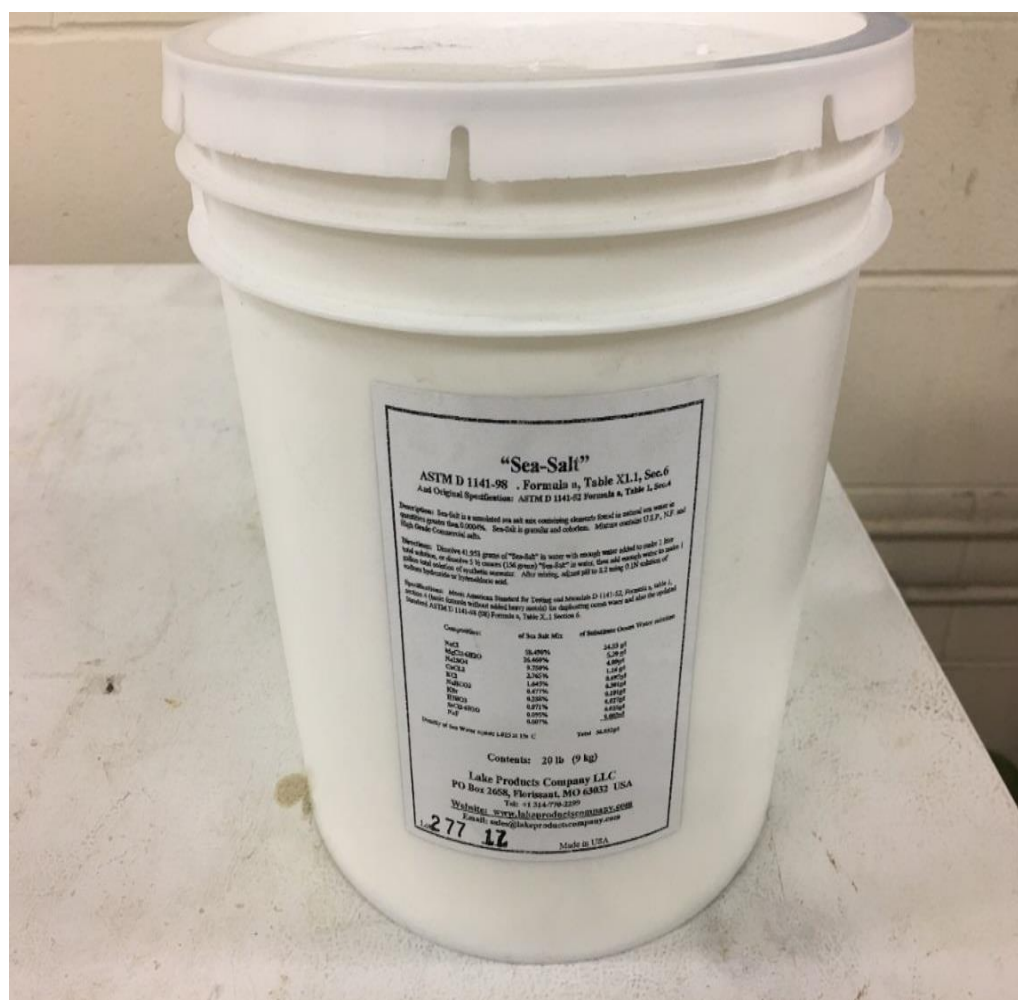
6.2.2. Methods. Simulated **s**eawater was prepared as per the ASTM D 1141-98 standard.To make a 1 liter solution, 41.953 grams of sea salt was added to deionized water. After mixing pH of the solution was adjusted to 8.2 using 0.1 N sodium hydroxide.

6.2.2.1. Design of experiments. The face-centered rotatable central composite design was used to design both the flotation and froth stability experiments. Table 6.1 lists the detail of experiment sets carried out during this study. Each set consisted of two experiments. A total of 56 sets of experiments were performed. Twenty-eight flotation experiment sets were carried out including 14 sets of seawater experiments and 14 sets of freshwater experiments. Similarly, 28 sets of froth stability experiments were performed including 14 sets of experiments for each water type.

6.2.2.2. Froth flotation experiments. Bulk flotation of galena and chalcopyrite was carried out in a Denver flotation cell with an impeller diameter of 3.88 in and a 1L flotation tank. In all experiments, solids concentration (as per industrial application) was kept constant at 45% , while pH for fresh and sea water were maintained at unadjusted values of 7.9 and 8.2 respectively. The optimum operation parameters that were found through statistical analysis in Section 3 were also kept constant. Only frother (MIBC) and collector dosage were varied, as these have a pronounced effect on froth stability as shown in Table 6.1. The sequence of reagent addition in froth flotation experiments is given in Figure 6.3.

6.2.2.3. Froth stability experiments. For each flotation experiment, an identical froth stability experiments was run. Froth stability experiments were carried out in two types of process water, sea and tap water to test the effect of seawater on froth stability. All conditions were kept same as in the flotation experiment, except the size of the cell

Table 6.1. General experimental design for flotation and froth stability tests.

StdOrder	RunOrder	PtType	Blocks	Frother (g/ton)	Collector (g/ton)	Water
23	1	-1	2	349	400	Fresh
19	2	0	2	180	400	Sea
25	3	-1	2	180	682	Fresh
18	4	-1	2	180	682	Sea
27	5	0	2	180	400	Fresh
24	6	-1	2	180	117	Fresh
20	7	0	2	180	400	Sea
26	8	0	2	180	400	Fresh
21	9	0	2	180	400	Sea
28	10	0	2	180	400	Fresh
16	11	-1	2	349	400	Sea
17	12	-1	2	180	117	Sea
15	13	-1	2	10	400	Sea
22	14	-1	2	10	400	Fresh
14	15	0	1	180	400	Fresh
13	16	0	1	180	400	Fresh
1	17	1	1	60	200	Sea
9	18	1	1	300	200	Fresh
10	19	1	1	60	600	Fresh
3	20	1	1	60	600	Sea
8	21	1	1	60	200	Fresh
4	22	1	1	300	600	Sea
12	23	0	1	180	400	Fresh
5	24	0	1	180	400	Sea
2	25	1	1	300	200	Sea
11	26	1	1	300	600	Fresh
7	27	0	1	180	400	Sea
6	28	0	1	180	400	Sea
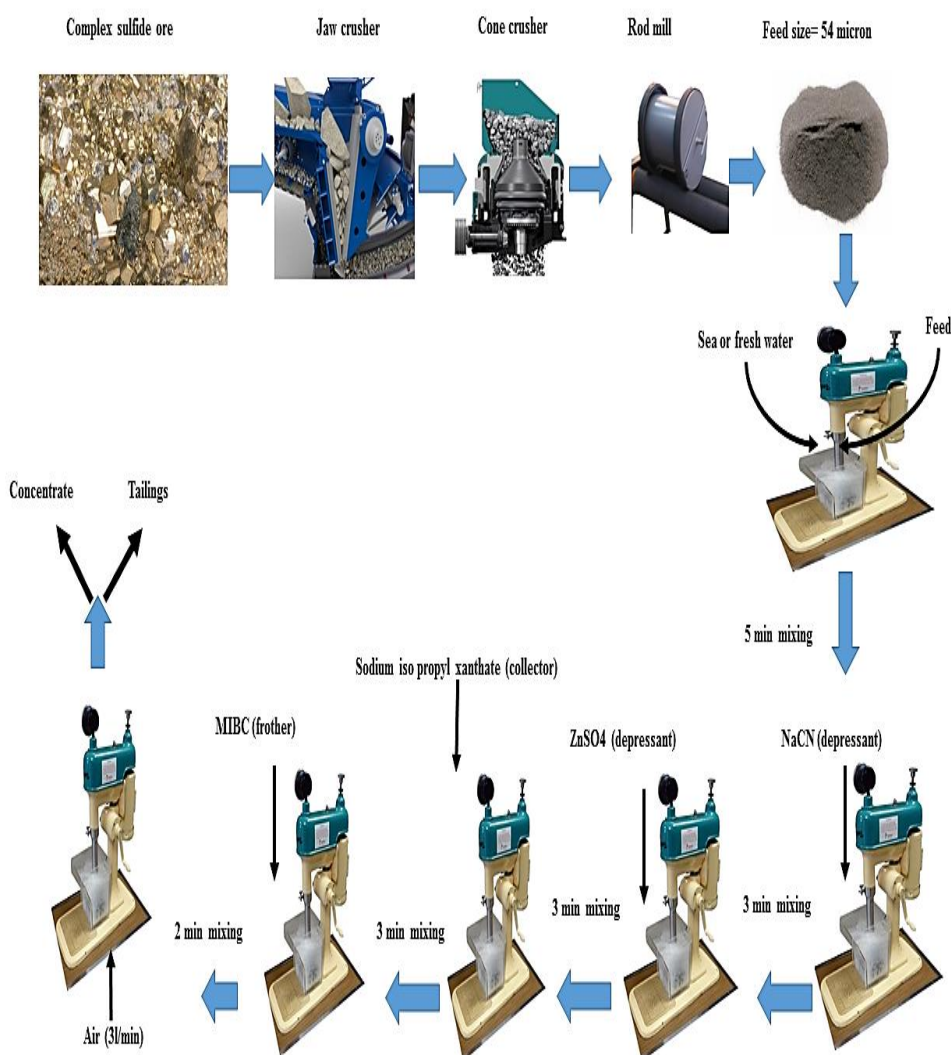
Figure 6.3. Sequence of reagent addition for froth flotation tests for both sea and fresh water [152]–[156].

used. As mentioned in Section 4, froth stability experiments were conducted in a specially designed high-wall cell to prevent the overflow of froth. This allowed the rise of froth in the cell to be recorded and its velocity and maximum equilibrium height to be measured.

6.3. RESULTS

Fifty-six sets of experiments using the face-centered central composite design method were designed and conducted. In these tests, impeller speed, air rate, pyrite depressant (NaCN) dosage, sphalerite depressant ($ZnSO_4$) dosage, and flotation time were kept constant. Frother dosage, collector dosage and type of process water were varied to test the effect of these on flotation performance and froth stability. Each set consisted of two experiments. The results were analyzed using "Minitab 17.0" software.

6.3.1. Froth Flotation Results. Fourteen sets of flotation experiments were performed for each type of process water to study its effect on flotation performance of bulk flotation of galena and chalcopyrite. After flotation, the froth (concentrate) was collected, dried, weighed, and assayed for Pb, Cu, Zn, and Fe. The assays were determined using ICEP-OES and EDTA titration methods as applicable. Recovery was then calculated using Equation 6 in Section 3. Table 6.2 shows the grade and recovery of different metals achieved in the ore when fresh water was used in flotation.

Grade and recovery of Pb, Cu, Zn and Fe achieved in application of seawater as process water is depicted by Table 6.3.

6.3.2. Froth Stability Results. For each type of process water, 14 sets of froth stability tests were carried out to analyze the effect of each on the dynamic froth stability. Data collected from froth stability tests using fresh water is shown in Figure 6.4.

Seawater was also used in 14 sets of experiments to find out its effect on froth stability. Figure 6.5 shows froth height vs time; measured during these experiments. All data was obtained through Tracker software.

Table 6.2. Grade and recovery of Pb, Zn, Cu and Fe plus dynamic froth stability obtained in flotation when fresh water was used.

Dynamic Froth Stability	26.73	32.5	31.45	25.13	30.50	31.11	30.09	28.84
Fe Recovery (%)	22.29	19.67	18.30	15.72	15.63	17.58	10.90	16.75
Fe Grade (%)	3.58	3.26	4.04	4.75	4.54	3.9	4.35	4.08
Cu Recovery (%)	56.88	31.20	46.18	38.87	43.93	44.61	33.34	45.59
Cu Grade (%)	2.28	2.1	2.42	2.94	2.54	2.4	2.58	2.21
Zn Recovery (%)	10.28	3.35	8.72	4.23	9.03	11.96	4.25	9.03
Zn Grade (%)	2.3	2.68	2.52	2.4	2.61	2.52	2.52	2.67
Pb Recovery (%)	62.19	56.10	52.40	40.70	38.86	40.48	25.33	38.49
Pb Grade (%)	31.96	26.83	28.24	25.71	23.59	27.5	27.9	23.1
Water	Fresh	Fresh	Fresh	Fresh	Fresh	Fres	Fresh	Fresh
Collector	400	682.8	400	117.15	400	400	400	400
Frother	349.7	180	180	180	180	180	10.29437	180
Blocks	2	2	2	2	2	2	2	1
Pt Type	-1	-1	0	-1	0	0	-1	0
Run Order	1	3	5	6	8	10	14	15
Std Order	23	25	27	24	26	28	22	14

Table 6.2. Grade and recovery of Pb, Zn, Cu and Fe plus dynamic froth stability obtained in flotation when fresh water was used (cont.).

13	16	0	1	180	400	Fresh	23.63	43.63	2.69	8.05	2.3	47.42	4.54	19.61	28.44
9	18	1	1	300	200	Fresh	26.8	40.57	2.48	5.62	3.02	45.23	4.79	14.28	17.17
10	19	1	1	60	600	Fresh	26.04	36.20	2.73	5.83	2.47	36.06	3.98	12.67	27.50
8	21	1	1	60	200	Fresh	26.66	40.22	2.67	6.05	2.92	46.26	4.85	15.29	27.68
12	23	0	1	180	400	Fresh	22.39	37.00	2.69	7.92	2.19	49.65	4.32	16.30	30.096
11	26	1	1	300	600	Fresh	24.1	66.00	2.61	5.43	2.06	50.76	3.679	21.50	29.24

6.3.3. Mathematical Modelling. Quadratic models were fitted to the results of flotation and froth stability experimental results. A total of nine models were fitted for experiments involving each type of water. These models describe equations for response variables including Pb grade, Pb recovery, Cu grade, Cu recovery, Zn grade, Zn recovery, Fe grade, Fe recovery, and dynamic froth stability. Models for the response variables were chosen through a stepwise procedure with an alpha (α) value of 0.05. Resulting models from froth stability and flotation experiments involving fresh water are given by the Equations 25 through 33.

Table 6.3. Grade and recovery of Pb, Zn, Cu and Fe plus dynamic froth stability obtained in flotation when seawater was used.

Dynamic Froth sSability	20.06	27.08	26.99	21.15	20.67	17.73	22.93
Fe Recovery (%)	22.29	24.60	27.83	24.66	21.10	20.79	25.22
Fe Grade (%)	2.85	2.75	2.75	3.06	3.05	2.9	2.67
Cu Recovery (%)	60.50	43.21	61.91	63.17	56.30	48.53	66.91
Cu Grade (%)	1.69	1.5	1.36	1.56	1.52	1.93	1.41
Zn Recovery (%)	18.90	12.63	20.77	17.72	15.11	9.65	20.31
Zn Grade (%)	2.62	2.6	2.6	2.63	2.45	2.44	2.59
Pb Recovery (%)	71.52	74.52	75.22	80.18	62.00	69.02	93.06
Pb Grade (%)	17.58	16.53	19.53	20.79	21.73	20.15	20.59
Water	Sea	Sea	Sea	Sea	Sea	Sea	Sea
Collector (g/ton)	400	682.84	400	400	400	117.16	400
Frother (g/ton)	180	180	180	180	349.71	180	10.29
Blocks	2	2	2	2	2	2	2
Pt Type	0	-1	0	0	-1	-1	-1
Run Order	2	4	7	9	11	12	13
Std Order	19	18	20	21	16	17	15

Table 6.3. Grade and recovery of Pb, Zn, Cu and Fe plus dynamic froth stability obtained in flotation when seawater was used (cont.).

Water															
Sea	24.97	28.28	2.58	66.08	1.74	23.04	2.71	85.90	16.38	200	60	1	1	17	1
Sea	17.26	25.96	2.99	61.06	1.4	20.61	2.85	75.12	14.32	600	60	1	1	20	3
Sea	19.64	25.30	2.81	66.19	1.19	23.78	2.81	78.13	14.75	600	300	1	1	22	4
Sea	19.24	26.40	2.8	68.38	1.15	25.10	2.81	79.62	14.06	400	180	1	0	24	5
Sea	17.15	22.70	2.906	62.59	1.6	20.45	2.62	60.09	16.22	200	300	1	1	25	2
Sea	22.57	26.15	2.69	68.80	1.57	26.73	2.82	83.21	15.4	400	180	1	0	27	7
Sea	19.31	26.94	2.85	71.02	1.79	24.50	2.77	78.33	16.2	400	180	1	0	28	6

. Figure 6.4. Time vs froth height data obtained via tracker software for 14 experiment runs conducted using fresh water.

Figure 6.4. Time vs froth height data obtained via tracker software for 14 experiment runs conducted using fresh water.(cont.).
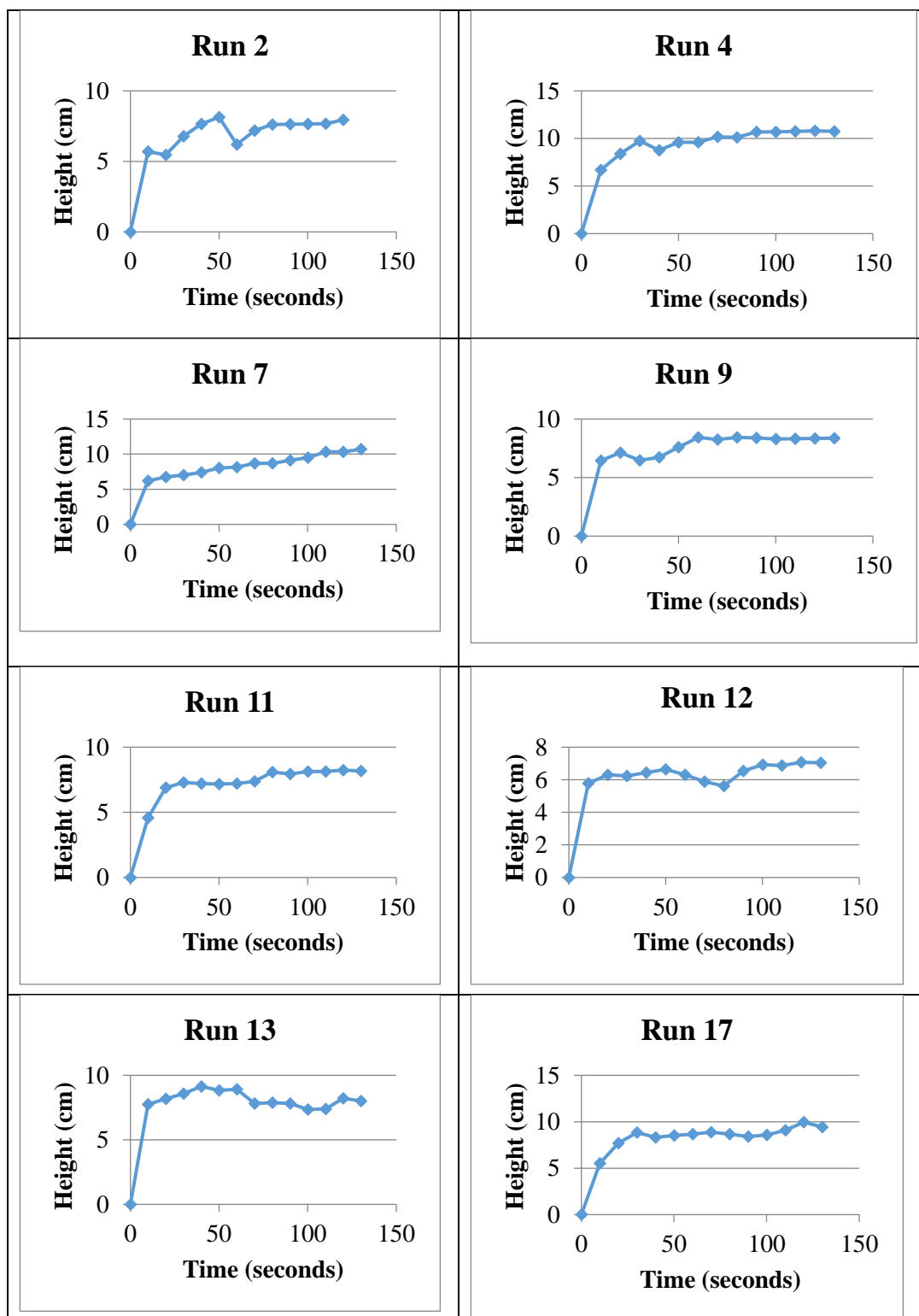
Figure 6.5. Time vs froth height data obtained via tracker software for 14 experiment runs conducted using seawater.
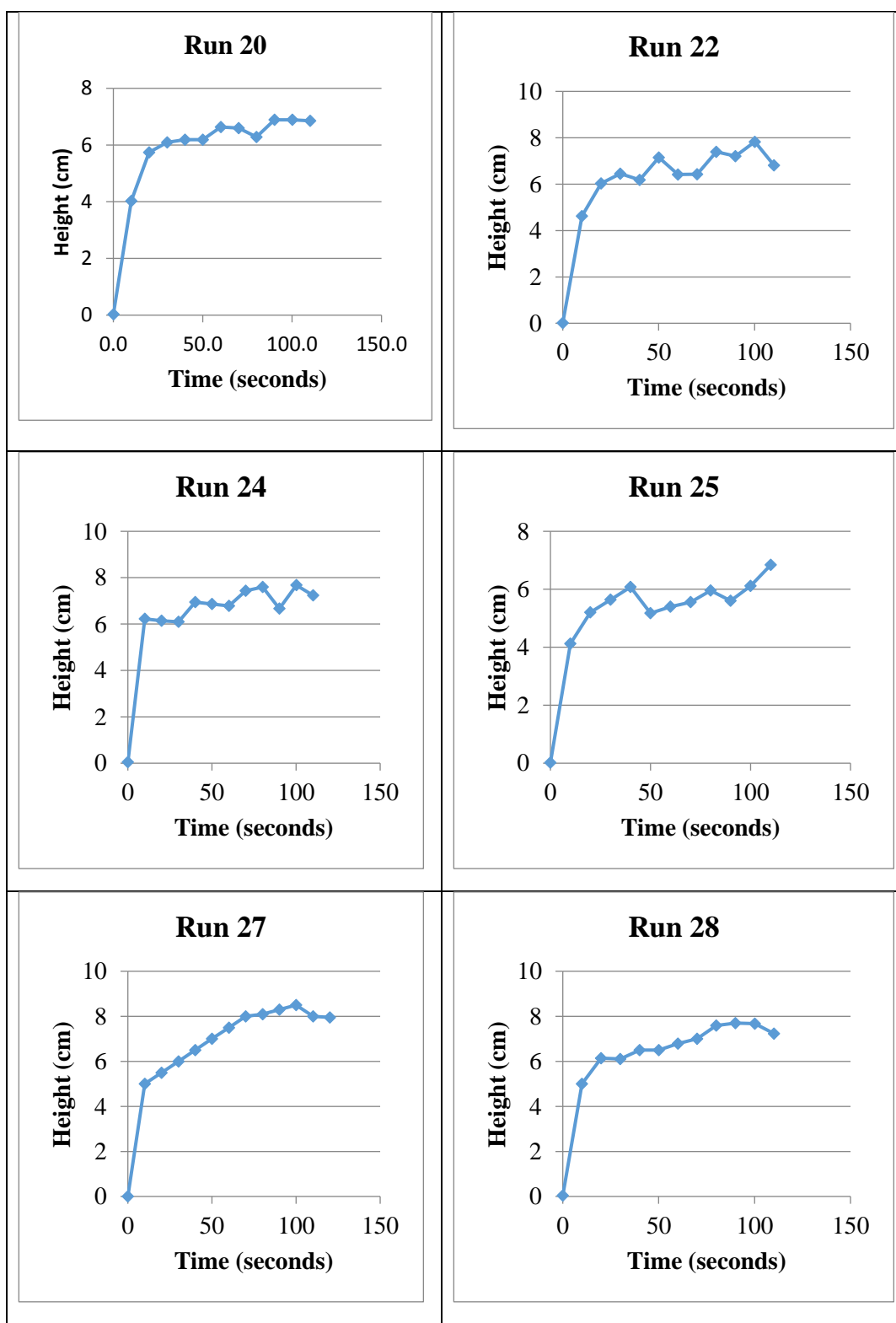
Figure 6.5. Time vs froth height data obtained via tracker software for 14 experiment runs conducted using seawater (cont.).

$$\text{Pb grade(\%)} = 27.951 - 0.0337 \text{ frother} + 0.000102 \text{ frother*frother} \qquad (25)$$

$$\text{Pb Recovery(\%)} = 43.30 - 0.0357 \text{ frother} - 0.0364 \text{ collector} \qquad (26)$$
$$+ 0.000304 \text{ frother*collector}$$

$$\text{Cu grade (\%)} = 3.284 - 0.003163 \text{ collector} + 0.000002 \text{ collector*collector} \qquad (27)$$

$$\text{Cu Recovery (\%)} = 27.02 - 0.0018 \text{ frother} + 0.0883 \text{ collector} \qquad (28)$$
$$- 0.000148 \text{ collector*collector} + 0.000127 \text{ frother*collector}$$

$$\text{Zn grade (\%)} = 2.4395 + 0.000765 \text{ frother} + 0.000357 \text{ collector} \qquad (29)$$
$$- 0.000003 \text{ frother*frother}$$

$$\text{Zn Recovery (\%)} = -3.94 + 0.0631 \text{ collector} - 0.000078 \text{ collector*collector} \qquad (30)$$

$$\text{Fe grade (\%)} = 5.484 - 0.001510 \text{ frother} - 0.002555 \text{ collector} \qquad (31)$$

$$\text{Fe Recovery (\%)} = 15.96 - 0.0058 \text{ frother} - 0.00889 \text{ collector} \qquad (32)$$
$$+ 0.000077 \text{ frother*collector}$$

$$\text{Dynamic froth stability} = 35.03 - 0.0583 \text{ frother} - 0.01157 \text{ collector} \qquad (33)$$
$$+ 0.000117 \text{ frother*collector}$$

Models obtained through flotation and froth stability experiments involving seawater with a 95 % confidence interval are given through Equations 34 to 42.

$$\text{Pb grade(\%)} = 19.363 - 0.0337 \text{ frother} + 0.000102 \text{ frother*frother} \qquad (34)$$

$$\text{Pb Recovery(\%)} = 103.22 - 0.1909 \text{ frother} - 0.0364 \text{ collector} \qquad (35)$$

$$Cu\ grade\ (\%) = 2.354 - 0.003163\ collector \\ + 0.000002\ collector*collector \tag{36}$$

$$Cu\ Recovery\ (\%) = 56.09 - 0.0646\ frother + 0.0883\ collector \\ - 0.000148\ collector*collector + 0.000127\ frother*collector \tag{37}$$

$$Zn\ grade\ (\%) = 2.5273 + 0.000765\ frother + 0.000357\ collector \\ - 0.000003\ frother*frother \tag{38}$$

$$Zn\ Recovery\ (\%) = 8.89 + 0.0631\ collector \\ - 0.000078\ collector*collector \tag{39}$$

$$Fe\ grade\ (\%) = 2.679 + 0.000712\ frother + 0.000064\ collector \tag{40}$$

$$Fe\ Recovery\ (\%) = 30.69 - 0.0433\ frother - 0.00889\ collector \\ + 0.000077\ frother*collector \tag{41}$$

$$Dynamic\ froth\ stability = 27.90 - 0.0583\ frother - 0.01157\ collector \tag{42}$$

For estimation of the significance of these models, analysis of variance (ANOVA) was applied. Table 6.4 describes the results of the ANOVA analysis performed on these models. It can be seen that all fitted models are significant (p-value < 0.05).

Figure 6.6 represents the predicted against actual values for dynamic froth stability along with % grade and % recovery of Pb, Cu, Zn and Fe for fresh and seawater. A 1:1 correlation line for each of the plot is also shown in Figure 6.6. The closer the points to the line, the better the agreement between the predicted values and the actual values.The coefficient of multiple determinations, R^2 was found to be 92.01%, 94.26%, 90.25% , 94.12% ,90.64%, 88.67%, 94.41%, 88.64%, and 80.55% for Pb grade, Pb recovery, Cu grade, Cu recovery, Zn grade, Zn recovery, Fe grade, Fe recovery, and

dynamic froth stability, respectively. The R^2 value is higher than 80% in all cases. This means that these models could explain more than 80% of the total variations in the system. The high value of R^2 indicates that the quadratic equations are capable of representing the system under the given experimental domain.

Table 6.4. ANOVA analysis results of the developed models for flotation and froth stability experiments using fresh and seawater.

		Sum of square	DOF	Mean square	F-value	P-value
Pb grade	Model	634.604	4	158.651	72.29	<0.05
	Residual	559.90	23	2.395		
Pb Recovery	Model	9199.00	5	1839.80	61.84	<0.05
	Residual	559.90	22	25.45		
Zn grade	Model	0.443972	5	0.088794	42.62	<0.05
	Residual	0.045839	22	0.002084		
Zn recovery	Model	1367.96	1	341.99	44.98	<0.05
	Residual	174.88	23	7.60		
Cu grade	Model	7.1704	3	2.39012	74.06	<0.05
	Residual	0.7745	24	0.03227		
Cu recovery	Model	2256.93	2	1128.46	84.06	<0.05
	Residual	147.67	11	13.42		
Fe grade	Model	15.3085	5	3.0617	74.34	<0.05
	Residual	0.9061	22	0.0412		
Fe recovery	Model	578.549	5	115.710	34.35	<0.05
	Residual	74.115	22	3.369		
Dynamic froth stability	Model	550.70	5	110.140	18.22	<0.05
	Residual	132.97	22	6.044		
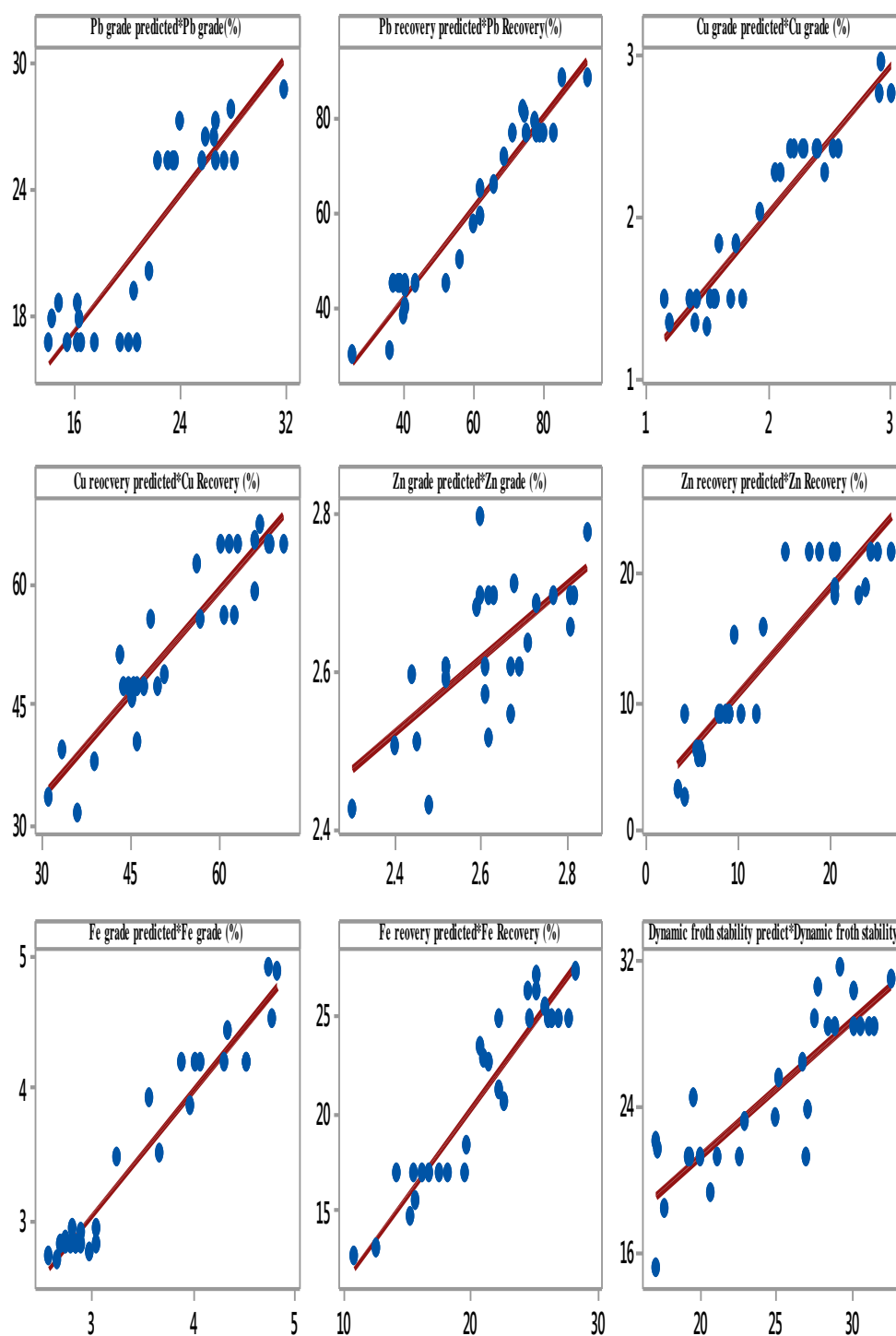
Figure 6.6. Plot showing the actual values vs predicted values of Pb grade, Pb recovery, Cu grade, Cu recovery, Zn grade, Zn recovery, Fe grade, Fe recovery and dynamic froth stability for fresh and seawater in flotation.

6.3.4. Optimization. The response optimizer in Minitab 17 was employed to find the optimum conditions to achieve maximum Pb grade, Pb recovery, Cu grade, Cu recovery, and dynamic froth stability while minimizing the grade and recovery of Zn and Fe in both Al_2O_3 and SiO_2 nanoparticles-aided flotation. All the results were computed using model Equations 25-42 within the experimental range of the study. The optimum flotation conditions for frother and collector found when seawater was used in flotation were 92.57 g/ton of frother (MIBC) and 117.15g/ton of collector, as shown in Figure 6.7. The corresponding values of Pb grade, Pb recovery, Cu grade, Cu recovery, Zn grade, Zn recovery ,Fe grade, Fe recovery and dynamic froth stability achieved at these conditions were 17.13 %, 84.57%, 2.01%, 59.79%, 2.6%, 15.25%, 2.75% and 26.47% and 22.41% ,respectively. Figure 6.8 gives the optimum flotation conditions of frother (MIBC) and collector for the desired results in freshwater. The optimum values of MIBC and collector were found to be 349.7 g/ton and 551.4 g/ton respectively. The values of Pb grade, Pb recovery, Cu grade, Cu recovery, Zn grade, Zn recovery, Fe grade, Fe recovery and dynamic froth stability obtained at optimum flotation conditions were 28.64%, 69.25%, 2.27%, 54.39 %, 2.47%, 7.28%, 3.54%, 23.84% and 30.80%, respectively.

6.4. CONTOUR PLOTS

To help view the changes in dynamic froth stability, Pb recovery and Cu recovery when process water is changed from fresh to sea water, contour plots were generated. Figure 6.9 and 6.10 show the effect of varying dosages of collector and frother on dynamic froth stability in the case of sea and fresh water respectively.

It can be seen from Figures 6.9 and 6.10 that a higher value of dynamic froth stability is achieved when fresh water is used as process water. It can therefore be inferred that in sulfide mineral flotation, ions present in sea water decrease the stability of froth. Another interesting observation from Figure 6.9 and 10 is that, in both fresh or sea water case, froth is found to be more stable below a collector dosage of 400 g/ton and frother dosage of 100 g/ton. As collector and frother dosage is increased above these values in both fresh and seawater cases, froth starts to become unstable. Froth again becomes stable as the collector and frother dosages exceed 500 g/ton and 150 g/ton respectively.

Figures 6.11 and 12 illustrate the effect of varying dosages of collector and frother on Pb recovery when sea or fresh water is used respectively. When sea water is used 20 % higher recovery of Pb is achieved as compared to fresh water. Sea water also consumes less amount of collector and frother to achieve this recovery. This clearly shows that sea water can be used effectively and economically when high Pb recovery is required in complex sulfide ore flotation.Effect of type of process water on recovery of Cu with varying dosages of collector and frother is elucidated in Figures 6.13 and 6.14. Again in sea water, a higher Cu recovery of 65 % is achieved as compared to fresh water, in which case a cu recovery of 50 % is accomplished. Moreover, less amount of reagents are consumed in seawater

6.5. DISCUSSION

Results from froth flotation tests carried with sea and fresh water are plotted in Figure 6.15. From Figure 6.15, it can be seen that while using seawater as process water
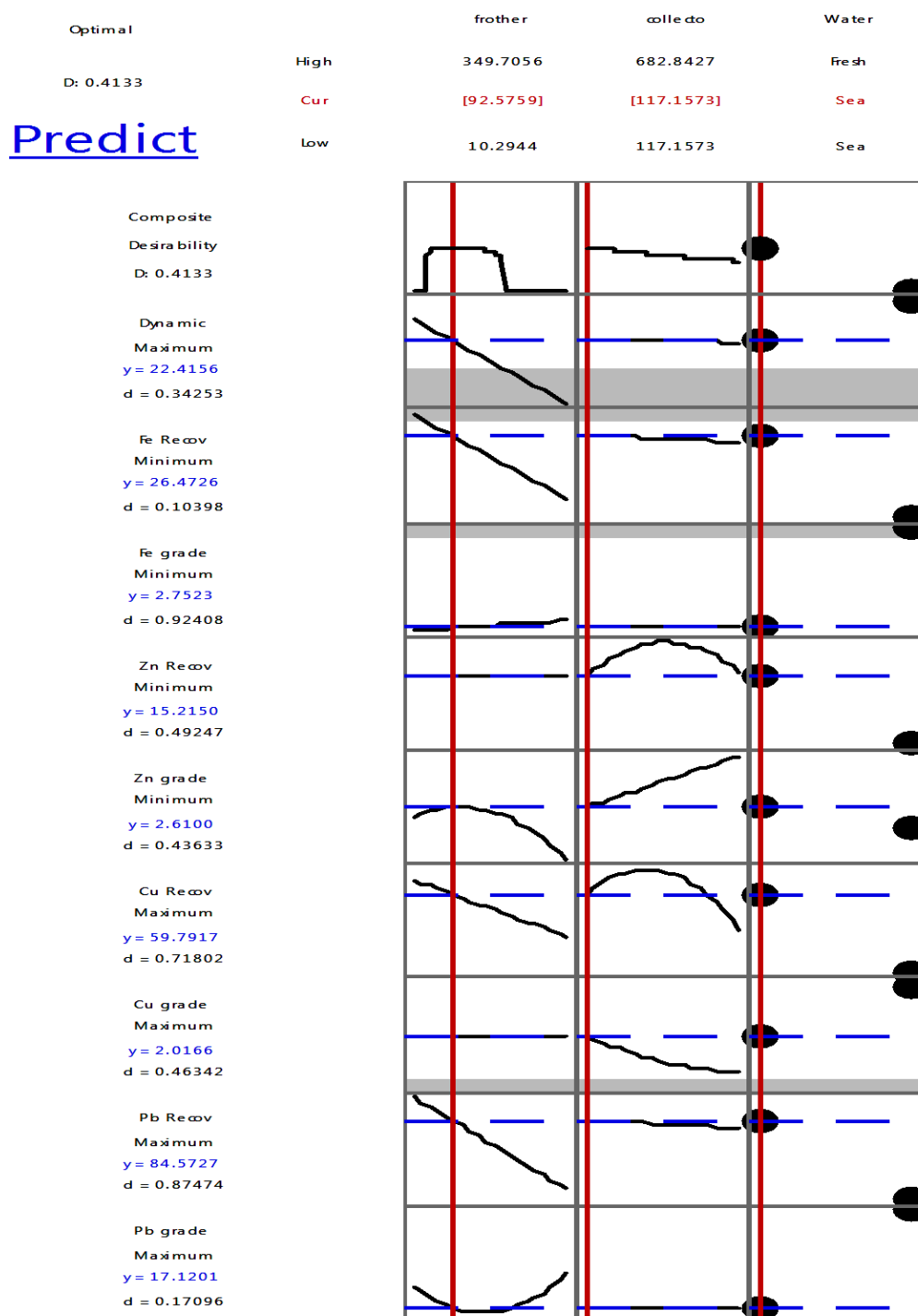
Figure 6.7. Optimum concentrations of frother (MIBC) and collector and corresponding values of Pb grade, Pb recovery, Cu grade, Cu recovery, Zn grade, Zn recovery, Fe grade, Fe recovery and dynamic froth stability in the case of seawater.
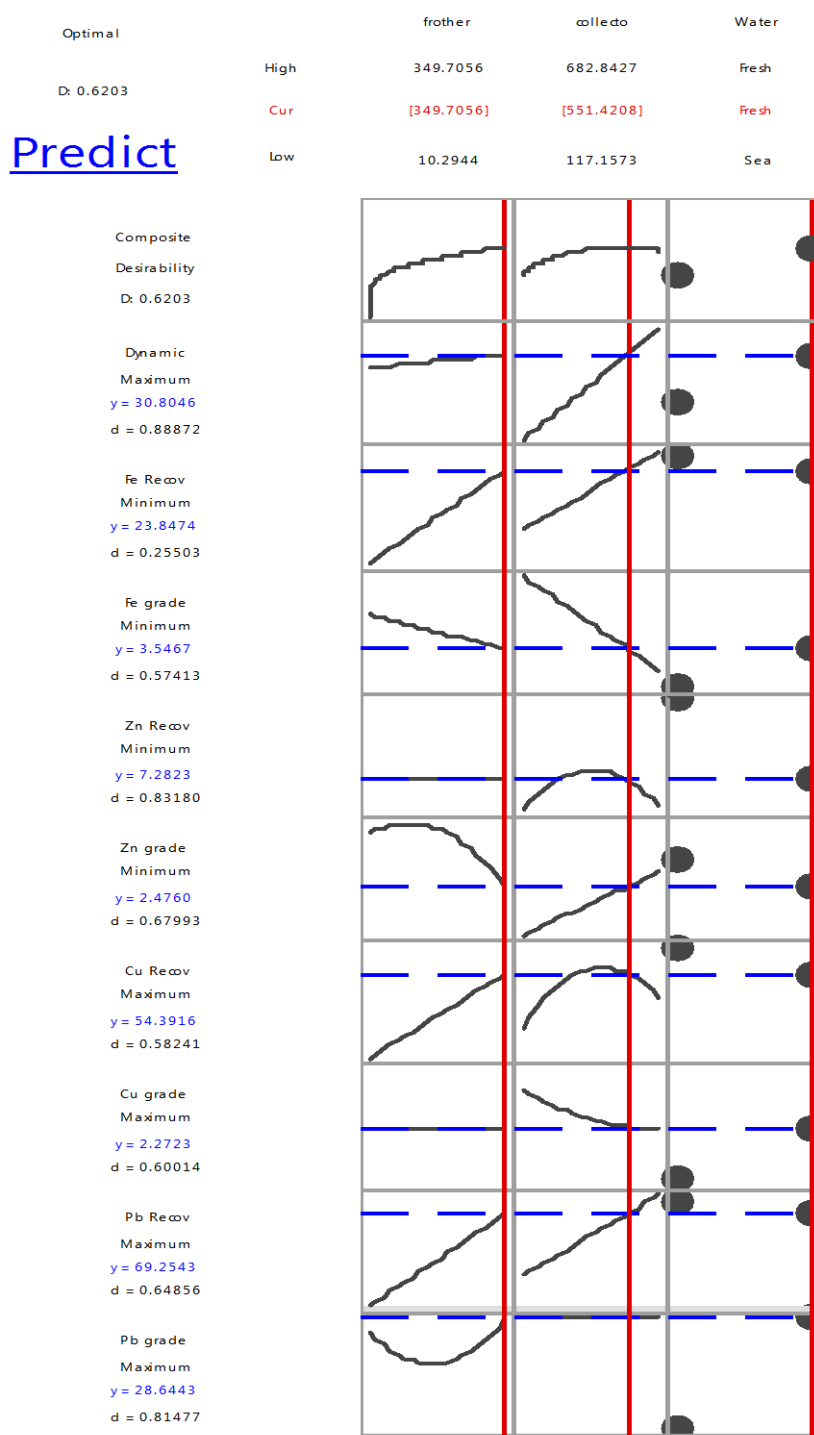
Figure 6.8. Optimum concentrations of frother (MIBC) and collector and corresponding values of Pb grade, Pb recovery, Cu grade, Cu recovery, Zn grade, Zn recovery, Fe grade, Fe recovery and dynamic froth stability in the case of freshwater.
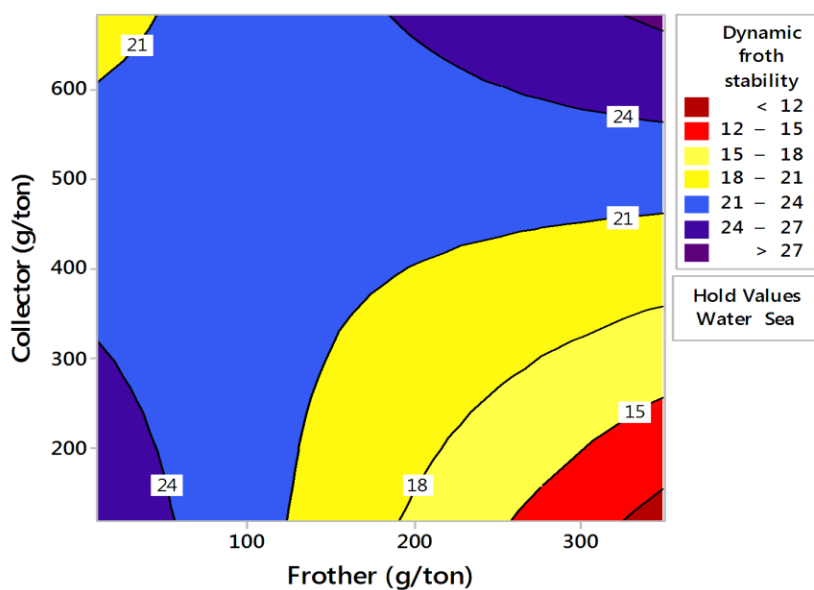
Figure 6.9. Contour plot of dynamic froth stability with varying dosages of frother and collector in seawater.
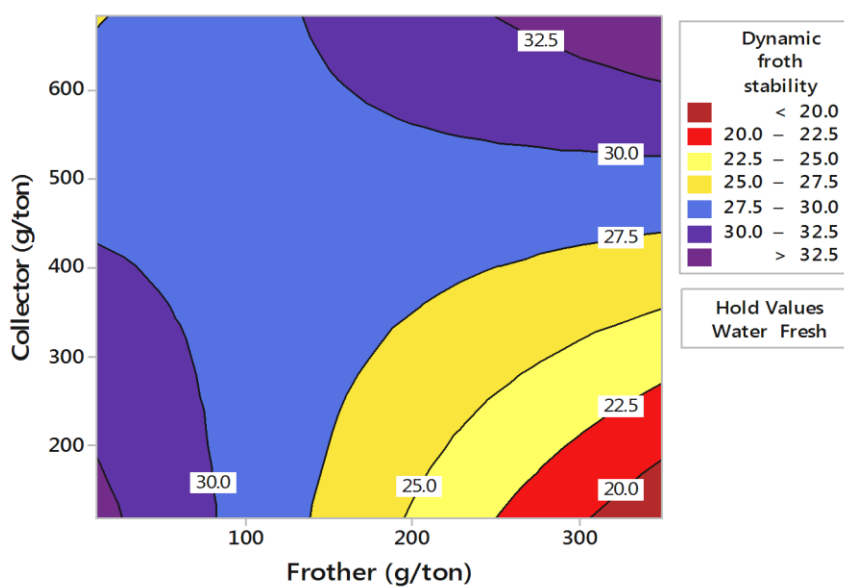
Figure 6.10. Contour plot of dynamic froth stability with varying dosages of frother and collector in fresh water.
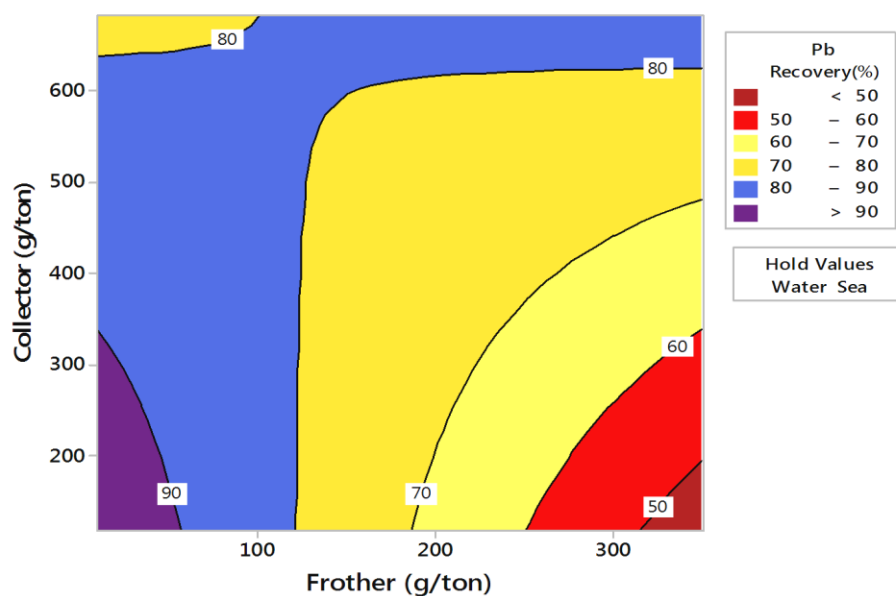
Figure 6.11. Contour plot of Pb recovery with varying dosages of frother and collector in seawater.
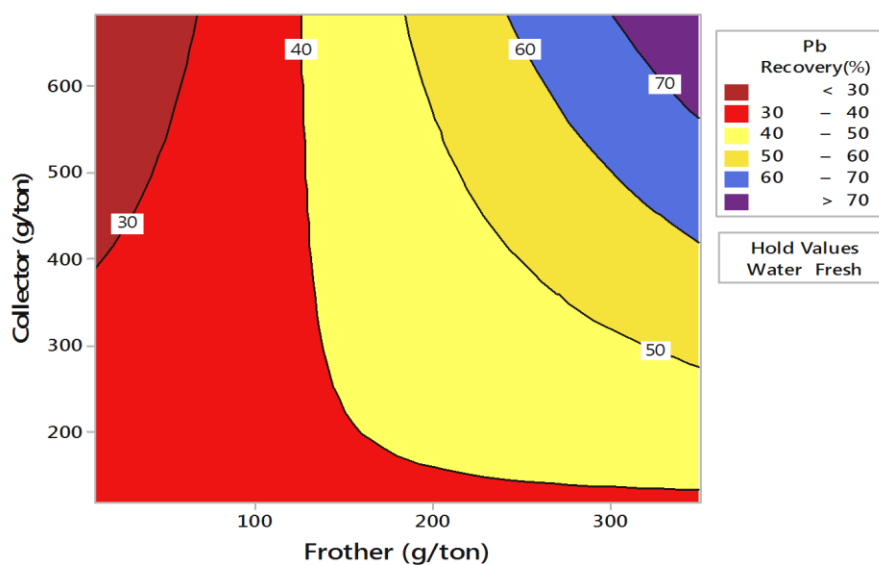
Figure 6.12. Contour plot of Pb recovery with varying dosages of frother and collector in fresh water.
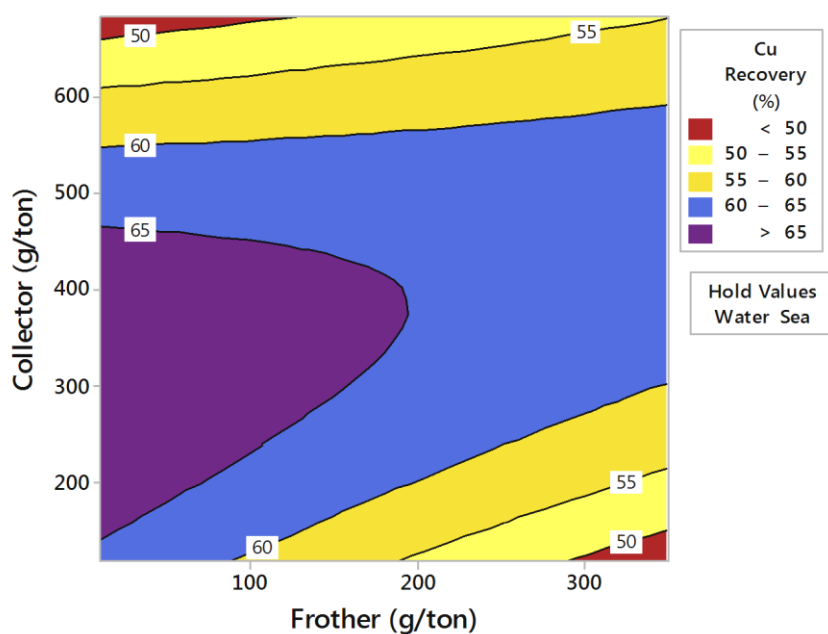
Figure 6.13. Contour plot of Cu recovery with varying dosages of frother and collector in sea water.
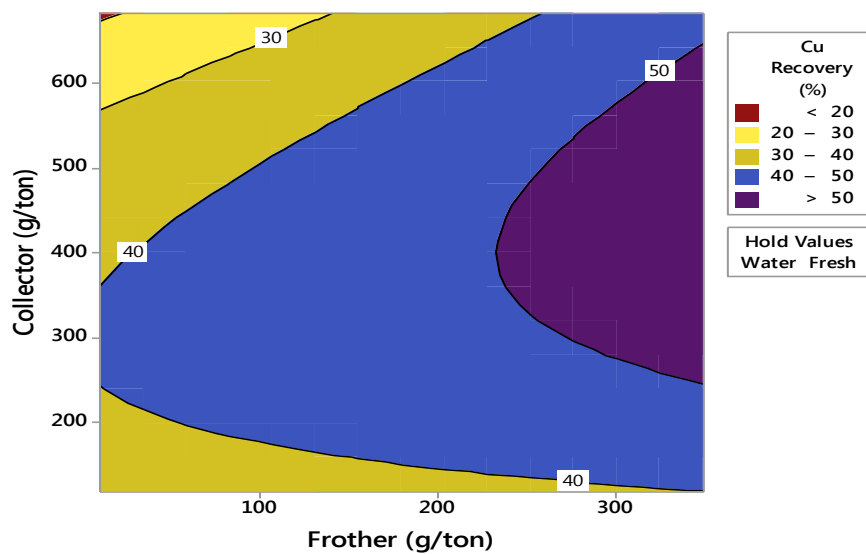
Figure 6.14. Contour plot of Cu recovery with varying dosages of frother and collector in fresh water.
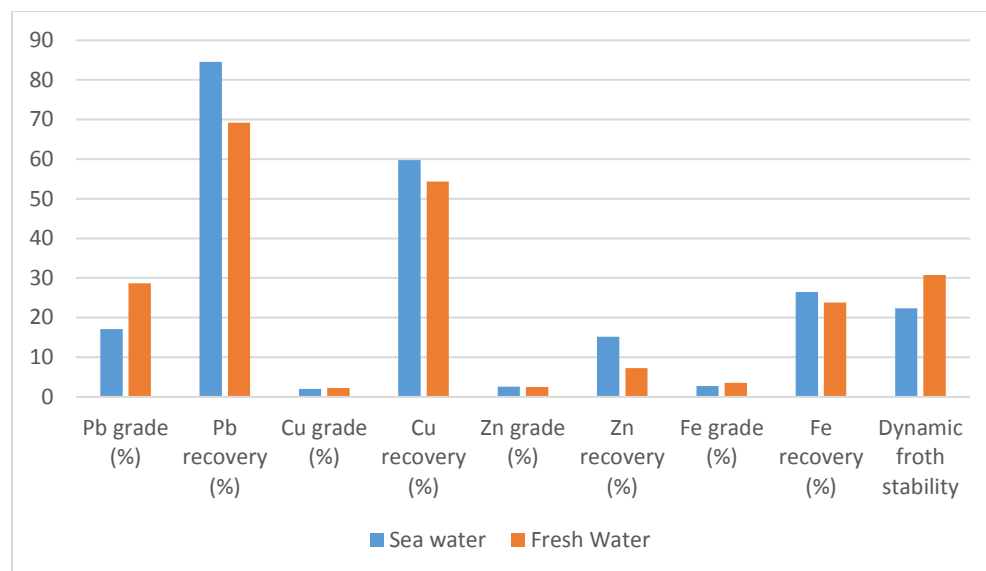
Figure 6.15. Comparison of Pb grade, Pb recovery, Cu grade, Cu recovery, Zn grade, Zn recovery, Fe grade, Fe recovery, and dynamic froth stability achieved in froth flotation tests with fresh and seawater as process water.

dynamic froth stability decreased by 8% as compared to when fresh water was used. This decrease in froth stability can be explained based on the joint effect of frothers and collectors with seawater. Much research has been done on the joint action of frother and inorganic salts on froth stability. It is well known that both frothers and salts have the ability of reduce bubble size and stop bubble coalescence. Frothers do this by reducing the surface tension of the solution. This ability of frothers is enhanced in a saline atmosphere, and thus an increase in froth stability is observed in saline water [125], [126]. Collector, on the other hand, has quite an opposite effect on froth stability. Sodium isopropyl xanthate was found to decrease the froth stability in a saline solution [127]. Xanthate collectors are specifically found to cause bubble coalescence and destabilization of froth in saline water flotation [128]. In addition to the part of collector to reduce froth

stability, ions in seawater also play a role in decreasing foam thickness as shown in Figure 6.16 [129].
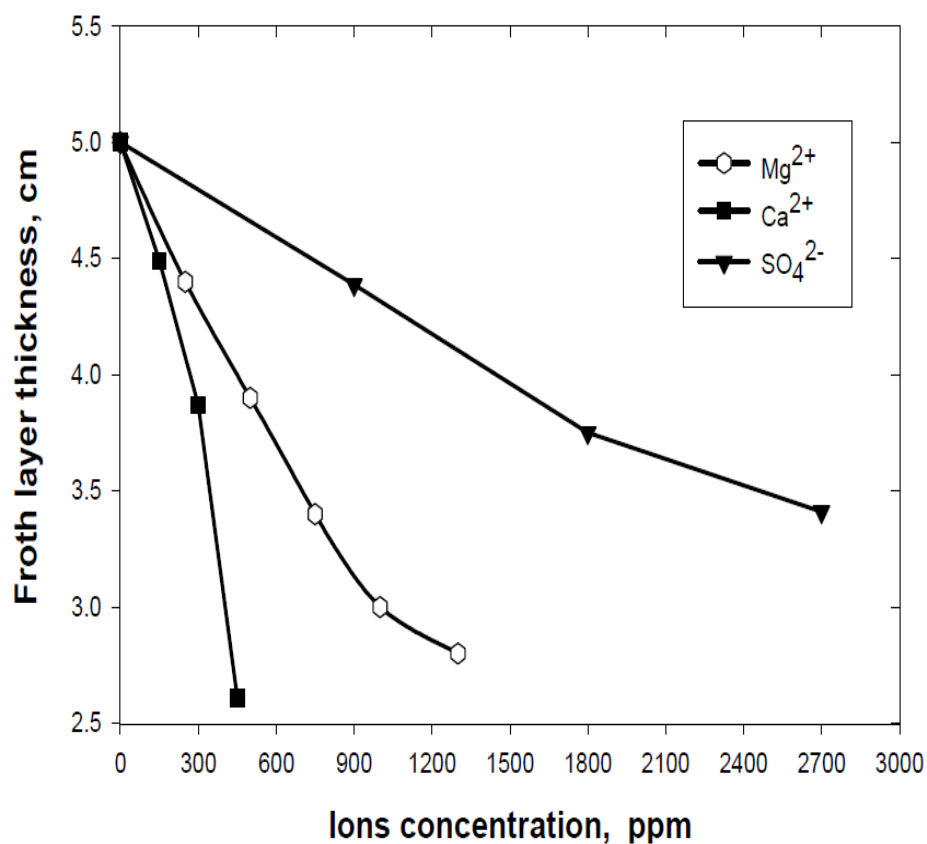
Figure 6.16. Thickness of froth layer affected by concentration of Ca^{2+}, Mg^{2+} and $(SO_4)^{2-}$ [129].

Based on the literature and the experimental results gathered in this study, the decrease in froth stability in the case of seawater flotation can be attributed to the joint action of sodium isopropyl xanthate and saline water augmented by the destabilizing effect of ions on froth stability. Regarding the effect of seawater on flotation

performance, it was observed that recovery of the metals Pb, Cu, Zn, and Fe was enhanced by 15.37 %, 5.4 %, 7.9%, and 2.6% respectively, when seawater was used. This increase is in line with the previous literature conducted in different ores. Use of seawater resulted a decrease in grade of all the metals except Zn, where change was negligible. Reduction in Pb, Cu, and Fe grade was found to be 11.52%, 0.26%, and 0.8%, respectively. This decrease in grades may be attributed to the depressing action of ions present in seawater on certain metals. This assumption is based on the evidence as observed in molybedenite depression in seawater due to the action of ions present in seawater [129].

Based on the observations done during this study it can be concluded that seawater reduces froth stability in complex sulfide ore flotation. However, the effect of seawater on flotation performance is positive overall. However it is important to adjust the frother and collector dosages when using seawater. This study has laid the foundation of selecting the proper reagent dosages for complex sulfide ore flotation by generating mathematical models as given by Equations 34 to 42.

It is recommended that fundamental research be conducted to determine the depressing effect of different ions in seawater on different metals in complex sulfide ore flotation. It is also suggested to test nano materials in seawater which may enhance the froth stability, thus helping to achieve grades comparable to fresh water.

7. ARTIFICIAL INTELLIGENCE AND MACHINE LEARNING MODELS FOR PREDICTING THE METALLURGICAL PERFORMANCE OF COMPLEX SULFIDE ORE FLOTATION PROCESS

7.1. BACKGROUND

In recent times, artificial intelligence (AI) methods particularly artificial neural network (ANN) have been used for predicting the metallurgical performance based on certain important operational variables for a flotation set-up. ANN with a single hidden layer have been used to predict the flotation performance by using the froth visual parameters including bubble size and bubble color as the only two inputs [157]. A comparison was carried out for the prediction performance of non-linear ARMAX, Takagi and Sugeno Fuzzy Logic, fuzzy combinational, projection on latent states (PLS), wavelet based models and Multi layered ANN for concentrate grade. It was concluded that PLS performed slightly better than ANN and significantly better than rest of the methods [158]. Least square support vector machine (LS – SVM) had been employed for predicting grade of both the concentrate and tailing from a floatation plant [159]. Multilayered ANN and Random Forest (RF) models were used for predicting the platinum concentrate grade by using froth images. Air flow rate, level of pulp along with the collector, activator, depressant and frother dosage were used as the inputs. ANN was found to outperform RF [160]. Adaptive principle component analysis (APCA) and composite kernel support vector regression (CK – SVR) have been used for predicting the concentrate grade and recovery of a for a flotation circuit [161]. An improved back propagation neural network method for predicting the concentrate grade for mineral floatation process has been recently introduced. PCA algorithm has been used in this

method to extract bubble characteristics by processing the digital images obtained

during the process [162]. Multi layered ANN and Multivariate Non-Linear Regression

(MNLR) have been used for predicting the grade and recovery of copper and

molybdenum for a flotation column plant. It was found that back propagation ANN has

better prediction capability than MNLR [163]. Artificial Neural Network (ANN) has also

been used for metallurgical performance prediction of copper and molybdenum grades

[114]. Performance of a copper flotation plant has been maintained through a controller

using fuzzy logic model [115]. ANN has been successfully used for predicting the iron,

phosphorus, sulfur and iron oxide recoveries from the final concentrate of iron ore

flotation plant. Particle size along with iron, phosphor, sulfur and iron oxide percentage

contents of run-on-mine were used as the inputs for the model [164]. Satisfactory results

were obtained via Mamdani Fuzzy logic (MFL) model to predict the iron and copper

recoveries for a copper flotation plant. Operational method, bacteria type and time was

used as the input parameters for the model and satisfactory prediction results were

obtained [116]. In another study, Multi layered ANN were employed for developing

predict models for grade and recovery of copper and molybdenum. Collector dosage,

frother dosage, F-oil dosage, pH of pulp, particle size, moisture content, solid percentage

and copper, molybdenum and iron grade in feed were used as the input parameters to

predict the metallurgical performance [117]. Work has been done to compare the non-

linear regression technique, ANN and Adaptive Neuro Fuzzy Inference System (ANFIS)

for predicting copper grade and recovery. Flow rate of the gas, solid percentage, pH of

the slurry, frother & collector dosages were used as the input parameters. It was shown

that ANN and ANFIS performed better than the statistical method [165].

Various artificial intelligence (AI) methods, mainly neural networks have been used by previous researchers for predicting the performance of a flotation process. This study is the first attempt in developing five of the main artificial intelligence (AI) and machine learning (ML) models for predicting the grade and recovery of bulk flotation of chalcopyrite and galena. All the credit for programming the models goes to Danish Ali, who is a current PhD student in Mining engineering department at Missouri S & T.This work when up scaled to plant level, will provide the required framework to test various flotation configurations with no cost and time expense, obtain the optimal values for all the variables and design the plant as per the required specifications.

7.2. FLOTATION EXPERIMENTS

Two sets of 62 flotation experiments were carried out to test the effect of seven operational variables on flotation performance (Table 3.1). Details of the process and results are discussed in Section 3. Same results are being used to apply AI and ML models to predict the flotation performance.

7.3. MACHINE LEARNING (ML) & ARTIFICIAL INTELLIGENCE (AI) MODELS

Five of the main ML and AI models namely Artificial Neural Network (ANN), Adaptive Neuro Fuzzy Inference System (ANFIS), Mamdani Fuzzy logic (MFL), Random Forest (RF) and Hybrid Neuro Fuzzy Inference System (HyFIS) introduced by Rosenblatt [166], Jang [167], Mamdani [168], Breiman [169] and Kim and Kasabov [170], respectively, were used for predicting the metallurgical performance of bulk flotation of galena and chalcopyrite.

7.3.1. Tree Based Method. Random forest method, was developed by Breiman (2001). This method not only looks at the correlation, but also takes into account the interactions between the features. Random forest has a binary tree as its basic component. This tree is constructed by using the Recursive partitioning (RPART). After this, classification and regression tree (CART) is used to expand the base learner. Partinioing of each tree is done into consistent or near consistent nodes. Random trees are combined to build a complete random forest. Each tree is constructed using data set from the training data, also known as bootstrap data sample.The remaining training data set samples are known as out–of –bag observations. Set of variables at each node split of a tree are also assigned randomly. Correlation among the trees is ensured through these randomness inducing layers and therefore low variance forest is constructed. Figure 7.1 shows the working of a random forest algorithm [169].

7.3.2. Artificial Neural Network. Artificial neural network (ANN) is a intensive computation method based on mimicking the functioning of human brain [171]. ANN consists of three main layers consisting of Input, Output and single or multiple Hidden layers. Each layer in the networks comprises several neurons or nodes. The neurons in different layers are connected with each other through weighted connections. Each connection between the neurons of different layers is assigned a random weight [172]. Input data is provided to the input layer which transmits it to the first hidden layer. From the first hidden layer, data is transmitted to anyother hidden layer culminating in the output layer. Neurons present in the hidden layer and the output layer of ANN, process the data and apply weights to them based on the closeness of the predicted and actual results. There is bias provided for each hidden and output layer neuron to
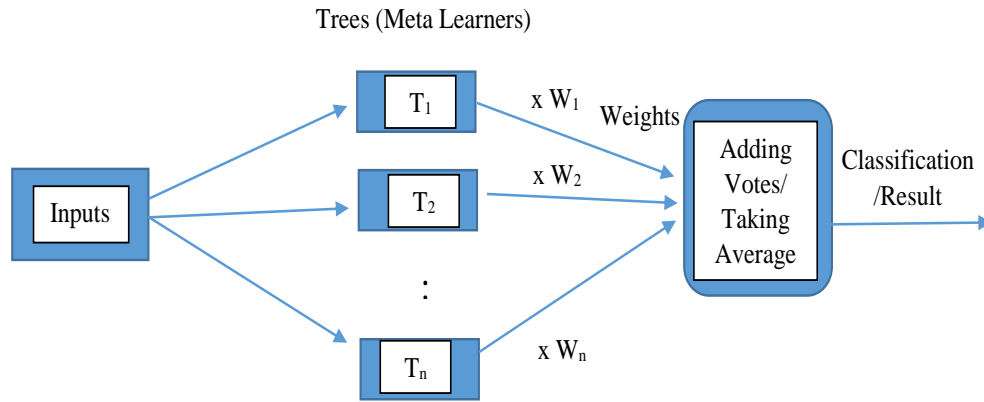
Figure 7.1. RF Algorithm. T_n and W_n indicates the nth tree and weight, respectively. If un-weighted method is used: $W_1 = W_2 = \ldots = W_n = 1$ [173].

make sure the neuron produces a non-zero output even if inputs are zero. An activation or transfer function is used by the neurons to process the weighted inputs and the output is generated. Most commonly used transfer functions include Sigmoid, Gaussian, Hyperbolic Tangent and Hyperbolic Secant [174].

The most commonly used ANN method is Multi-layer perceptron (MLP) in supervised learning [175]. Figure 7.2 shows the general MLP structure with a single hidden layer. Expression providing the output for MLP model is given by Equation 43[176]–[178].

$$y_k = f_0 \left[\sum_{j=1}^{H_N} W_{kj} \cdot f_h \left(\sum_{i=1}^{I_N} W_{ji} \cdot X_i + W_{j0} \right) + W_{k0} \right] \tag{43}$$

Where,

W_{ji} = Hidden layer weight connecting hidden layer jth neuron and input layer ith

neuron

W_{j0} = hidden layer jth neuron bias

f_h = Hidden neuron transfer (activation) function

W_{kj} = Output layer weight connecting hidden layer jth neuron and output layer jth neuron

W_{k0} = Output layer kth neuron bias

f_0 = Output neuron transfer (activation) function

X_i = ith input variable

y_k = Output variable

I_N = Total number of neurons in input layer

H_N = Total number of neurons in hidden layer

7.3.3. Fuzzy Logic Approach. Fuzzy set theory was developed by

Zadeh (1965). Fuzzy sets have tremendous ability to accommodate human and sytem

uncertainities [180]. Membership values in fuzzy logic syatems range from [0, 1] with

value of 1 stating a complete acceptance of membership and vice versa.

Figure 7.3 shows the illustrates the fuzzy logic approach. Fuzzy logic approach consists

of three stages named Fuzzification, Inference, and Defuzzification. During first stage

transformation of normal input variable values, known as crisp inputs, to linguistic terms

takes place. Second stage consists of mapping the linguistic inputs to linguistic output

values using some fuzzy if-then rules. In third stage linguistic out put values are

transformed into normal/real values known as crisp outputs. The two main fuzzy logic

methods include Mamdani fuzzy logic method [168] and Sugeno fuzzy logic method

[181]. These methods differ on the basis of the way fuzzy if-then rule base is formed.
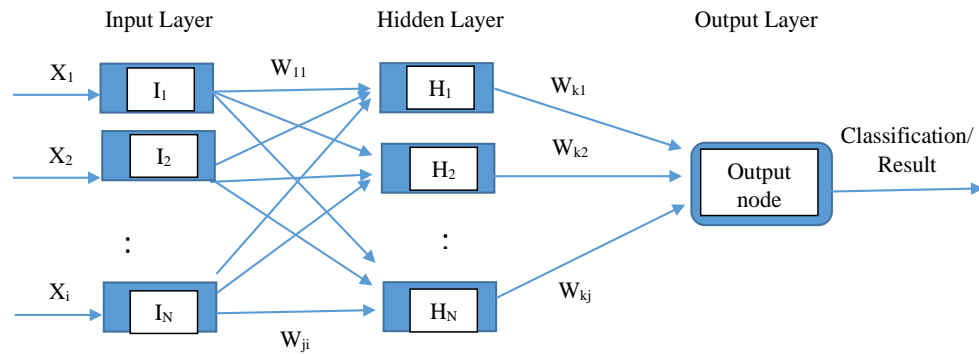
Figure 7.2. Schematic for MLP model with single hidden layer. Here: X_i = ith input variable, I_N = Total number of neurons in input layer, H_N = Total number of neurons in hidden layer, W_{ji} = Hidden layer weight connecting hidden layer jth neuron and input layer ith neuron, W_{kj} = Output layer weight connecting hidden layer jth neuron and output layer jth neuron [173].

Data sets in these methods can be clustered using either Fuzzy c-means (FCM) or subtractive clustering for Mamdani model. 'Min' operator is used as the implication method [182] and 'max' operator is utilized for rule aggregation [183] in Mamdani fuzzy logic model.

As an example, consider following a rule base: RB^i: if x is A_i and y is B_i then Z is C_i where i = 1, 2, 3, ... , n, Then; $RB^i = (A_i \wedge B_i) => C_i$ is defined by $\mu_{RB}{}^i = \mu_{(Ai \wedge Bi) => Ci}$ (x,y,z). With two inputs (x_o and y_o), following output will be produced by using the above rule as in Equation 44:

$$
\begin{cases}
\mu_{C_i'}(Z) = \left[\mu_{A_i}(x_o) \wedge \mu_{B_i}(y_o)\right] \to \mu_{C_i}(Z) = \alpha_i \wedge \mu_{C_i}(Z) \\
\mu_{C'}(Z) = \mu_{C_1}(Z) \vee \mu_{C_2}(Z) = \left[\alpha_1 \wedge \mu_{C_2}(Z)\right] \vee \left[\alpha_2 \wedge \mu_{C_2}(Z)\right] \\
\mu_{C'}(Z) = \cup_{i=1}^n \left[\alpha_i \wedge \mu_{C_i}(Z)\right] = \cup_{i=1}^n \mu_{C_i'}(Z), \ C' = <=_{i=1}^n C_i'
\end{cases}
\quad (44)
$$

7.3.4. Adaptive Neuro Fuzzy Inference System. ANFIS is a hybrid intelligent method combining ANN and fuzzy logic system. It uses Takagi Sugeno fuzzy inference model for creating an inference system for the input data values and then uses artificial neural network for membership function parameters adjustment [184].
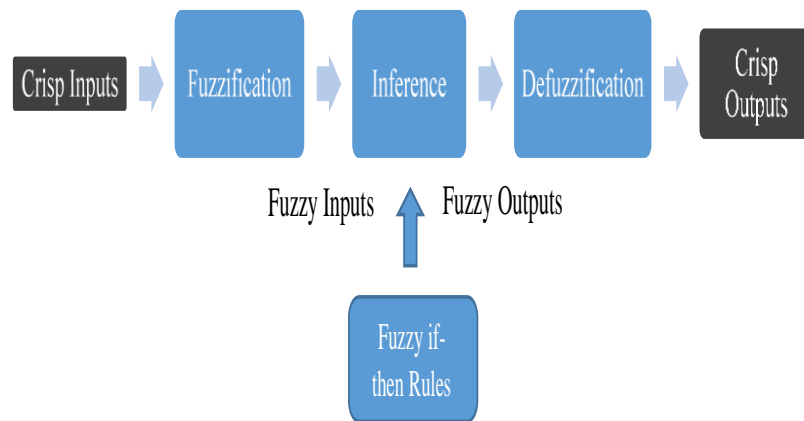
Figure 7.3. General schematic for Fuzzy logic system [173].

Figure 7.4 shows the structure of ANFIS. It consists of five layers. Working of ANFIS can be elaborated through and example having only two inputs with single output. Let these two inputs to be 'x' and 'y' as shown in Figure 7.2. Following is the relationship between the inputs and the outputs of each layer as explained by [167] [173]:

Layer 1: Each node 'i' in this layer constructs membership grade for each input variable. The output for each node can be defined as in Equations 45 & 46:

$$O_{1,i} = \mu_{A_i}(x) \; ; \; i = 1, 2 \tag{45}$$

$$O_{1,i} = \mu_{B_{i-2}}(y) \; ; \; i = 3, 4 \tag{46}$$

Where, 'A$_i$' and 'B$_{i-2}$' are the linguistic fuzzy input variables of the corresponding node with its shape being defined through a particular membership function (μ). Various membership functions are available, most commonly used are as given in Equations 47 & 48:

$$\mu_{A_i}(x) = e^{-\frac{1}{2}\left(\frac{x-c_i}{SD_i}\right)^2} \quad \text{(Gaussian MF)} \tag{47}$$

$$\mu_{A_i}(x) = \frac{1}{1 + \left[\left(\frac{x-c_i}{SD_i}\right)^2\right]^{b_i}} \tag{48}$$

In this layer, $\{SD_i, b_i, c_i\}$ are the set of parameters that defines the membership function shape and are commonly regarded as "premise parameters"

Layer 2: Firing strength of the rule 'w$_i$' is computed by each of node in this layer. Output of each node in this layer is basically a product of all its inputs for each node as given by Equation 49:

$$O_{2,i} = w_i = \mu_{A_i}(x) \times \mu_{B_i}(y) \; ; \; i = 1, 2 \tag{49}$$

Layer 3: Each node in this layer computes the normalized firing strength '$\overline{w_i}$' by calculating a ratio of a particular node firing strength to the sum of all the firing strengths (Equation 50):

$$O_{3,i} = \overline{w_i} = \frac{w_i}{w_1 + w_2} \; ; \quad i = 1, 2 \tag{50}$$

Layer 4: In this layer an overall rule contribution (ith rule) in the overall model output is computed for each node (ith node) via Equation 51:

$$O_{4,i} = \overline{w_i} f_i = \overline{w_i} \, (p_i x + q_i y + r_i) \; ; \quad i = 1, 2 \tag{51}$$

In this layer, $\{p_i, q_i, r_i\}$ are the set of parameters that are known as "consequent parameters".

Layer 5: This layer consists of a single node for each output variable which computes the overall ANFIS output by taking the sum of all the inputs to that particular node as expressed by Equation 52:

$$O_{5,i} = \sum_{i=1}^{2} \overline{w_i} f_i = \frac{\sum_{i=1}^{2} w_i f_i}{\sum_{i=1}^{2} w_i} = \overline{w_i} \, (p_i x + q_i y + r_i) \tag{52}$$

7.3.5. Hybrid Neuro Fuzzy Inference System. Hybrid Neuro Fuzzy Inference System (HyFIS) was developed by Kim and Kasabov (1999). HYFIS has two lerning phases termed as knowledge acquisition and parameter learning. Wang and Mendel
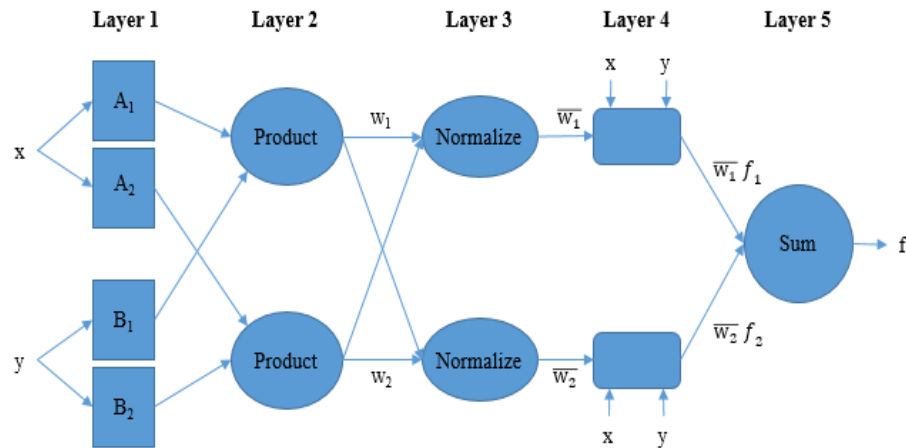
Figure 7.4. General ANFIS schematic with two crisp inputs 'x' and 'y' and one output. Here: 'A$_i$' and 'B$_i$' are the linguistic fuzzy input variables with i = 1,2 [173].

technique is used for knowledge acquisition from the input data. A supervised learning method with gradient descent based algorithm is used afterwards for parameter and structure learning. Through a combination of these two phases a database consisting of rules along with the membership function parameters is generated. Gaussian function is used as the membership function in HyFIS [170][185][173].

7.3.6. Model Performance Criteria. Coefficient of determination (R^2) and Root Mean Square Errors (RMSE), as given by Equations (53) and (54), respectively, were used as the statistical indicators in order to evaluate the performance of each of the machine learning and artificial intelligence model in this work. The value for the coefficient of determination (R2), describing the degree of correlation, ranges between [0, 1]. The closer the value of R2 to 1, the better the correlation between the predicted and the actual values. RMSE ranges between [0, ∞] indicating the variance of errors. The

closer the value of RMSE to 0, the better the match between the actual and the

predicted values [186].

$$R^2 = \frac{[\sum_{i=1}^{n}(P_i - \bar{P})(A_i - \bar{A})]^2}{[\sum_{i=1}^{n}(P_i - \bar{P})^2 (A_i - \bar{A})^2]} \tag{53}$$

$$RMSE = \sqrt{\frac{\sum_{i=1}^{n}(P_i - A_i)^2}{n}} \tag{54}$$

Where,

n = Total number of observations in the data being used

P_i = Predicted value by the model

A_i = Actual value in data

$\bar{P}$ = Mean of all the predicted values

$\bar{A}$ = Mean of all the actual values

7.4. DATA PREPARATION AND AI MODELING

Data preparation involves division of the total data (flotation experiment inputs

and outputs) into training and testing subsets containing 80% and 20% of the total data,

respectively for training and validating ML and AI models. Each observation in the

subset includes data containing five inputs and six outputs. Division of the data was done

by using cross validation method [187]. Table 7.1 displays the statistical quality analysis

results for training and test data set with providing the minimum value, maximum value,

mean/average value, standard deviation and the coefficient of variation for all the

variables (both the input and the output).

Software R was used for ML and AI modelling. Both the training and testing data

sets were normalized between 0 and 1, through linear mapping as given by Equation (55).

Denormalization of the output values was done once model training was finished [188].

$$X_n[0, 1] = \frac{X - X_{min}}{X_{max} - X_{min}} \qquad (55)$$

Where,

X_n = Normalized value for variable 'x'

X_{max} = Maximum value of variable 'x'

X_{min} = Minimum value of variable 'x'

X = Actual value of variable 'x'

7.5. IMPLEMENTATION AND RESULTS OF MODELLING

Detailed implementation of each of the AI and ML models and results obtained

are discussed below.

7.5.1. Random Forest Model Results. All the input and output variable

identifications were provided through a formula for training phase in supervised mode.

Number of trees 'ntree' to be randomly grown in the forest and the number of variables to

be randomly selected at each node split 'mtry' are the two most important parameters for

RF model. There is no limitation on number of trees so 'ntree' was set to 1000. For

obtaining an optimal value for 'mtry', parameter tuning process was employed. After

running the model multiple times for a fixed 'ntree' of 1000, an optimum value of '7'

was obtained through cross validation (CV) method. Then the optimal value was used

during the training phase for model development.

Figures 7.5A, 7.5B, 7.6A and 7.6B display the plots between real and predicted

values (by random forest model) for lead recovery, lead grade, copper recovery and

copper grade, respectively for the model training phase. Figures 7.7A, 7.7B, 7.8A and

7.8B display plots between real and predicted values (by random forest model) for lead

recovery, lead grade, copper recovery and copper grade, respectively for the model

testing phase. Figure 7.9 illustrates the importance of all the input variables in forest

building. It can be seen that impeller speed is the most important input variable for all the

output variables prediction based on RF model.

   7.5.2. Artificial Neural Network Results. ANN was developed for predicting

the metallurgical performance of the froth floatation of complex sulfide ore. Resilient

backpropagation with weight backtracking was used as the training algorithm for single

hidden layer ANN. Trial and error methodology [189] was used to obtain the optimal

number of hidden neurons. The range based on the Equations (56) and (57) provided by

Wanas et al. [190] and Mishra and Desai [191], respectively, came out to be between 2

and 15 .

However, the optimal number of hidden neurons was selected based on the point

where the model performance stabilized. Value for the number of hidden neurons came

out to be 30 and was used to develop the final ANN model. TANSIG and PURELIN

functions were used as the activation functions for hidden and output layer, respectively.

Training data set was used during the training phase and the iterations stopped as soon as

the specified threshold error of 0.01 was reached. After training, the model was validated through the testing phase.

The predicted outcomes were compared with the original values to evaluate the performance of ANN model. The developed ANN model is displayed in Figure 7.10. In order to reach a final threshold 0.01, the model had to go through a total 862 steps during the training phase. Weight vectors, connecting the neurons, are represented with black lines in Figure 7.10. Whereas, bias is represented with blue lines. Figure 7.11 shows the ANN model with no visual cluttering issue. Thickness of line shows the magnitude of the weight and color shows the weight sign (black indicates positive, grey indicates negative).
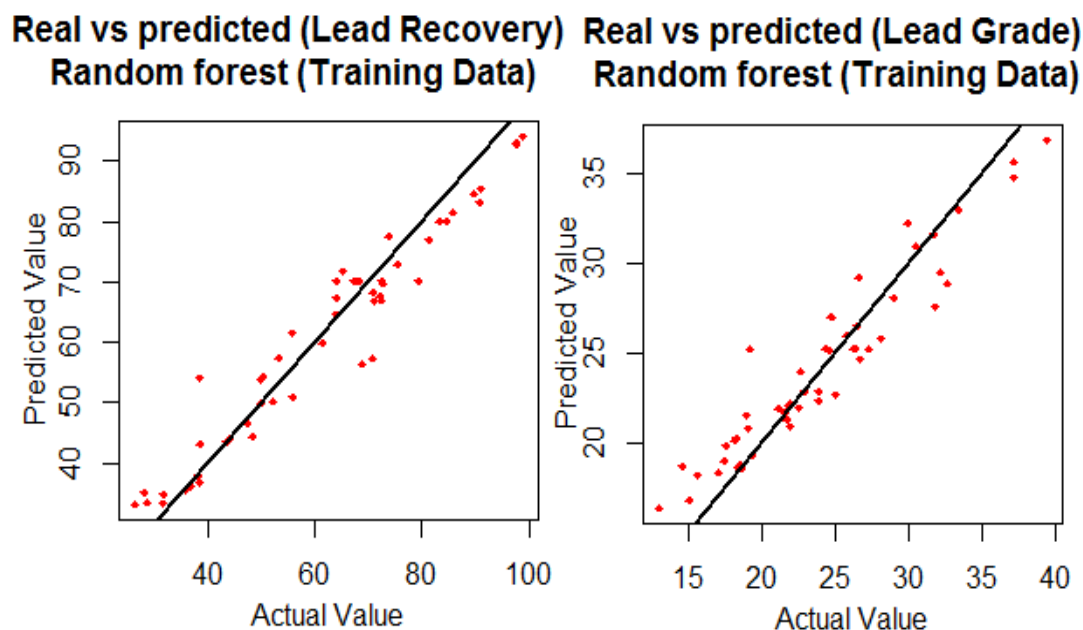
Figure 7.5. Real vs Predicted values plot for the training phase of the Random Forest (RF) model (A) Lead recovery and (B) Lead grade.

Table 7.1. Quality analysis of Training and Test Data Sets.

	Minimum	Maximum	Mean	Standard Deviation (SD)	Coefficient of Variation (COV)
Training Data					
Sodium Isopropyl Xanthate (ppm)	100	450	271.5	107.8205	39.71287
Sodium Cyanide (ppm)	50	350	191	87	45.54974
MIBC (ppm)	5	100	51.55	32.20206	62.46762
Zinc Sulfate (ppm)	200	700	445	161.9413	36.39131
Impeller Speed	3	9	6.18	1.840543	29.78226
Air Rate (l/min)	800	1800	1290	308.0584	23.8805
Flotation Time	2	8	4.94	1.748256	35.3898
Lead Grade (%)	13.02	39.46	24.084	6.132633	25.46309
Lead Recovery (%)	26.21	98.94	60.969	19.58045	32.11531
Copper Grade (%)	0.772	5.1	2.7478	1.002568	36.48578
Copper Recovery (%)	7.09	70.2	37.464	12.96619	34.60943
Test Data					
Sodium Isopropyl Xanthate (ppm)	100	450	260.41	112.0167	43.01442
Sodium Cyanide (ppm)	50	350	212.5	96.01432	45.18321
MIBC (ppm)	5	100	48.541	23.41782	48.24271
Zinc Sulfate (ppm)	200	700	470.83	123.2517	26.17734
Impeller Speed	3	9	5.75	1.920286	33.39629
Air Rate (l/min)	800	1800	1341.6	320.0477	23.85449
Flotation Time	2	8	5.25	2.277608	43.38302
Lead Grade (%)	14.67	39.33	26.259	9.089104	34.61307
Lead Recovery (%)	19.26	75.54	57.721	17.35179	30.06113
Copper Grade (%)	0.035	3.127	2.1507	0.794644	36.94787
Copper Recovery (%)	11.19	55.74	35.76103	14.30665	40.00626

Figure 7.6. Real vs Predicted values plot for the training phase of the Random Forest (RF) model (A) Copper recovery and (B) Copper grade.

Figure 7.7. Real vs Predicted values plot for the testing phase of the Random Forest (RF) model (A) Lead recovery and (B) Lead grade.

Real vs predicted (Copper Rec.) Random forest (Test Data)

Real vs predicted (Copper Grade) Random forest (Test Data)

Figure 7.8. Real vs Predicted values plot for the testing phase of the Random Forest (RF) model (A) Copper recovery and (B) Copper grade.
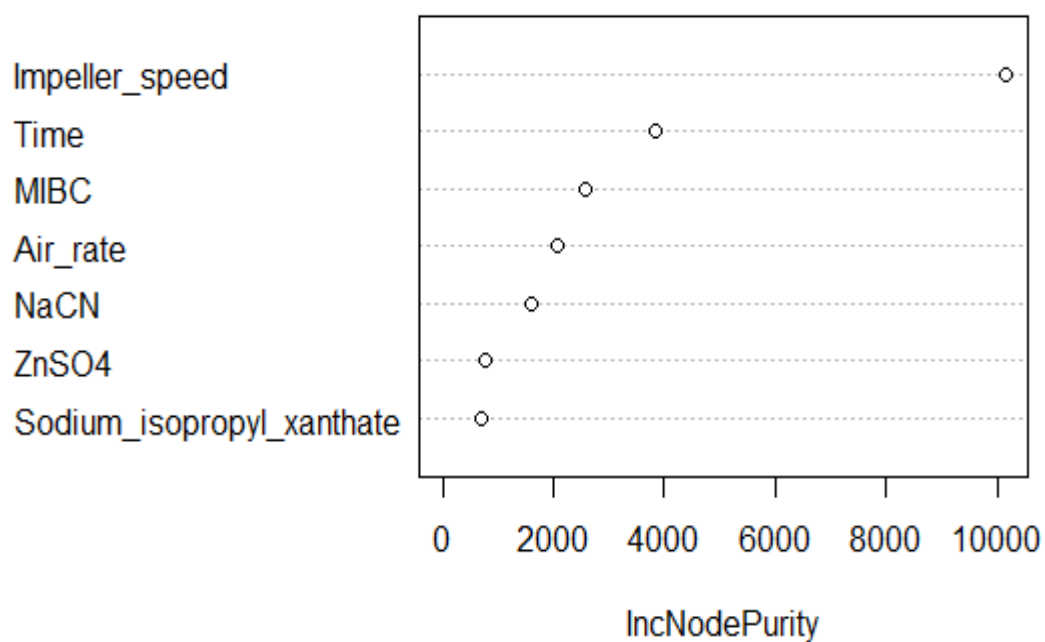
Figure 7.9. Variable Importance within Forest Model.

$$H_N = \log(n) \quad [190] \tag{56}$$

$$H_N = 2(I_N) + 1 \quad [191] \tag{57}$$

Where,

H_N = Total number of hidden neurons

n = Total number of training data samples

I_N = Total number of input neurons

Figures 7.12A, 7.12B, 7.13A and 7.13B display the plots between real and predicted values (of ANN model) for lead recovery, lead grade, copper recovery and copper grade, respectively for the model training phase. Figures 7.14A, 7.14B, 7.15A and 7.15B display the plots between real and predicted values (ANN model) for lead recovery, lead grade, copper recovery and copper grade, respectively for the model training phase.

7.5.3. Mamdani Fuzzy Logic. The prediction model for metallurgical performance was trained using Mamdani Fuzzy Logic (MFL). In order to form the fuzzy if-then rules, the task of pattern recognition was done by using Fuzzy c-Means (FCM) clustering method, developed by Dunn [192]. Parameter 'm' is the most important parameter in FCM and its value was set to 2 as recommended by Hathaway and Bezdek [193]. A total of 57 fuzzy if-then rules were developed and further used for training of the model. Model was developed with Gaussian membership functions for both input and output variables. Gaussian membership functions for all the five input variables are shown in Figure 7.16.

Plots for experimental vs predicted values of training phase of the Mamdani Fuzzy logic model for lead recovery, lead grade, copper recovery and copper grade have been shown in Figures 7.17A, 7.17B, 7.18A and 7.18B, respectively. Plots for real vs predicted values of testing phase of the Mamdani Fuzzy logic model for lead recovery, lead grade, copper recovery and copper grade have been shown in Figures 7.19A, 7.19B, 7.20A and 7.20B, respectively.

7.5.4. ANFIS Model. ANFIS model is trained using the least square method with back propagation for parameter learning in which the membership function are optimized for antecedent & consequent parts [194]. Membership grade for each input variable is developed with Gaussian membership functions in the fuzzification process. For model development, t-norm and s-norm are set to 'min' and 'max', respectively. Total number of iterations were fixed to 1500. Step size of '0.01' was used for the back propagation optimization. Fifty five fuzzy if-then rules were used to construct the ANFIS model using Takagi Sugeno (TSK) method. Gaussian membership functions for ANFIS model are shown in Figure 7.21. Plots for real vs predicted values of training phase of the ANFIS model for lead recovery, lead grade, copper recovery and copper grade have been shown in Figures 7.22A, 7.22B, 7.23A and 7.23B, respectively. Plots for experimental vs predicted values of testing phase of the Mamdani Fuzzy logic model for lead recovery, lead grade, copper recovery and copper grade have been shown in Figures 7.24A, 7.24B, 7.25A and 7.25B, respectively.

7.5.5. HyFIS Model. HyFIS model was developed with a rule base consisting of 55 fuzzy if-then rules. Prediction phase is carried out through Mamdani fuzzy logic method. Whereas, parameter tuning phase is done by gradient decent based error back

propagation. Fuzzification is done with Gaussian membership functions with t-norm and maximum number of iterations set to 'min' and 1000, respectively. Defuzzification is done by employing the Modified Center of Gravity (COG) function for the output variables. Figure 7.26 displays the Gaussian membership functions for developed HyFIS model. Figures 7.27A, 7.27B, 7.28A and 7.28B display the plots between real and predicted values (of HyFIS model) for lead recovery, lead grade, copper recovery and copper grade, respectively for the model training phase. Figures 7.29A, 7.29B, 7.30A and 7.30B display the plots between experimental and predicted values (of HyFIS model) for lead recovery, lead grade, copper recovery and copper grade, respectively for the model testing phase.

7.6. RESULTS

A total of five AI or ML models namely ANN, RF, Mamdani, ANFIS and HyFIS were developed during the course of this study. The performance of these five models was evaluated and compared for the prediction of metallurgical performance of bulk flotation of galena and chalcopyrite in complex sulfide ore flotation process. The developed models were validated once the training phase was completed. Table 7.2 contains all the R^2 and RMSE results for each of the five developed models for both the training and testing phase. On the basis of these statistical performance indicator results, it is evident that all the models predicted the recovery and the grade of both copper and lead, during the complex sulfide ore flotation process of galena and chalcopyrite , with considerable accuracy.
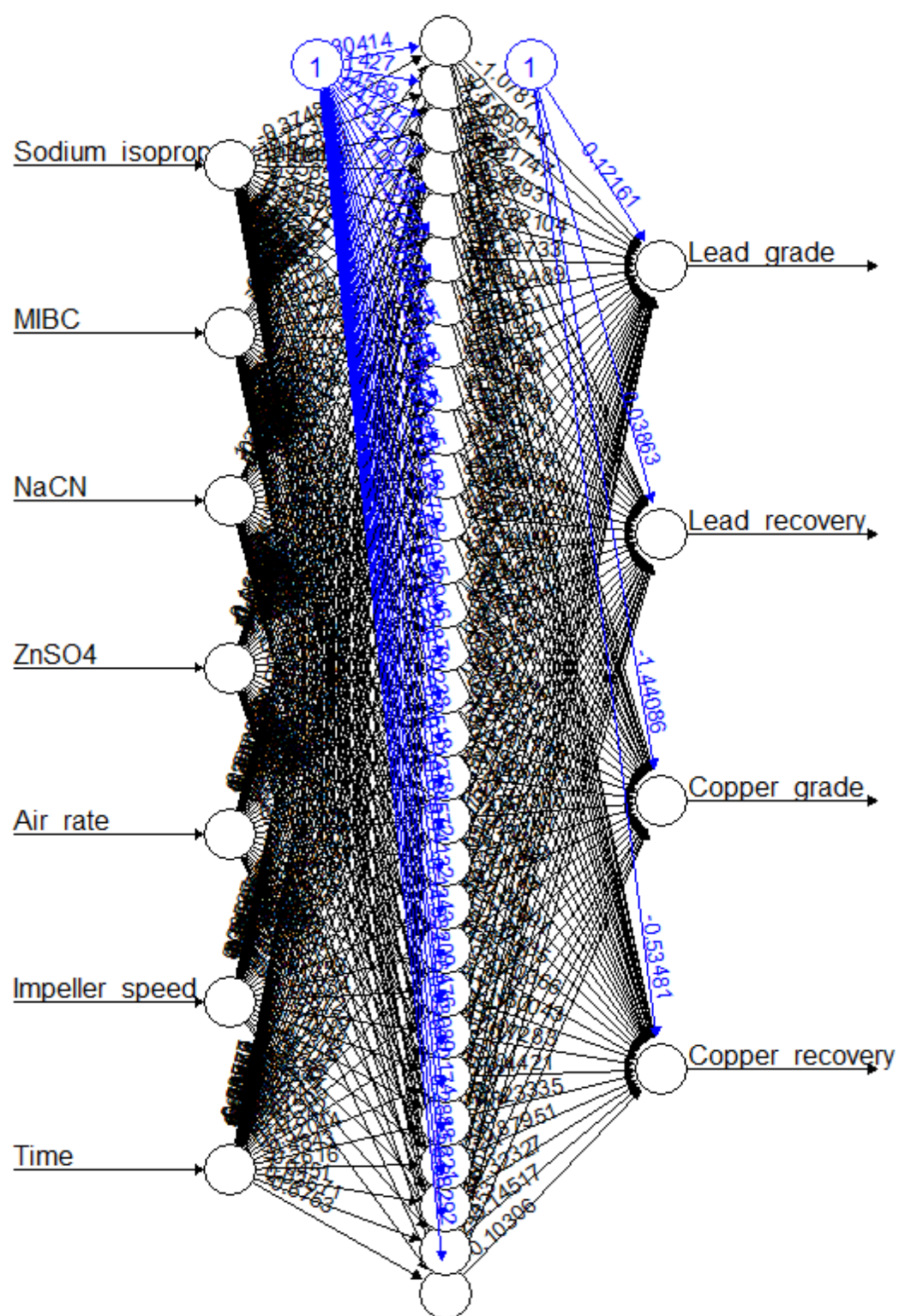
Figure 7.10. Developed ANN model. Note: Black lines display the weight vectors b/w the neurons and blue lines show the added bias.
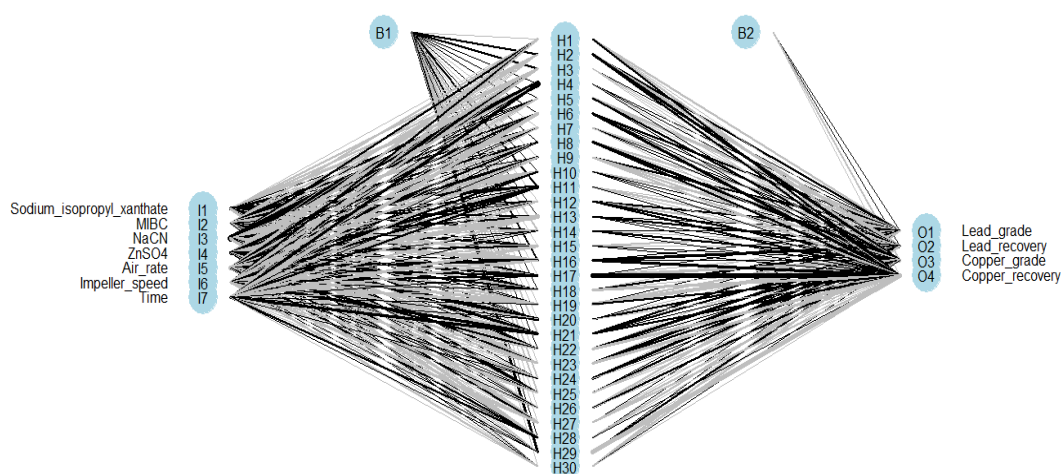
Figure 7.11. Developed neural network with relative weight magnitudes and directions being displayed with the thickness and color of the line, respectively. Note: black = positive, grey = negative.
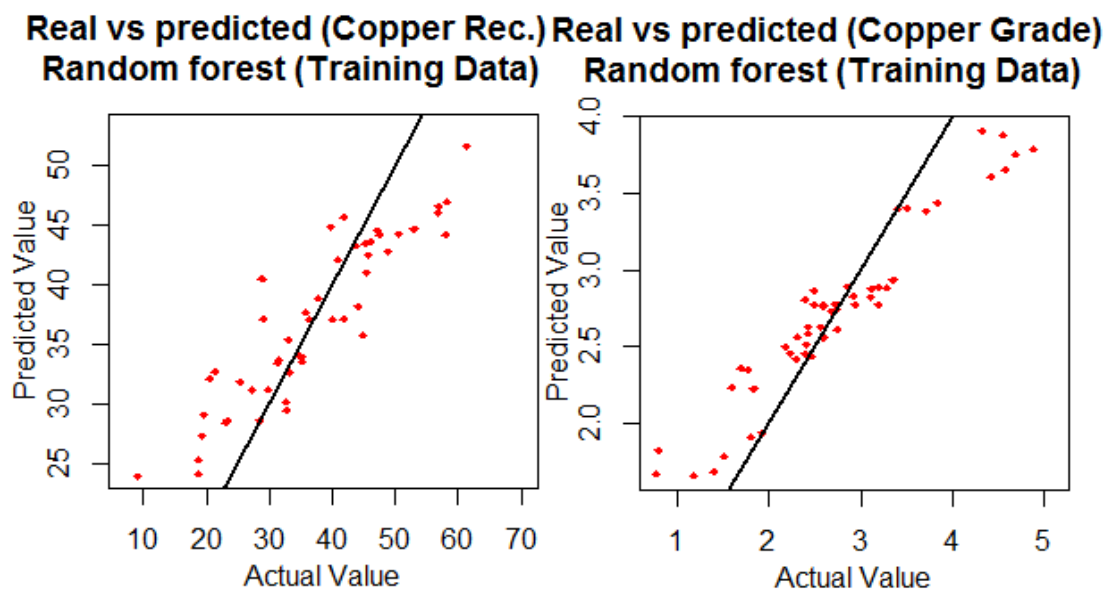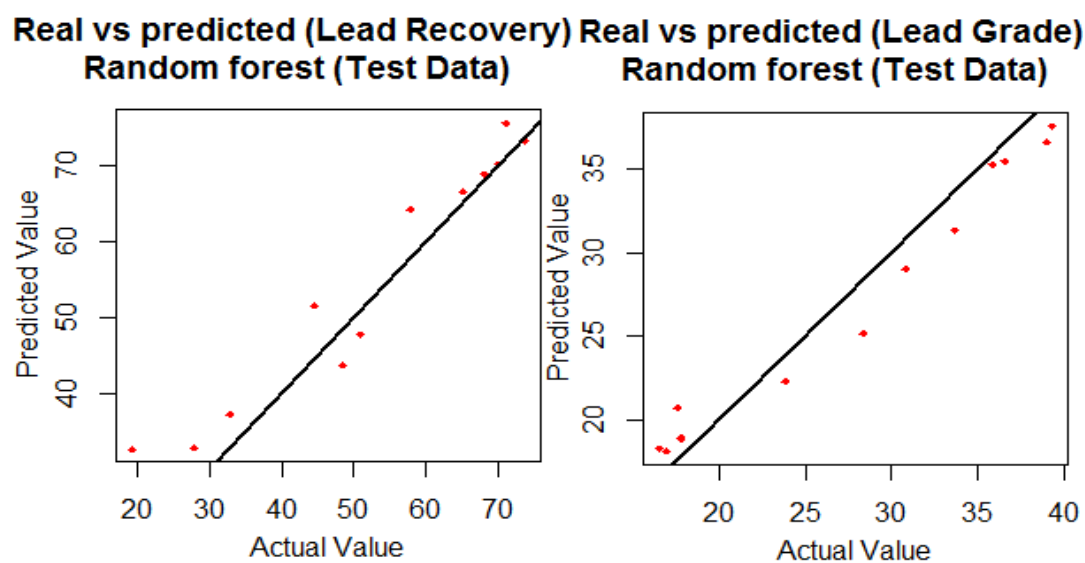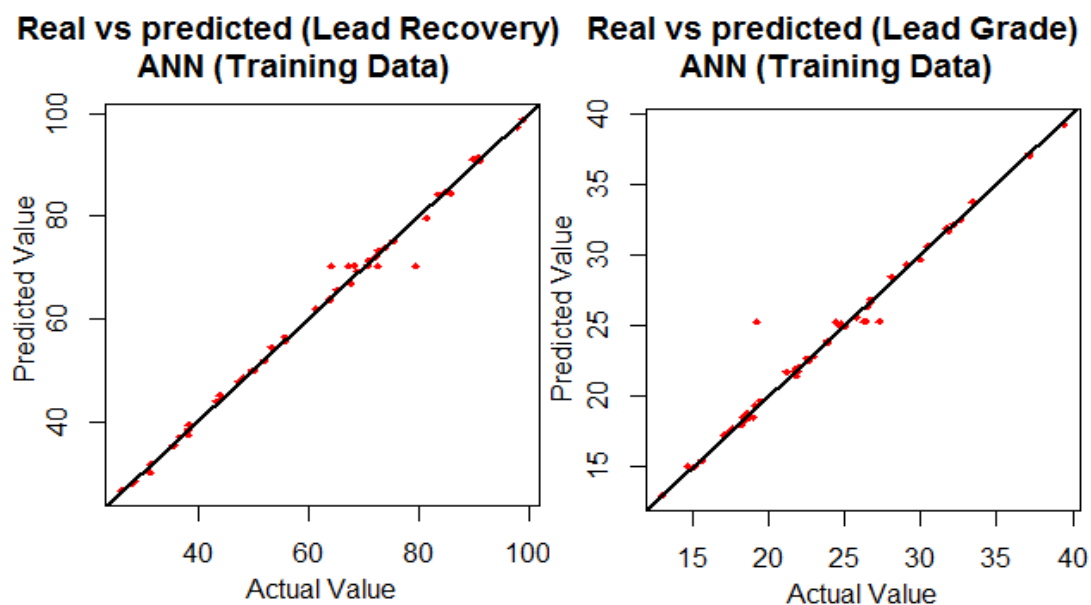

Figure 7.12. Real vs Predicted values plot for the training phase of the ANN model (A) Lead recovery and (B) Lead grade.
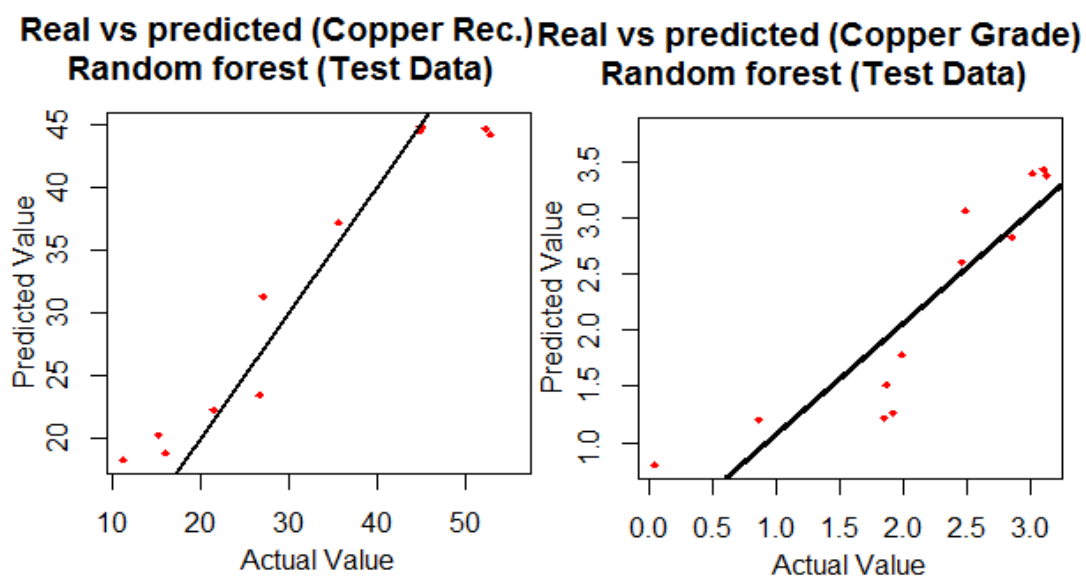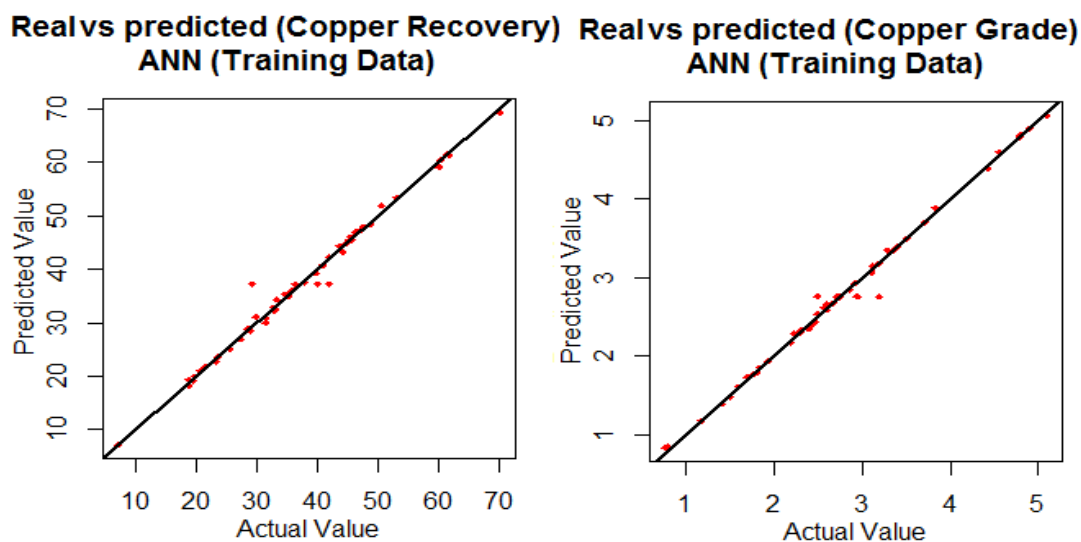
Figure 7.13. Real vs Predicted values plot for the training phase of the ANN model (A) Copper recovery and (B) Copper grade.
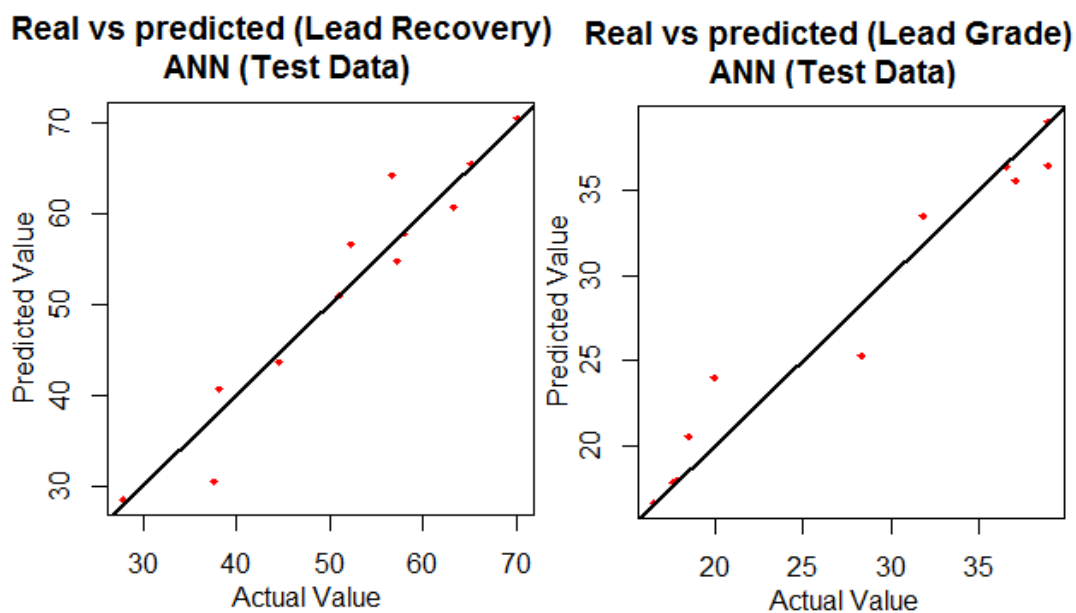
Figure 7.14. Real vs Predicted values plot for the testing phase of the ANN model (A) Lead recovery and (B) Lead grade.
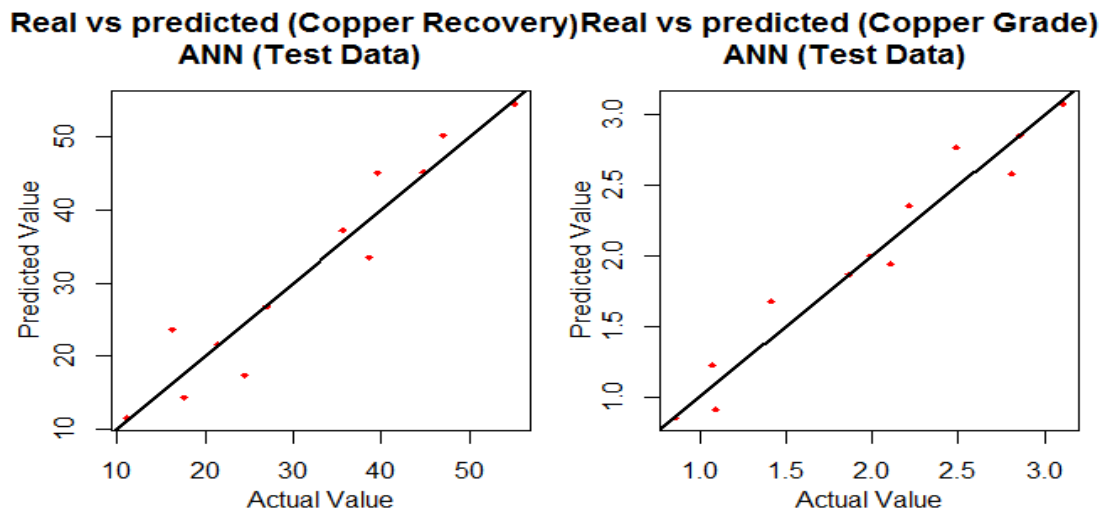
Figure 7.15. Real vs Predicted values plot for the testing phase of the ANN model (A) Copper recovery and (B) Copper grade.
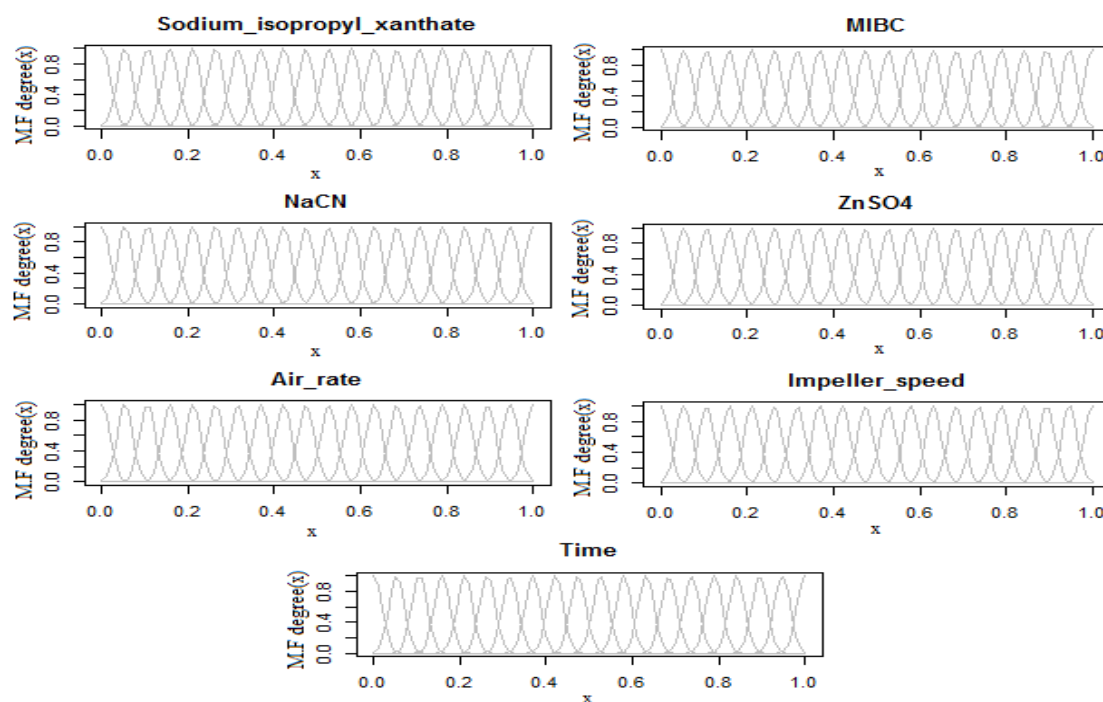
Figure 7.16. Gaussian membership functions for all the input variables of the Mamdani Fuzzy logic model.
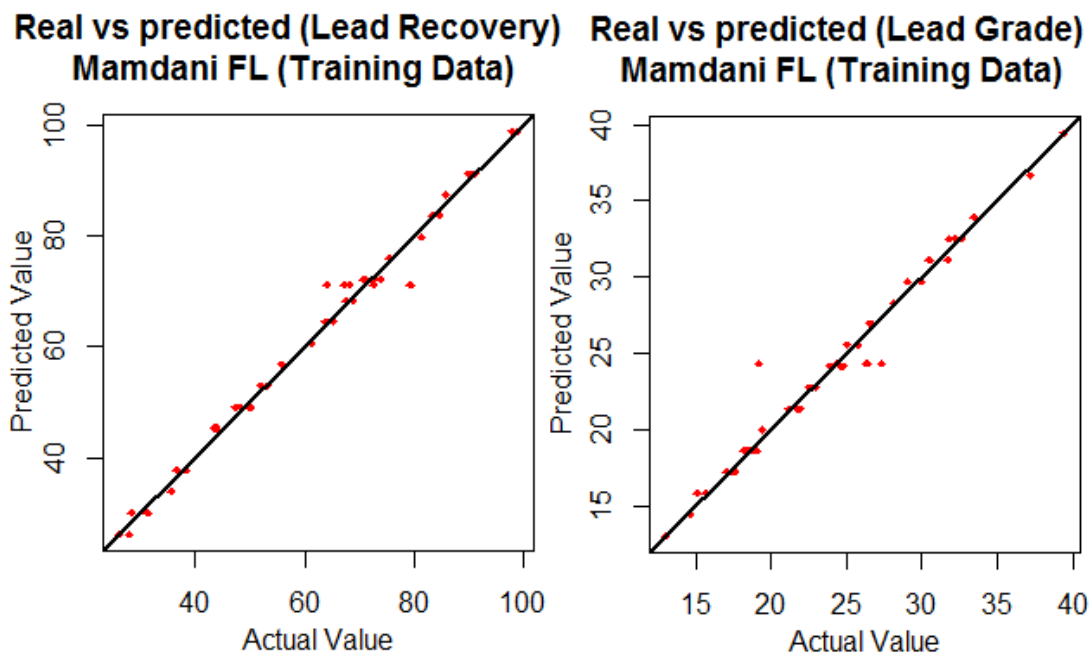
Figure 7.17. Real vs Predicted values plot for the training phase of the MFL model (A) Lead recovery and (B) Lead grade.
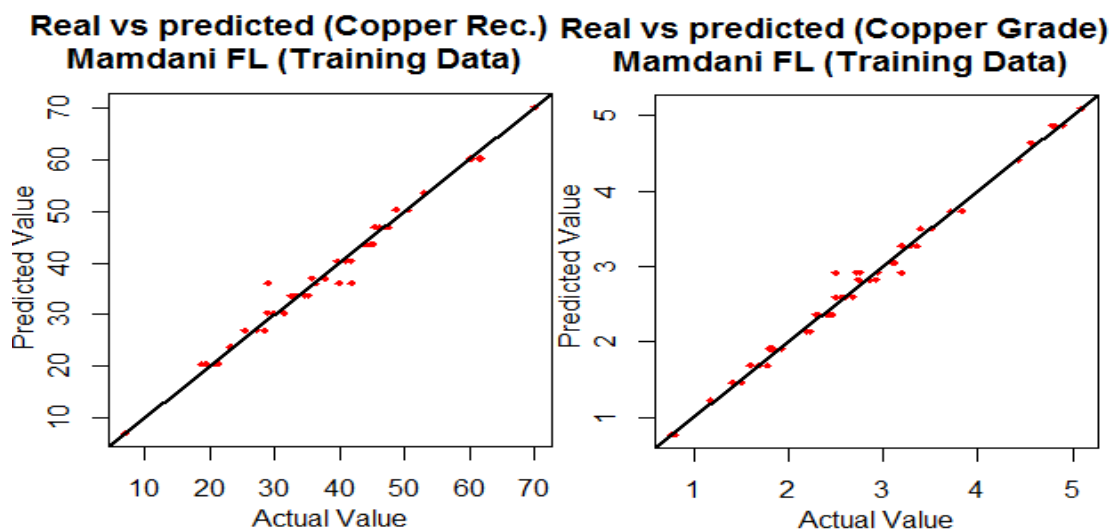
Figure 7.18. Real vs Predicted values plot for the training phase of the MFL model (A) Copper recovery and (B) Copper grade.
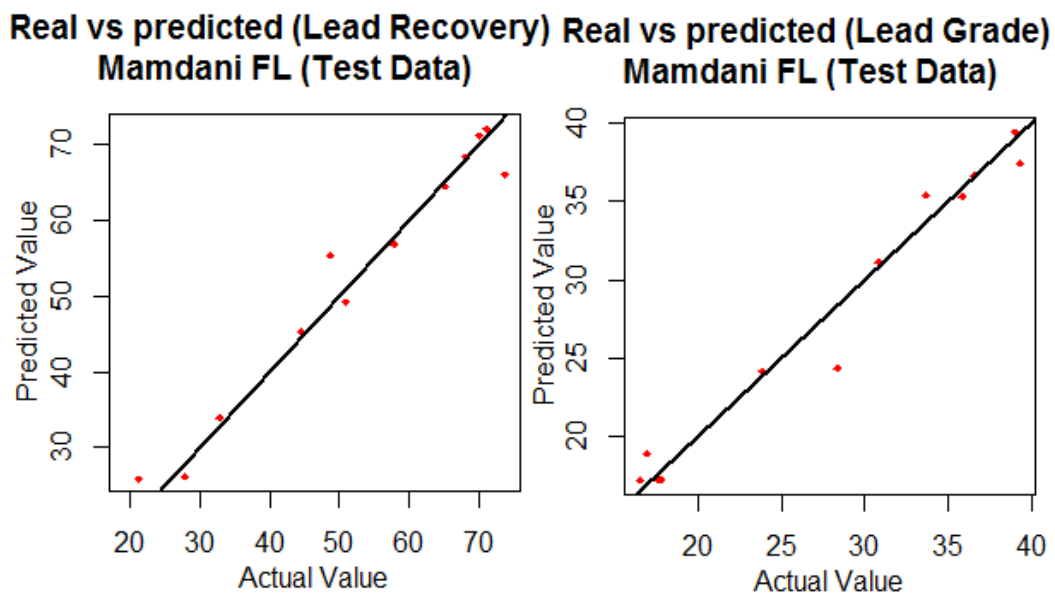
Figure 7.19. Real vs Predicted values plot for the testing phase of the MFL model (A) Lead recovery and (B) Lead grade.
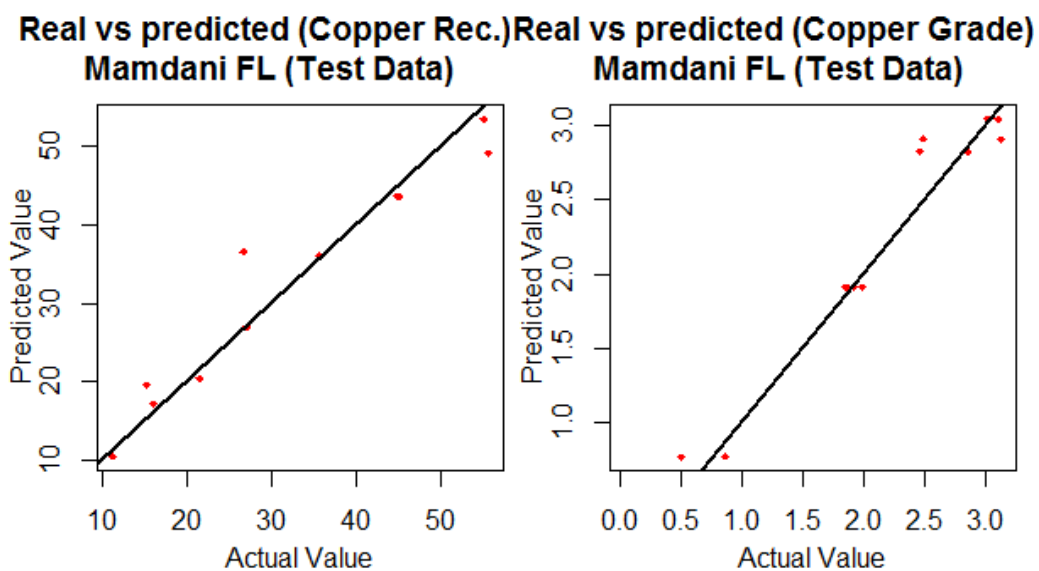
Figure 7.20. Real vs Predicted values plot for the testing phase of the MFL model (A) Copper recovery and (B) Copper grade.
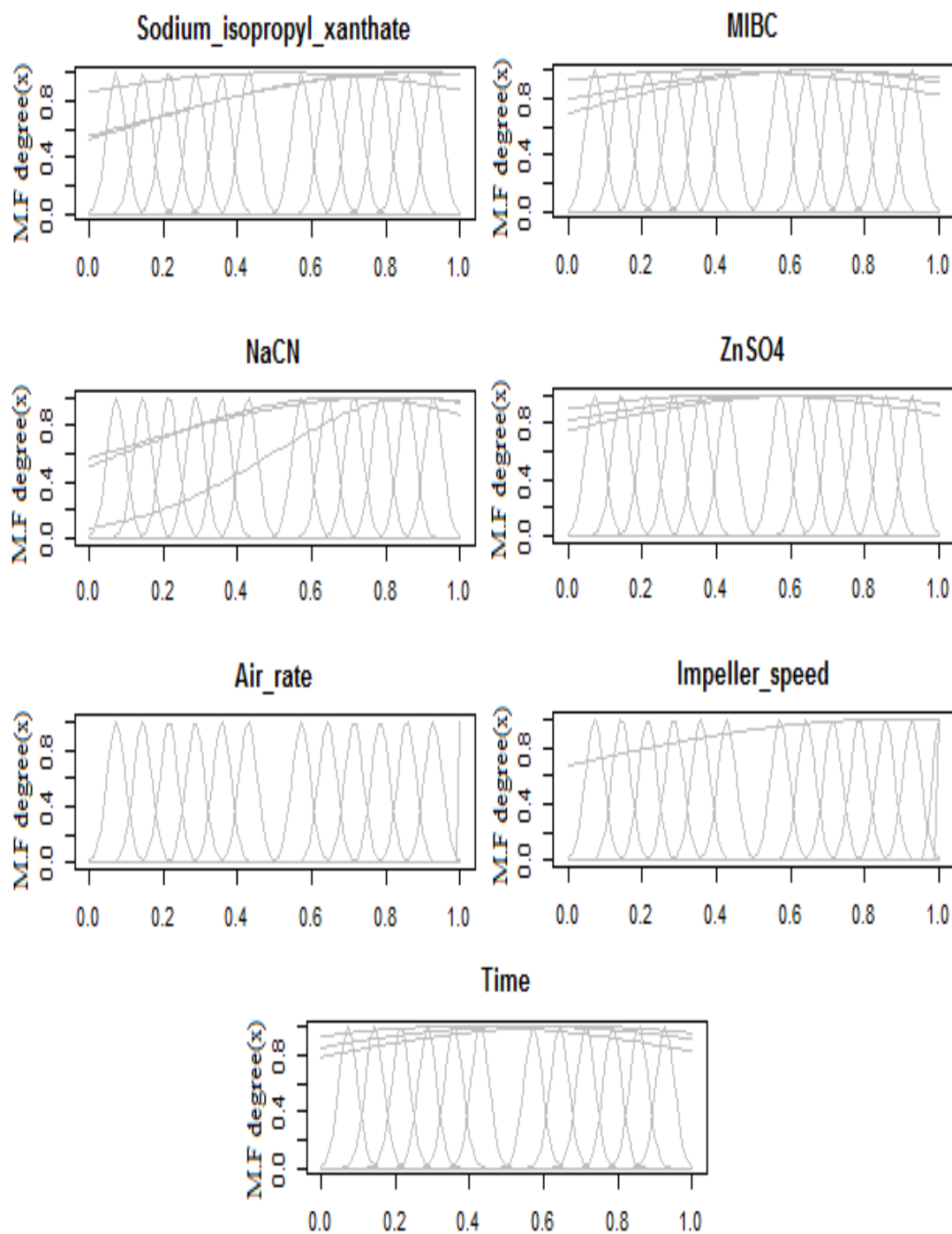
Figure 7.21. Gaussian membership functions for all the input variables of the ANFIS model.
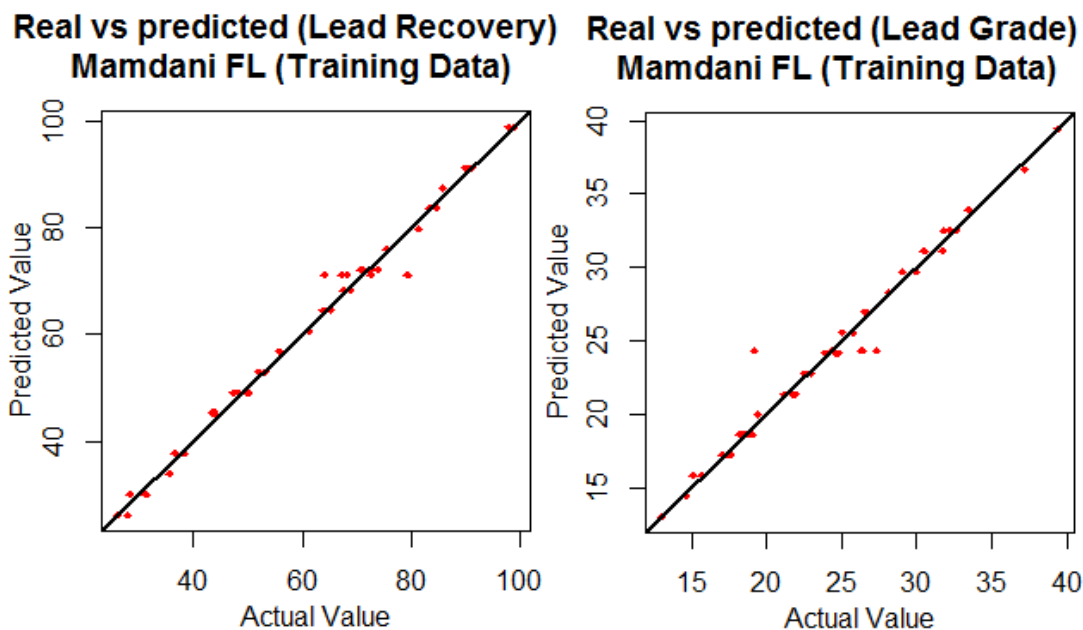
Figure 7.22. Real vs Predicted values plot for the training phase of the ANFIS model (A) Lead recovery and (B) Lead grade.
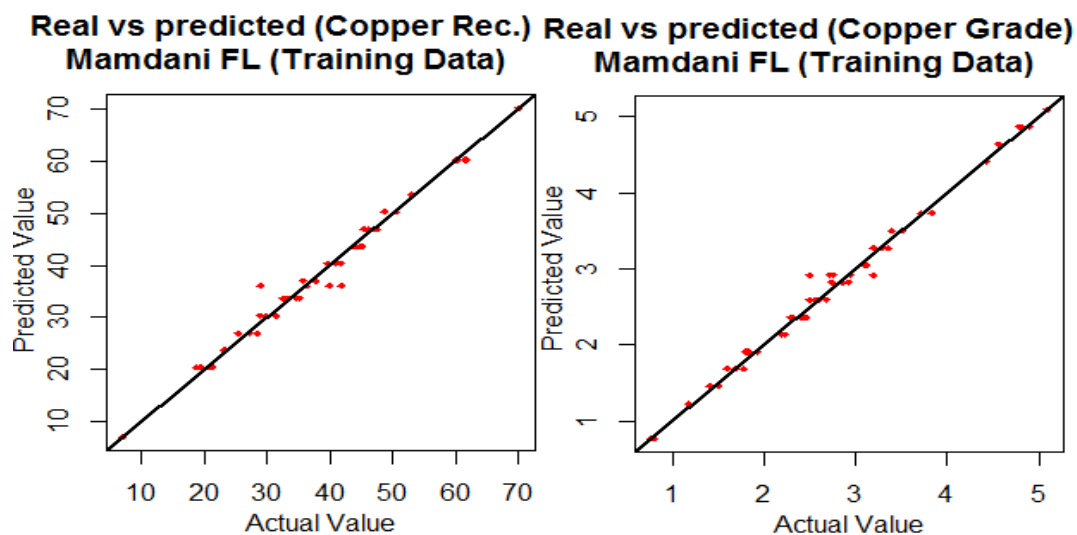
Figure 7.23. Real vs Predicted values plot for the training phase of the ANFIS model (A) Copper recovery and (B) Copper grade.
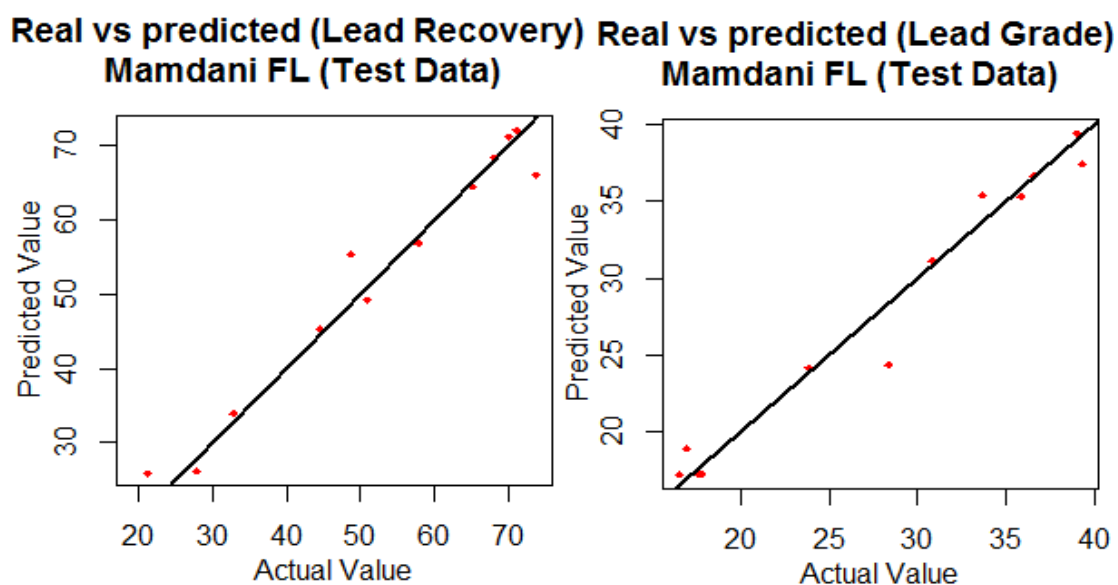
Figure 7.24. Real vs Predicted values plot for the testing phase of the ANFIS model (A) Lead recovery and (B) Lead grade.
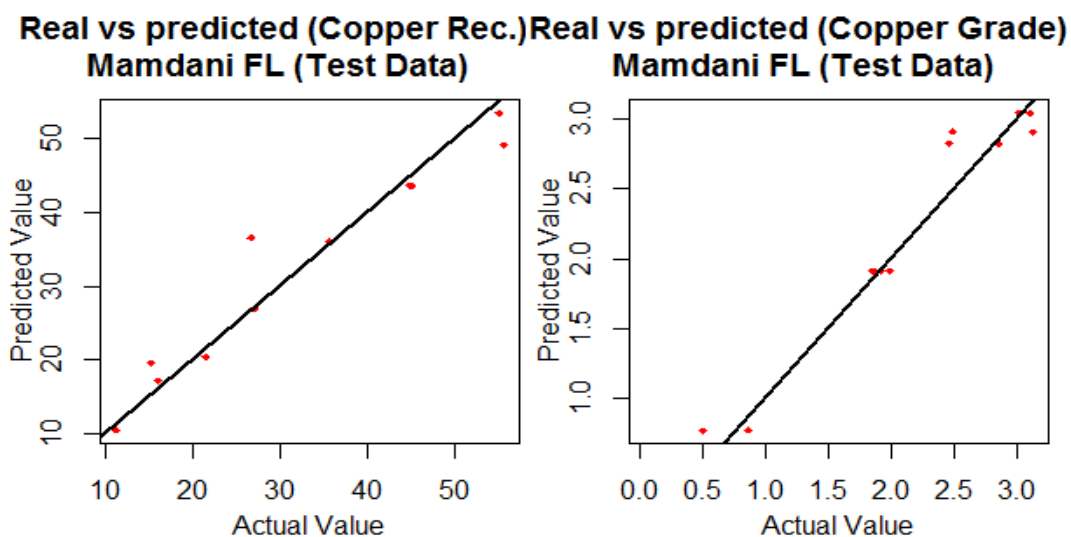
Figure 7.25. Real vs Predicted values plot for the testing phase of the ANFIS model (A) Copper recovery and (B) Copper grade.
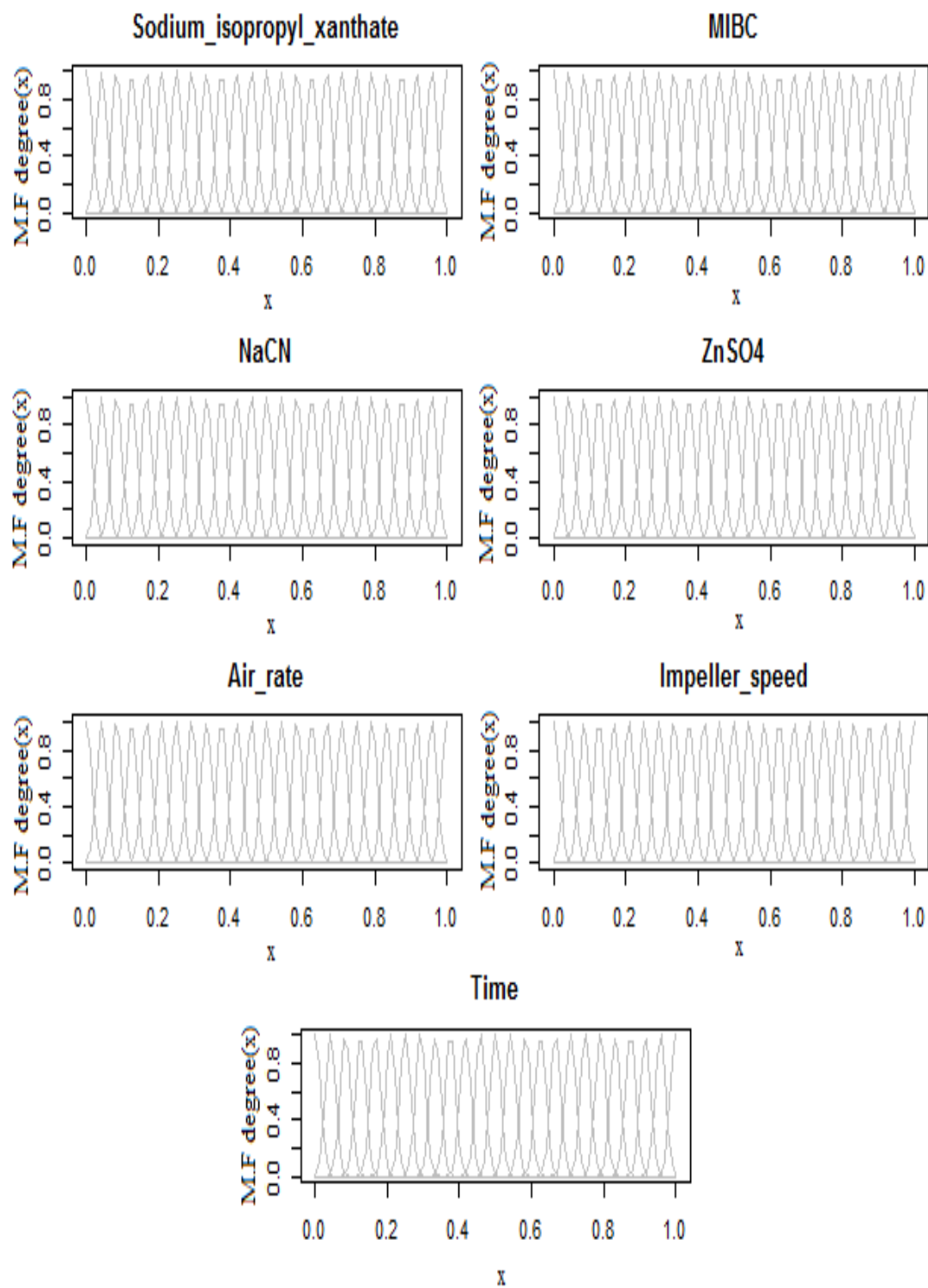
Figure 7.26. Gaussian membership functions for all the input variables of the HyFIS model.
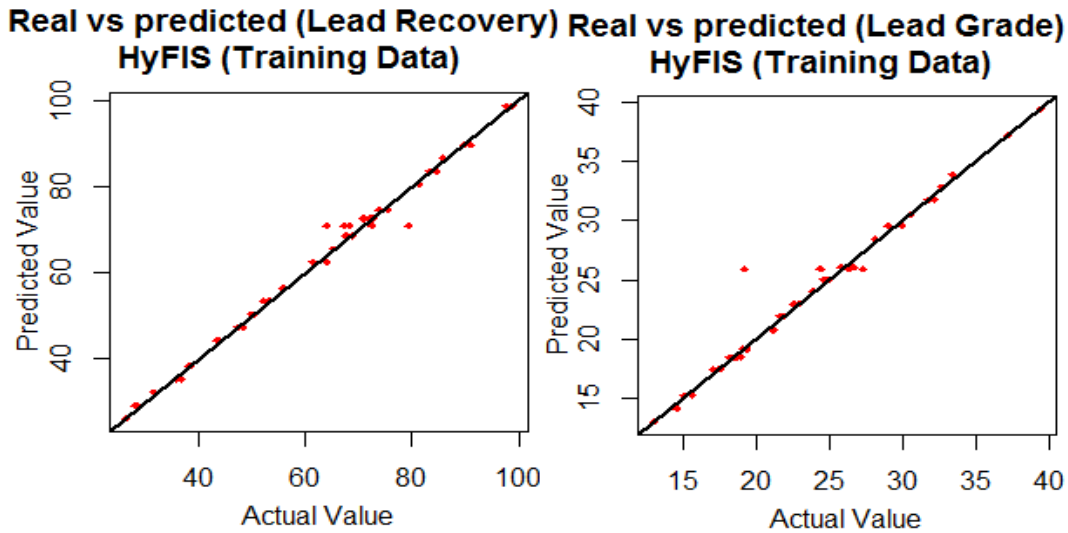
Figure 7.27. Real vs Predicted values plot for the training phase of the HyFIS model (A) Lead recovery and (B) Lead grade.

It can be seen from the results that the prediction error rates were higher for the testing phase in comparison to the training phase for each of the AI models. With ANN model, the obtained R^2 and RMSE values were 0.99 and 1.09 for the training step, respectively, and for the testing phase the respective values were 0.9 and 2.98. With ANFIS model, the obtained R^2 and RMSE values were 0.95 and 1.87 for the training step respectively. For the testing phase respective values were 0.87 and 3.34. Comparing these indicators, it can be seen that ANN model performed much better than ANFIS. It can further be noted that corresponding values of R^2 and RMSE for RF model came out to be 0.92 and 2.82, respectively for the training step, and 0.82 and 3.79, respectively for the testing phase. For HyFIS model, obtained R^2 and RMSE values were 0.98 and 1.06
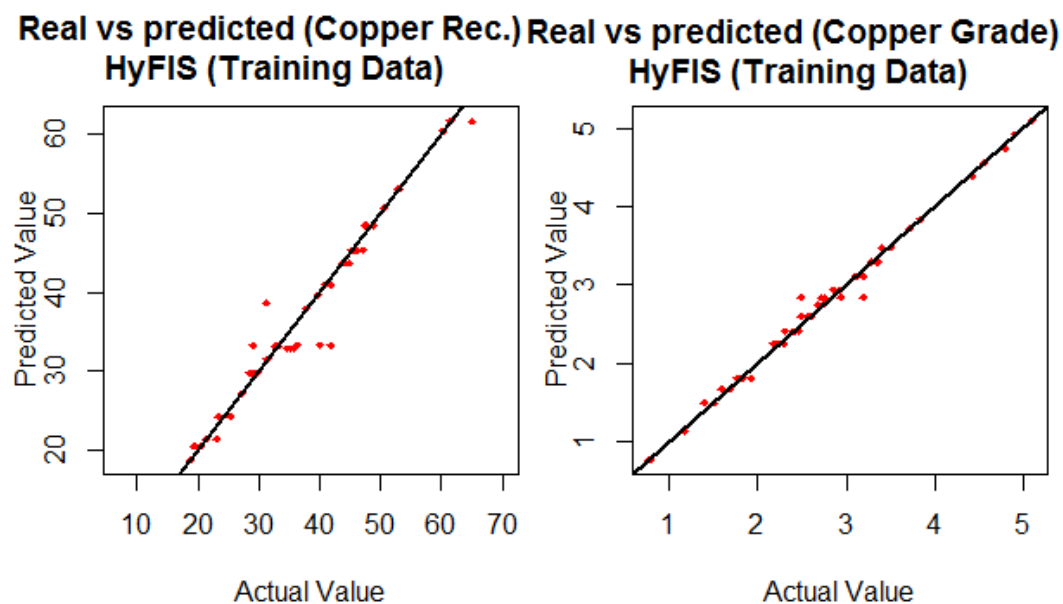
Figure 7.28. Real vs Predicted values plot for the training phase of the HyFIS model (A) Copper recovery and (B) Copper grade.
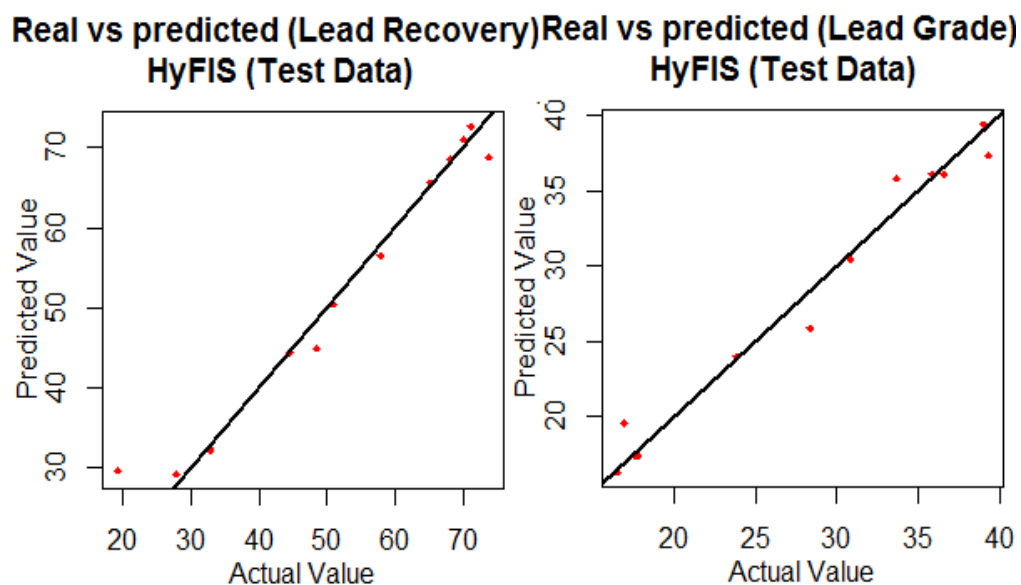
Figure 7.29. Real vs Predicted values plot for the testing phase of the HyFIS model (A) Lead recovery and (B) Lead grade.
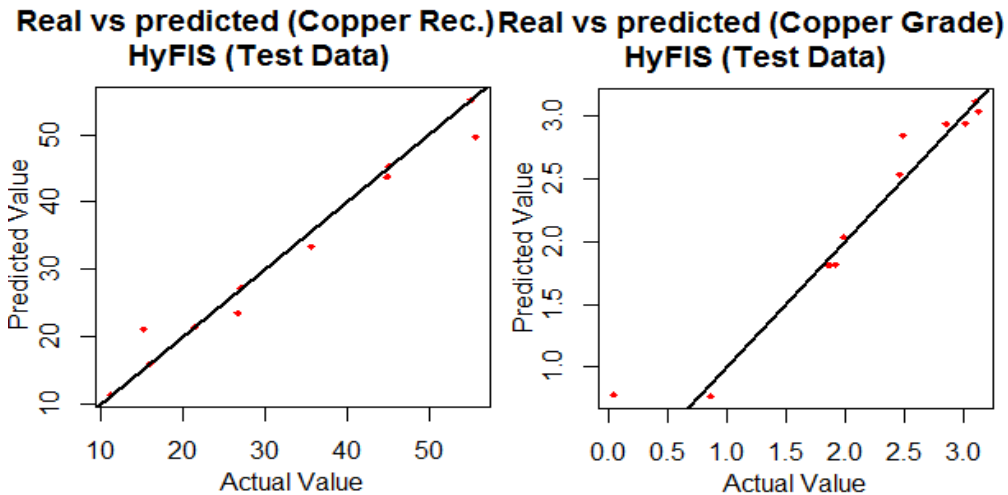
Figure 7.30. Real vs Predicted values plot for the testing phase of the HyFIS model (A) Copper recovery and (B) Copper grade.

for the training step, respectively, and for the testing phase the respective values were 0.91 and 2.85. The values for R^2 and RMSE for Mamdani FL model appeared to be 0.98 and 1.21 in the training step, respectively, whereas during the testing phase the respective values were 0.90 and 2.94. Mamdani FL model performed better than ANFIS and RF model as evident through the indictors' comparison.

The overall accuracy appeared to be in the following order, HyFIS > ANN > Mamdani FL ANFIS > RF. The hybrid intelligent model performed the best but the margin between the ANN, MFL and HyFIS was minimal.

7.7. DISCUSSION

The values for R^2 and RMSE for HyFIS model, came out to be 0.98 and 1.06 for the training phase, respectively, whereas for the testing step the respective values were

Table 7.2. Performance Indicators for all the developed AI models.

	Training		Testing	
	R^2	RMSE	R^2	RMSE
ANN	0.98647094	1.09359905	0.90082834	2.989
Mamdani	0.98341725	1.21792542	0.90188536	2.941
RF	0.91592695	2.82448383	0.82281637	3.792
ANFIS	0.95574083	1.87647238	0.87927651	3.347
HyFIS	0.98954153	1.06884344	0.91275861	2.859

0.91 and 2.85. By comparing these performance indicators results for all the developed

models, it is evident that the hybrid intelligent model namely HyFIS performed better

than any other model. Results obtained from this work will contribute to the research that

has been devoted to build an intelligent autonomous system to predict the process

outcomes. If this model is trained on the plant data, plant can be run at the highest

possible efficiency.

8. CONCLUSIONS AND RECOMMENDATIONS

8.1. CONCLUSION

This research work was aimed at making froth flotation of sulfide minerals sustainable and environment-friendly process. To accomplish this purpose, bulk flotation of complex sulfide ores containing galena, sphalerite, pyrite, chalcopyrite and dolomite was optimized and mathematical models were derived for the process. Biodegradable chitosan polymer was utilized to replace the toxic pyrite depressants that are currently used in the process. Nanoparticles process aids; SiO_2 and Al_2O_3, were added to optimize the flotation performance and froth stability. Sea water was used to replace fresh water in the flotation process of polymetallic sulfide ores and its effect on the flotation performance was quantified. Artificial intelligence and machine learning models were used to predict the flotation performance of the ore under different influencing parameters which will allow the building of intelligent systems that can be used to predict the process outcomes of polymetallic sulfides that have similar ore characteristics. The following conclusions may be drawn from this study:

1. The optimum flotation conditions found for maximum Pb grade were 450 g/ton of sodium isopropyl xanthate, 350 g/ton of MIBC, 73g/ton of NaCN, 700 g/ton of $ZnSO_4$, 3 l/min of air, 1200 rpm of impeller speed and 8 minutes of flotation time. Optimum flotation variables for maximum Pb recovery were found to be 100 g/ton of sodium isopropyl xanthate, 95 g/ton of MIBC, 5g/ton of NaCN, 200 g/ton of $ZnSO_4$, 3 l/min of air, 1800 rpm of impeller speed and 6.6 minutes of flotation time. For maximizing Cu grade; 450 g/ton of sodium isopropyl xanthate, 50 g/ton of MIBC, 200 g/ton of $ZnSO_4$, 800 rpm of impeller speed and 2 minutes of

flotation time were found to be the best fit values of significant operation parameters.

2. Optimal flotation conditions for Cu recovery were determined to be 100 g/ton of sodium isopropyl xanthate, 350 g/ton of MIBC, 5 g/ton of NaCN, 200 g/ton of $ZnSO_4$, 1800 rpm of impeller speed and 2 minutes of flotation time.

3. To achieve the combined desired results of bulk flotation of galena and chalcopyrite, which were minimizing the grade and recovery of Zn & Fe and maximizing the grade and recovery of Pb and Cu, following values of flotation variables are suggested; 450 g/ton of sodium isopropyl xanthate, 50 g/ton of MIBC, 80g/ton of NaCN, 700 g/ton of $ZnSO_4$, 3 l/min of air, 1456 rpm of impeller speed and 8 minutes of flotation time.

4. Bulk flotation tests carried out to compare the depression capability of NaCN and chitosan polymer revealed that chitosan was effective in depressing pyrite minerals. Chitosan depressed 5.6% more pyrite as compared to conventional depressant. It was however noted that at higher dosages, chitosan depressed chalcopyrite and galena which was not desired in this case. The optimum dosage of chitosan was 50 g/ton. At this dosage, galena had the highest recovery while pyrite had the lowest recovery. An inverse relationship was found between dynamic froth stability and chitosan dosage which may be attributed to the decrease in the number of pyrite particles in froth layer due to depressing effect of Chitosan.

5. Addition of Al_2O_3 nanoparticles increased dynamic froth stability by 26.4 % while there was no significant increase in the dynamic froth stability when SiO_2

nanoparticles were used. There was 0.85 % increase in Pb grade when Al_2O_3 nanoparticles were added in the system while Pb grade decreased by 2% when SiO_2 nanoparticles were added. Addition of Al_2O_3 nanoparticles increased Pb recovery by 3 % while there was no significant increase observed in case of SiO_2 nanoparticles. Cu grade was not significantly influenced by the addition of both type of nanoparticles. Cu recovery, however unexpectedly decreased when both types of nanoparticles were added. The decrease in Cu recovery was found to be 4 % in case of SiO_2 nanoparticles and 3.5 % in case of Al_2O_3 nanoparticles. Both type of nanoparticles had no effect on Zn grade. A decrease of 0.8 % was detected in Zn recovery by virtue of addition of both type of nanoparticles. Al_2O_3 nano particle addition decreased both Fe grade and recovery. SiO_2 nanoparticles however resulted in rise of 0.6 % in Fe grade and 0.7 % in Fe recovery which was not desired as Fe was targeted to be depressed.

6. While using seawater as process water, dynamic froth stability decreased by 8 % as compared to the case when fresh water was used. This decrease in froth stability in case of seawater flotation can be attributed to the joint action of sodium isopropyl xanthate and saline water augmented by the destabilizing effect of ions on froth stability. Recovery of all the metals including Pb, Cu, Zn, and Fe was enhanced by 15.37 %, 5.4 %, 7.9 % and 2.6 % respectively when seawater was used. Use of seawater resulted a decrease in grade of all the metals except Zn in which change was negligible. Reduction in Pb, Cu and Fe grade was found to be 11.52 %, 0.26 % and 0.8 % respectively. This decrease in grades may be attributed to the depressing action of ions present in sea water on certain metals.

Based on the observations done during this study it can be concluded that seawater reduces froth stability in complex sulfide ore flotation. However the effect of sea water on flotation performance is positive overall. It is however important to adjust the frother and collector dosages when using seawater. This study has laid the foundation of selecting the proper reagent dosages for complex sulfide ore flotation by generating mathematical models as given by Equations 34 to 42.

7. Five different machine learning and artificial intelligence models including Artificial Neural Networks (ANN), Random Forest (RF), Adaptive Neuro Fuzzy Interference System (ANFIS), Mamdani Fuzzy Logic (MFL) and Hybrid Neural Fuzzy Interference System (HyFIS) were developed and trained in this study for prediction of flotation performance of bulk flotation of galena and chalcopyrite. Coefficient of determination and root mean square error were employed as the performance indicators for evaluating the performance of these developed models. The values for R^2 and RMSE for HyFIS model, came out to be 0.98 and 1.06 for the training phase, respectively, whereas for the testing step the respective values were 0.91 and 2.85. By comparing these performance indicators results for all the developed models, it was evident that the hybrid intelligent model namely HyFIS performed better than any other model. This finding can pave the path for implementation of HyFIS model to automate the plants processing Mississippi valley type ore in future.

8.2. RECOMMENDATIONS

The findings obtained from this research work indicate that sulfide mineral flotation process can be made environment friendly by introducing chitosan polymer instead of NaCN for pyrite dosage. Moreover, sustainability and controllability of flotation can be enhanced by using sea water and nanoparticles. Effect of all these materials have been quantified on froth stability. HyFIS model has been found to effectively run the sulfide ore processing plant. In short, large amount of data has been generated through this study which will enhance the current state of knowledge on froth stability and sustainability of the froth flotation process of polymetallic sulfide ores. However, further studies are needed to investigate the application of polymers, nanomaterials ,seawater and ML models on stability and performance of sulfide ore flotation process at pilot and industrial scale. The following studies are recommended for future work:

1. This study showed that chitosan may have a bright prospect for use in sulfide mineral flotation as pyrite depressant. However effect of chitosan on sphalerite needs to be investigated. There is a possibility that chitosan may be able to depress both sphalerite and pyrite simultaneously.

2. It is recommended that fundamental research be conducted to find out the reason for preferential adsorption of Al_2O_3 nanoparticles on liquid air interface in case of sulfide ore flotation. More types of nanoparticles should be tested to find out the most suitable type of nanoparticles to control froth stability and flotation performance of complex sulfide ores.

3. Fundamental research should be carried out to find the depressing effect of different ions in seawater on different metals in complex sulfide ore flotation. It is also suggested to try nanomaterials in seawater which may enhance the froth stability, thus help in achieving the grades comparable to fresh water.

4. Computational fluid dynamic models used to define the froth flotation process needs to be simplified to lessen the computational cost and time to run the process simulations.

5. AI and ML models should be employed at mineral processing plants as it will cut the labor cost to operate the plant. Less sampling will be required as AI algorithms will be able to control the plant input parameters very efficiently according to the changing situation. Peak performance of plant will be achieved at all times.

8.3. FUTURE WORK

In addition to above recommendations , this study aims to carry out CFD simulation on effect of solid concentration on froth stability. Experimental work to validate the CFD simulations have already been completed. Preliminary simulations have also been carried out. Details of this future work and it'sare given below.

8.3.1. Background. Froth structure and stability plays a very important part in the ability of a froth flotation process to achieve the desired grade and recovery [68]. There are a number of factors effecting froth stability among which most important are drainage of liquid in the lamellae , particle size, hydrophobicity of particles, zeta

potential of the particles, surface viscosity, solid concentration, and type and quantity of surface active reagents in the solution [195].

Bubble coalescence and breakage plays a very important role in stability of froth. A higher bubble coalescence and burst rate results in unstable froths. Bubble coalescence results from the collision of two gas bubbles. During collision, thickness of liquid film between the bubbles shrinks, which reaching a certain thickness collapses resulting in coalescence [196]. However, small solid particles attached to the planar or curved liquid interfaces can act as a steric hindrance to the drainage of the liquid film. This role of solid particles results in stabilizing the froth in dynamic conditions of froth flotation. It is now well known that solid particles can stabilize the froth up to weeks in very harsh conditions [94][109]. The effect of solid particles on froth stability mainly depends upon the concentration of solid particles, particle size and shape. The stability of the foam has been observed to be inversely proportional to particle size and directly proportional to solid particle concentration [81], [83].

In mineral processing industry most of the flotation is carried out using cells with mechanical agitators. These cells can range up to a size of 1L in lab to 300 m^3 at plant scale. The flotation process is divided in three sub-processes involving collision, attachment and detachment. Flotation cells have been designed using empirical relations in the past. The shift now, however, is to design these based on the Computational fluid dynamic (CFD) studies. In CFD studies of flotation, flotation cell is divided into discrete elements of finite volume. This allows the local values of the flow to be calculated at each finite volume. The understanding of flotation process gained through this approach

has allowed great advancements in both flotation cell designs and flotation performance [197]–[199].

Eulerian–Eulerian approach has been used recently in a CFD model to study the effect of solid concentration on froth stability. Simulation included bubble break-up, bubble coalescence rate, the interfacial exchange of mass and momentum and bubble–particle attachment and detachment. Good agreement was found between experimental and simulation results regarding the effect of solid concentration on gas hold-up and axial pressure profile [109].

The aim of this work is to use computational fluid dynamic modelling to understand the impact of solid concentration on froth stability in a mechanically agitated cell. The developed 3D CFD model will measure the froth stability by analyzing the velocity of mixture of phases through the cell after aeration. Experiments determining the effect of solid concentration on froth stability have been carried out in a 1L Denver flotation cell. CFD modelling has been done through Ansys Fluent 18 and is still in process.

8.3.2. Model Description. In this study, three-dimensional flow of a 2 L Denver flotation cell used throughout this study for froth stability measurement will be simulated using Ansys Fluent 18 software. Figure 8.1 illustrates the geometrical aspects of the cell used in this study. This figure has been generated through 3 dimensional design modeler of Ansys Work Bench 18. The flotation cell used is 216 mm in height and 108 mm in width. Agitator is placed at the centre of the flotation cell and has a height of 216 mm and has a shaft of diameter 21.44 mm. Fan attached to the agitator handle measures a diameter of 66.04 mm. Agitator is encapsulated inside an air duct of 43.18

diameter. Air is introduced at the top of this inlet and is dispersed throughout the cell via the agitator fan. Froth outlet is at the top of the cell and has an area of 11,664 mm^2. In this study cell is divided into 221320 number of elements as shown in Figure 8.2.

Simulations will be carried out to predict the froth stability at concentrations of 30% and 40 % by volume. Impeller speed will be maintained at 146 rad/s which was found to be optimum during initial experiments.
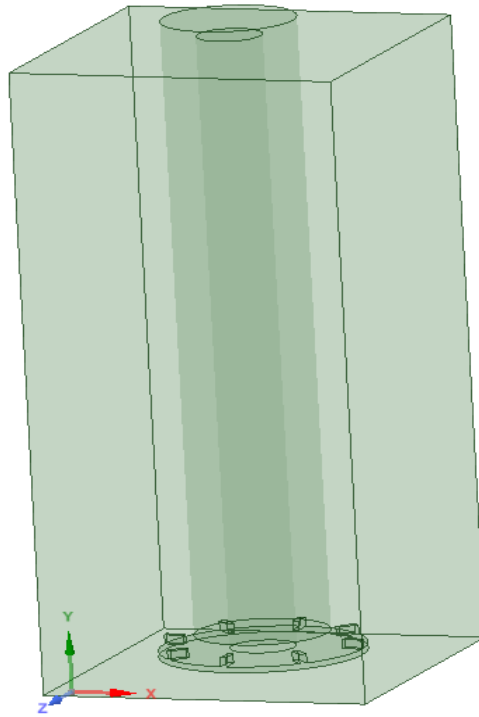
Figure 8.1. 3D sketch of 2L Denver flotation cell.

In this study, water is the primary fluid phase with a density of 998.2 kg/m^3. Air introduced in the cell in form of air bubbles was secondary fluid phase. Air bubles size

range modeled in the CFD model is from 500 to 1000 microns as shown in Figure

8.3.Third phase in this study was sulfide ore. Density of ore is 2917 kg/m^3 and 80 %

passing size is 53 micron For modelling purpose, all particles and bubbles are assumed to

have spherical shape.
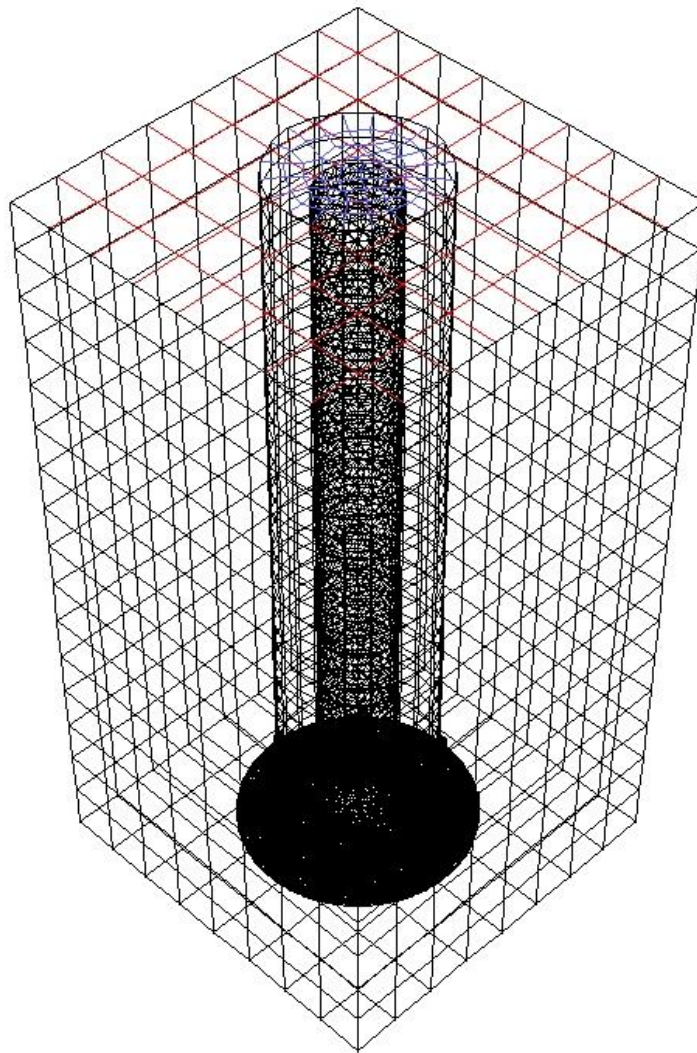
Figure 8.2. Detailed meshing of flotation cell with 221320 elements.
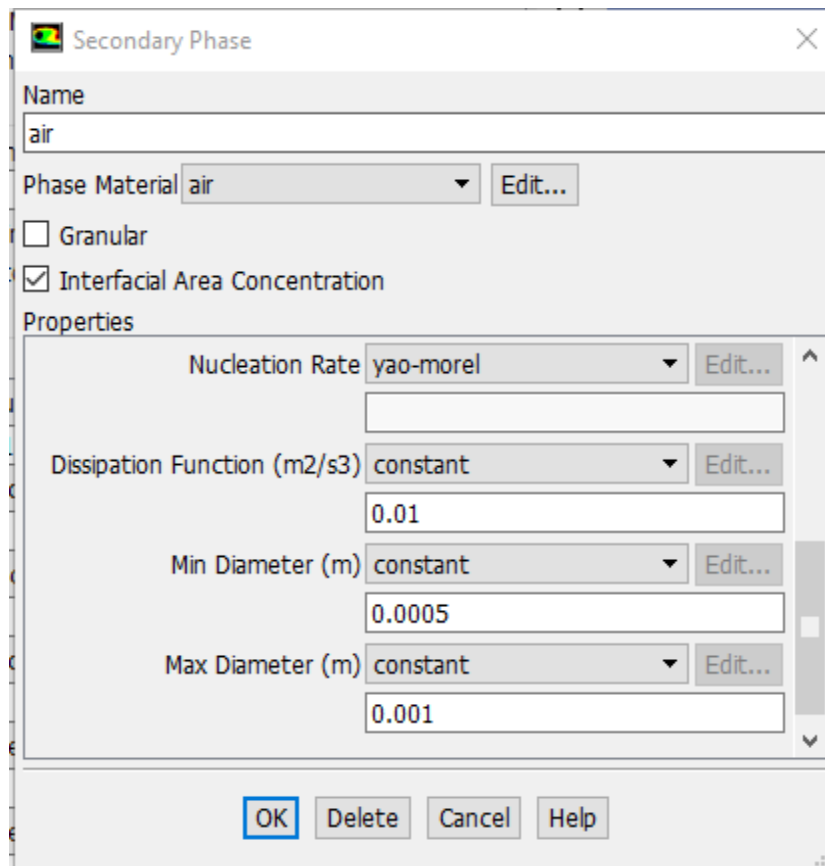
Figure 8.3. Properties of air used in the CFD model.

8.3.3. Hydrodynamic Model . The commercial CFD software package Ansys Fluent 18 is used to model the hydrodynamics of the mechanical flotation cell. Eulerian-Eulerian multiphase approach was used to calculate the conservation of mass, energy and momentum for each phase. Water is the primary continuous phase, while ore and air are dispersed phases. All three phases are however modeled in Eulerian frame of reference to cut down the computation time. The turbulent viscosity of the primary phase is calculated using standard k - ε turbulence model. Details of viscous model and its constant are given in Figure 8.4.
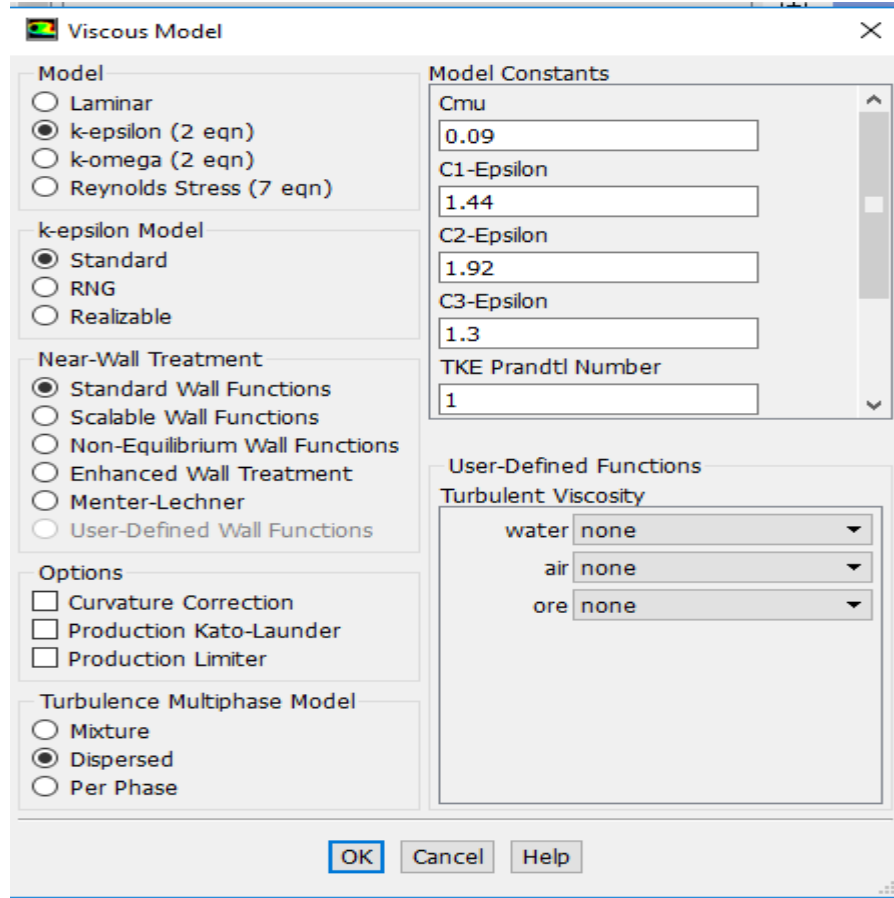
Figure 8.4. Details of the standard turbulence model used to calculate viscosity of primary phase.

8.3.4. Governing Equations The equations solved by Fluent for fluid-fluid multiphase flows are presented below. The volume fraction for each phase in Fluent is calculated through a continuity equation as represented by Equation 58 [200].

$$\frac{1}{\rho_{rq}}\left(\frac{\partial}{\partial t}(\alpha_q\rho_q) + \nabla\cdot(\alpha_q\rho_q\vec{v}_q) = \sum_{p=1}^{n}(\dot{m}_{pq} - \dot{m}_{qp})\right) \tag{58}$$

Where ρ_{rq} is the phase reference density of the qth phase in the solution domain.The conservation of momentum for a fluid phase q is given by **E**quation 59 [200].

$$\frac{\partial}{\partial t}\left(\alpha_q \rho_q \vec{v}_q\right) + \nabla.\left(\alpha_q \rho_q \vec{v}_q \vec{v}_q\right) = -\alpha_q \nabla p + \nabla.\bar{\bar{\tau}}_q + \alpha_q \rho_q \vec{g} +$$
$$\sum_{p=1}^{n}\left(K_{pq}\left(\vec{v}_p - \vec{v}_q\right) + \dot{m}_{pq}\vec{v}_{pq} - \dot{m}_{qp}\vec{v}_{qp}\right) + \left(\vec{F}_q + \vec{F}_{lift,q} + \vec{F}_{wl,q} +\right.$$
$$\left.\vec{F}_{vm,q} + \vec{F}_{td,q}\right) \tag{59}$$

where μ_q is the phase stress-strain tensor. Here μ_q and λ_q are the shear and bulk viscosity of phase q, F_q is an external body force, $F_{lift,q}$ is a lift force, $F_{wl,q}$ is a wall lubrication force , F_{vmq} is a virtual mass force, and F_{tdq} is a turbulent dispersion force. R_{pq} is an interaction force between phases, and p is the pressure shared by all phases. V_{pq} is the interphase velocity.The equation solved by ANSYS Fluent for the conservation of energy is given by Equation 60 [200].

$$\frac{\partial}{\partial t}\left(\alpha_q \rho_q h_q\right) + \nabla.\left(\alpha_q \rho_q \vec{u}_q h_q\right) = \alpha_q \frac{dp_q}{dt} + \bar{\bar{\tau}}_q : \nabla \vec{u}_q - \nabla \vec{q}_q + S_q +$$
$$\sum_{p=1}^{n}\left(Q_{pq} + \dot{m}_{pq}h_{pq} - \dot{m}_{qp}h_{qp}\right) \tag{60}$$

where h_q is the specific enthalpy of the qth phase, q_q is the heat flux, S_q is a source term that includes sources of enthalpy, Q_{pq} is the intensity of heat exchange between the pth and q^{th} phases, and h_{pq} is the interphase enthalpy .The heat exchange between phases must comply with the local balance conditions $Q_{pq} = - Q_{qp}$ and $Q_{pq} = 0$.

The Interfacial Area Concentration predicts the mass, momentum and energy transfer through the phases. The interfacial area concentration model in this study uses a single transport equation per secondary phase which is given by Equation 61 [200].

$$\frac{\partial(\rho_g X_p)}{\partial t} + \nabla.(\rho_g \vec{u}_g X_p) = \frac{1}{3}\frac{D\rho_g}{Dt}X_p + \frac{2}{3}\frac{\dot{m}_g}{\alpha_g}X_p + \rho_g(S_{RC}S_{WE}S_{TI}) \tag{61}$$

where X_p is the interfacial area concentration and α_g is the gas volume fraction. The first two terms on the right hand side of are of gas bubble expansion due to compressibility and mass transfer (phase change). $\dot{m}_g$ is the mass transfer rate into the gas phase per unit mixture volume. S_{RC} and S_{WE} are the coalescence sink terms due to random collision and wake entrainment, respectively. S_{TI} is the breakage source term due to turbulent impact. In this study Hibiki-Ishi model is employed to account for bubble coalescence and breakage terms.

BIBLIOGRAPHY

[1]   J. F. W. Bowles, R. A. Howie, D. J. Vaughan, and J. Zussman, "Non-silicates: Oxides, hydroxides and sulphides, The Rock Forming Minerals, 5a," in *London: The Geological Society, 920pp*, 2011, vol. 5A, p. 920.

[2]   V. P. Kohad, "Flotation of Sulphide Ores-HZL Experience," in *Workshop on Froth Flotation: Recent Trends*, 1998, pp. 18–41.

[3]   D. J. Vaughan and C. L. Corkhill, "Mineralogy of Sulfides," *Elements*, vol. 13, no. 2, pp. 81–87, 2017.

[4]   The Editors of Encyclopædia Britannica, "Sulfide mineral," *Encyclopædia Britannica*. Encyclopædia Britannica, inc., 2011.

[5]   J. R. Craig and D. J. Vaughan, "Compositional and textural variations of the major iron and base-metal sulphide minerals," in *Sulphide deposits---their origin and processing*, P. M. J. Gray, G. J. Bowyer, J. F. Castle, D. J. Vaughan, and N. A. Warner, Eds. Dordrecht: Springer Netherlands, 1990, pp. 1–16.

[6]   S. M. Bulatovic and S. M. Bulatovic, "14 – Flotation of Lead–Zinc Ores," in *Handbook of Flotation Reagents*, 2007, pp. 323–366.

[7]   S. M. Bulatovic and S. M. Bulatovic, "15 – Flotation of Copper–Lead–Zinc Ores," in *Handbook of Flotation Reagents*, 2007, pp. 367–400.

[8]   J. M. Cases, "Finely Disseminated Complex Sulfide Ores," *Complex Sulphide Ores*, vol. 4, pp. 234–247, 1980.

[9]   B. A. Wills and T. Napier-Munn, "12 - Froth flotation BT - Wills' Mineral Processing Technology (Seventh Edition)," Oxford: Butterworth-Heinemann, 2005, pp. 267–352.

[10]   S. Sumiya, "Froth flotation system," US3032199 A, 01-May-1962.

[11]   S. J. Neethling and J. J. Cilliers, "Modelling flotation froths," *Int. J. Miner. Process.*, vol. 72, no. 1–4, pp. 267–287, 2003.

[12]   C. Aldrich, D. W. Moolman, F. S. Gouws, and G. F. Schmitz, "Machine Learning Strategies for Control of Flotation Plants," *IFAC Proc. Vol.*, vol. 28, no. 17, pp. 99–105, 1995.

[13] G. Hilson and A. J. Monhemius, "Alternatives to cyanide in the gold mining industry: what prospects for the future?," *J. Clean. Prod.*, vol. 14, no. 12, pp. 1158–1167, 2006.

[14] M. Logsdon and T. Hagelstein, Karen Mudder, "The management of cyanide in gold extraction," in *International Council of Metals and the Environment*, 1999.

[15] F. Korte and F. Coulston, "From Single-Substance Evaluation to Ecological Process Concept: The Dilemma of Processing Gold with Cyanide," *Ecotoxicol. Environ. Saf.*, vol. 32, no. 1, pp. 96–101, 1995.

[16] D. I. Bleiwas, "Estimated water requirements for the conventional flotation of copper ores," Reston, VA, 2012.

[17] T. C. Shumba, "Relationship between flotation operational factors and froth behaviour," University of Cape Town, 2014.

[18] G. D. Clayton and F. E. Clayton, "Cyanides and nitriles. Patty's industrial hygiene and toxicology. Vol. 2C," *Toxicol. New York, NY John Wiley Sons, Inc*, vol. 2C, no. 3rd.rev ed, pp. 4845–4856, 1982.

[19] E. C. Cilek and S. Karaca, "Effect of nanoparticles on froth stability and bubble size distribution in flotation," *Int. J. Miner. Process.*, vol. 138, pp. 6–14, 2015.

[20] B. Shahbazi, B. Rezai, and S. M. Javad Koleini, "Bubble–particle collision and attachment probability on fine particles flotation," *Chem. Eng. Process. Process Intensif.*, vol. 49, no. 6, pp. 622–627, 2010.

[21] S. Ahmed and S. Ahmed, "Cavitation Nanobubble Enhanced Flotation Process For More Efficient Coal Recovery," University of Kentucky, 2013.

[22] R. H. Yoon and G. H. Luttrell, "The Effect of Bubble Size on Fine Particle Flotation," *Miner. Process. Extr. Metall. Rev.*, vol. 5, no. 1–4, pp. 101–122, 1989.

[23] R. H. Yoon, "Microbubble flotation," *Miner. Eng.*, vol. 6, no. 6, pp. 619–630, 1993.

[24] A. V Nguyen, J. Ralston, and H. J. Schulze, "On modelling of bubble–particle attachment probability in flotation," *Int. J. Miner. Process.*, vol. 53, no. 4, pp. 225–249, 1998.

[25] A. Sobhy, "Cavitation nanobubble enhanced flotation process for more efficient coal recovery," Ph. D Thesis, College of Engineering-University of Kentucky, 145p, 2013.

[26] B. Albijanic, O. Ozdemir, A. V. Nguyen, and D. Bradshaw, "A review of induction and attachment times of wetting thin films between air bubbles and particles and its relevance in the separation of particles by flotation," *Advances in Colloid and Interface Science*, vol. 159, no. 1. pp. 1–21, 2010.

[27] R. H. Yoon, "The role of hydrodynamic and surface forces in bubble-particle interaction," *Int. J. Miner. Process.*, vol. 58, no. 1–4, pp. 129–143, 2000.

[28] D. Tao, "Role of Bubble Size in Flotation of Coarse and Fine Particles—A Review," *Sep. Sci. Technol.*, vol. 39, no. 4, pp. 741–760, 2005.

[29] B. J. Shean and J. J. Cilliers, "A review of froth flotation control," *Int. J. Miner. Process.*, vol. 100, no. 3, pp. 57–71, 2011.

[30] G. Bartolacci, P. Pelletier, J. Tessier, C. Duchesne, P.-A. Bossé, and J. Fournier, "Application of numerical image analysis to process diagnosis and physical parameter measurement in mineral processes—Part I: Flotation control based on froth textural characteristics," *Miner. Eng.*, vol. 19, no. 6, pp. 734–747, 2006.

[31] J. Finch, "Column flotation," in *Froth Flotation: A Century of Innovation*, 2007, pp. 681–737.

[32] C. Bhondayi, "A study of flotation froth phase behaviour," University of the Witwatersrand, 2015.

[33] 911 metallurgists, "Flotation Collectors," 2017. [Online]. Available: https://www.911metallurgist.com/blog/flotation_collectors. [Accessed: 19-Dec-2017].

[34] J. Ramberg, "Effect of the reagents and minerals on froth electrical conductivity in pilot scale froth flotation process," University of Oulu Faculty of Technology, 2015.

[35] D. J. Bradshaw, P. J. Harris, and C. T. O'Connor, "Synergistic interactions between reagents in sulphide flotation," *J. South African Inst. Min. Metall.*, vol. 98, no. 4, pp. 189–194, 1998.

[36] S. M. Bulatovic and S. M. Bulatovic, "3 – Frothers," in *Handbook of Flotation Reagents*, 2007, pp. 43–51.

[37] S. M. Bulatovic, "4 - Modifying Reagents BT - Handbook of Flotation Reagents," Amsterdam: Elsevier, 2007, pp. 53–79.

[38]   R. D. Crozier, *Flotation: Theory, Reagents and Ore Testing*, First. Oxford,Newyork,Tokyo,Seoul: Elsevier Science & Technology Books, 1992.

[39]   J. B. Yianatos, J. A. Finch, and A. R. Laplante, "Selectivity in column flotation froths," *Int. J. Miner. Process.*, vol. 23, no. 3, pp. 279–292, 1988.

[40]   J. B. Yianatos, "Fluid Flow and Kinetic Modelling in Flotation Related Processes: Columns and Mechanically Agitated Cells—A Review," *Chem. Eng. Res. Des.*, vol. 85, no. 12, pp. 1591–1603, 2007.

[41]   A. P. van der Westhuizen and D. A. Deglon, "Solids suspension in a pilot-scale mechanical flotation cell: A critical impeller speed correlation," *Miner. Eng.*, vol. 21, no. 8, pp. 621–629, 2008.

[42]   M. C. Fuerstenau, G. J. Jameson, and R.-H. Yoon, *Froth flotation: a century of innovation*. SME, 2007.

[43]   R. Pugh and P. Stenius, "Solution chemistry studies and flotation behaviour of apatite, calcite and fluorite minerals with sodium oleate collector," *Int. J. Miner. Process.*, vol. 15, no. 3, pp. 193–218, 1985.

[44]   N. O. Lotter and D. J. Bradshaw, "The formulation and use of mixed collectors in sulphide flotation," *Miner. Eng.*, vol. 23, no. 11, pp. 945–951, 2010.

[45]   S. M. Bulatovic and S. M. Bulatovic, "2 – Collectors," in *Handbook of Flotation Reagents*, 2007, pp. 5–41.

[46]   D. Montgomery, *Design and Analysis of Experiments*, vol. 5th. 2001.

[47]   M. A. Bezerra, R. E. Santelli, E. P. Oliveira, L. Silveira Villar, and L. A. Elia Escaleira, "Response surface methodology (RSM) as a tool for optimization in analytical chemistry," *Talanta*, vol. 76, no. 5, pp. 965–977, 2008.

[48]   K. M. Carley, N. Y. Kamneva, and J. Reminga, "Response Surface Methodology," 2004.

[49]   A. Martinez L., A. Uribe S., F. R. Carrillo P., J. Coreno A., and J. C. Ortiz, "Study of celestite flotation efficiency using sodium dodecyl sulfonate collector: Factorial experiment and statistical analysis of data," *Int. J. Miner. Process.*, vol. 70, no. 1–4, pp. 83–97, 2003.

[50] D. P. Obeng, S. Morrell, and T. J. Napier-Munn, "Application of central composite rotatable design to modelling the effect of some operating variables on the performance of the three-product cyclone," *Int. J. Miner. Process.*, vol. 76, no. 3, pp. 181–192, 2005.

[51] V. K. Kalyani, Pallavika, T. Gouri Charan, and S. Chaudhuri, "Optimization of a Laboratory-Scale Froth Flotation Process Using Response Surface Methodology," *Coal Prep.*, vol. 25, no. 3, pp. 141–153, Jul. 2005.

[52] N. Aslan and R. Fidan, "Optimization of Pb flotation using statistical technique and quadratic programming," *Sep. Purif. Technol.*, vol. 62, no. 1, pp. 160–165, 2008.

[53] N. Aslan, F. Cifci, and D. Yan, "Optimization of process parameters for producing graphite concentrate using response surface methodology," *Sep. Purif. Technol.*, vol. 59, no. 1, pp. 9–16, 2008.

[54] J. V. Mehrabani, M. Noaparast, S. M. Mousavi, R. Dehghan, and A. Ghorbani, "Process optimization and modelling of sphalerite flotation from a low-grade Zn-Pb ore using response surface methodology," *Sep. Purif. Technol.*, vol. 72, no. 3, pp. 242–249, 2010.

[55] M. J. Anderson and P. J. Whitcomb, *DOE Simplified: Practical Tools for Effective Experimentation*, vol. 53, no. 9. 2013.

[56] S. L. C. Ferreira *et al.*, "Box-Behnken design: An alternative for the optimization of analytical methods," *Analytica Chimica Acta*, vol. 597, no. 2. pp. 179–186, 2007.

[57] N. Magdalinovic, M. Trumic, Z. Petkovic, and V. Rajic, "Cyanide elimination from lead-zinc flotation," *ejmp ep (European J. Miner. Process. Environ. Prot.*, vol. 4, no. 1, pp. 30–35, 2004.

[58] J. Zhang, Y. Hu, D. Wang, and J. Xu, "Depressing effect of hydroxamic polyacrylamide on pyrite," *J. Cent. South Univ. Technol.*, vol. 11, no. 4, pp. 380–384, Dec. 2004.

[59] P. Huang, L. Wang, and Q. Liu, "Depressant function of high molecular weight polyacrylamide in the xanthate flotation of chalcopyrite and galena," *Int. J. Miner. Process.*, vol. 128, pp. 6–15, 2014.

[60] A. Boulton, D. Fornasiero, and J. Ralston, "Selective depression of pyrite with polyacrylamide polymers," *Int. J. Miner. Process.*, vol. 61, no. 1, pp. 13–22, Jan. 2001.

[61] Y. Guévellou, C. Noïk, J. Lecourtier, and D. Defives, "Polyacrylamide adsorption onto dissolving minerals at basic pH," *Colloids Surfaces A Physicochem. Eng. Asp.*, vol. 100, no. C, pp. 173–185, 1995.

[62] O. Molatlhegi and L. Alagha, "Ash Depression in Fine Coal Flotation Using a Novel Polymer Aid," *Int. J. Clean Coal Energy*, vol. 5, no. 04, p. 65, 2016.

[63] P. Huang, "Chitosan in differential flotation of base metal sulfides," University of Alberta, 2013.

[64] P. Huang, M. Cao, and Q. Liu, "Using chitosan as a selective depressant in the differential flotation of Cu–Pb sulfides," *Int. J. Miner. Process.*, vol. 106–109, pp. 8–15, 2012.

[65] P. Huang, M. Cao, and Q. Liu, "Selective depression of pyrite with chitosan in Pb-Fe sulfide flotation," *Miner. Eng.*, vol. 46–47, pp. 45–51, 2013.

[66] Y. Xiang, "Carboxymethyl Chitosan as a Selective Depressant in Differential Flotation of Galena and Chalcopyrite," University of Alberta, 2015.

[67] M. B. Hayat, L. Alagha, and S. M. Sannan, "Flotation Behavior of Complex Sulfide Ores in the Presence of Biodegradable Polymeric Depressants," *Int. J. Polym. Sci.*, vol. 2017, pp. 1–9, 2017.

[68] N. Barbian, K. Hadler, E. Ventura-Medina, and J. J. Cilliers, "The froth stability column: linking froth stability and flotation performance," *Miner. Eng.*, vol. 18, no. 3, pp. 317–324, 2005.

[69] T. V Subrahmanyam and E. Forssberg, "Froth stability, particle entrainment and drainage in flotation — A review," *Int. J. Miner. Process.*, vol. 23, no. 1, pp. 33–53, 1988.

[70] C. Aldrich and D. Feng, "The effect of mothers on bubble size distributions in flotation pulp phases and surface froths," *Miner. Eng.*, vol. 13, no. 10, pp. 1049–1057, 2000.

[71] S. J. Neethling, H. T. Lee, and J. J. Cilliers, "Simple relationships for predicting the recovery of liquid from flowing foams and froths," *Miner. Eng.*, vol. 16, no. 11, pp. 1123–1130, 2003.

[72] J. Cilliers, "Understanding froth behaviour with CFD," in *5th international conference on CFD in the process industries CSIRO, Melbourne*, 2006, p. 7.

[73] S. Farrokhpay, "The significance of froth stability in mineral flotation — A review," *Adv. Colloid Interface Sci.*, vol. 166, no. 1–2, pp. 1–7, 2011.

[74] T. Marozva, "Investigating the effect of frother type on froth structure, froth recovery and entrainment," University of Cape Town, 2015.

[75] H. Khoshdast, "Flotation Frothers: Review of Their Classifications, Properties and Preparation," *Open Miner. Process. J.*, vol. 4, no. 1, pp. 25–44, 2011.

[76] A. K. Gupta, P. K. Banerjee, and A. Mishra, "Effect of frothers on foamability, foam stability, and bubble size," *Coal Prep.*, vol. 27, no. 1–3, pp. 107–125, 2007.

[77] S. N. Tan, R. J. Pugh, D. Fornasiero, R. Sedev, and J. Ralston, "Foaming of polypropylene glycols and glycol/MIBC mixtures," in *Minerals Engineering*, 2005, vol. 18, no. 2 SPEC. ISS., pp. 179–188.

[78] Y. S. Cho and J. S. Laskowski, "Effect of flotation frothers on bubble size and foam stability," *Int. J. Miner. Process.*, vol. 64, no. 2, pp. 69–80, 2002.

[79] Z. Aktas, J. J. Cilliers, and A. W. Banford, "Dynamic froth stability: Particle size, airflow rate and conditioning time effects," *Int. J. Miner. Process.*, vol. 87, no. 1–2, pp. 65–71, 2008.

[80] C. Chen, "Development of measurement of froth characteristics," Chalmers University of Technology Gothenburg, Sweden, 2012.

[81] H. J. Liu, W. Zhang, and C. B. Sun, "Influence of bubble diameter and solids concentration on bubble stability: Development of a novel analytical approach," *J. Cent. South Univ.*, vol. 21, no. 9, pp. 3588–3595, 2014.

[82] D. Tao, G. H. Luttrell, and R.-H. Yoon, "A parametric study of froth stability and its effect on column flotation of fine particles," *Int. J. Miner. Process.*, vol. 59, no. 1, pp. 25–43, 2000.

[83] S. W. Ip, S. W. Wang, and J. M. Toguri, "Aluminum Foam Stabilization by Solid Particles," *Can. Metall. Q.*, vol. 38, no. 1, pp. 81–92, Jan. 1999.

[84] G. Li, L. Deng, Y. Cao, B. Wang, J. Ran, and H. Zhang, "Effect of sodium chloride on fine coal flotation and discussion based on froth stability and particle coagulation," *Int. J. Miner. Process.*, vol. 169, no. Supplement C, pp. 47–52, 2017.

[85] S. Gredelj, M. Zanin, and S. R. Grano, "Selective flotation of carbon in the Pb–Zn carbonaceous sulphide ores of Century Mine, Zinifex," *Miner. Eng.*, vol. 22, no. 3, pp. 279–288, 2009.

[86] N. Barbian, E. Ventura-Medina, and J. J. Cilliers, "Dynamic froth stability in froth flotation," *Miner. Eng.*, vol. 16, no. 11, pp. 1111–1116, 2003.

[87] M. Zanin, E. Wightman, S. R. Grano, and J.-P. Franzidis, "Quantifying contributions to froth stability in porphyry copper plants," *Int. J. Miner. Process.*, vol. 91, no. 1, pp. 19–27, 2009.

[88] K. Hadler and J. J. Cilliers, "The relationship between the peak in air recovery and flotation bank performance," *Miner. Eng.*, vol. 22, no. 5, pp. 451–455, 2009.

[89] X. Zheng, J. P. Franzidis, and N. W. Johnson, "An evaluation of different models of water recovery in flotation," *Miner. Eng.*, vol. 19, no. 9, pp. 871–882, 2006.

[90] X. Qu, L. Wang, and A. V Nguyen, "Correlation of air recovery with froth stability and separation efficiency in coal flotation," *Miner. Eng.*, vol. 41, no. Supplement C, pp. 25–30, 2013.

[91] S. H. Morar, D. J. Bradshaw, and M. C. Harris, "The use of the froth surface lamellae burst rate as a flotation froth stability measurement," *Miner. Eng.*, vol. 36–38, no. Supplement C, pp. 152–159, 2012.

[92] S. H. Morar, M. C. Harris, and D. J. Bradshaw, "The use of machine vision to predict flotation performance," *Miner. Eng.*, vol. 36–38, no. Supplement C, pp. 31–36, 2012.

[93] S. H. Morar, D. P. Hatfield, N. Barbian, D. J. Bradshaw, J. J. Cilliers, and B. Triffett, "A comparison of flotation froth stability measurements and their use in the prediction of concentrate grade," in *Proceedings of the XXIII International Minerals Processing Congress*, 2006, pp. 739–744.

[94] T. S. Horozov, "Foams and foam films stabilised by solid particles," *Curr. Opin. Colloid Interface Sci.*, vol. 13, no. 3, pp. 134–140, 2008.

[95] G. Bournival, S. Ata, and E. J. Wanless, "The roles of particles in multiphase processes: Particles on bubble surfaces," *Adv. Colloid Interface Sci.*, vol. 225, pp. 114–133, 2015.

[96] R. M. Rahman, S. Ata, and G. J. Jameson, "Froth recovery measurements in an industrial flotation cell," *Miner. Eng.*, vol. 53, pp. 193–202, 2013.

[97] S. Ata, "Phenomena in the froth phase of flotation — A review," *Int. J. Miner. Process.*, vol. 102–103, pp. 1–12, 2012.

[98] Y. Zhang, Z. Chang, W. Luo, S. Gu, W. Li, and J. An, "Effect of starch particles on foam stability and dilational viscoelasticity of aqueous-foam," *Chinese J. Chem. Eng.*, vol. 23, no. 1, pp. 276–280, 2015.

[99] S. Yang, R. Pelton, A. Raegen, M. Montgomery, and K. Dalnoki-Veress, "Nanoparticle flotation collectors: mechanisms behind a new technology," *Langmuir*, vol. 27, no. 17, pp. 10438–10446, 2011.

[100] S. Yang and R. Pelton, "Nanoparticle flotation collectors II: the role of nanoparticle hydrophobicity," *Langmuir*, vol. 27, no. 18, pp. 11409–11415, 2011.

[101] B. McFadzean, T. Marozva, and J. Wiese, "Flotation frother mixtures: Decoupling the sub-processes of froth stability, froth recovery and entrainment," *Miner. Eng.*, vol. 85, pp. 72–79, 2016.

[102] T. Wei, Y. Peng, and S. Vink, "The joint action of saline water and flotation reagents in stabilizing froth in coal flotation," *Int. J. Miner. Process.*, vol. 148, pp. 15–22, 2016.

[103] G. Bournival, R. J. Pugh, and S. Ata, "Examination of NaCl and MIBC as bubble coalescence inhibitor in relation to froth flotation," *Miner. Eng.*, vol. 25, no. 1, pp. 47–53, 2012.

[104] V. Simanzhenkov and R. Idem, *Crude Oil Chemistry*. CRC Press, 2003.

[105] S. Castro, C. Miranda, P. Toledo, and J. S. Laskowski, "Effect of frothers on bubble coalescence and foaming in electrolyte solutions and seawater," *Int. J. Miner. Process.*, vol. 124, pp. 8–14, 2013.

[106] M. Ejtemaei, C. Plackowski, and A. V Nguyen, "The effect of calcium, magnesium, and sulphate ions on the surface properties of copper activated sphalerite," *Miner. Eng.*, vol. 89, pp. 42–51, 2016.

[107] T. M. Moimane, K. C. Corin, and J. G. Wiese, "Investigation of the interactive effects of the reagent suite in froth flotation of a Merensky ore," *Miner. Eng.*, vol. 96–97, no. Special Issue: Froth Flotation, pp. 39–45, 2016.

[108] C. Bhondayi and M. H. Moys, "Measurement of a proxy for froth phase bubble sizes as a function of froth depth in flotation machines Part 1. Theoretical development and testing of a new technique," *Int. J. Miner. Process.*, vol. 130, pp. 8–19, 2014.

[109] A. R. Sarhan, J. Naser, and G. Brooks, "CFD simulation on influence of suspended solid particles on bubbles' coalescence rate in flotation cell," *Int. J. Miner. Process.*, vol. 146, pp. 54–64, 2016.

[110] H. Park and L. Wang, "Experimental studies and modeling of surface bubble behaviour in froth flotation," *Chem. Eng. Res. Des.*, vol. 101, pp. 98–106, 2015.

[111] E. Jorjani, S. Chehreh Chelgani, and S. Mesroghli, "Prediction of microbial desulfurization of coal using artificial neural networks," *Miner. Eng.*, vol. 20, no. 14, pp. 1285–1292, Nov. 2007.

[112] S. Al-Thyabat, "On the optimization of froth flotation by the use of an artificial neural network," *J. China Univ. Min. Technol.*, vol. 18, no. 3, pp. 418–426, Sep. 2008.

[113] S. Mohanty, "Artificial neural network based system identification and model predictive control of a flotation column," *J. Process Control*, vol. 19, no. 6, pp. 991–999, Jun. 2009.

[114] F. Nakhaeie, A. Sam, and M. R. Mosavi, "Concentrate Grade Prediction in an Industrial Flotation Column Using Artificial Neural Network," *Arab. J. Sci. Eng.*, vol. 38, no. 5, pp. 1011–1023, May 2013.

[115] A. J. Saravani, N. Mehrshad, and M. Massinaei, "Fuzzy-based Modelling and Control of an Industrial Flotation Column," *Chem. Eng. Commun.*, vol. 201, no. 7, pp. 896–908, Jul. 2014.

[116] A. Ahmadi and M. R. Hosseini, "A Fuzzy Logic Model to Predict the Bioleaching Efficiency of Copper Concentrates in Stirred Tank Reactors," *Int. J. Nonferrous Metall.*, vol. 4, no. 4, pp. 1–8, 2015.

[117] E. Allahkarami, O. S. Nuri, A. Abdollahzadeh, B. Rezai, M. Chegini, and E. Allahkarami, "Estimation of Copper and Molybdenum Grades and Recoveries in the Industrial Flotation Plant Using the Artificial Neural Network Prediction of Grade and Recovery, Artificial Neural Network, Copper Flotation, Copper Concentrator Plant," *Int. J. Nonferrous Metall.*, vol. 5, no. 5, pp. 23–32, 2016.

[118] M. N. V. R. Kumar, "A review of chitin and chitosan applications," *React. Funct. Polym.*, vol. 46, no. 1, pp. 1–27, 2000.

[119] G. Crini and P.-M. Badot, "Application of chitosan, a natural aminopolysaccharide, for dye removal from aqueous solutions by adsorption processes using batch studies: A review of recent literature," *Prog. Polym. Sci.*, vol. 33, no. 4, pp. 399–447, 2008.

[120] G. Egger, D. Cameron-Smith, and R. Stanton, "The effectiveness of popular, non-prescription weight loss supplements," *Med. J. Aust.*, vol. 171, no. 11–12, pp. 604–608, 1999.

[121] Y.-S. Chung, K.-K. Lee, and J.-W. Kim, "Durable press and antimicrobial finishing of cotton fabrics with a citric acid and chitosan treatment," *Text. Res. J.*, vol. 68, no. 10, pp. 772–775, 1998.

[122] D. Jocić, M. R. Julia, and P. Erra, "Application of a chitosan/nonionic surfactant mixture to wool assessed by dyeing with a reactive dye," *Color. Technol.*, vol. 113, no. 1, pp. 25–31, 1997.

[123] Z. J. Piao, D. Z. Wei, Z. L. Liu, W. G. Liu, S. L. Gao, and M. Y. Li, "Selective depression of galena and chalcopyrite by O,O-bis(2,3- dihydroxypropyl) dithiophosphate," *Trans. Nonferrous Met. Soc. China (English Ed.*, vol. 23, no. 10, pp. 3063–3067, 2013.

[124] B. Feng, Y. Lu, and X. Luo, "The effect of quartz on the flotation of pyrite depressed by serpentine," *J. Mater. Res. Technol.*, vol. 4, no. 1, pp. 8–13, 2015.

[125] P. Huang, M. Cao, and Q. Liu, "Selective depression of pyrite with chitosan in Pb-Fe sulfide flotation," *Miner. Eng.*, vol. 46–47, pp. 45–51, 2013.

[126] P. Huang, M. Cao, and Q. Liu, "Using chitosan as a selective depressant in the differential flotation of Cu-Pb sulfides," *Int. J. Miner. Process.*, vol. 106–109, pp. 8–15, 2012.

[127] P. Huang, L. Wang, and Q. Liu, "Depressant function of high molecular weight polyacrylamide in the xanthate flotation of chalcopyrite and galena," *Int. J. Miner. Process.*, vol. 128, pp. 6–15, 2014.

[128] M. S. Yen, "Application of chitosan/nonionic surfactant mixture in reactive dyes for dyeing wool fabrics," *J. Appl. Polym. Sci.*, vol. 80, no. 14, pp. 2859–2864, 2001.

[129] P. Huang, M. Cao, and Q. Liu, "Adsorption of chitosan on chalcopyrite and galena from aqueous suspensions," *Colloids Surfaces A Physicochem. Eng. Asp.*, vol. 409, pp. 167–175, 2012.

[130] A. Burke, E. Yilmaz, N. Hasirci, and O. Yilmaz, "Iron(III) ion removal from solution through adsorption on chitosan," *J. Appl. Polym. Sci.*, vol. 84, no. 6, pp. 1185–1192, 2002.

[131] W. S. Wan Ngah, L. C. Teong, and M. A. K. M. Hanafiah, "Adsorption of dyes and heavy metal ions by chitosan composites: A review," *Carbohydrate Polymers*, vol. 83, no. 4. pp. 1446–1456, 2011.

[132] C. Gerente, V. K. C. Lee, P. Le Cloirec, and G. McKay, "Application of chitosan for the removal of metals from wastewaters by adsorption - Mechanisms and models review," *Critical Reviews in Environmental Science and Technology*, vol. 37, no. 1. pp. 41–127, 2007.

[133] S. Sun and A. Wang, "Adsorption properties and mechanism of cross-linked carboxymethyl-chitosan resin with Zn(II) as template ion," *React. Funct. Polym.*, vol. 66, no. 8, pp. 819–826, 2006.

[134] X. Wang, Y. Du, and H. Liu, "Preparation, characterization and antimicrobial activity of chitosan-Zn complex," *Carbohydr. Polym.*, vol. 56, no. 1, pp. 21–26, 2004.

[135] I. Saucedo, E. Guibal, J. Roussy, C. Roulph, and P. Le Cloirec, "Uranium sorption by glutamate glucan. A modified chitosan. Part I. Equilibrium studies," *Water SA*, vol. 19, no. 2, pp. 113–118, 1993.

[136] G. L. Rorrer, T. Y. Hsien, and J. D. Way, "Synthesis of Porous-Magnetic Chitosan Beads for Removal of Cadmium Ions from Waste Water," *Ind. Eng. Chem. Res.*, vol. 32, no. 9, pp. 2170–2178, 1993.

[137] I. M. N. Vold, K. M. Vårum, E. Guibal, and O. Smidsrød, "Binding of ions to chitosan - Selectivity studies," *Carbohydr. Polym.*, vol. 54, no. 4, pp. 471–477, 2003.

[138] R. G. Parr and R. G. Pearson, "Absolute Hardness: Companion Parameter to Absolute Electronegativity," *J. Am. Chem. Soc.*, vol. 105, no. 26, pp. 7512–7516, 1983.

[139] A. Boulton, D. Fornasiero, and J. Ralston, "Selective depression of pyrite with polyacrylamide polymers," *Int. J. Miner. Process.*, vol. 61, no. 1, pp. 13–22, 2001.

[140] P. Huang, "CHITOSAN IN DIFFERENTIAL FLOTATION OF BASE METAL SULFIDES," University of Alberta, 2013.

[141] D. Exerowa and P. M. Kruglyakov, *Foam and foam films: theory, experiment, application*, vol. 5. Amsterdam: Elsevier, 1997.

[142] S. Schwarz and S. Grano, "Effect of particle hydrophobicity on particle and water transport across a flotation froth," *Colloids Surfaces A Physicochem. Eng. Asp.*, vol. 256, no. 2, pp. 157–164, 2005.

[143] A. K. Gupta, P. K. Banerjee, A. Mishra, P. Satish, and Pradip, "Effect of alcohol and polyglycol ether frothers on foam stability, bubble size and coal flotation," *Int. J. Miner. Process.*, vol. 82, no. 3, pp. 126–137, 2007.

[144] B. P. Binks, "Particles as surfactants—similarities and differences," *Curr. Opin. Colloid Interface Sci.*, vol. 7, no. 1, pp. 21–41, 2002.

[145] V. N. Paunov, B. P. Binks, and N. P. Ashby, "Adsorption of Charged Colloid Particles to Charged Liquid Surfaces," *Langmuir*, vol. 18, no. 18, pp. 6946–6955, Sep. 2002.

[146] Z. Du, M. P. Bilbao-Montoya, B. P. Binks, E. Dickinson, R. Ettelaie, and B. S. Murray, "Outstanding Stability of Particle-Stabilized Bubbles," *Langmuir*, vol. 19, no. 8, pp. 3106–3108, Apr. 2003.

[147] E. Dickinson, R. Ettelaie, T. Kostakis, and B. S. Murray, "Factors Controlling the Formation and Stability of Air Bubbles Stabilized by Partially Hydrophobic Silica Nanoparticles," *Langmuir*, vol. 20, no. 20, pp. 8517–8525, Sep. 2004.

[148] B. P. Binks and T. S. Horozov, "Aqueous Foams Stabilized Solely by Silica Nanoparticles," *Angew. Chemie Int. Ed.*, vol. 44, no. 24, pp. 3722–3725, Jun. 2005.

[149] Q. Liu, S. Zhang, D. Sun, and J. Xu, "Foams stabilized by Laponite nanoparticles and alkylammonium bromides with different alkyl chain lengths," *Colloids Surfaces A Physicochem. Eng. Asp.*, vol. 355, no. 1, pp. 151–157, 2010.

[150] O. Zech, M. F. Haase, D. G. Shchukin, T. Zemb, and H. Moehwald, "Froth flotation via microparticle stabilized foams," *Colloids Surfaces A Physicochem. Eng. Asp.*, vol. 413, pp. 2–6, 2012.

[151] Carroll Croarkin, "NIST/SEMATECH e-Handbook of Statistical Methods," *NIST*, 2003. [Online]. Available: http://www.itl.nist.gov/div898/handbook/index.htm. [Accessed: 03-Dec-2018].

[152] Eriez Flotation, "Rod/Ball Mill," 2018. [Online]. Available: https://www.eriezlabequipment.com/products/size-reduction/rod-ball-mill/. [Accessed: 06-Jul-2018].

[153] Blue group, "Cone Crusher Applications," 1AD. [Online]. Available: https://blue-group.com/en/news/cone-crusher-applications/. [Accessed: 06-Jul-2018].

[154] Kleemann GmbH, "Jaw Crusher," 2018. [Online]. Available: https://www.kleemann.info/en/technologies/crushing-technology/.

[155] Gekko, "SULPHIDE GOLD." [Online]. Available: http://www.gekkos.com/minerals/sulphide-gold. [Accessed: 06-Jul-2018].

[156] I. SEPOR, "SEPOR Lab D-12 Flotation Machine." [Online]. Available: https://www.sepor.com/d-12-lab-flotation-machine/. [Accessed: 06-Jul-2018].

[157] J. M. Hargrave and S. T. Hall, "Diagnosis of concentrate grade and mass flowrate in tin flotation from colour and surface texture analysis," *Miner. Eng.*, vol. 10, no. 6, pp. 613–621, 1997.

[158] G. D. Gonzalez, M. Orchard, J. L. Cerda, A. Casali, and G. Vallebuona, "Local models for soft-sensors in a rougher flotation bank," *Miner. Eng.*, vol. 16, no. 5, pp. 441–453, 2003.

[159] Z. X. Geng and T. Y. Chai, "Soft sensor of technical indices based on LS-SVM for flotation process," *J. Syst. Simul.*, vol. 20, no. 23, pp. 6321–6324, 2008.

[160] C. Marais, "Estimation of concentrate grade in platinum flotation based on froth image analysis," 2010.

[161] H. Yang and S. Zhao, "Prediction Model for Production Indexes of a Flotation Circuit Based on Adaptive PCA and Composite Kernel Support Vector Regression," in *2010 International Conference on Biomedical Engineering and Computer Science*, 2010, pp. 1–4.

[162] Y. Wang, W. Ou, C. Yang, and W. Gui, "Online prediction of concentrate grade in flotation process based on PCA and improved BP neural networks," in *Control Conference (CCC), 29th Chinese. IEEE.*, 2010, pp. 2347–2353.

[163] F. Nakhaei, M. R. Mosavi, A. Sam, and Y. Vaghei, "Recovery and grade accurate prediction of pilot plant flotation column concentrate: Neural network and statistical techniques," *Int. J. Miner. Process.*, vol. 110–111, pp. 140–154, 2012.

[164] S. H. Hosseini and M. Samanipour, "Prediction of Final Concentrate Grade Using Artificial Neural Networks from Gol-E-Gohar Iron Ore Plant," *Am. J. Min. Metall. Vol. 3, 2015, Pages 58-62*, vol. 3, no. 3, pp. 58–62, 2015.

[165] A. Jahedsaravani, M. H. Marhaban, and M. Massinaei, "Application of Statistical and Intelligent Techniques for Modeling of Metallurgical Performance of a Batch Flotation Process," *Chem. Eng. Commun.*, vol. 203, no. 2, pp. 151–160, Feb. 2016.

[166] F. Rosenblatt, "The perceptron: A probabilistic model for information storage and organization in the brain.," *Psychol. Rev.*, vol. 65, no. 6, pp. 386–408, 1958.

[167] J.-S. R. Jang, "ANFIS: adaptive-network-based fuzzy inference system," *IEEE Trans. Syst. Man. Cybern.*, vol. 23, no. 3, pp. 665–685, 1993.

[168] E. H. Mamdani, "Advances in the linguistic synthesis of fuzzy controllers," *Int. J. Man. Mach. Stud.*, vol. 8, no. 6, pp. 669–678, Nov. 1976.

[169] L. Breiman, "Random Forests," *Mach. Learn.*, vol. 45, no. 1, pp. 5–32, 2001.

[170] J. Kim and N. Kasabov, "HyFIS: adaptive neuro-fuzzy inference systems and their application to nonlinear dynamical systems," *Neural Networks*, vol. 12, no. 9, pp. 1301–1319, Nov. 1999.

[171] S.-C. Wang, "Artificial Neural Network," in *Interdisciplinary Computing in Java Programming*, Boston, MA: Springer US, 2003, pp. 81–100.

[172] K. G. Sheela and S. N. Deepa, "Review on Methods to Fix Number of Hidden Neurons in Neural Networks," *Math. Probl. Eng.*, vol. 2013, pp. 1–11, 2013.

[173] D. Ali, M. Hayat, L. Alagha, and O. Molatlhegi, "An Evaluation of Machine Learning and Artificial Intelligence Models for Predicting the Flotation Behavior of Fine High-Ash Coal," *Adv. powder Technol.*, 2018 (submitted).

[174] I. Malekmohamadi, M. R. Bazargan-Lari, R. Kerachian, M. R. Nikoo, and M. Fallahnia, "Evaluating the efficacy of SVMs, BNs, ANNs and ANFIS in wave height prediction," *Ocean Eng.*, vol. 38, no. 2–3, pp. 487–497, Feb. 2011.

[175] K. Hornik, M. Stinchcombe, and H. White, "Multilayer feedforward networks are universal approximators," *Neural Networks*, vol. 2, no. 5, pp. 359–366, Jan. 1989.

[176] V. Nourani, A. H. Baghanam, J. Adamowski, and M. Gebremichael, "Using self-organizing maps and wavelet transforms for space–time pre-processing of satellite precipitation and runoff data in neural network based rainfall–runoff modeling," *J. Hydrol.*, vol. 476, pp. 228–243, Jan. 2013.

[177] R. Barzegar and A. Asghari Moghaddam, "Combining the advantages of neural networks using the concept of committee machine in the groundwater salinity prediction," *Model. Earth Syst. Environ.*, vol. 2, no. 1, p. 26, Mar. 2016.

[178] R. Barzegar, M. Sattarpour, M. R. Nikudel, and A. A. Moghaddam, "Comparative evaluation of artificial intelligence models for prediction of uniaxial compressive strength of travertine rocks, Case study: Azarshahr area, NW Iran," *Model. Earth Syst. Environ.*, vol. 2, no. 2, p. 76, Jun. 2016.

[179] L. A. Zadeh, "Fuzzy sets," *Inf. Control*, vol. 8, no. 3, pp. 338–353, Jun. 1965.

[180] I. Pulido-Calvo and J. C. Gutiérrez-Estrada, "Improved irrigation water demand forecasting using a soft-computing hybrid model," *Biosyst. Eng.*, vol. 102, no. 2, pp. 202–218, Feb. 2009.

[181] M. Sugeno, *Industrial applications of fuzzy control*. Amsterdam, 1985.

[182] E. H. Mamdani and S. Assilian, "An experiment in linguistic synthesis with a fuzzy logic controller," *Int. J. Man. Mach. Stud.*, vol. 7, no. 1, pp. 1–13, Jan. 1975.

[183] I. Iancu, *A Mamdani type fuzzy logic controller, in: E. Dadios (Ed.), Fuzzy Logic: Controls, Concepts, Theories and Applications*, vol. 3. Rijeka: InTech Croatia, 2012.

[184] J. Jang, C. Sun, and E. Mizutani, *Neuro-Fuzzy and Soft Computing : A Computational Approach to Learning and Machine Intelligence*. Upper Saddle River, NJ: Prentice Hall, 1997.

[185] L.-X. Wang and J. M. Mendel, "Generating fuzzy rules by learning from examples," *IEEE Trans. Syst. Man. Cybern.*, vol. 22, no. 6, pp. 1414–1427, 1992.

[186] X. Dou and Y. Yang, "Comprehensive Evaluation of Machine Learning Techniques for Estimating the Responses of Carbon Fluxes to Climatic Forces in Different Terrestrial Ecosystems," *Atmosphere (Basel).*, vol. 9, no. 3, p. 83, 2018.

[187] E. Fijani, A. A. Nadiri, A. Asghari Moghaddam, F. T.-C. Tsai, and B. Dixon, "Optimization of DRASTIC method by supervised committee machine artificial intelligence to assess groundwater vulnerability for Maragheh–Bonab plain aquifer, Iran," *J. Hydrol.*, vol. 503, pp. 89–100, Oct. 2013.

[188] A. Kumar, "Data Science – How to Scale or Normalize Numeric Data using R," 2014. .

[189] A. Belayneh, J. Adamowski, B. Khalil, and B. Ozga-Zielinski, "Long-term SPI drought forecasting in the Awash River Basin in Ethiopia using wavelet neural network and wavelet support vector regression models," *J. Hydrol.*, vol. 508, pp. 418–429, Jan. 2014.

[190] N. Wanas, G. Auda, M. S. Kamel, and F. Karray, "On the optimal number of hidden nodes in a neural network," in *Conference Proceedings. IEEE Canadian Conference on Electrical and Computer Engineering (Cat. No.98TH8341)*, 1998, vol. 2, pp. 918–921.

[191] A. K. Mishra and V. R. Desai, "Drought forecasting using feed-forward recursive neural network," *Ecol. Modell.*, vol. 198, no. 1–2, pp. 127–138, Sep. 2006.

[192] J. C. Dunn, "A Fuzzy Relative of the ISODATA Process and Its Use in Detecting Compact Well-Separated Clusters," *J. Cybern.*, vol. 3, no. 3, pp. 32–57, Jan. 1973.

[193] R. J. Hathaway and J. C. Bezdek, "Fuzzy c-means clustering of incomplete data," *IEEE Trans. Syst. Man Cybern. Part B*, vol. 31, no. 5, pp. 735–744, 2001.

[194] M. Zounemat-Kermani and M. Teshnehlab, "Using adaptive neuro-fuzzy inference system for hydrological time series prediction," *Appl. Soft Comput.*, vol. 8, no. 2, pp. 928–936, Mar. 2008.

[195] R. M. Rahman, S. Ata, and G. J. Jameson, "The effect of flotation variables on the recovery of different particle size fractions in the froth and the pulp," *Int. J. Miner. Process.*, vol. 106–109, pp. 70–77, 2012.

[196] P. M. J. and B. H. W., "Bubble coalescence and break-up in air-sparged bubble columns," *AIChE J.*, vol. 36, no. 10, pp. 1485–1499, Jun. 2018.

[197] P. T. L. Koh, M. P. Schwarz, Y. Zhu, P. Bourke, R. Peaker, and J. P. Franzidis, "Development of CFD models of mineral flotation cells," in *Third International Conference on Computational Fluid Dynamics in the Minerals and Process Industries, Melbourne, Australia*, 2003, pp. 171–175.

[198] P. T. L. Koh and M. P. Schwarz, "CFD model of a self-aerating flotation cell," *Int. J. Miner. Process.*, vol. 85, no. 1, pp. 16–24, 2007.

[199] P. T. L. Koh and M. P. Schwarz, "CFD modelling of bubble–particle collision rates and efficiencies in a flotation cell," *Miner. Eng.*, vol. 16, no. 11, pp. 1055–1059, 2003.

[200] by G. J. D. and J. A. Swanson, *ANSYS engineering analysis system user's manual*. Houston, Pa. : Swanson Analysis Systems, 1985., 1985.

VITA

Muhammad Badar Hayat grew up in Mianwali, Pakistan. In 2008, he received his Bacheolar of Science in Mining Engineering from the University of Engineering & Technology (UET) Lahore, Pakistan. He worked as a blasting Engineer from 2008 to 2010 at Bestway Cement Limited in Chakwal, Pakistan. In 2010, he joined the Department of Mining Engineering at UET Lahore as a lecturer. Alongside his teaching responsibilities, he successfully finished his Master of Science in Mining Engineering from UET Lahore in 2012.

In 2013, he started his PhD in Mining Engineering at Missouri University of Science & Technology (S&T) in Rolla, Missouri, USA. He worked as a Teaching Fellow at Saudi Mining Polytechnic (a project of Mining & Nuclear Engineering Department of Missouri S&T) in Arar, Saudi Arabia for almost one year. During his PhD at Missouri S&T, he worked as a Graduate Research Assistant and Graduate Teaching Assistant for mineral processing courses. He received his PhD in Mining Engineering from Missouri S&T in July 2018.